A novel multi-dimensional Eulerian approach to computational solid dynamics

Philip Trevor Barton

PhD Thesis

SCHOOL OF ENGINEERING
CRANFIELD UNIVERSITY

Cranfield University

Philip Trevor Barton

A novel multi-dimensional Eulerian approach to computational solid dynamics

School of Engineering

PhD Thesis

Academic Year 2009-2010

Supervisor: Dimitris Drikakis

December 2009

Acknowledgements

First and foremost I would like to thank Prof. Dimitris Drikakis for his supervision and guidance on all aspects of the project, from whom I have learnt a great deal, and who provides inspiration for persuing an academic career. It was a pleasure to have worked with Prof. Evgeniy Romenski, who I thank kindly for devoting much time and patience to answering all my questions on the employed continuum model, and who has instilled in me a keen interest in model development which I hope to one day persue. Also for contacting Prof. Anatoly Resnyansky to provide some much needed material constants for the employed equation of state. In the multi-scale modelling method it was a pleasure to have worked in collaboration with Dr. Marco Kalweit, and I thank him for patiently describing the art of molecular dynamics.

I am extremely grateful to Dr. Graham Ball and Nigel Park for organising my use of the Atomic Weapons Establishment's (AWE's) facilities and for providing many stimulating discussions about dynamic friction and shock physics. Also from AWE I thank David Youngs for discussions on multi-phase flows and interface tracking methods.

I would like to acknowledge the Engineering and Physical Sciences Research Council and the Ministry of Defence-AWE for financial support of the project under which this work was conducted.

I benefitted hugely from many conversations with Dr. Vladimir Titarev on aspects of numerical modelling, particularly high-order methods, and it was our common interest in non-linear elasticity which led to a joint publication. I thank Dr. Evgeniy Shapiro for providing instruction on the base code HIRECOM used for the bulk of the work and for his first class advice on programming with Fortran. Within the FMaCS group there are many colleagues who I have benefitted from either technical conversations, useful software packages, or friendly moral support including Max Starr, Dr. Ben Thornber, Nikolaos Asproulis, and Mathis Dahlqvist.

My family have been behind me throughout my entire education which I suppose formally comes to an end with this PhD and would not have been possible without their continued encouragement. I make a special 'thank you' to my parents for also providing free all-inclusive accommodation whenever I required it whilst at AWE.

I reserve my biggest thanks for my wife Louise who has supported me every step of the way through my PhD (and whilst miraculously keeping her winging to a minimum), which has arguably been quite tough at times. It is without question that I dedicate this work to her.

Philip Barton

Abstract

Many problems in solid dynamics involve moving boundaries, finite elasto-plastic deformations, and strong non-linear waves. Continuum modelling of such events is difficult on account of these characteristics, and there exist a number of inadequacies in current numerical algorithms. Furthermore, a comprehensive understanding of certain underlying processes is yet to be achieved which places a limit on the derivation of engineering models to simulate these occurrences. Much needed atomistic studies, capable of revealing much about the governing physical processes, remain limited by current computational resources. This thesis is devoted to targeting these difficulties by proposing new continuum numerical schemes and a means of studying both micro- and macro-scale behaviours via a dynamic coupling of continuum mechanics and molecular dynamics theory.

Eulerian shock-capturing schemes have advantages for modelling problems involving complex non-linear wave structures and large deformations in solid media. Various numerical methods now exist for solving hyperbolic conservation laws that have yet to be applied to solid dynamics. A three-dimensional finite-volume scheme on fixed grids is proposed for elastoplastic solids. The scheme is based upon the Godunov flux method and thus requires solution of the Riemann problem. Both exact and approximate solutions are proposed for the special case of non-linear elasticity. An implicit algorithm is developed to allow for resolving rate-dependent inelastic deformations. The methods are tested against exact solutions in one-dimension, and symmetrical polar solutions in two- and three-dimensions.

To account for multiple immiscible materials it is necessary to include some means of tracking material boundaries within a numerical scheme. A moving grid scheme is a simple means of accommodating transient boundaries. Interface tracking based on the use of level set functions is an attractive alternative for problems with sliding interfaces since it allows discontinuous velocity profiles at the material boundaries whilst employing fixed grids. Both of these methods are explored in the current context. A series of one-dimensional testcases have been carried out that demonstrate the ability of the numerical schemes to accurately resolve complex boundary conditions between interacting free surfaces.

Where singularities occur in a system comprising solid materials, atomistic studies are invaluable for achieving a fundamental insight into the governing physical processes. However where non-linear waves are generated, domain size proves to be a limiting factor in achieving solutions free from numerical artifacts. A domain decomposition multi-scale modelling strategy is developed that couples the Eulerian shock capturing scheme with a molecular dynamics solver. The method is demonstrated for one-dimensional testcases involving strong shear waves and multiple components. Attention is devoted to resolving transient wave propagation free from spurious wave reflections through investigation of the numerical parameters.

Contents

List of Figures

List of Tables

1

Introduction

For modelling events such as high velocity impact and explosive loading of solid materials there is strong demand on the numerical methods to simultaneously achieve high wave resolution, maintain sharp interfaces, and accurately impose interfacial boundary conditions. One can single out two modelling approaches: atomistic methods, such as molecular dynamics (MD), that consider the motion of each individual atom in a system and thus naturally handle wave propagation and multi-materials; continuum mechanics (CM) methods which rely upon the provision of constitutive models to describe the motion of specific bulk volumes of material and require complex algorithms to resolve non-linear waves and multiple components. On the basis of these concise definitions of two very different techniques, one might be tempted to resort simply to MD since this ticks all the boxes for the above stated requirements without any apparent difficulties. Furthermore atomistic methods lend a fundamental insight into the physical processes governing a material's behaviour. However such methods are computationally intensive and, with current resources, are limited only to nano-scale samples. CM methods are suited to resolving macroscale systems, but in conventional approaches it is difficult to achieve all of the above requirements within a single numerical algorithm. Furthermore, the range of applicability, or even the availability, of certain constitutive equations can be a limiting factor before any analysis takes place. It is these predicaments that motivates the development of new multi-material, multi-scale modelling techniques for compressible solids.

It is the development of a continuum mechanics method, tailored to the above outlined requirements, that will form the majority of this work and should therefore be the primary focus of background review. If one was to list the requirements of any model of compressible solids based upon historically documented behaviour, then the more fundamental of these would include the ability to resolve high strain rates, finite elastoplastic deformations, strain hardening, thermal softening, and melting. Within the bulk material, constitutive models covering each of these requirements, whilst still the subject of considerable research efforts, have been established to a high level of confidence for many of the common metallic elements and alloys. One flaw of conventional models appears to be the inadequacy of the mathematical formulation of the governing laws such that solution methodologies do not meet the

above requirements. Another more fundamental deficiency is singularities in certain systems where constitutive equations, or even a comprehensive understanding of the physical behaviour itself, remain outstanding. Since overcoming each of these problems represents quite different challenges they shall be considered independently in the first instance; but it will soon become apparent that a solution to one can be equally beneficial to the other.

1.1 Continuum methods for multiple compressible solids

Various models and numerical methods have been developed to simulate processes in solid media and a users choice will depend largely on the problem and the available resources. Benson [6] provides a detailed review of the most common of these (see also [87, 91]). The governing laws of compressible solids in the Lagrangian frame comprise conservation of mass, momentum, and energy, in conjunction with constitutive models for the strength of the material. Alternatively, transformation to the Eulerian frame of reference requires additional laws to transport the material history, such as elastoplastic strains; the number of additional equations depends largely on the complexity of the employed constitutive models. This distinct difference in complexity is of course then reflected in the numerical algorithms one must employ to find soutions to a given problem. Lagrangian methods, where the computational grid conforms to the material, are efficient and can resolve material interfaces exactly. Furthermore, since there is zero mass transfer across the cell boundaries, implementation of complex constitutive equations for material strength is relatively straightforward since the history is stored for each element. However, in circumstances where the material undergoes large distortions, accuracy cannot be guaranteed and in some cases the methods can fail. Eulerian methods on the other hand use fixed grids and allow the material to flow through it. Aside from the solution of more complicated algorithms for each material, Eulerian methods must be supplemented by some means of tracking the boundaries of each component in a system. As such they are expensive, not least since one must designate in the first instance a computational mesh that spans the entire potential range of space through which the materials might pass, the details of which might not be known prior to a calculation. However, the use of fixed grids avoids any danger of mesh entanglement and premature code failure as a result of large deformations.

It is inevitable then that several methods have been developed that either combine the Lagrangian and Eulerian approaches, such as arbitrary Lagrangian Eulerian (ALE) methods [80, 30], or attempt to combat the deficiencies of one by modifying the numerical methods, such as meshless Lagrangian smoothed particle hydrodynamics (SPH) techniques, and the free Lagrange approach [31]. Considerable efforts

are directed to improving these methods in view of their potential over the conventional approaches. However, difficulties in each of these do remain and therefore justifies the exploration of further alternatives. For compressible solids targeting difficulties of the pure Eulerian approach is of particular interest here. It is mentioned however that developments in this specific framework could be used in conjunction with the ALE method, which might yield greater efficiency overall since the Eulerian counterpart need only be used under large deformations. Concentrating in the first instance on just the pure Eulerian approach, one can highlight two difficulties:

- Immiscible multi-material calculations require interface tracking algorithms which typically are based upon the volume-of-fluid (VOF) method, which, for reasons which will be discussed in detail shortly, can introduce artificial smearing of discontinuous profiles across material boundaries over a finite number of grid points.

- The governing models used in Eulerian approaches typically consist of the conservation laws for mass, momentum and energy, complemented by constitutive equations for the time dependent stress deviator, and closure models for hydrostatic pressure and material strength. Traditional Eulerian methods employ the finite element or finite difference methods, requiring the explicit inclusion of artificial viscosity to avoid numerical artifacts in problems involving shock waves. Whilst this works in practice it is desirable to introduce the necessary viscosity in a more natural way.

With this in mind it is intuitive to explore specific schemes employed by physics disciplines outside of solid mechanics; in particular computational fluid dynamics (CFD).

In view of the complex behaviour that can occur in solid materials, the requirements from the employed numerical algorithms is akin to those of hydrodynamics: the algorithm must be capable of handling large distortions and achieve high wave resolution. High-order shock capturing methods, based upon solving Riemann problems locally at each cell edge throughout a computational domain, have emerged as a favourable approach to meeting these requirements. Their success in fluid mechanics has led to a wealth of research and consequently methods of increasing accuracy and efficiency are now available. Many of these numerical tools are derived on the basis of arbitrary systems of conservation laws; thus retrofitting these techniques to other physics disciplines is possible given that the governing models are written in adequate form.

Application of these numerical tools to solid mechanics has been made possible by formulations of the governing theory as first-order hyperbolic systems of conservation laws in the Eulerian frame of reference [40, 57, 58, 62, 28]. Considering first the special case of non-linear elasticity, the governing systems of equations presented

in these previous works are comparable, differing in the chosen state parameters: in [57, 58, 62] the conservation of strain is achieved through transport equations for the components of the inverse deformation gradient tensor, whereas in [40, 62, 28] the deformation gradients are used as the state variables. In both cases the equations are supplemeted by additional constraining steady conservation laws for the respective gradients. The relative differences in each formulation constitutes an interesting mathematical conundrum as discussed in [82] but is outside the scope of the present study. From the viewpoint of numerical evaluation, both formulations have the distinct advantage of being suitable for the application shock capturing tools such as the widely recognised Godunov flux method. It is mentioned that the Godunov approach has been applied to conventional models for solids [41], but in the deformation gradient based models, material strength, an important source of non-linearity, can be accounted for in the Riemann problem solution. Developments of Godunov methods for such formulations include the works of LeFloch and Olsson [42] and Titarev *et al* [72]. It is also worth mentioning the use of Godunov methods for these formulations in the Lagrangian frame in [78, 79]. Modifications to these algorithms to include inelastic deformations need not be overly complicated.

Inelastic deformations can be accounted for by modifying the governing model in a number of ways. The multiplicative decomposition of the total deformation tensor into elastic and plastic parts (see [68]) can be used to yield additional conservation laws for the plastic deformation tensor [40, 58]. Developments using these models include the work of Vorobiev *et al* [80], Wang *et al* [85], Walter *et al* [83, 84], and Miller and Colella [48]. A disadvantage of this approach is the additional expense of solving a much larger system of equations. In a different approach, a modified elastic potential was proposed in [39] such that the resultant constitutive equations for stress obey von Mises yield criterion, but is restricted to idealised plasticity theory. Developments of Godunov methods for such formulations include the work of Trangenstein and Colella [76], Trangenstein and Pember [77] Vorobiev *et al.* [80], Wang *et al.* [85], Walter *et al.* [84], and Miller and Colella [48]. In the present study the elastic-plastic formulation of Godunov and Romenski [28] is used, specifically the formulation presented in [62], where plasticity is introduced via source terms for the equations of the elastic deformation tensor. It is mentioned that in accessory to rate dependent plasticity, thermal softening and melting, additional equations in some of the above works have been used to resolve strain hardening and fracture behaviours.

Finally it is necessary to discuss the extension of the shock capturing schemes for elastoplastic solids to multi-component systems. If grid motion is deemed acceptable then material boundaries can be accommodated using a moving mesh strategy where the grid boundaries conform to the material boundaries, but interior nodes are distributed such that mesh tangling is avoided (see [89, 80, 81] for a use of this method for solid dynamics problems). Such methods are commonly categorised as

simplified ALE (SALE). It is mentioned that true ALE methods do indeed employ moving grids, and material boundaries can be defined by grid lines; but in the limit that deformations become large there will be some mechanism that will resort to using one of the interface tracking methods, to be described next, to evolve the internal boundaries. This hybrid approach considerably extends the range of stability of a moving grid method alone. The numerous numerical methods for solving multi-material problems using fixed grids can be broadly classed as either *interface capturing* or *interface tracking*. The former has been applied extensively to problems in fluid mechanics where the resultant interface smearing may be deemed acceptable on the basis that the flow is miscible. For many problems in solid mechanics however interfaces need to remain sharp and interface tracking methods are more suitable. Included in this category are level-set methods, volume-of-fluid (VOF) methods, and marker particle methods. A detailed presentation of the means by which an interface is evolved in each of these shall be omitted, and instead the interested reader is directed to the review in [61]. Such methods have been successfully applied to the aforementioned models in conservative form, including in [49] where the VOF method is used in a coupled solid/fluid scheme, and in [84, 85] where marker particles are used to track boundaries in the simulation of impacting solid materials.

When interfaces of two solid materials come into contact two limits can be identified for the resulting behaviour: *stick* where both the traction and velocity vectors of each material normal to the common interface are equal; *slip* where tangential components of the traction normal to the interface are zero and the components slide freely over one another. In reality, for high velocity impacts the behaviour will lie somewhere in between these two limits [88], with the tangential motion a complex non-linear function of the interfacial state. An accurate numerical scheme for modelling such processes must incorporate an interface tracking method where the boundary evolution reflects the motion dictated by the physics. That is it allows unconstrained sliding between components. These requirements single out the level-set and marker particle methods. VOF methods on the other hand require a common velocity vector between interacting components within mixed cells. The next question then is how to incorporate these within a numerical scheme and more importantly how to account for the interaction between components, and will be subject to investigation in this thesis.

1.2 Multi-scale modelling

It is apparent that in some circumstances either or both of the CM and previously described MD methods may be inadequate. An example might be some interfacial phenomenon that exists as a singularity in a multi-component system of interest. Ideally one would like to perform MD simulations of relatively long time scales to

draw conclusions on the physical processes such that an engineering model might be developed for use in a CM solver. This is of course provided that reliable potentials exist for the materials of interest. However, any waves generated in the MD domain may at some point reach the boundaries of the simulation domain resulting in numerical artifacts that soil the solution. Furthermore, there exist difficulties with certain aspects of MD, such as modelling heat conduction, that may indeed benefit from overlaying continuum models. Instead a multiscale strategy could be employed where MD is used in the near interface region and CM methods elsewhere, with a dynamic coupling between the two. In this way the CM provides time-accurate boundary conditions for the MD solver allowing generated waves to propagate naturally through the system, and on-the-other-hand the MD eliminates the requirement for constitutive models in the CM solver to describe the unknown interfacial state. This example is somewhat specific but gives a flavour of the potential of a multiscale strategy. Keeping this in mind it is intuitive to discuss in greater detail the approach to such a strategy.

The different approaches to multi-scale modelling are summarised nicely in [15] as algorithm refinement methods, or domain decomposition methods. An example of the former was proposed in [11] for problems involving dry sliding where for computational cells adjacent to a component's boundary a sub-grid model is used to determine the interfacial state, and subsequently leads to improved continuum predictions of sliding components. The objective here is to achieve an atomistic study of a singularity in a solid material by targeting limitations on the range of applicability of MD simulations, and in turn eliminate the reliance on particular constitutive models used in the continuum mechanics (CM) methods. In this way the simulation domain can be decomposed into regions Γ^{MD} where MD is applied, and regions Γ^{CM} where CM models are sufficient.

A widely accepted hybrid domain decomposition approach is the class of coarse grain molecular dynamics (CGMD) methods (see for example [52]). GCMD methods rely on assigning groups of atoms to (time-dependent) continuum grid nodes. Alternative hybrid continuum-molecular methods based upon coupling either by the exchange of states or through the implementation of fluxes via a *hybrid surface interface* (HSI) [37], eliminating the restraint of molecules and grid nodes, are comparably new and show significant potential for problems involving finite deformations. In this approach an Eulerian computational fluid dynamics (CFD) solver can be employed with boundary cells overlapping in the MD regions on to which a state deduced from the MD solver can be applied. Conversely, the fluxes subsequently predicted across the face of the boundary cells can be enforced on the atoms within a flux implementation zone to provide physical, time-dependent bounds for the MD solver. Coupling MD with a CFD finite volume method also has the advantage that the latter employing solutions of local Riemann problems at cell edges to approximate numerical flux functions tend to exhibit improved resolution of non-

linear waves. This is especially true when cell centred piecewise averaged data is reconstructed using state-of-the-art polynomial reconstruction methods of increasingly high-orders of accuracy (see [13, 2]). Furthermore, flux functions predicted in this way and employed by the MD simulation in the flux coupling approach may well lead to a more accurate implementation method as opposed to using simple averages between piecewise averaged data from cells adjoining the MD/CM interface. Using governing models of continuum mechanics in adequate form it is possible to employ such a multiscale technique for the problems in solid mechanics of interest here.

In light of the behaviour historically observed in solid materials, such as rate-dependent elastoplastic deformations and thermal softening, one would ideally prefer to have a method general to condensed media, thus capable of resolving the behaviour of both solid and liquid phases should the phase change occur. MD naturally simulates material across the phase space, including liquid and solid phases, as long as a suitable model for the potential interactions is available. It is therefore an excellent method for the simulation of systems where the complex physical processes remain unknown in their entirety. Provided the required constitutive equations are known continuum models are too capable of handling transitions between phases; the difficulty lies more in the numerical methods which must be capable of handling large deformations and achieve high wave resolution. Eulerian methods for solid mechanics using shock capturing schemes have emerged as a viable means of achieving high wave resolution and allowing finite elastoplastic deformations whilst employing Cartesian computational grids [48, 3, 4]. For problems in solid media where the resolving of strong non-linear waves is paramount, the combination of these two methods within a single Eulerian multiscale modelling strategy has significant potential.

1.3 Summary of content

The rest of the thesis proceeds as follows. Chapter 2 is devoted to establishing and verifying a shock capturing scheme for non-linear elastic materials, including a detailed description of the employed model, proposal of a high-order characteristics based method for the approximation of numerical flux functions, and derivation of a proceedure for obtaining exact solutions of the Riemann problem for hyperelastic materials for the purpose of verification. These numerical methods form the basis for extension to multiple space dimensions and the inclusion of inelastic deformations in Chapter 3. Since a moving boundary capability is required for modelling systems comprising multiple components, interface tracking approaches are proposed in Chapter 4 using modifications of the single component numerical methods estab-

lished in the previous Chapters 2 and 3. Chapter 5 is concerned with combining all of these techniques with molecular dynamics to form a multi-scale physics code for the purpose of studying solid systems comprising certain singularities, and concentrates on establishing the numerical framework with an emphasis on the continuum counterpart. Finally, conclusions are drawn in Chapter 6.

1.4 Publications

Aspects of the work in this thesis has been reported in the following publications:

- M. Kalweit, **P.T. Barton** & D. Drikakis, Hybrid molecular dynamics - continuum mechanics method for solid materials, *under review* (2009).
- **P.T. Barton** & D. Drikakis, An Eulerian method for multi-component problems in non-linear elasticity with sliding interfaces, *under review* (2009).
- **P.T. Barton**, D. Drikakis & E. Romenski, An Eulerian finite-volume scheme for large elastoplastic deformations in solids, *International Journal for Numerical Methods in Engineering*, DOI: 10.1002/nme.2695 (2009).
- **P.T. Barton**, D. Drikakis, E. Romenski & V.A. Titarev, Exact and approximate solutions of Riemann problems in non-linear elasticity, *Journal of Computational Physics*, **228**, 7046–7068 (2009).

Furthermore aspects of the work have been presented at the following conferences:

- **P. Barton** & D. Drikakis, An Eulerian method for sliding interfaces, *Numerical Methods for Multi-material Fluids and Structures, Pavia, Italy*, 21–25 Sep (2009).
- M. Kalweit, **P. Barton** & D. Drikakis, Simulation of high speed sliding friction using a hybrid molecular-continuum method, *Numerical Methods for Multi-material Fluids and Structures, Pavia, Italy*, 21–25 Sep (2009).
- M. Kalweit, **P. Barton**, D. Drikakis & G. Ball, Hybrid molecular-continuum simulation for multiscale simulations of dynamic friction, *World Tribology Congress, Kyoto*, 6–11 Sep (2009).

2

Exact and approximate solutions of Riemann problems in non-linear elasticity[†]

Synopsis

Eulerian shock-capturing schemes have advantages for modelling problems involving complex non-linear wave structures and large deformations in solid media. Various numerical methods now exist for solving hyperbolic conservation laws that have yet to be applied to non-linear elastic theory. In this chapter one such class of solver is examined based upon characteristic tracing in conjunction with high–order monotonicity preserving weighted essentially non-oscillatory (MPWENO) reconstruction. Furthermore, a new iterative method for finding exact solutions of the Riemann problem in non-linear elasticity is presented. Access to exact solutions enables an assessment of the performance of the numerical techniques with focus on the resolution of the seven wave structure. The governing model represents a special case of more general theory describing additional physics such as material plasticity. The numerical scheme therefore provides a firm basis for extension to simulate more complex physical phenomena. Comparison of exact and numerical solutions of one-dimensional initial values problems involving three-dimensional deformations is presented.

2.1 Introduction

The Riemann problem is an initial value problem consisting of two uniform conditions where the state varies discontinuously. Depending on how these uniform states are chosen the Riemann problem for the equations of non-linear elasticity can result in up to six genuinely non-linear waves propagating away from a central linearly degenerate contact. Between each wave the state is uniform and hence the wavespeeds are constant, leading to a self similar profile of up to eight piecewise constant states.

Solution of the Riemann problem has gained significant importance in numerical schemes for systems of hyperbolic conservation laws. Considering a computational

[†]Much of the work in this chapter was presented in [3]: **P.T. Barton**, D. Drikakis, E. Romenski & V.A. Titarev, Exact and approximate solutions of Riemann problems in non-linear elasticity, *Journal of Computational Physics*, **228**, 7046–7068 (2009).

mesh with piecewise constant data stored at each discrete point, Godunov proposed solving Riemann problems locally at each intercell boundary. What has now become commonly known as the Godunov method permits numerical computation of more general Cauchy problems where discontinuities may exist in the solution. For such problems these shock-capturing schemes are popular since they avoid the need to explicitly include artificial viscosity to ensure convergence to the correct weak solution.

Here, the interest is in developing Godunov methods for solid media in the Eulerian reference frame. Although more complicated than Lagrangian schemes, Eulerian formulations are better suited for modelling problems involving discontinuous waves and large deformations. Several authors have proposed Eulerian schemes based on solving Riemann problems for solid materials. In [42, 72] approximate one-dimensional Riemann solvers are presented for two-dimensional deformations. Godunov methods for elastic-plastic media are demonstrated in [77, 85] for one-dimension, in [80] for two-dimensions, and in [48] for three dimensions.

The application of these numerical tools for solid mechanics is made possible by formulations of the governing laws as first order hyperbolic systems of conservation laws in the Eulerian reference frame [26, 40, 58, 28]. Here, the formulation proposed by Godunov and Romenski [28] is used, where the state of solid media is governed by conservation laws for mass, momentum, strain and energy, in conjunction with compatibility constraints (see also [57]). It should be mentioned that solution of the Riemann problem in non-linear elasticity is a stepping stone towards developing numerical schemes for elastic-plastic media. Indeed it is shown in [28, 62] that plasticity can be governed by the addition of source terms and thus with no change to the Riemann solver employed for the convective fluxes. Another interesting approach is proposed in [39] where the elastic potential is modified to obey Von-Mises yield criterion.

In this study the motivation for developing an exact solution to the Riemann problem in non-linear elasticity is not for use within a numerical scheme, but rather as a tool for validating approximate techniques. In general, exact solutions of Riemann problems are iterative processes and their use in a numerical scheme would constitute an expensive overhead. Instead one can find approximate solutions, or solve exactly an approximation of the governing theory. Indeed in those studies mentioned above the numerical schemes employ approximate Riemann solvers. Titarev *et al.* [72] recently studied several approximate solvers for non-linear elasticity. It was shown that, except in some special circumstances, such approximate methods are sufficient to obtain high accuracy solutions.

Few authors have considered exact solutions of the Riemann problem in non-linear elasticity. In all but one of these studies solutions are obtained only for the special case of uniaxial deformations. Garaizar [25] presents a theoretical evaluation of the equations of elasticity and proposes an algorithm for uniaxial deformations;

however, no numerical results are given. Titarev *et al.* [72] also solve the Riemann problem exactly for uniaxial deformations. Miller [50] proposed an exact iterative method for the solution of the Riemann problem of arbitrary hyperbolic systems of conservation laws, using the equations of non-linear elasticity as an example. Here, they appear to be the first to consider exact solutions for three-dimensional deformations. Their results highlighted large discrepancies between exact and approximated solutions of initial value problems and stands as an example of the need for exact solutions.

The purpose of the present chapter is to apply certain well established high–order shock capturing methods to the augmented one-dimensional equations of non-linear elasticity. The model of Godunov and Romenski [28] is considered and a characteristic-tracing based approximate Riemann solver is derived considering three-dimensional deformations. In comparison to the one-dimensional system for two-dimensional deformations [72], this requires the evaluation of an additional six equations, and an examination of the eigensystem reveals a total of seven characteristic fields. Similar wave profiles are found in magnetohydrodynamics (MHD) and in [2] it is shown that improved wave resolution can be achieved via high–order monotonicity preserving weighted essentially non-oscillatory (MPWENO) reconstruction. In particular these have benefits for for such problems where slow shocks proceed a faster moving wave, where the former can otherwise be insufficiently resolved. In order to assess these methods for non-linear elasticity exact solutions are desirable.

The proposed exact solution method requires systematic evaluation of the solutions across each characteristic wave. It is assumed that the Riemann problem solution comprises a central linearly degenerate contact wave, with all other waves being genuinly non-linear. In [50], where a similar approach is adopted, it is reported that these assumptions limit the applicability of the algorithm as a result of certain conditions, such as lack of genuine non-linearity, that can occur for non-linear elastic materials. Analysis of these conditions is not repeated here, but a discussion of the impact on the range of applicability of the scheme proposed in this paper is given in § 2.4.6. Concisely, as a result of these conditions the present proposed exact solution proceedure is valid only for cases where all seven waves are distinct.

The rest of the chapter proceeds as follows. In § 1.2 the governing equations are presented along with an analysis of the characteristic decomposition. In § 1.3 details are given of an exact iterative solution to the Riemann problem, while § 1.4 outlines a numerical scheme. A comparative analysis between exact and numerical methods using example testcases is presented in § 1.5 and finally conclusions are drawn in § 1.6.

2.2 Model of non-linear elastic solids

To describe processes in condensed media in the Eulerian reference frame the model of Godunov and Romenski [26] (and more recently [28]) is used. Here, the state of a solid is characterised by the elastic deformation gradient $\mathbf{F} = [F_{ij}] = \partial x_i / \partial x_{0_j}$ (where $\mathbf{x} = [x_i]$ and $\mathbf{x_0} = [x_{0_j}]$ denote the fixed spatial coordinates and material coordinates of the unstressed reference state respectively), velocity $\mathbf{u} = [u_i]$, and entropy $\mathscr{S}$. The complete three dimensional system forms a hyperbolic system of conservation laws for momentum, strain, and energy. In Cartesian coordinates

$$\frac{\partial \rho u_i}{\partial t} + \frac{\partial \left(\rho u_i u_\alpha - \sigma_{i\alpha}\right)}{\partial x_\alpha} = 0 \tag{2.1a}$$

$$\frac{\partial \rho F_{ij}}{\partial t} + \frac{\partial \left(\rho F_{ij} u_\alpha - \rho F_{\alpha j} u_i\right)}{\partial x_\alpha} = 0 \tag{2.1b}$$

$$\frac{\partial \rho E}{\partial t} + \frac{\partial \left(\rho u_\alpha E - u_i \sigma_{i\alpha}\right)}{\partial x_\alpha} = 0 \tag{2.1c}$$

Here, ρ is the density, $\sigma = [\sigma_{ij}]$ the Cauchy stress tensor, $E = (\mathscr{E} + |\mathbf{u}|^2/2)$ the total energy, with $\mathscr{E}$ the specific internal energy. Repeated indices denote summation (see Appendix A). The system is closed by analytic formulae for the specific internal energy in terms of the parameters of state

$$\mathscr{E} = \mathscr{E}(F_{11},\, F_{12},\, \ldots,\, F_{33},\, \mathscr{S}). \tag{2.2}$$

Density, temperature and the stress tensor are given by

$$\rho = \rho_0 / \det|\mathbf{F}|, \tag{2.3}$$

$$T = \frac{\partial \mathscr{E}}{\partial \mathscr{S}}, \tag{2.4}$$

$$\sigma_{ij} = \rho F_{ik} \frac{\partial \mathscr{E}}{\partial F_{jk}}, \tag{2.5}$$

respectively, where ρ_0 denotes the density of the initial unstressed medium.

Using Eq. (2.3) in (2.1b) it is possible to show that the combination of equations governing the conservation of strain conserve mass, by means of recovering the continuity equation

$$\frac{\partial \rho}{\partial t} + \frac{\partial \rho u_\alpha}{\partial x_\alpha} = 0. \tag{2.6}$$

(see Appendix B for proof).

Remark: It is useful to consider that the continuity equation can be used in place of one equation for the deformation gradient tensor in order to provide conservation of mass (see [72]). In particular it will be shown in Chapter 3 that this property plays a crucial role in developing stable numerical algorithms for elastoplastic deformations.

2.2.1 Constitutive relations for isotropic hyperelastic materials

Using the form of the potential Eq. (2.2) does not guarantee that the stress tensor, Eq. (2.5), is symmetric. It is first necessary to discuss the frame indifference of the internal energy density. This point is discussed in detail in [51] where it is shown that in order to satisfy frame indifference the internal energy must instead be expressed in terms of any symmetric strain tensor. Consider some symmetric strain tensor $\mathbf{E} = [E_{ij}] = \mathbf{E}(\mathbf{F})$ then one can instead have

$$\mathscr{E} = \mathscr{E}(E_{11},\ E_{12},\ \ldots,\ E_{33},\ \mathscr{S}). \tag{2.7}$$

Formulations of a number of the common strain tensors in terms of $\mathbf{F}$ are given in [28]. In this work two strain tensors will be used. One strain tensor considered is the Finger tensor:

$$\mathbf{G} = \mathbf{F}^{-\mathrm{T}}\mathbf{F}^{-1}, \tag{2.8}$$

It is shown in [28] that in terms of $\mathbf{G} = [G_{ij}]$ the Murnaghan formula for Cauchy stresses, Eq. (2.5), becomes

$$\sigma_{ij} = -2\rho G_{ik}\frac{\partial \mathscr{E}}{\partial G_{kj}}. \tag{2.9}$$

Another strain tensor considered is the elastic Green's tensor

$$\mathbf{C} = \mathbf{F}^{\mathrm{T}}\mathbf{F} \tag{2.10}$$

and in terms of $\mathbf{C} = [C_{ij}]$, the Murnaghan formulas Eq. (2.5) become

$$\sigma_{ij} = 2\rho C_{ik}\frac{\partial \mathscr{E}}{\partial C_{kj}}. \tag{2.11}$$

In [28] it is also pointed out that the symmetry of Eq. (2.9) or Eq. (2.11), using Eq. (2.7), with $\mathbf{E}$ representing the respective strain tensor, still remains unclear, but that this can easily be established on the grounds that the internal energy density for a hyperelastic isotropic medium is not an arbitrary function of $\mathbf{E}$ but rather depends on the principle invariants $\mathcal{I}_1 := \mathrm{tr}(\mathbf{E})$, $\mathcal{I}_2 := \frac{1}{2}\left[(\mathrm{tr}(\mathbf{E}))^2 - \mathrm{tr}(\mathbf{E}^2)\right]$, $\mathcal{I}_3 := \det|\mathbf{E}|$:

$$\mathscr{E} = \mathscr{E}(\mathcal{I}_1,\ \mathcal{I}_2,\ \mathcal{I}_3,\ \mathscr{S}). \tag{2.12}$$

It is mentioned that for the Finger strain tensor

$$\mathcal{I}_3 = (\rho/\rho_0)^2 \tag{2.13}$$

and that for the Green's tensor

$$\mathcal{I}_3 = (\rho_0/\rho)^2 \tag{2.14}$$

Further specification can be made on the general form of the equation of state Eq. (2.12) for a hyperelastic isotropic material. The specific internal energy can be decomposed into potentials describing the hydrostatic and thermal energy density, $\mathscr{U}(\mathcal{I}_3, \mathscr{S})$ (since $\mathcal{I}_3 = \mathcal{I}_3(\rho, \rho_0)$), and the contribution due to shear deformations $\mathscr{W}(\mathcal{I}_1, \mathcal{I}_2, \mathcal{I}_3, \mathscr{S})$. Thus

$$\mathscr{E}(\mathcal{I}_1, \mathcal{I}_2, \mathcal{I}_3, \mathscr{S}) = \mathscr{U}(\mathcal{I}_3, \mathscr{S}) + \mathscr{W}(\mathcal{I}_1, \mathcal{I}_2, \mathcal{I}_3, \mathscr{S}). \tag{2.15}$$

Derivations of the terms in Eq. (2.15) can be found in [27, 24, 65, 49]

2.2.2 Compatibility constraints

The equations for deformation gradients satisfy three compatibility constraints [28]

$$\frac{\partial \rho F_{\alpha j}}{\partial x_\alpha} = 0, \qquad j = 1, 2, 3, \tag{2.16}$$

which hold for any time $t > 0$ if true for the initial data at $t = 0$. Note that the compatibility constraints stem from compatibility conditions which are analogous to St. Venant's conditions (see [53]). These conditions are required such that the deformations are continuous. This is elucidated by considering the problem in the Lagrangian frame; if for any element one knows the deformation gradients but wishes to determine the functions x_i then one has nine equations for the three unknowns; thus six conditions are required. The constraints Eq. (2.16) can be shown to be a consequence of six compatibility conditions for the Lagrangian deformation gradient $\mathbf{g} = [g_{ij}] = \mathbf{F}^{-1}$ (see [28, 3]):

$$\frac{\partial g_{mn}}{\partial x_i} - \frac{\partial g_{mi}}{\partial x_n} = 0, \tag{2.17}$$

which hold for any time $t > 0$ if true for the initial data at $t = 0$. In [3] it is shown that the following relation can be obtained

$$\frac{\partial \rho F_{\alpha j}}{\partial x_\alpha} = \rho F_{ij} F_{nm} \left(\frac{\partial g_{mn}}{\partial x_i} - \frac{\partial g_{mi}}{\partial x_n} \right), \tag{2.18}$$

from which it can be concluded that the three constraints Eq. (2.16) are a consequence of six compatibility constraints Eq. (2.18).

The compatibility constraints Eq. (2.16) play an integral part in the necessary characteristic analysis. It is reported in [76] that for a similar Eulerian formulation of equations for non-linear elastic materials, a characteristic analysis of the

quasi-linear system deduced directly by differentiation of the conservative equations produces characteristic speeds which are unphysical and leads to spurious eigenvector deficiency. The conservation laws used in [76] are based upon the inverse of the deformation gradient, $\mathbf{g}$, rather than the present formulation in terms of $\mathbf{F}$. Direct reduction of the conservative system Eq. (2.1) too leads to unphysical wave families. To overcome this, certain derivatives in the quasi-linear equations for $\mathbf{F}$ obtained from Eq. (2.1b) can be replaced using the constraints Eq. (2.16). An alternative approach which elucidates the necessary use of the constraints and arrives at the same result is to replace Eq. (2.1b) with the following modified form derived in [62]:

$$\frac{\partial \rho F_{ij}}{\partial t} + \frac{\partial \left(\rho F_{ij} u_\alpha - \rho F_{\alpha j} u_i\right)}{\partial x_\alpha} = -u_i \beta_j, \tag{2.19}$$

where

$$\beta_j := \frac{\partial \rho F_{\alpha j}}{\partial x_\alpha}. \tag{2.20}$$

can be considered an artificial vector variable providing the conservative form of the equations for $\mathbf{F}$. If deformations are elastic then $\beta_j = 0$ for all time if true for the initial conditions, and Eq. (2.1b) and Eq. (2.19) are equivalent. Direct reduction of Eq. (2.19) to quasi-linear form (see Appendix D) gives the following equations for $\mathbf{F}$:

$$\frac{\partial F_{ij}}{\partial t} + u_\alpha \frac{\partial F_{ij}}{\partial x_\alpha} - F_{\alpha j} \frac{\partial u_i}{\partial x_\alpha} = 0, \tag{2.21}$$

which leads to physically correct wavespeeds and a complete set of independent eigenvectors. Thus, equations for the deformation gradient can be considered in two different equivalent forms: conservative and non-conservative. The conservative form is used below for studying discontinuous solutions (shock and contact waves). As a result of the consequences discussed above the non-conservative form, Eq. (2.21), is used to obtain eigenfunctions required for the construction of rarefaction waves.

Remark: Similar modified form of the governing system, Eq. (2.19), is performed in [48] for the equations for $\mathbf{g}$. Not only is this done for the purpose of obtaining physically correct wavespeeds for the quasi-linear system, but also with the aim of improving the numerical algorithm. It is indicated that by performing a numerical discretisation of Eq. (2.1) one can expect not to be finding a solution $\mathbf{U}$ but instead some modification of it, say $\mathbf{U}^{\text{MOD}}$, as a result of truncation errors. In turn it cannot be guaranteed that $\mathbf{U}^{\text{MOD}}$ satisfies the compatibility constraints, which by definition if equal to zero in the initial conditions should remain equal to zero at all other times. Further it is pointed out that the subsequent effects of errors remain unresolved in their entirety for equations of this form. It is suggested in [48] that Eq. (2.19) should instead be solved, i.e. a single set of transport equations, leaving only the question

of whether the solution complies with the original system Eq. (2.1), Eq. (2.16). Whilst these complications do not arise in the one-dimensional system in the x_1-direction studied in this paper (since $\partial(\rho F_{1j})/\partial t = 0$), the methods are developed in the prospect of later application to multi-dimensional problems, in which case it is likely that these modifications are necessary.

2.3 Characteristic analysis: 1-dimensional

The ensuing numerical methods are derived on the basis of the augmented one-dimensional system in the x_1-direction (taking $\alpha = 1$ in Eqs. (2.1a),(2.1c),(2.19)), which can be written in matrix form as

$$\frac{\partial \mathbf{U}}{\partial t} + \frac{\partial \mathscr{F}}{\partial x_1} = -\mathbf{S}^{\mathrm{C}}. \tag{2.22}$$

with

$$\mathbf{U} := \begin{pmatrix} \rho\mathbf{u} \\ \rho\mathbf{F}^{\mathrm{T}}\mathbf{e}_1 \\ \rho\mathbf{F}^{\mathrm{T}}\mathbf{e}_2 \\ \rho\mathbf{F}^{\mathrm{T}}\mathbf{e}_3 \\ \rho E \end{pmatrix}, \ \mathscr{F} := \begin{pmatrix} u_1\rho\mathbf{u} - \sigma\mathbf{e}_1 \\ 0 \\ u_1\rho\mathbf{F}^{\mathrm{T}}\mathbf{e}_2 - u_2\rho\mathbf{F}^{\mathrm{T}}\mathbf{e}_1 \\ u_1\rho\mathbf{F}^{\mathrm{T}}\mathbf{e}_3 - u_3\rho\mathbf{F}^{\mathrm{T}}\mathbf{e}_1 \\ u_1\rho E - (\sigma u)\mathbf{e}_1 \end{pmatrix}, \ \mathbf{S}^{\mathrm{C}} := \begin{pmatrix} 0 \\ 0 \\ u_2\frac{\partial}{\partial x}(\rho\mathbf{F}^{\mathrm{T}}\mathbf{e}_1) \\ u_3\frac{\partial}{\partial x}(\rho\mathbf{F}^{\mathrm{T}}\mathbf{e}_1) \\ 0 \end{pmatrix},$$

where $\mathbf{e}_k$ are the Cartesian unit vectors and $\mathbf{M}^{\mathrm{T}}$ denotes the transpose of the vector or tensor $\mathbf{M}$. By introducing the vector of primitive variables

$$\mathbf{W} := (\mathbf{u},\ \mathbf{F}^{\mathrm{T}}\mathbf{e}_1,\ \mathbf{F}^{\mathrm{T}}\mathbf{e}_2,\ \mathbf{F}^{\mathrm{T}}\mathbf{e}_3,\ \mathscr{S})^{\mathrm{T}}, \tag{2.23}$$

Eq. (2.22) can be rewritten as a quasi-linear system (see Appendix D):

$$\frac{\partial \mathbf{W}}{\partial t} + \mathscr{A}\frac{\partial \mathbf{W}}{\partial x_1} = 0, \tag{2.24}$$

with the Jacobian

$$\mathscr{A} := \begin{pmatrix} u_1\mathbf{I} & -\mathbf{A}^{11} & -\mathbf{A}^{12} & -\mathbf{A}^{13} & -\mathbf{b}^1 \\ -\mathbf{F}^{\mathrm{T}}\mathbf{D}^{11} & u_1\mathbf{I} & 0 & 0 & 0 \\ -\mathbf{F}^{\mathrm{T}}\mathbf{D}^{12} & 0 & u_1\mathbf{I} & 0 & 0 \\ -\mathbf{F}^{\mathrm{T}}\mathbf{D}^{13} & 0 & 0 & u_1\mathbf{I} & 0 \\ 0 & 0 & 0 & 0 & u_1 \end{pmatrix}. \tag{2.25}$$

Here, $\mathbf{D}^{\alpha\beta} = [D_{ij}^{\alpha\beta}]$ represents the unit dyads $\mathbf{D}^{\alpha\beta} := \mathbf{e}_\alpha \otimes \mathbf{e}_\beta^{\mathrm{T}}$, $\mathbf{I}$ is the identity matrix, and the following coefficients are defined:

$$\mathbf{A}^{\alpha\beta} = [A_{ij}^{\alpha\beta}] := \frac{1}{\rho}\frac{\partial \sigma_{\alpha i}}{\partial F_{\beta j}}, \qquad \mathbf{b}^{\alpha} = [b_i^{\alpha}] := \frac{1}{\rho}\frac{\partial \sigma_{\alpha i}}{\partial \mathscr{S}}. \tag{2.26}$$

If λ denotes the wavespeeds then the characteristic polynomial for Eq. (2.25) ($|\mathscr{A} - \lambda\mathbf{I}| = 0$) has the following form

$$(u_1 - \lambda)^7 \det\left|\mathbf{\Omega} - (u_1 - \lambda)^2\mathbf{I}\right| = 0,$$

where $\mathbf{\Omega} = [\Omega_{ij}]$ is the *acoustic tensor*

$$\Omega_{ij} := A^{1j}_{ik} F_{1k}. \tag{2.27}$$

Due to the hyperbolicity of the system Eq. (2.22), the tensor $\mathbf{\Omega}$ is positive definite and thus by defining the diagonal matrix of positive eigenvalues

$$\mathscr{D} = \operatorname{diag}\left(\sqrt{\lambda_{\mathrm{ac}_1}},\ \sqrt{\lambda_{\mathrm{ac}_2}},\ \sqrt{\lambda_{\mathrm{ac}_3}}\right), \tag{2.28}$$

with $\lambda_{\mathrm{ac}_3} \leq \lambda_{\mathrm{ac}_2} \leq \lambda_{\mathrm{ac}_1}$, and the orthogonal matrix $\mathbf{Q}$, Eq. (2.27) can be rewritten as

$$\mathbf{\Omega} = \mathbf{Q}^{-1}\mathscr{D}^2\mathbf{Q}. \tag{2.29}$$

The diagonal matrix of eigenvalues is thus given by (assuming the canonical order $u_1 - \sqrt{\lambda_{\mathrm{ac}_1}} \leq u_1 - \sqrt{\lambda_{\mathrm{ac}_2}} \leq \ldots \leq u_1 \leq \ldots \leq u_1 + \sqrt{\lambda_{\mathrm{ac}_1}}$)

$$\mathbf{\Lambda} = \operatorname{diag}\left(u_1\mathbf{I} - \mathscr{D},\ u_1\mathbf{I},\ u_1\mathbf{I},\ u_1,\ u_1\mathbf{I} + \pi\mathscr{D}\pi\right), \tag{2.30}$$

where the permutation matrix π is defined as

$$\pi = \begin{pmatrix} 0 & 0 & 1 \\ 0 & 1 & 0 \\ 1 & 0 & 0 \end{pmatrix}, \tag{2.31}$$

with the following matrix of left eigenvectors

$$\mathbf{L} = \begin{pmatrix} \mathscr{D}\mathbf{Q} & \mathbf{Q}\mathbf{A}^{11} & \mathbf{Q}\mathbf{A}^{12} & \mathbf{Q}\mathbf{A}^{13} & \mathbf{Q}\mathbf{b}^1 \\ 0 & \frac{1}{F_{11}}(F_{12}\mathbf{D}^{11} + F_{13}\mathbf{D}^{21}) - \mathbf{D}^{12} - \mathbf{D}^{23} & \frac{1}{F_{11}}(F_{12}\mathbf{D}^{31}) - \mathbf{D}^{32} & 0 & 0 \\ 0 & 0 & \frac{1}{F_{11}}(F_{13}\mathbf{D}^{11}) - \mathbf{D}^{13} & \frac{1}{F_{11}}(F_{12}\mathbf{D}^{21} + F_{13}\mathbf{D}^{31}) - \mathbf{D}^{22} - \mathbf{D}^{33} & 0 \\ 0 & 0 & 0 & 0 & 1 \\ \pi\mathscr{D}\mathbf{Q} & -\pi\mathbf{Q}\mathbf{A}^{11} & -\pi\mathbf{Q}\mathbf{A}^{12} & -\pi\mathbf{Q}\mathbf{A}^{13} & -\pi\mathbf{Q}\mathbf{b}^1 \end{pmatrix}. \tag{2.32}$$

Using the assumption that the right eigenvectors are orthonormal to the left ($\mathbf{RL} = \mathbf{I}$) then the matrix of right eigenvectors is given as follows

$$\mathbf{R} = \left(\begin{array}{cc} \frac{1}{2}(\mathscr{D}\mathbf{Q})^{-1} & 0 \\ \frac{1}{2}\left(\mathbf{F}^{\mathrm{T}}\mathbf{e}_1\right) \otimes \left(\mathbf{e}_1^{\mathrm{T}}\mathbf{Q}^{-1}\mathscr{D}^{-2}\right) & \left(\mathbf{F}^{\mathrm{T}}\mathbf{e}_1\right) \otimes \left(\mathbf{e}_1^{\mathrm{T}}\mathbf{T}^1\right) - \mathbf{D}^{21} - \mathbf{D}^{32} \\ \frac{1}{2}\left(\mathbf{F}^{\mathrm{T}}\mathbf{e}_1\right) \otimes \left(\mathbf{e}_2^{\mathrm{T}}\mathbf{Q}^{-1}\mathscr{D}^{-2}\right) & \left(\mathbf{F}^{\mathrm{T}}\mathbf{e}_1\right) \otimes \left(\mathbf{e}_2^{\mathrm{T}}\mathbf{T}^1\right) - \mathbf{D}^{23} \\ \frac{1}{2}\left(\mathbf{F}^{\mathrm{T}}\mathbf{e}_1\right) \otimes \left(\mathbf{e}_3^{\mathrm{T}}\mathbf{Q}^{-1}\mathscr{D}^{-2}\right) & \left(\mathbf{F}^{\mathrm{T}}\mathbf{e}_1\right) \otimes \left(\mathbf{e}_3^{\mathrm{T}}\mathbf{T}^1\right) \\ 0 & 0 \end{array} \right.$$

$$\left(\begin{array}{cc} 0 & 0 \\ \left(\mathbf{F}^{\mathrm{T}}\mathbf{e}_1\right) \otimes \left(\mathbf{e}_1^{\mathrm{T}}\mathbf{T}^2\right) & -\left(\mathbf{e}_1^{\mathrm{T}}\mathbf{\Omega}^{-1}\mathbf{b}^1\right)\mathbf{F}^{\mathrm{T}}\mathbf{e}_1 \\ \left(\mathbf{F}^{\mathrm{T}}\mathbf{e}_1\right) \otimes \left(\mathbf{e}_2^{\mathrm{T}}\mathbf{T}^2\right) - \mathbf{D}^{31} & -\left(\mathbf{e}_2^{\mathrm{T}}\mathbf{\Omega}^{-1}\mathbf{b}^1\right)\mathbf{F}^{\mathrm{T}}\mathbf{e}_1 \\ \left(\mathbf{F}^{\mathrm{T}}\mathbf{e}_1\right) \otimes \left(\mathbf{e}_3^{\mathrm{T}}\mathbf{T}^2\right) - \mathbf{D}^{22} - \mathbf{D}^{33} & -\left(\mathbf{e}_3^{\mathrm{T}}\mathbf{\Omega}^{-1}\mathbf{b}^1\right)\mathbf{F}^{\mathrm{T}}\mathbf{e}_1 \\ 0 & 1 \end{array} \right. \tag{2.33}$$

$$\left. \begin{array}{c} \frac{1}{2}(\mathscr{D}\mathbf{Q})^{-1}\pi \\ -\frac{1}{2}\left(\left(\mathbf{F}^{\mathrm{T}}\mathbf{e}_1\right) \otimes \left(\mathbf{e}_1^{\mathrm{T}}\mathbf{Q}^{-1}\mathscr{D}^{-2}\right)\right)\pi \\ -\frac{1}{2}\left(\left(\mathbf{F}^{\mathrm{T}}\mathbf{e}_1\right) \otimes \left(\mathbf{e}_2^{\mathrm{T}}\mathbf{Q}^{-1}\mathscr{D}^{-2}\right)\right)\pi \\ -\frac{1}{2}\left(\left(\mathbf{F}^{\mathrm{T}}\mathbf{e}_1\right) \otimes \left(\mathbf{e}_3^{\mathrm{T}}\mathbf{Q}^{-1}\mathscr{D}^{-2}\right)\right)\pi \\ 0 \end{array} \right),$$

with

$$\mathbf{T}^1 := \mathbf{\Omega}^{-1}\left(\mathbf{A}^{11}\mathbf{D}^{21} + \mathbf{A}^{11}\mathbf{D}^{32} + \mathbf{A}^{12}\mathbf{D}^{23}\right),$$
$$\mathbf{T}^2 := \mathbf{\Omega}^{-1}\left(\mathbf{A}^{12}\mathbf{D}^{31} + \mathbf{A}^{13}\mathbf{D}^{22} + \mathbf{A}^{13}\mathbf{D}^{33}\right).$$

Using these results it can be easily shown that there are seven linear degenerate ($\mathbf{r}^i \cdot \nabla_{\mathbf{W}}\lambda_i = 0$, where $\mathbf{r}^i = [r^i_j] := R_{ji}$ denotes the i-th eigenvector and thus the i-th column vector of $\mathbf{R}$, and $\nabla_{\mathbf{W}}$ is the gradient operator with respect to $\mathbf{W}$) waves with equal velocity u_1, and six genuinly non-linear ($\mathbf{r}^i \cdot \nabla_{\mathbf{W}}\lambda_i \neq 0$) waves with velocities $u_1\mathbf{I} - \mathscr{D}$ and $u_1\mathbf{I} + \mathscr{D}$.

Remark: Here, the eigenvectors have been written in compact form. Since they play a fundamental role in solving the Riemann problem both exactly and approximately, and to improve reproducibility, the expanded matrices are presented in Appendix D.

Remark: Ideally one would like to evaluate the acoustic tensor, Eq. (2.27), analytically during computations, which requires the evaluation of a large number of thermodynamic derivatives to formulate the coefficients $\mathbf{A}^{\alpha\beta}$, Eq. (2.26). Appendix F is thus devoted to detailing this relatively straightforward but combersome task. Computation of the diagonal matrix $\mathscr{D}$ and orthogonal matrix $\mathbf{Q}$ is performed numerically using those methods in [69].

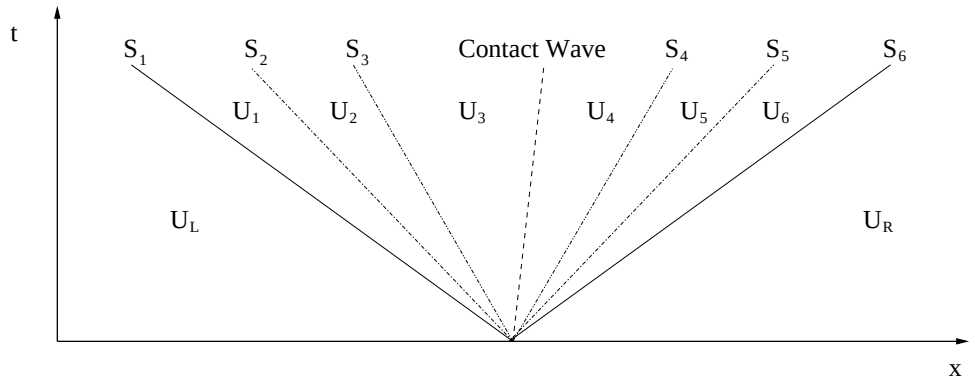

Figure 2.1: Illustration of the Riemann problem for non-linear elasticity in x-t space. The wavespeeds for the six genuinely non-linear waves are denoted by $\mathfrak{S}_j$, $1 \leq j \leq 6$. Between each wave the state is constant denoted by $\mathbf{U}^{(j)}$, $1 \leq j \leq 6$. The states $\mathbf{U}^{\text{L}}$ and $\mathbf{U}^{\text{R}}$ correspond to the initial left and right conditions respectively.

2.4 Exact Riemann problem solution

In this section an exact iterative method is derived for the solution of the Riemann problem: solutions of the system Eq. (2.22) subject to the initial conditions

$$\mathbf{U}(x, t=0) = \begin{cases} \mathbf{U}^{\text{L}} & \text{if} \quad x \leq x_0 \\ \mathbf{U}^{\text{R}} & \text{if} \quad x > x_0 \end{cases}, \tag{2.34}$$

where x_0 is the position of the discontinuity in the initial data. Depending on how the initial states in Eq. (2.34) are chosen the solution of the Riemann problem for non-linear elasticity can consist of up to eight constant states separated by seven distinct waves. These are from left to right: a longitudinal wave, two tranverse shear waves, a contact wave, two more shear waves and a further longitudinal wave (Figure 2.1).

Considering all waves to be distinct, then the solution across each is uniquely determine once one state either side and the wavespeed $\mathfrak{S}$ are known. To elaborate, given the states on the left and right in the initial data, Eq. (2.34), and also estimates of the intermediate six constant states $\mathbf{U}^{(j)}$, $1 \leq j \leq 6$, then the the type of wave present can be determined by analysing for each the inclination of characteristics:

$$\begin{cases} |\lambda^+| < |\lambda^-| & \Longrightarrow & \text{shock wave,} \\ |\lambda^+| > |\lambda^-| & \Longrightarrow & \text{rarefaction wave.} \end{cases} \tag{2.35}$$

Here λ is the respective characteristic speed, whilst $\pm$ indicates the state from which this is analysed: for any quantity ϕ, ϕ^+ denotes evaluation from the up-stream state and ϕ^- denotes evaluation from the downstream state. This notation

shall be adopted throughout. Based upon the determination of the wave types the wavespeeds, $\mathfrak{S}_j$, $1 \leq j \leq 6$, which are determined differently for either shocks or refractions, can be evaluated using the upstream and downstream data.

Following the determination of these initial properties, each iteration of the exact solution proceedure comprises firstly determining the inner most states either side of the contact wave ($\mathbf{U}^{(3)}$ and $\mathbf{U}^{(4)}$ in Figure 2.1) given the wave types and speeds and initial left and right data in Eq. (2.34). Treating the collective waves to the left and to the right of the contact independently, the solution across the three waves to the left are first evaluated, and then likewise for those to the right. The found states must satisfy by definition certain continuity conditions across the contact. Any residual error then is reflective of errors in the estimates of the wavespeeds. For each iteration the residual errors can be used to obtain improved estimates of the wavespeeds until some convergence criteria is satisfied.

It is intuitive to now consider solutions for each of the non-linear waves before summarising the implementation.

2.4.1 Contact waves

Consider a discontinuity propagating with velocity $\mathfrak{D}$. For the system Eq. (2.22) the Rankine-Hugoniot relations connecting the left and right states are given by

$$[\![\mathbf{U}]\!]\mathfrak{D} = [\![\mathscr{F}]\!], \tag{2.36}$$

where for any quantity ϕ, $[\![\phi]\!] = \phi^- - \phi^+$. An isolated contact discontinuity is defined by the condition that the normal velocity component does not change across it, thus for the one-dimensional system under consideration in the x_1-direction

$$u_1^+ = u_1^- = \mathfrak{D}. \tag{2.37}$$

From Eq. (2.22) the following equalities are obtained

$$\left[\!\!\left[\begin{array}{c} u_1 \\ u_2 \\ u_3 \end{array} \right]\!\!\right] = \left[\!\!\left[\begin{array}{c} F_{11} \\ F_{12} \\ F_{13} \end{array} \right]\!\!\right] = \left[\!\!\left[\begin{array}{c} \sigma_{11} \\ \sigma_{12} \\ \sigma_{13} \end{array} \right]\!\!\right] = 0. \tag{2.38}$$

The inner most states either side of the contact wave, $\mathbf{U}^{(3)}$ and $\mathbf{U}^{(4)}$, are uniquely determined by the initial left and right states in Eq. (2.34), and estimates of the wavespeeds $\mathfrak{S}_j$, $1 \leq j \leq 6$. In turn these inner states should satisfy those continuity conditions in Eq. (2.38). Therefore using Eq. (2.38) six non-linear equations can be

written for the six unknown wavespeeds

$$\mathscr{R}^{\mathrm{c}}(\mathfrak{S}_1, \mathfrak{S}_2, \ldots, \mathfrak{S}_6) := \begin{pmatrix} u_1^+ - u_1^- \\ u_2^+ - u_2^- \\ u_3^+ - u_3^- \\ \sigma_{11}^+ - \sigma_{11}^- \\ \sigma_{12}^+ - \sigma_{12}^- \\ \sigma_{13}^+ - \sigma_{13}^- \end{pmatrix} = 0, \tag{2.39}$$

with $\mathbf{U}^+ = \mathbf{U}^{(3)}$ and $\mathbf{U}^- = \mathbf{U}^{(4)}$.

In general Eq. (2.39) will not be satisfied by the initial guess, and instead it is expected that $|\mathscr{R}_j^{\mathrm{c}}| > 0$, $1 \leq j \leq 6$. Therefore Eq. (2.39) can be solved for improved estimates of the wavespeeds using Newton's method:

$$\mathfrak{S}^n = \mathfrak{S}^{n-1} - \left(\frac{\partial \mathscr{R}^{\mathrm{c}^{n-1}}}{\partial \mathfrak{S}^{n-1}} \right)^{-1} \mathscr{R}^{\mathrm{c}^{n-1}}. \tag{2.40}$$

The six-by-six Jacobian in Eq. (2.40) can be evaluated using perturbations of each wavespeed; a second order approximation can be written

$$\frac{\partial \mathscr{R}_i^{\mathrm{c}^{n-1}}}{\partial \mathfrak{S}_j^{n-1}} = \frac{\mathscr{R}_i^{\mathrm{c}^{n-1}}(\mathfrak{S}_j^{n-1} + \varepsilon) - \mathscr{R}_i^{\mathrm{c}^{n-1}}(\mathfrak{S}_j^{n-1} - \varepsilon)}{2\varepsilon} + O(\varepsilon^2). \tag{2.41}$$

Experience shows that choosing $\varepsilon = 1{\cdot}10^{-6}$ is sufficient to obtain converged solutions. The Jacobian was inverted using LU-decomposition.

2.4.2 Shock waves

Consider a shock wave propagating with a velocity $\mathfrak{D}$. Based upon the Rankine-Hugoniot relations Eq. (2.36) then

$$\mathscr{R}^{\mathrm{s}} := \mathscr{F}(\mathbf{U}^+) - \mathscr{F}(\mathbf{U}^-) - \mathfrak{D}\left(\mathbf{U}^+ - \mathbf{U}^-\right) = 0. \tag{2.42}$$

Recall that in the exact solution method, for each wave one solves for the upstream state $\mathbf{U}^+$ from the known downstream state $\mathbf{U}^-$ and wave speed. Thus for shock waves it is deduced that Eq. (2.42) is a set of non-linear relations for $\mathbf{U}^-$ in terms of $\mathbf{U}^+$ and the shock speed $\mathfrak{D}$. Using Newton's method then

$$\mathbf{U}^{-^n} = \mathbf{U}^{-^{n-1}} - \left(\frac{\partial \mathscr{R}^{\mathrm{s}^{n-1}}}{\partial \mathbf{U}^{-^{n-1}}} \right)^{-1} \mathscr{R}^{\mathrm{s}^{n-1}}. \tag{2.43}$$

As in § 2.4.1 the Jacobian in Eq. (2.43) can be discretised using perturbations of each variable

$$\frac{\partial \mathscr{R}_i^{s^{n-1}}}{\partial U_j^{-^{n-1}}} = \frac{\mathscr{R}_i^{s^{n-1}}(U_j^{-^{n-1}} + \varepsilon) - \mathscr{R}_i^{s^{n-1}}(U_j^{-^{n-1}} - \varepsilon)}{2\varepsilon} + O(\varepsilon^2), \tag{2.44}$$

and again taking $\varepsilon = 1 \cdot 10^{-6}$. If Eq. (2.43) is being solved from the left then $\mathfrak{D} = \mathfrak{S}_j$, $\mathbf{U}^+ = \mathbf{U}^{(j-1)}$ with $\mathbf{U}^{(0)} = \mathbf{U}^{\mathrm{L}}$, giving $\mathbf{U}^{(j)} = \mathbf{U}^-$, $1 \leq j \leq 3$. Similarly for the right $\mathfrak{D} = \mathfrak{S}_j$, $\mathbf{U}^+ = \mathbf{U}^{(j+1)}$ with $\mathbf{U}^{(7)} = \mathbf{U}^{\mathrm{R}}$, giving $\mathbf{U}^{(j)} = \mathbf{U}^-$, $4 \leq j \leq 6$.

2.4.3 Rarefaction waves

For solutions across rarefaction waves the theory presented in [43] is followed. If $\mathbf{r}^j$ denotes the j-th column vector in Eq. (2.33) then across a rarefaction wave

$$\frac{\partial \mathbf{W}}{\partial \xi} = \frac{\mathbf{r}^j(\mathbf{W})}{\mathbf{r}^j(\mathbf{W}) \cdot \nabla_{\mathbf{w}} \lambda_j(\mathbf{W})}, \tag{2.45}$$

where $\lambda_j(\mathbf{W}^-) \leq \xi \leq \lambda_j(\mathbf{W}^+)$ and $\nabla_{\mathbf{w}}$ denotes the gradient operator with respect to components of the vector of primitive variables, $\mathbf{W}$.

An important consideration when solving Eq. (2.45) is that the solution is parameterised by the characteristic evaluated from the upstream state, $\lambda(\mathbf{W}^-)$, and solving Eq. (2.45) otherwise would lead to a multi-valued function [43]. In the solution of the Riemann problem it is assumed that for each genuinely non-linear wave the corresponding downstream state is known. Solving across rarefaction waves is therefore an iterative process. It is convenient to consider the solutions across rarefaction waves on each side of the contact wave independently: for waves on the left one could pose the following non-linear equations

$$\mathscr{R}^{\mathrm{r}^{n-1}} := \mathbf{W}^{(j-1)} - \mathbf{W}^+(\mathbf{W}^{(j)}) = 0; \tag{2.46}$$

and likewise for the right

$$\mathscr{R}^{\mathrm{r}^{n-1}} := \mathbf{W}^{(j+1)} - \mathbf{W}^+(\mathbf{W}^{(j)}) = 0; \tag{2.47}$$

where in each case $\mathbf{W}^+(\mathbf{W}^{(j)})$ denotes solution of Eq. (2.45) using an estimate of the upstream state $\mathbf{W}^- = \mathbf{W}^{(j)}$. In the same way as the residual functions in § 2.4.1, Eq. (2.46) and Eq. (2.47) can be solved using Newton's method:

$$\mathbf{W}^{-^n} = \mathbf{W}^{-^{n-1}} - \left(\frac{\partial \mathscr{R}^{\mathrm{r}^{n-1}}}{\partial \mathbf{W}^{-^{n-1}}} \right)^{-1} \mathscr{R}^{\mathrm{r}^{n-1}}. \tag{2.48}$$

As an initial guess the last known solution of $\mathbf{W}^{(j)}$ can be taken.

Eq. (2.45) can be integrated using the classical fourth-order Runge–Kutta method. The step size can be taken as $\Delta\xi_j = \lambda_j(\mathbf{W}^{(j-1)}) - \mathfrak{S}_j$, $1 \leq j \leq 3$, for the left and $\Delta\xi_j = \lambda_{j+7}(\mathbf{W}^{(j+1)}) - \mathfrak{S}_j$, $4 \leq j \leq 6$, for the right. It is necessary in some cases to subdivide the integral into N parts; experience shows that taking $N = 10$ is sufficient.

An additional complexity of solving across rarefaction waves is the evaluation of the right-hand-side of Eq. (2.45). Taking as an example the wave $\lambda = u_1 - \sqrt{\lambda_{ac_k}}$, expanding the denominator in gives

$$\mathbf{r}^k \cdot \nabla_{\mathbf{w}}(u_1 - \mathscr{D}_{kk}) = \left(\mathbf{Q}^{-1}\mathscr{D}^{-1}\right)_{1k} - \sum_{j,m=1}^{3} F_{1j}\left(\mathbf{Q}^{-1}\mathscr{D}^{-2}\right)_{mk}\frac{\partial \mathscr{D}_{kk}}{\partial F_{mj}}. \tag{2.49}$$

When computing the diagonalisation of the acoustic tensor, Eq. (2.29), it is more convenient to do so numerically rather than derive lengthy expressions for the corresponding third order polynomial. This omission of closed form solutions for the acoustic wavespeeds means some other approach is required if the derivatives with respect to deformation in Eq. (2.49) are to be evaluated analytically. The method in [50] provides a convenient reformulation of the wave derivatives from which it is straightforward to find analytic solutions for each of these terms. Considering the diagonalisation of the acoustic tensor, Eq. (2.29), the following equalities are obtained

$$\nabla_{\mathbf{F}}\left(\mathbf{\Omega}\mathbf{Q}^{-1}\right) = \nabla_{\mathbf{F}}\left(\mathbf{Q}^{-1}\mathscr{D}^2\right), \tag{2.50}$$

$$\nabla_{\mathbf{F}}\left(\mathbf{\Omega}\right)\mathbf{Q}^{-1} + \mathbf{\Omega}\nabla_{\mathbf{F}}\left(\mathbf{Q}^{-1}\right) = \nabla_{\mathbf{F}}\left(\mathbf{Q}^{-1}\right)\mathscr{D}^2 + \mathbf{Q}^{-1}\nabla_{\mathbf{F}}\left(\mathscr{D}^2\right), \tag{2.51}$$

$$\mathbf{Q}\nabla_{\mathbf{F}}\left(\mathbf{\Omega}\right)\mathbf{Q}^{-1} + \mathscr{D}^2\mathbf{Q}\nabla_{\mathbf{F}}\left(\mathbf{Q}^{-1}\right) = \mathbf{Q}\nabla_{\mathbf{F}}\left(\mathbf{Q}^{-1}\right)\mathscr{D}^2 + \mathbf{I}\nabla_{\mathbf{F}}\left(\mathscr{D}^2\right), \tag{2.52}$$

where $\nabla_{\mathbf{F}}$ denotes the gradient operator with respect to deformation. Taking only the diagonal components in Eq. (2.52) gives

$$\nabla_{\mathbf{F}}\left(\mathscr{D}_{kk}^2\right) = Q_{km}\nabla_{\mathbf{F}}\left(\Omega_{mj}\right)Q_{jk}^{-1}. \tag{2.53}$$

Evaluating derivatives of the acoustic tensor, although rather lengthy, is relatively straightforward (see Appendix G).

2.4.4 Solution proceedure

Here, the implementation is summarised:

Step 1: *Initialise solution.* Given an initial estimate of the piecewise constant states $\mathbf{U}^{(j)}$, $1 \leq j \leq 6$, between each of the non-linear waves, and the initial left and right states $\mathbf{U}^{\mathrm{L}}$, $\mathbf{U}^{\mathrm{R}}$ in Eq. (2.34), one determines the wave types by assessing the inclination of characteristics Eq. (2.35). Once the wave types are known,

proceed to evaluate an initial estimate of the wave speeds $\mathfrak{S}_j$, $1 \leq j \leq 6$ using $\mathfrak{S}_j = \mathfrak{D}$ from Eq. (2.42) for a shock, and $\mathfrak{S}_j = \lambda_j$, $1 \leq j \leq 3$, or $\mathfrak{S}_j = \lambda_{j+7}$, $4 \leq j \leq 6$, from Eq. (2.30) for left and right waves respectively in the case of a rarefaction.

Step 2: *Compute residual errors.* Given an estimate of the wavespeeds $\mathfrak{S}_j$, $1 \leq j \leq 6$ and the left and right states $\mathbf{U}^{\text{L}}$, $\mathbf{U}^{\text{R}}$, and knowing the wave types, systematically find the solution $\mathbf{U}^-$ across each wave (in each case the corresponding downstream state $\mathbf{U}^+$ is known). Starting with the left hand state $\mathbf{U}^{\text{L}}$ move upstream solving across each wave for $\mathbf{U}^{(j)} = \mathbf{U}^-$, $1 \leq j \leq 3$, taking $\mathbf{U}^+ = \mathbf{U}^{(j-1)}$, with $\mathbf{U}^{(0)} = \mathbf{U}^{\text{L}}$. Continue this procedure until a solution is found for the state immediately left of the contact wave $\mathbf{U}^{(3)}$. Likewise evaluate upstream starting from the right initial state $\mathbf{U}^{\text{R}}$, where for each wave take $\mathbf{U}^+ = \mathbf{U}^{(j+1)}$, $1 \leq j \leq 3$, with $\mathbf{U}^{(7)} = \mathbf{U}^{\text{R}}$, until a solution is found for the state immediately to the right of the contact wave $\mathbf{U}^{(4)}$. Thus evaluate the truncation errors, Eq. (2.39), in continuity across the contact wave.

Step 3: *Estimate new wavespeeds.* If from *Step 2* $\sum_{i=1}^{6} |\mathscr{R}_i^{\text{c}}| > \varepsilon$, where ε is the desired tolerance, then use Eq. (2.40) to improve the estimates of the wavespeeds. Evaluate the Jacobian in Eq. (2.40) using small perturbations of each wavespeed and re-evaluating in each case *Step 2*. With the new wavespeeds, again re-evaluate *Step 2* until $\sum_{i=1}^{6} |\mathscr{R}_i^{\text{c}}| < \varepsilon$ is satisfied.

Experience shows that with a good initial guess the solution will converge in three to four iterations to a tolerance of $\sum_{i=1}^{6} |\mathscr{R}_i^{\text{c}}| < 10^{-8}$.

2.4.5 Provision of the initial guess

The final detail of the exact solution method is the specification of initial estimates of the states $\mathbf{U}^{(j)}$, $1 \leq j \leq 6$. One choice would be to use the linearised solver proposed in the next section. In most cases a linearised solution is sufficient, but in some special cases will fail (see [72]). In such circumstances one could instead interpolate a solution from the results of any scheme such as Lax-Friedrich, which approximates directly the governing model rather than solves exactly an approximation of it, run on a sufficiently fine grid. Such a method has no knowledge of the characteristic structure and although diffusive (hence the need for fine meshes, especially where amplitudes of waves or the difference in speeds of adjacent waves is small) one can be assured that the solution is a faithful representation of the exact solution. The method of solving the Riemann problem exactly hinges on this ability to obtain a

good initial guess of the states either side of each of the waves in order to determine the wavetypes.

2.4.6 Limitations of the exact solver

The proposed method of obtaining exact solutions to Riemann problems in non-linear elasticity is limited to those cases where all waves are distinct as a result of the following assumptions that are made: all waves are genuinly non-linear except for the central contact wave which is linearly degenerate; the wave type is determinable by analysing the inclination of characteristics. In [50] conditions are discussed where these assumptions would cause the method to fail to reach an exact solution. For example it is reported that for the case where transverse wavespeeds coincide, which for an isotropic hyperelastic material occurs when the internal energy density resides on the reference hydrostat, there is a lack of genuine non-linearity. Modifications are proposed in [50] that overcome these difficulties and restore the generality of the scheme. These modifications have not been implemented in the present study, hence the limitation to cases where all waves are distinct. The sought solutions cannot therefore be considered general, but do provide adequate tests for examining certain capabilites of the proposed numerical algorithms discussed next.

2.5 Numerical scheme

The system Eq. (2.22) is solved numerically using a computational mesh where cell centred quantities are denoted by the indices i and cell boundaries by $i \pm 1/2$; thus each cell is denoted $I_i := [x_{i-1/2}, x_{i+1/2}]$ and has the size $(\Delta x)_i = x_{i+1/2} - x_{i-1/2}$. Cell averaged data are stored at cell centres. Discretisation of the time derivatives is achieved by re-expressing Eq. (2.22) as

$$\frac{\mathrm{d}}{\mathrm{d}t}\mathbf{U}(x_i, t) = \mathscr{L}(\mathbf{U}_i^n), \tag{2.54}$$

with

$$\mathscr{L}(\mathbf{U}_i^n) = -\frac{\mathscr{F}\left(\mathbf{U}(x_{i+1/2}, t^n)\right) - \mathscr{F}\left(\mathbf{U}(x_{i-1/2}, t^n)\right)}{\Delta x}, \tag{2.55}$$

where $\mathbf{U}_i^n$ is the space average of the solution in the i-th cell at time t^n:

$$\mathbf{U}_i^n = \frac{1}{\Delta x}\int_{x_{i-1/2}}^{x_{i+1/2}} \mathbf{U}(x, t^n)\mathrm{d}x. \tag{2.56}$$

Eq. (2.54) is integrated using the third-order TVD Runge–Kutta scheme [67]

$$\begin{aligned}
\mathbf{U}_i^{(1)} &= \mathbf{U}_i^n + \Delta t \left[\mathscr{L}(\mathbf{U}_i^n)\right], \\
\mathbf{U}_i^{(2)} &= \mathbf{U}_i^n + \frac{\Delta t}{4}\left[\mathscr{L}(\mathbf{U}_i^n) + \mathscr{L}(\mathbf{U}_i^{(1)})\right], \\
\mathbf{U}_i^{n+1} &= \mathbf{U}_i^n + \frac{\Delta t}{6}\left[\mathscr{L}(\mathbf{U}_i^n) + \mathscr{L}(\mathbf{U}_i^{(1)}) + 4\mathscr{L}(\mathbf{U}_i^{(2)})\right].
\end{aligned} \tag{2.57}$$

The global timestep is evaluated at the start of each time iteration and computed according to

$$\Delta t = \mathscr{C} \times \min_i \left(\frac{\Delta x}{|u_1| + \sqrt{\lambda_{\mathrm{ac1}}}} \right), \tag{2.58}$$

where $0 < \mathscr{C} \leq 1$ is an adjustable scaler parameter used to control the timestep so as to satisfy the Courant-Friedrichs-Lewy condition (thus commonly referred to as the CFL number).

In the numerical method the convective flux functions in Eq. (2.55) are discretised using the well known method of Godunov. Therefore solution of a Riemann problem is required at the boundaries of each cell in the computational mesh. Exact solutions to these problems following the procedure outlined in the preceeding section, are somewhat complex and expensive. In general one can instead apply an approximate solution method, such as those described in [74]. Titarev *et al.* [72] examined the performance of a number of different approximate Riemann solvers for the equations of non-linear elasticity. They found that a linearised solver based upon characteristic tracing yielded a good balance between accuracy and cost. It also has the advantage of recognising all waves in the solution and is shown to exceed the ability of some alternative upwind methods in resolving delicate features such as contact discontinuities. Although approximate Riemann solvers based upon linearising the governing equations have well known drawbacks, such as the production of entropy violating shock waves where there are sonic rarefactions, it is pointed out in [72] that these conditions are rare in solid media. For all intended purposes a characteristics based method can be expected to perform well.

2.5.1 Flux approximation

Consider the non-linear system Eq. (2.24). If it is assumed that the Jacobian $\mathscr{A}$ is evaluated at some constant state $\widehat{\mathbf{W}}$ such that $\widehat{\mathscr{A}} := \mathscr{A}(\widehat{\mathbf{W}})$ consists entirely of constant coefficients, then in turn the corresponding eigenvalues and eigenvectors are constant, $\widehat{\mathbf{\Lambda}} := \mathbf{\Lambda}(\widehat{\mathbf{W}})$, $\widehat{\mathbf{L}} := \mathbf{L}(\widehat{\mathbf{W}})$, $\widehat{\mathbf{R}} := \mathbf{R}(\widehat{\mathbf{W}})$. If

$$\mathscr{Q} := \widehat{\mathbf{L}}\mathbf{W}, \tag{2.59}$$

is defined as the vector of characteristic variables, then Eq. (2.24) can be rewritten in the decoupled characteristic form

$$\left(\frac{\partial}{\partial t}+\widehat{\lambda}_j\frac{\partial}{\partial x}\right)\mathscr{Q}_j=0, \qquad 1\leq j\leq 13. \tag{2.60}$$

Since, from Eq. (2.60), $\mathscr{Q}_j$ is invariant along the characteristic of slope $\widehat{\lambda}_j$, the solution for any Cauchy problem is simply

$$\mathscr{Q}_j(x,t)=\mathscr{Q}_j\left(x-\widehat{\lambda}_j t\right), \tag{2.61}$$

which gives the following solution to the Riemann problem

$$\mathbf{W}(x,t)=\widehat{\mathbf{R}}\mathscr{Q}(x,t). \tag{2.62}$$

Explicit expressions can thus be written for each of the primitive variables, but are here omitted and instead left to the Appendix D.

In order to maintain high order accuracy it is necessary to reexpress the invariants in terms of conserved variables. The extension is based upon the ideas in [16] for the compressible Euler equations. The resultant Riemann solver has also been successfully applied to incompressible fluid dynamics [13]. The derivation here follows the tensorial approach presented in [66]. From Eq. (2.60) the invariants $\partial\mathscr{Q}=\widehat{\mathbf{L}}\cdot\partial\mathbf{W}$ can be transformed simply as $\partial\mathscr{Q}=\widehat{\mathbf{L}}\widehat{\mathbf{C}}\cdot\partial\mathbf{U}$, where $\widehat{\mathbf{C}}:=(\partial\widehat{\mathbf{W}}/\partial\widehat{\mathbf{U}})$. Partial derivatives of the velocity vector and deformation tensor can be expressed in terms of partial derivatives of conserved variables according to

$$\partial\mathbf{u}=\frac{1}{\rho}(\partial(\rho\mathbf{u})-\mathbf{u}\partial\rho), \tag{2.63}$$

$$\partial\mathbf{F}=\frac{1}{\rho}(\partial(\rho\mathbf{F})-\mathbf{F}\partial\rho). \tag{2.64}$$

For entropy, recall the general form of the internal energy density as a function of the state parameters, Eq. (2.2), thus $\mathscr{S}=\mathscr{S}(\mathscr{E},\ F_{11},\ F_{12},\ \ldots,\ F_{33})$, which leads to the following identity

$$\partial\mathscr{S}=\frac{\mathrm{d}\mathscr{S}}{\mathrm{d}\mathscr{E}}\partial\mathscr{E}+\sum_{i,j=1}^{3}\frac{\mathrm{d}\mathscr{S}}{\mathrm{d}F_{ij}}\partial F_{ij}. \tag{2.65}$$

Using the definition of total energy $E=(\mathscr{E}+|\mathbf{u}|^2/2)$, the following partial derivatives can be written

$$\partial(\rho\mathscr{E})=\partial(\rho E)-u_i\partial(\rho\mathbf{u})_i+\frac{1}{2}|\mathbf{u}|^2\partial\rho, \tag{2.66}$$

thus

$$\partial\mathscr{E} = \frac{1}{\rho}\left[\partial(\rho E) - u_i\partial(\rho\mathbf{u})_i + \frac{1}{2}|\mathbf{u}|^2\partial\rho - \mathscr{E}\partial\rho\right]. \tag{2.67}$$

Substituting Eq. (2.64) and Eq. (2.67) into Eq. (2.65) gives

$$\begin{aligned}\partial\mathscr{S} = \ \frac{1}{\rho}\Bigg[\frac{\mathrm{d}\mathscr{S}}{\mathrm{d}\mathscr{E}}\left(\partial(\rho E) - u_i\partial(\rho\mathbf{u})_i + \frac{1}{2}|\mathbf{u}|^2\partial\rho - \mathscr{E}\partial\rho\right) + \\ \sum_{i,j=1}^{3}\frac{\mathrm{d}\mathscr{S}}{\mathrm{d}F_{ij}}\left(\partial(\rho F)_{ij} - F_{ij}\partial\rho\right)\Bigg].\end{aligned} \tag{2.68}$$

Since density is a function of $\det|\rho\mathbf{F}|$ via the following relationship

$$\rho^2 = \det|\rho\mathbf{F}|/\rho_0, \tag{2.69}$$

then partial derivatives of density can be found in terms of $(\rho\mathbf{F})$:

$$\partial\rho = \frac{1}{2}\sum_{i,j=1}^{3} F_{ij}^{-\mathrm{T}}\partial(\rho\mathbf{F})_{ij}. \tag{2.70}$$

Partial derivatives with respect to density then in Eq. (2.63), Eq. (2.64) and Eq. (2.68) can be replaced with the expression in Eq. (2.70).

In matrix form the transformation can be found using

$$\mathbf{C} = -\frac{1}{2\rho}\begin{pmatrix} -2\mathbf{I} & \mathbf{u}\otimes(\mathbf{e}_1^{\mathrm{T}}\mathbf{F}^{-\mathrm{T}}) & \mathbf{u}\otimes(\mathbf{e}_2^{\mathrm{T}}\mathbf{F}^{-\mathrm{T}}) & \mathbf{u}\otimes(\mathbf{e}_3^{\mathrm{T}}\mathbf{F}^{-\mathrm{T}}) & 0 \\ 0 & (\mathbf{F}^{\mathrm{T}}\mathbf{e}_1)\otimes(\mathbf{e}_1^{\mathrm{T}}\mathbf{F}^{-\mathrm{T}}) - 2\mathbf{I} & (\mathbf{F}^{\mathrm{T}}\mathbf{e}_1)\otimes(\mathbf{e}_2^{\mathrm{T}}\mathbf{F}^{-\mathrm{T}}) & (\mathbf{F}^{\mathrm{T}}\mathbf{e}_1)\otimes(\mathbf{e}_3^{\mathrm{T}}\mathbf{F}^{-\mathrm{T}}) & 0 \\ 0 & (\mathbf{F}^{\mathrm{T}}\mathbf{e}_2)\otimes(\mathbf{e}_1^{\mathrm{T}}\mathbf{F}^{-\mathrm{T}}) & (\mathbf{F}^{\mathrm{T}}\mathbf{e}_2)\otimes(\mathbf{e}_2^{\mathrm{T}}\mathbf{F}^{-\mathrm{T}}) - 2\mathbf{I} & (\mathbf{F}^{\mathrm{T}}\mathbf{e}_2)\otimes(\mathbf{e}_3^{\mathrm{T}}\mathbf{F}^{-\mathrm{T}}) & 0 \\ 0 & (\mathbf{F}^{\mathrm{T}}\mathbf{e}_3)\otimes(\mathbf{e}_1^{\mathrm{T}}\mathbf{F}^{-\mathrm{T}}) & (\mathbf{F}^{\mathrm{T}}\mathbf{e}_3)\otimes(\mathbf{e}_2^{\mathrm{T}}\mathbf{F}^{-\mathrm{T}}) & (\mathbf{F}^{\mathrm{T}}\mathbf{e}_3)\otimes(\mathbf{e}_3^{\mathrm{T}}\mathbf{F}^{-\mathrm{T}}) - 2\mathbf{I} & 0 \\ 2\dfrac{\mathrm{d}\mathscr{S}}{\mathrm{d}\mathscr{E}}\mathbf{u}^{\mathrm{T}} & -2\dfrac{\mathrm{d}\mathscr{S}}{\mathrm{d}\mathbf{e}_1^{\mathrm{T}}\mathbf{F}} - \mathbf{e}_1^{\mathrm{T}}\mathbf{F}^{-\mathrm{T}}T_3 & -2\dfrac{\mathrm{d}\mathscr{S}}{\mathrm{d}\mathbf{e}_2^{\mathrm{T}}\mathbf{F}} - \mathbf{e}_2^{\mathrm{T}}\mathbf{F}^{-\mathrm{T}}T_3 & -2\dfrac{\mathrm{d}\mathscr{S}}{\mathrm{d}\mathbf{e}_3^{\mathrm{T}}\mathbf{F}} - \mathbf{e}_3^{\mathrm{T}}\mathbf{F}^{-\mathrm{T}}T_3 & -2\dfrac{\mathrm{d}\mathscr{S}}{\mathrm{d}\mathscr{E}} \end{pmatrix}, \tag{2.71}$$

with

$$T_3 := \frac{\mathrm{d}S}{\mathrm{d}\mathscr{E}}\left(\frac{1}{2}|\mathbf{u}|^2 - \mathscr{E}\right) - \sum_{i,j=1}^{3}\frac{\mathrm{d}S}{\mathrm{d}F_{ij}}F_{ij}.$$

The inverse of Eq. (2.71), $\mathbf{C}^{-1} := \partial\mathbf{U}/\partial\mathbf{W}$, is given by

$$\mathbf{C}^{-1} = -\rho \begin{pmatrix} -\mathbf{I} & \mathbf{u}\otimes(\mathbf{e}_1^{\mathrm{T}}\mathbf{F}^{-\mathrm{T}}) & \mathbf{u}\otimes(\mathbf{e}_2^{\mathrm{T}}\mathbf{F}^{-\mathrm{T}}) & \mathbf{u}\otimes(\mathbf{e}_3^{\mathrm{T}}\mathbf{F}^{-\mathrm{T}}) & 0 \\ 0 & (\mathbf{F}^{\mathrm{T}}\mathbf{e}_1)\otimes(\mathbf{e}_1^{\mathrm{T}}\mathbf{F}^{-\mathrm{T}}) - \mathbf{I} & (\mathbf{F}^{\mathrm{T}}\mathbf{e}_1)\otimes(\mathbf{e}_2^{\mathrm{T}}\mathbf{F}^{-\mathrm{T}}) & (\mathbf{F}^{\mathrm{T}}\mathbf{e}_1)\otimes(\mathbf{e}_3^{\mathrm{T}}\mathbf{F}^{-\mathrm{T}}) & 0 \\ 0 & (\mathbf{F}^{\mathrm{T}}\mathbf{e}_2)\otimes(\mathbf{e}_1^{\mathrm{T}}\mathbf{F}^{-\mathrm{T}}) & (\mathbf{F}^{\mathrm{T}}\mathbf{e}_2)\otimes(\mathbf{e}_2^{\mathrm{T}}\mathbf{F}^{-\mathrm{T}}) - \mathbf{I} & (\mathbf{F}^{\mathrm{T}}\mathbf{e}_2)\otimes(\mathbf{e}_3^{\mathrm{T}}\mathbf{F}^{-\mathrm{T}}) & 0 \\ 0 & (\mathbf{F}^{\mathrm{T}}\mathbf{e}_3)\otimes(\mathbf{e}_1^{\mathrm{T}}\mathbf{F}^{-\mathrm{T}}) & (\mathbf{F}^{\mathrm{T}}\mathbf{e}_3)\otimes(\mathbf{e}_2^{\mathrm{T}}\mathbf{F}^{-\mathrm{T}}) & (\mathbf{F}^{\mathrm{T}}\mathbf{e}_3)\otimes(\mathbf{e}_3^{\mathrm{T}}\mathbf{F}^{-\mathrm{T}}) - \mathbf{I} & 0 \\ -\mathbf{u}^{\mathrm{T}} & \dfrac{\mathrm{d}\mathscr{E}}{\mathrm{d}\mathbf{e}_1^{\mathrm{T}}\mathbf{F}} - \mathbf{e}_1^{\mathrm{T}}\mathbf{F}^{-\mathrm{T}}(\dfrac{1}{2}|\mathbf{u}|^2 + \mathscr{E}) & \dfrac{\mathrm{d}\mathscr{E}}{\mathrm{d}\mathbf{e}_2^{\mathrm{T}}\mathbf{F}} - \mathbf{e}_2^{\mathrm{T}}\mathbf{F}^{-\mathrm{T}}(\dfrac{1}{2}|\mathbf{u}|^2 + \mathscr{E}) & \dfrac{\mathrm{d}\mathscr{E}}{\mathrm{d}\mathbf{e}_3^{\mathrm{T}}\mathbf{F}} - \mathbf{e}_3^{\mathrm{T}}\mathbf{F}^{-\mathrm{T}}(\dfrac{1}{2}|\mathbf{u}|^2 + \mathscr{E}) & -\dfrac{\mathrm{d}\mathscr{E}}{\mathrm{d}\mathscr{S}} \end{pmatrix}. \tag{2.72}$$

Thus the solution in terms of conserved variables becomes

$$\mathbf{U}(x,t) = \widehat{\mathbf{C}}^{-1}\widehat{\mathbf{R}}\mathscr{Q}^{\mathrm{c}}(x - \widehat{\lambda}t). \tag{2.73}$$

where $\mathscr{Q}^{\mathrm{c}} := \widehat{\mathbf{L}}\widehat{\mathbf{C}}\cdot\mathbf{U}$. As with the solution in terms of primitive variables, Eq. (2.62), explicit expressions can thus be written for each of the conserved variables, but are again omitted and instead left to Appendix D.

On a computational mesh these linearised problems are solved at each intercell boundary, $i \pm 1/2$. Locally then one is solving exactly an approximation of the non-linear system Eq. (2.22). There is no set way in which the constant state $\widehat{\mathbf{W}}_{i\pm1/2}$ should be chosen to evaluate the coefficients. Here, an arithmetic mean of the adjoining left and right cell centre states is used

$$\widehat{\mathbf{W}}_{i\pm1/2} = \frac{1}{2}\left(\mathbf{W}_i + \mathbf{W}_{i\pm1}\right). \tag{2.74}$$

A convenient function that achieves the solution Eq. (2.61) is [16]

$$\mathscr{Q}(x_{i+1/2} - \widehat{\lambda}_{j;i+1/2}t) = \left(\frac{1}{2} + \psi_{j;i+1/2}\right)\mathscr{Q}^{\mathrm{L}}_{i+1/2} + \left(\frac{1}{2} - \psi_{j;i+1/2}\right)\mathscr{Q}^{\mathrm{R}}_{i+1/2}, \tag{2.75}$$

with

$$\psi_{j;i+1/2} := \frac{1}{2}\frac{\widehat{\lambda}_{j;i+1/2}}{|\widehat{\lambda}_{j;i+1/2}| + \varepsilon}, \qquad \widehat{\lambda}_{j;i+1/2} := \lambda_j(\widehat{\mathbf{W}}_{i+1/2})$$

where $\mathscr{Q}^{\mathrm{L}}_{i+1/2}$ and $\mathscr{Q}^{\mathrm{R}}_{i+1/2}$ represent the left and right characteristic states adjacent to the boundary found by some high-order reconstruction method, and ε is a small number to prevent division by zero. Alternatively by choosing $\mathscr{Q}^{\mathrm{L}}_{i+1/2} = \mathscr{Q}(\mathbf{U}_i)$ and $\mathscr{Q}^{\mathrm{R}}_{i+1/2} = \mathscr{Q}(\mathbf{U}_{i+1})$ a first order upwind method is recovered.

The found solution Eq. (2.73) can then be used to construct the flux term in Eq. (2.55).

2.5.2 High-order spatial reconstruction

The outlined characteristic-based flux is used directly to construct high-order finite-volume schemes, in which the boundary-extrapolated values are obtained from cell averages by means of a high order polynomial reconstruction. In the examples that follow, weighted essentially non-oscillatory (WENO) schemes of third-, fifth- and ninth-order accuracy are used. Detailed descriptions of the WENO reconstruction method can be found in [33, 2] and the references therein. Below, a brief description is provided of the most practical fifth-order reconstruction procedure.

For a scalar function $\phi(x)$ the fifth order accurate left boundary extrapolated value $\phi^L_{i-1/2}$ is defined in terms of cell averaged values ϕ_i as

$$\begin{aligned}\phi^{\rm L}_{i-1/2} &= \frac{1}{6}\left[\omega_1(-\phi_{i+1}+5\phi_i+2\phi_{i-1})+\omega_2(-\phi_{i-2}+5\phi_{i-1}+2\phi_i)+\right.\\ &\left.\omega_3(2\phi_{i-3}-7\phi_{i-2}+11\phi_{i-1})\right],\end{aligned} \tag{2.76}$$

where ω_k, $k=1,2,3$, are nonlinear WENO weights given by

$$\omega_k := \frac{\alpha_k}{\sum_{l=1}^{3}\alpha_l}, \tag{2.77}$$

where

$$\alpha_1 := \frac{3}{10(\beta_1+\varepsilon)^2}, \qquad \alpha_2 := \frac{3}{5(\beta_2+\varepsilon)^2}, \qquad \alpha_3 := \frac{1}{10(\beta_3+\varepsilon)^2}. \tag{2.78}$$

The parameter ε is introduced to avoid division by zero and the recommended value of $\varepsilon = 10^{-6}$ is taken. The smoothness indicators are

$$\beta_1 = (13/12)(\phi_{i-1}-2\phi_i+\phi_{i+1})^2+(1/4)(3\phi_{i-1}-4\phi_i+\phi_{i+1})^2, \tag{2.79}$$

$$\beta_2 = (13/12)(\phi_{i-2}-2\phi_{i-1}+\phi_i)^2+(1/4)(\phi_{i-2}-\phi_i)^2, \tag{2.80}$$

$$\beta_3 = (13/12)(\phi_{i-3}-2\phi_{i-2}+\phi_{i-1})^2+(1/4)(\phi_{i-3}-4\phi_{i-2}+3\phi_{i-1})^2. \tag{2.81}$$

The right value $\phi^{\rm R}_{i+1/2}$ is obtained by symmetry.

It was found that component-wise reconstruction leads to severe oscillations for those testcases considered here and, more often than not failure to compute a solution. It is not surprising given the larger number of waves and complexity of the governing model that these artifacts are much worse than those observed for the Euler equations (see [59] for tests of the latter). Thus, in practical calculations the outlined scalar reconstruction procedure is carried out in characteristic variables rather than conservative variables and Eq. (2.76) is applied to each characteristic field. It was also found that for the nonlinear elasticity equations the WENO reconstructions of fifth- and higher-orders may still produce oscillatory results around

particularly steep gradients. To avoid spurious oscillations, the monotonicity preserving modification of [2] can be used, which is effectively a further limiting step applied to the WENO extrapolated values.

In what follows the j-th order WENO scheme will be referred to as WENO-j and likewise for the monotonicity preserving WENO scheme MPWENO-j.

2.6 Examples

Testcases are now provided to compare the numerical schemes against exact solutions. Before proceeding, the closure relation Eq. (2.15) must be specified. For all testcases the isotropic hyperelastic equation of state from [72] is used, where the hydrostatic internal energy is described by

$$\mathscr{U}(\mathcal{I}_3, \mathscr{S}) = \frac{K_0}{2\alpha^2}\left(\mathcal{I}_3^{\alpha/2} - 1\right)^2 + c_{\mathrm{v}} T_0 \mathcal{I}_3^{\gamma/2}\left[(\exp\left(\frac{\mathscr{S}}{c_{\mathrm{v}}}\right) - 1\right], \tag{2.82}$$

and the contribution due to small anisotropic shear is given by

$$\mathscr{W}(\mathcal{I}_1, \mathcal{I}_2, \mathcal{I}_3) = \frac{B_0}{2}\mathcal{I}_3^{\beta/2}\left(\mathcal{I}_1^2/3 - \mathcal{I}_2\right). \tag{2.83}$$

Here, the invariants correspond to those of the elastic Finger tensor $\mathbf{G}$, Eq. (2.8). The parameters $K_0 := c_0^2 - (4/3)b_0^2$, $B_0 := b_0^2$ are the squared bulk speed of sound and the squared speed of the shear wave, respectively; c_{v} is heat capacity at constant volume; T_0 is the reference temperature; α, β, γ are constants characterising nonlinear dependence of sound speeds and temperature on the mass density. Material constants for copper are given in Table 2.1.

Table 2.1: Equation of state parameters for copper

Parameter	Value	Units
ρ_0	8.9	$\mathrm{g\,cm^{-3}}$
c_0	4.6	$\mathrm{km\,s^{-1}}$
c_{v}	$3.9 \cdot 10^{-4}$	$\mathrm{kJ\,g^{-1}\,K^{-1}}$
T_0	300	K
b_0	2.1	$\mathrm{km\,s^{-1}}$
α	1.0	–
β	3.0	–
γ	2.0	–

In the examples below, initial value problems (IVPs) are solved in a computational domain $[0:1]$ cm. The position of the discontinuity in the initial data [cf. Eq. (2.34)] is $x_0 = 0.5$ cm. Where reference is made to first-order solutions, forward Euler time integration is used along with first-order reconstruction. Exact solutions in each case were found using the method in § 2.4 and are provided in Appendix H.

2.6.1 IVP 1

The first example considered is similar to the five wave testcase in [72]. In the present case an additional degree of shear deformation is added so as to study the full seven wave structure. The initial conditions are:

$$\begin{aligned}
\mathbf{U}^{\mathrm{L}}\left\{\begin{array}{l}\mathbf{u} = \begin{pmatrix} 0 \\ 0.5 \\ 1 \end{pmatrix}\ \mathrm{km\,s^{-1}},\ \mathbf{F} = \begin{pmatrix} 0.98 & 0 & 0 \\ 0.02 & 1 & 0.1 \\ 0 & 0 & 1 \end{pmatrix},\ \mathscr{S} = 1\cdot 10^{-3}\,\mathrm{kJ\,g^{-1}\,K^{-1}}\,,\end{array}\right. \\
\mathbf{U}^{\mathrm{R}}\left\{\begin{array}{l}\mathbf{u} = \begin{pmatrix} 0 \\ 0 \\ 0 \end{pmatrix}\ \mathrm{km\,s^{-1}},\quad \mathbf{F} = \begin{pmatrix} 1 & 0 & 0 \\ 0 & 1 & 0.1 \\ 0 & 0 & 1 \end{pmatrix},\quad \mathscr{S} = 0\,\mathrm{kJ\,g^{-1}\,K^{-1}}\,.\end{array}\right.
\end{aligned} \tag{2.84}$$

The solution comprises three left travelling rarefaction waves, a right travelling contact, and two right travelling rarefactions led by a right travelling shock wave.

Figure 2.2 shows various state profiles obtained using the MPWENO-5 scheme with $\mathscr{C}$=0.6 and 500 grid points and at time $t = 0.6$ μs. The results are quite satisfactory with no significant over- or under-shoots. The MPWENO-5 scheme was chosen because for this testcase it provided the best tradeoff between cost and resolution. Figure 2.3 shows density profiles using the first order scheme, WENO-3, MPWENO-5 and MPWENO-9 schemes. As expected WENO-3 and MPWENO-5 offer significant improvements on the first order method. Indeed the small amplitude second transverse waves on both sides of the contact are indistinguishable using first-order. While the MPWENO-9 scheme improves further the resolution of shock and contact waves, undershoots at the foot of rarefaction waves become amplified. Relative CPU-times are given in Table 2.2.

2.6.2 IVP 2

The second example is based upon that in [50]. In the original case the initial disturbance causes almost unnoticeable jumps in some parameters across certain transverse waves. It was found that these jumps can be amplified by using one

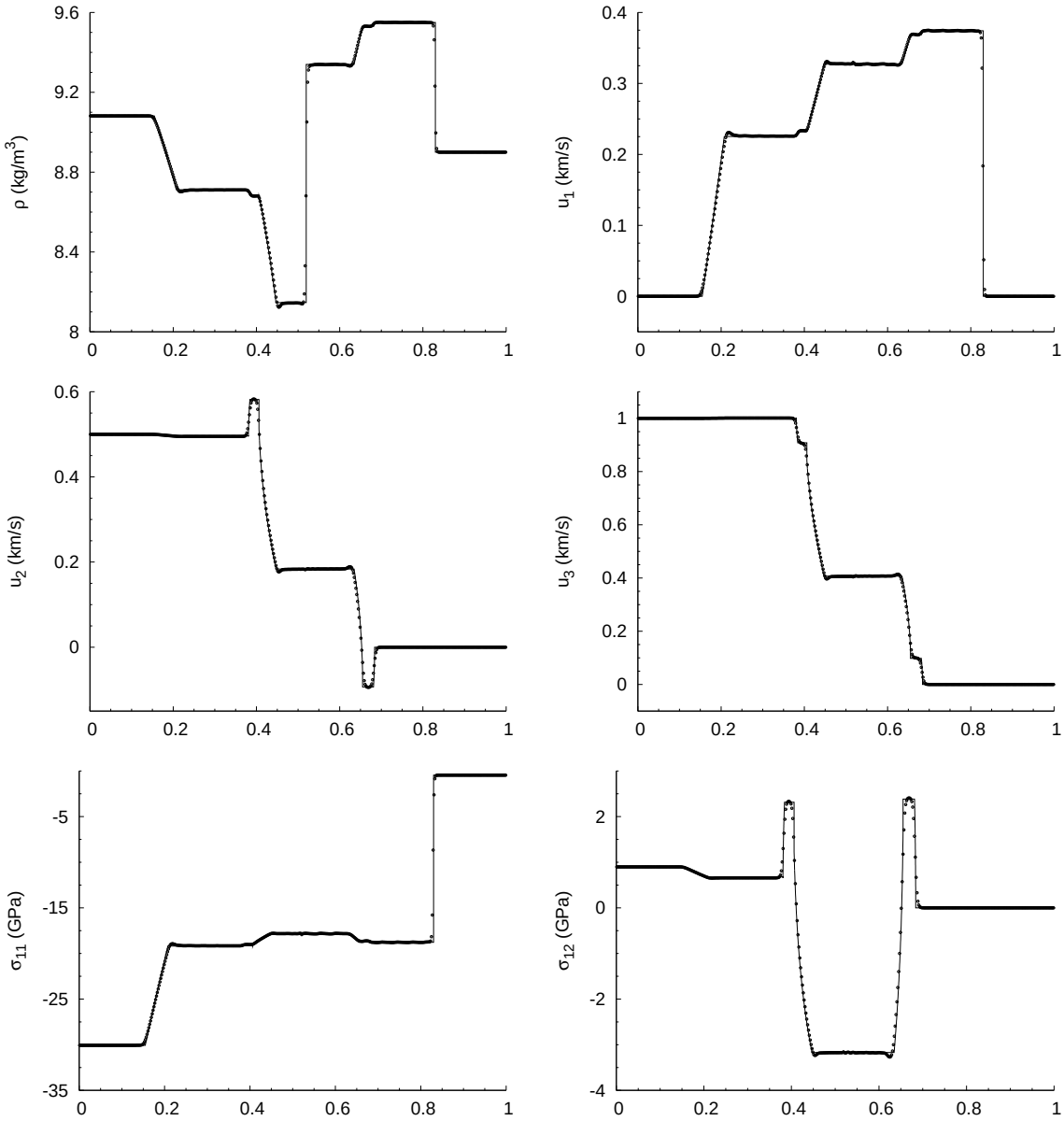

Figure 2.2: Comparison of exact (solid line) and numerical (points) solutions of IVP 1 at a time $t = 0.6\,\mu s$. Numerical solutions were obtained with a grid spacing $\Delta x = 1/500$, $\mathscr{C}$=0.6, and using the MPWENO 5th.

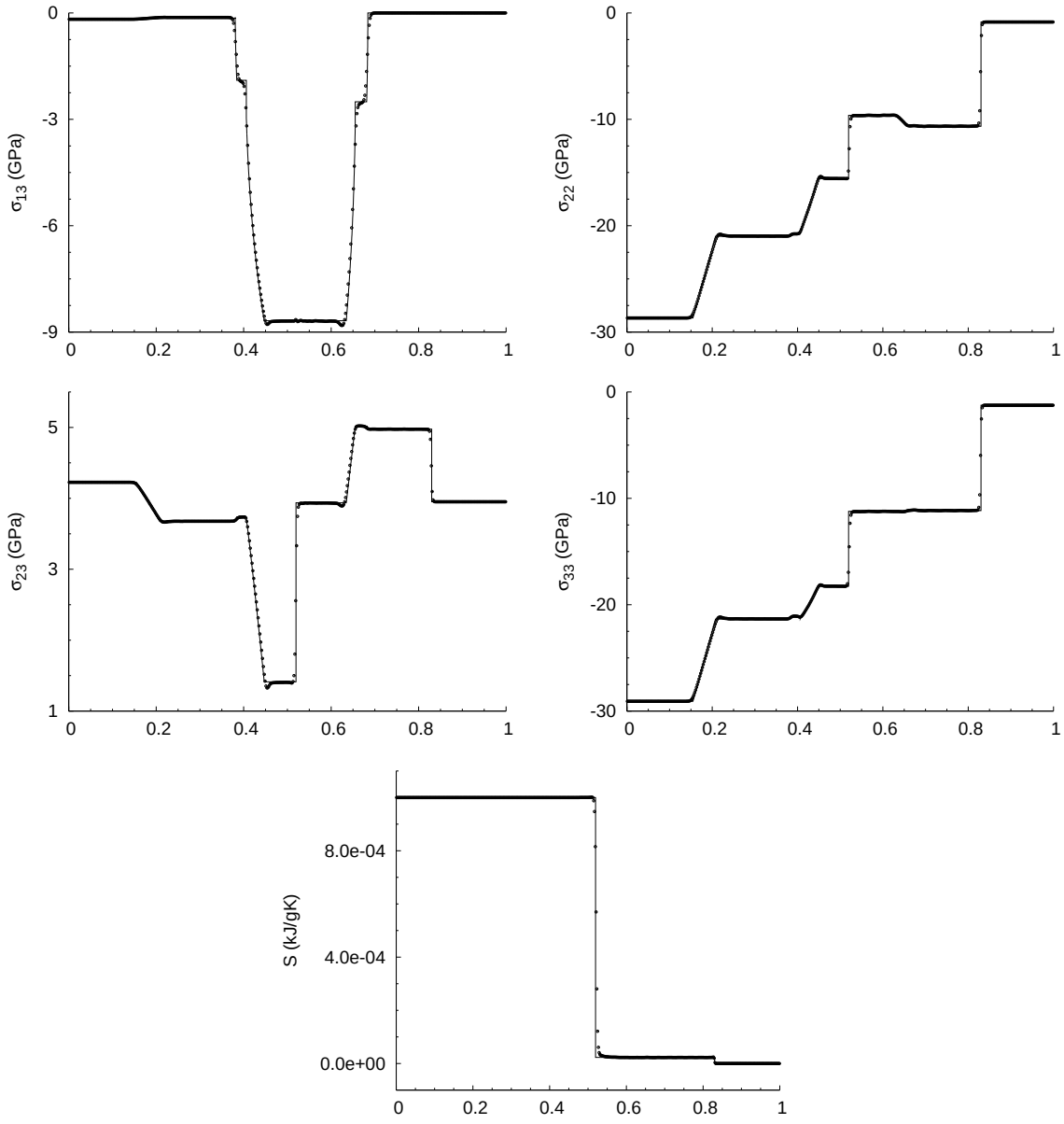

Figure 2.2: *(continued)*

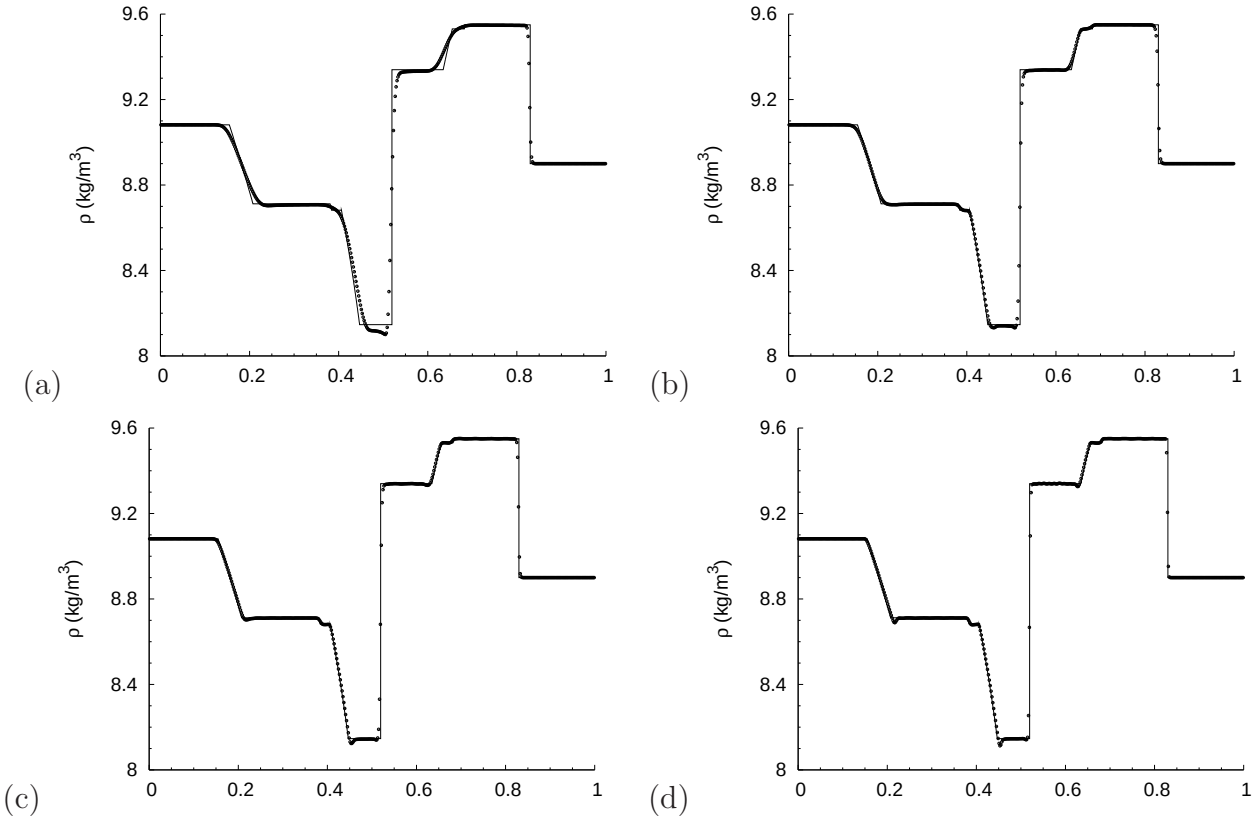

Figure 2.3: Comparison of exact (solid line) and numerical (points) solutions of IVP 1 at a time $t = 0.6\,\mu s$. Numerical solutions were obtained with a grid spacing $\Delta x = 1/500$; (a) first-order space and time with $\mathscr{C}$=0.9; (b) WENO-3, (c) MPWENO-5, (d) MPWENO-9, all with $\mathscr{C}$=0.6.

Table 2.2: Computation times for IVP 1. Times correspond to total CPU time required to reach a solution time $t = 0.6\,\mu$s using a grid with cell size $\Delta x = 1/N$.

Scheme	N	Relative CPU time[a]
1st order,	250	1.00
$\mathscr{C}$=0.9	500	3.57
	1000	14.40
	2000	55.56
1st order,	250	1.40
$\mathscr{C}$=0.6	500	5.24
	1000	21.02
	2000	81.13
WENO-3,	250	3.80
$\mathscr{C}$=0.6	500	14.24
	1000	53.96
	2000	209.83
MPWENO-5,	250	4.61
$\mathscr{C}$=0.6	500	16.83
	1000	64.53
	2000	255.27
MPWENO-9,	250	7.10
$\mathscr{C}$=0.6	500	23.26
	1000	88.77
	2000	346.82
MPWENO-9,	250	10.18
$\mathscr{C}$=1/3	500	39.64
	1000	154.82
	2000	618.49

[a] CPU times are shown relative to the first order scheme on the coarsest grid using $\mathscr{C}$=0.9.

additional degree of shear deformation. The initial conditions are

$$\mathbf{U}^{\mathrm{L}}\left\{\begin{array}{l}\mathbf{u}=\begin{pmatrix}2\\0\\0.1\end{pmatrix}\ \mathrm{km\,s^{-1}},\quad \mathbf{F}=\begin{pmatrix}1 & 0 & 0\\ -0.01 & 0.95 & 0.02\\ -0.015 & 0 & 0.9\end{pmatrix},\quad \mathscr{S}=0\ \mathrm{kJ\,g^{-1}\,K^{-1}}\ ,\\ \mathbf{u}=\begin{pmatrix}0\\-0.03\\-0.01\end{pmatrix}\ \mathrm{km\,s^{-1}},\quad \mathbf{F}=\begin{pmatrix}1 & 0 & 0\\ 0.015 & 0.95 & 0\\ -0.01 & 0 & 0.9\end{pmatrix},\quad \mathscr{S}=0\ \mathrm{kJ\,g^{-1}\,K^{-1}}\ .\end{array}\right.\quad \mathbf{U}^{\mathrm{R}}\tag{2.85}$$

The solution comprises symmetric left and right travelling wavetypes about the contact wave: a longitudinal shock followed by a tranverse rarefaction and a transverse shock. The central contact propagates to the right.

Results were again obtained using MPWENO-5, with $\mathscr{C}$=0.6 and 500 grid points, and run to a time $t = 0.6\ \mu$s. Spurious overshoots occur in those parameters not conserved across the contact wave (Figure 2.4). This behaviour was observed in [72] for similarly predominantly impact based testcases and is accountable to the Riemann solver. All waves and constant states are distinguishable using MPWENO-5 reconstruction and 500 grid points. It can be shown that the solution converges with decreasing grid spacing (Figure 2.5); the L_1-norm of error in primitive state variables exhibits approximately first-order convergence for the high-order schemes (Table 2.3), which is expected for such a problem comprising discontinuities. Trends in the L_1-error favour the higher-order methods (Figure 2.6); much fewer grid points are required to achieve a desired resolution than say the first-order method, especially in those variables that experience a jump across all non-linear waves. Note that CPU times for this problem were comparable to those for IVP 1 (Table 2.2). Taking for example then a comparison between the first-order and MPWENO-5 methods using 250 cells, the first-order method would require at least two times this number for some variabes, and significantly more for others. Since the MPWENO-5 method is only approximately five times more expensive than the first-order method on the coarsest grid, this makes it a better choice in practical computations for such a desired level of accuracy. A similar argument can be drawn between the MPWENO-5 and MPWENO-9 methods, although the differences are not so great.

Resolution of the first shocks and following rarefactions are good on both left and right sides of the contact. However, the slow transverse shocks are captured within quite a few more cells than the longitudinal shocks. This has also been observed for slow moving shocks in magnetohydrodynamics by Balsara et al. [2], where they show that the resolution can be improved using MPWENO-9. While similar improvements can be obtained in non-linear elasticity (Figure 2.7) it is found that using MPWENO-9 with $\mathscr{C}$=0.6 gives rise to oscillatory behaviour in the entropy profile. Instead, using $\mathscr{C}$=1/3 dampens almost all of these but of course doubles the overall cost.

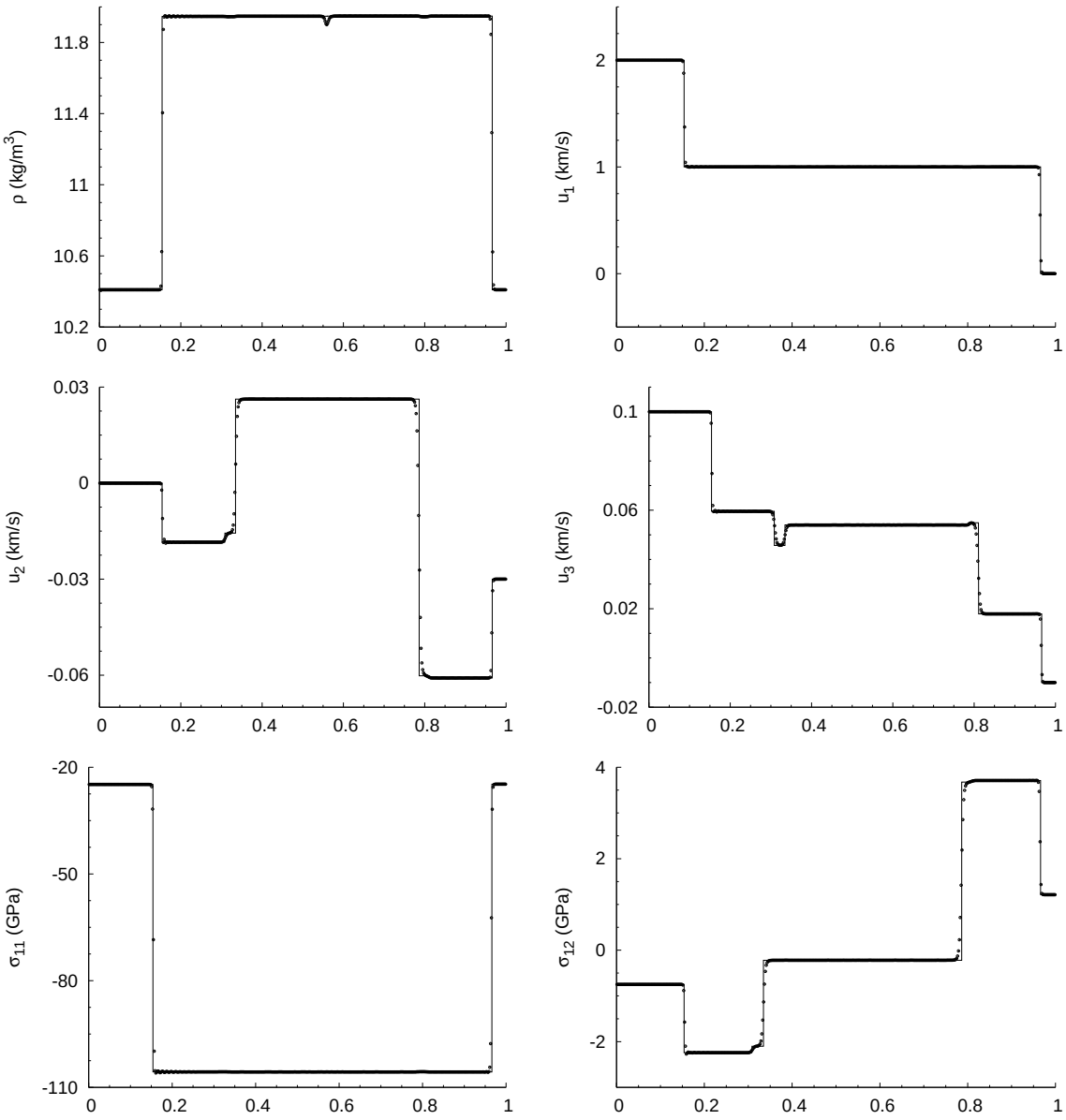

Figure 2.4: Comparison of exact (solid line) and numerical (points) solutions of IVP 2 at time $t = 0.6\,\mu s$. Numerical solutions were obtained with a grid spacing $\Delta x = 1/500$, $\mathscr{C}$=0.6, and using the 5th order WENO reconstruction scheme.

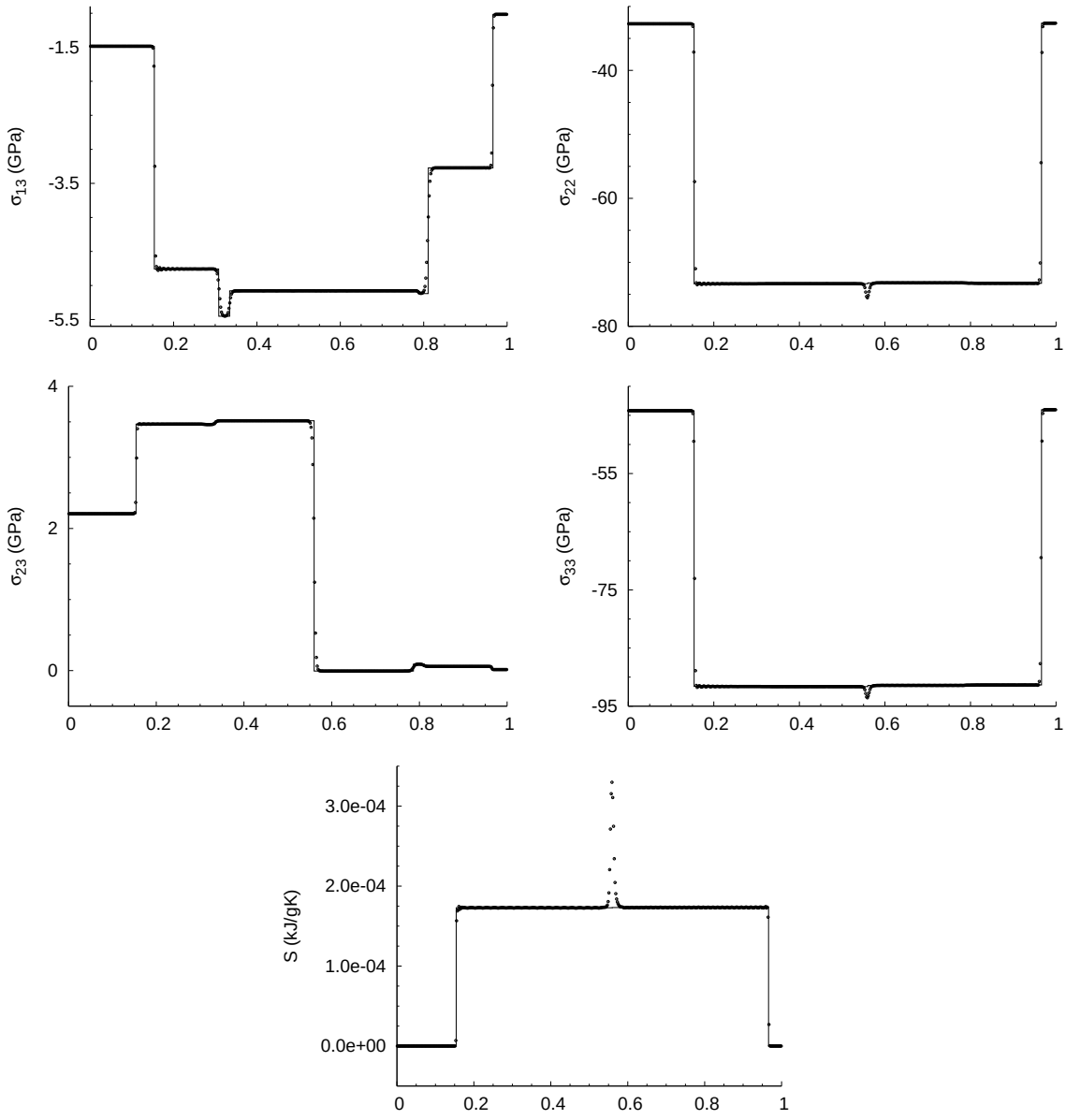

Figure 2.4: *(continued)*

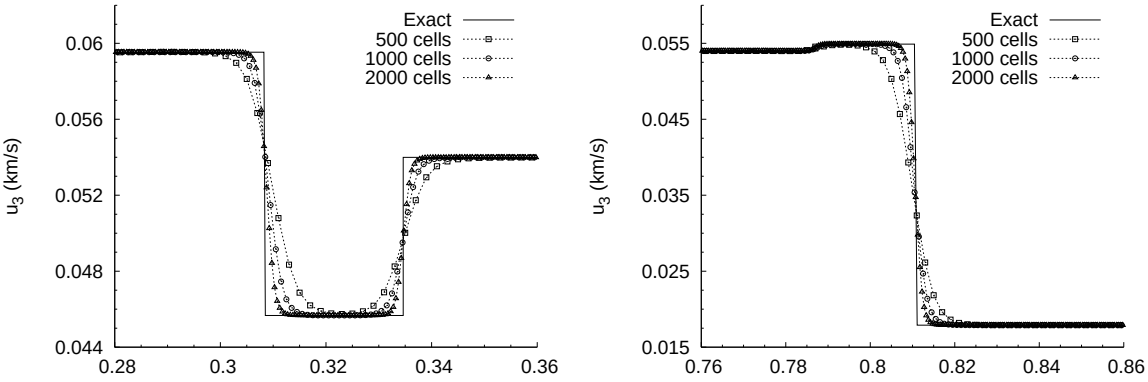

Figure 2.5: Comparison of exact and numerical solutions of IVP 2 at a time $t = 0.6\mu s$ for different grid spacings. As before: $\mathscr{C}$=0.6, and using the 5th order WENO reconstruction scheme.

Table 2.3: L_1-orders for IVP 2 for selected state parameters and using the different reconstruction methods.

		L_1 orders							
Scheme	N	u_1	u_2	u_3	F_{11}	F_{21}	F_{23}	F_{31}	$\mathscr{S}$
1st order,	250	–	–	–	–	–	–	–	–
$\mathscr{C}$=0.9	500	1.16	0.54	0.59	1.08	0.52	0.50	0.57	1.08
	1000	0.93	0.51	0.50	0.98	0.51	0.50	0.51	1.07
	2000	1.05	0.50	0.56	0.99	0.50	0.50	0.55	1.03
1st order,	250	–	–	–	–	–	–	–	–
$\mathscr{C}$=0.6	500	1.13	0.55	0.60	1.05	0.53	0.49	0.57	0.97
	1000	1.01	0.53	0.52	0.97	0.51	0.50	0.51	0.94
	2000	0.97	0.51	0.56	0.95	0.50	0.50	0.55	0.94
WENO-3,	250	–	–	–	–	–	–	–	–
$\mathscr{C}$=0.6	500	1.19	0.77	0.88	1.07	0.74	0.68	0.83	0.93
	1000	0.98	0.74	0.71	1.01	0.73	0.70	0.72	1.00
	2000	1.01	0.77	0.84	0.97	0.76	0.71	0.83	0.93
MPWENO-5,	250	–	–	–	–	–	–	–	–
$\mathscr{C}$=0.6	500	1.36	0.92	1.11	1.27	0.88	0.78	1.04	1.02
	1000	1.04	0.87	0.78	1.02	0.86	0.80	0.75	0.89
	2000	1.07	0.88	0.99	1.02	0.86	0.81	0.97	0.84
MPWENO-9,	250	–	–	–	–	–	–	–	–
$\mathscr{C}$=0.6	500	1.52	1.06	1.27	1.36	1.01	0.85	1.11	0.69
	1000	1.13	0.94	0.81	0.97	0.89	0.87	0.73	0.45
	2000	0.93	0.90	1.01	0.82	0.87	0.88	0.91	0.42
MPWENO-9,	250	–	–	–	–	–	–	–	–
$\mathscr{C}$=1/3	500	1.44	1.04	1.25	1.31	1.00	0.86	1.13	0.91
	1000	1.00	0.91	0.79	0.96	0.89	0.87	0.78	0.87
	2000	0.99	0.97	1.05	0.99	0.96	0.88	1.05	0.90

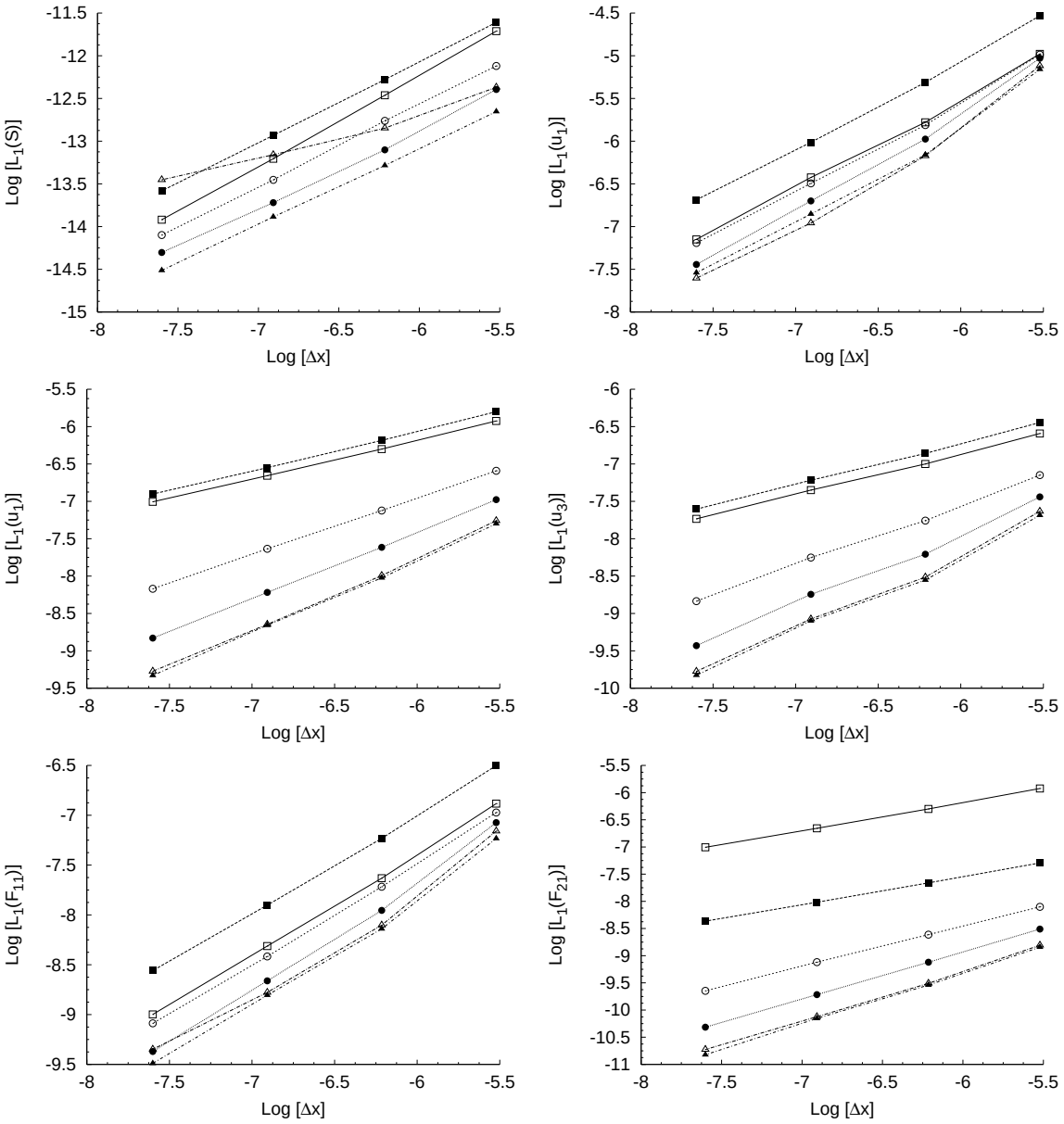

Figure 2.6: L_1-orders against cell size for various state parameters and for IVP 2 using the 1st order method, with $\mathscr{C} = 0.9$ (—□—); 1st order method, with $\mathscr{C} = 0.6$ (---■---); WENO-3 method (···○···); MPWENO-5 method (—●—); MPWENO-9 method, with $\mathscr{C} = 0.6$ (---△---); MPWENO-9 method, with $\mathscr{C} = 1/3$ (---▲---)

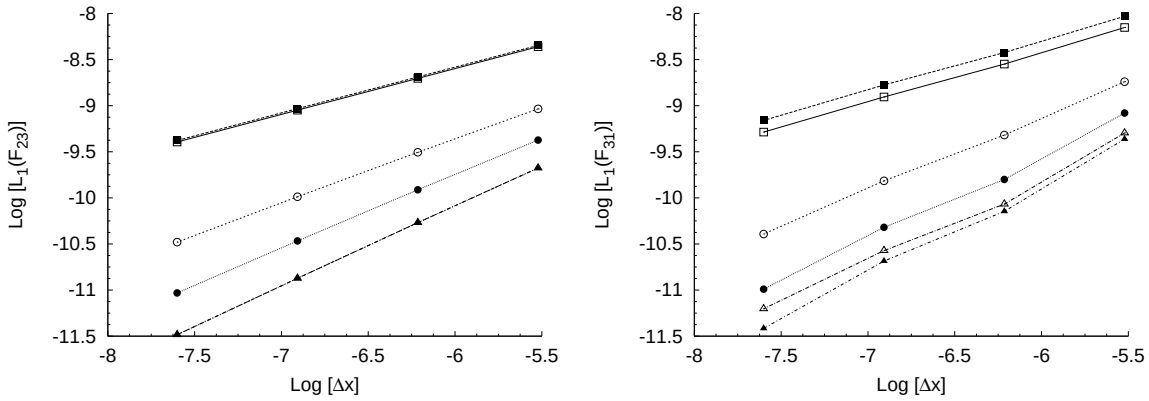

Figure 2.6: *(continued)*

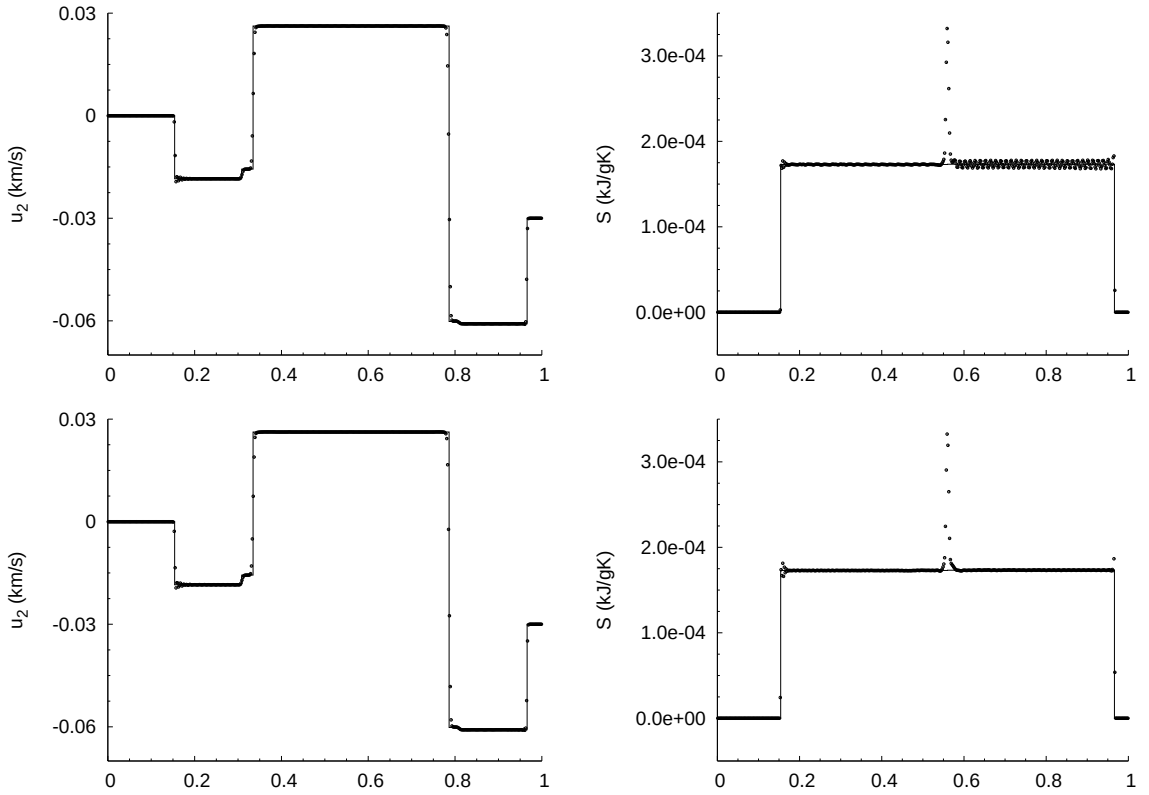

Figure 2.7: Comparison of exact (solid line) and numerical (points) solutions of IVP 2 at a time $t = 0.6\,\mu s$, with a grid spacing $\Delta x = 1/500$, using the 9th order WENO reconstruction scheme, with $\mathscr{C}$=0.6 (top) and $\mathscr{C}$=1/3 (bottom).

2.7 Summary and conclusions

The purpose of the present chapter was to apply existing high–order shock capturing methods to the governing theory of non-linear elasticity with three-dimensional deformations in one space dimension. Specifically, a characteristic based approximation of the Riemann problem was proposed, with high–order spatial accuracy achieved using MPWENO reconstruction and local characteristic decomposition. The methods were developed on the basis of the augmented one-dimensional system of equations and are easily extendable to multi-dimensions and have implications for more complex problems involving material plasticity. Associated compatibility constraints for the augmented system are exactly satisfied regardless of numerical error but may need special attention in multi-dimensional simulations and require further investigation.

The focus has been on using MPWENO schemes to resolve to a high degree structures where all seven waves are distinct in initial value problems. For this, exact solutions proved invaluable and were found using a proposed exact solver. Implementation of the exact solution method is relatively straightforward and although not entirely general has provided sufficient tests to draw the following conclusions

- Excellent agreement is achieved between numerical and exact results
- The close proximity of transverse waves makes jumps in some properties indistinguishable using first order methods. High order WENO and MPWENO resolve these well, even using WENO-3.
- Results using high order methods are essentially non-oscillatory. Spurious overshoots occur in the vicinity of contact waves for variables not conserved across linearly degenerate fields. These are apparent even with first order methods and remains to be improved.
- The increase in computational cost between first order and WENO-3 with three step time integration is quite significant. However, high-order schemes can be used to obtain the accuracy required at lower spatial resolution compared to lower order methods, thereby resulting in reduction of computational cost.
- MPWENO-5 offers the best tradeoff between accuracy and cost. Ninth order reconstruction lends further improvement in resolving slow moving shock waves, which are captured in more cells than longitudinal shocks, but requires lower CFL numbers to achieve monotonic solutions.

3

An Eulerian finite-volume scheme for large elastoplastic deformations in solids[†]

Synopsis

Conservative formulations of the governing laws of elastoplastic solid media have distinct advantages when solved using high-order shock capturing methods for simulating processes involving large deformations and shock waves. In this chapter one such model is considered where inelastic deformations are accounted for via conservation laws for elastic strain with relaxation source terms. Plastic deformations are governed by the relaxation time of tangential stresses. Compared to alternative Eulerian conservative models the governing system consists of fewer equations overall. A numerical scheme for the inhomogeneous system is proposed based upon temporal splitting. In this way the reduced system of non-linear elasticity is solved explicitly, with convective fluxes evaluated using high-order approximations of Riemann problems locally throughout the computational mesh. Numerical stiffness of the relaxation terms at high strain-rates is avoided by utilising certain properties of the governing model and performing an implicit update. The methods are demonstrated using testcases involving large deformations and high strain-rates in one-, two-, and three-dimensions.

3.1 Introduction

Under high strain-rate dynamic loading solid materials exhibit complex non-linear behaviour such as split elastic-plastic shock waves transporting large deformations. From the viewpoint of numerical modelling this represents a challenge since governing models must, in the very least, account for the materials ability to resist shear loads, and accurate models consist of highly non-linear constitutive equations. Neglecting inelastic deformations, the special case of non-linear elasticity studied in the previous chapter is governed by a homogeneous system of partial-differential-equations, conserving mass, momentum, strain and energy, in

[†]Much of the work in this chapter was presented in [4]: **P.T. Barton**, D. Drikakis & E. Romenski, An Eulerian finite-volume scheme for large elastoplastic deformations in solids, *International Journal for Numerical Methods in Engineering*, DOI: 10.1002/nme.2695 (2009).

conjunction with compatibility constraints. In reality, materials exhibit a limit to the deformations that can be maintained where further strains will be irreversible. It is the purpose of this chapter to both extend the established methods to multiple space dimensions, and to consider inelastic deformations.

Inelastic deformations can be accounted for by modifying the governing model in a number of ways. The multiplicative decomposition of the total deformation tensor into elastic and plastic parts can be used to yield additional conservation laws for the plastic deformation tensor [40, 58]. Developments using these models include the work of Vorobiev *et al.* [80], Wang *et al.* [85], Walter *et al.* [83, 84], and Miller and Colella [48]. A disadvantage of this approach is the additional expense of solving a much larger system of equations. In a different approach, a modified elastic potential was proposed in [39] such that the resultant constitutive equations for stress obey von Mises yield criterion, but is restricted to idealised plasticity theory. In the present study the elastic-plastic formulation of Godunov and Romenski [28] is used, where plasticity is introduced via source terms for the equations of the elastic deformation tensor.

In Chapter 2 a high-order Godunov method was developed for the model of Godunov and Romenski [28], using the special case of non-linear elasticity in one space dimension. Numerical results were compared to exact solutions of initial value problems involving three-dimensional deformations. High-order accuracy was achieved using monotonicity-preserving weighted essentially non-oscillatory (MP-WENO) reconstruction. Extension of these methods to inelastic deformations and multi-dimensions using this model requires little modifications of the method for discretising convective fluxes. The main difficulty becomes the evaluation of source terms of the now inhomogeneous system.

The rest of this chapter is organised as follows. In § 3.2 the governing theories are reviewed, whilst § 3.3 details the eigenstructure for the three dimensional system. § 3.4 discusses the necessary constitutive models. In § 3.5 the numerical scheme is proposed, and in § 3.6 these are tested using example testcases in one-, two- and three-dimensions. Finally in § 3.7 a concluding summary is given.

3.2 Governing model of elastoplastic materials

From the outset in the previous chapter only elastic deformations were considered. Before detailing modifications of the employed governing system of conservation laws it must be emphasised that when referring to $\mathbf{F}$ for the system accounting for inelastic deformations, one is in fact referring to the tensor of elastic, rather than total, deformation gradients.

In the model of Godunov and Romenski [26, 28] for a material that may undergo elastoplastic deformations the equations for F_{ij} providing the conservation of strain

become

$$\frac{\partial \rho F_{ij}}{\partial t} + \frac{\partial \left(\rho F_{ij} u_k - \rho F_{kj} u_i\right)}{\partial x_k} = \; -u_i \beta_j - \varphi_{ij}. \tag{3.1}$$

All other constitutive equations detailed in § 2.2 remain unchanged. The terms on the right-hand-side of Eq. (3.1) are given by Eq. (2.20) and

$$\varphi_{ij} := \frac{1}{2G\tau} \sigma'_{ik} \rho F_{kj}, \tag{3.2}$$

where $\sigma'_{ik} = \sigma_{ik} - \sigma_{mm}\delta_{ik}/3$ is the tensor of deviatoric stress, δ_{ik} is the Kronecker delta, and $G(\rho, \mathscr{S})$ is the shear modulus which can depend on the state of the material. The tensor φ provides the necessary mechanisims for decaying deviatoric stress via Maxwell's relaxation model; the relaxation time, τ, governs the rate of decay of deviatoric stress. For the case of small deformations a corresponding rheological law reads as

$$\frac{\mathrm{d}\sigma'_{ij}}{\mathrm{d}t} = 2G\dot{\epsilon}'_{ij} - \frac{\sigma'_{ij}}{\tau}, \tag{3.3}$$

where $\dot{\epsilon}'_{ij}$ is the strain rate deviator.

Remark: Note that in the case of pure elastic processes there is no plastic deformations and it is necessary to set $\varphi = 0$. Moreover if $\varphi = 0$, then $\beta = 0$ if it is equal to 0 in the initial data (see § 2.2.2). It is necessary only to keep in mind that the solutions to the reduced elasticity system must satisfy the compatibility constraints Eq. (2.16).

Remark: Despite the additional source terms on the equations for $\mathbf{F}$ in comparison to the equations for purely elastic flow, using Eq. (3.1) with Eq. (3.2) and Eq. (2.3), it is possible to show that the combination of equations governing the conservation of strain conserve mass, by means of recovering the continuity equation Eq. (2.6) (see Appendix B for the proof). Furthermore, the entropy balance law can be derived in the form

$$\frac{\partial \rho \mathscr{S}}{\partial t} + \frac{\partial \rho \mathscr{S} u_k}{\partial x_k} = Q. \tag{3.4}$$

Here Q is the entropy production, which is nonnegative due to the choice of the inelastic deformation source terms Eq. (3.2):

$$Q := \frac{1}{2G\tau T} \sigma'_{ij} \sigma'_{ji} \geq 0 \tag{3.5}$$

The system is closed by analytic formulae for the specific internal energy and relaxation time in terms of the parameters of state: Eq. (2.2) and

$$\tau = \tau(\sigma_{ij},\, T), \tag{3.6}$$

where $T = \partial\mathscr{E}/\partial\mathscr{S}$ is the temperature.

The complete three dimensional system forms a hyperbolic system of conservation laws in Cartesian coordinates. In matrix form these can be written

$$\frac{\partial \mathbf{U}}{\partial t} + \frac{\partial \mathscr{F}^{\alpha}}{\partial x_{\alpha}} = -\mathbf{S}^{\mathrm{C}} - \mathbf{S}^{\mathrm{P}}, \tag{3.7}$$

with

$$\mathbf{U} := \begin{pmatrix} \rho\mathbf{u} \\ \rho\mathbf{F}^{\mathrm{T}}\mathbf{e}_1 \\ \rho\mathbf{F}^{\mathrm{T}}\mathbf{e}_2 \\ \rho\mathbf{F}^{\mathrm{T}}\mathbf{e}_3 \\ \rho E \end{pmatrix}, \qquad \mathscr{F}^{\alpha} := \begin{pmatrix} u_{\alpha}\rho\mathbf{u} - \sigma\mathbf{e}_{\alpha} \\ u_{\alpha}\rho\mathbf{F}^{\mathrm{T}}\mathbf{e}_1 - u_1\rho\mathbf{F}^{\mathrm{T}}\mathbf{e}_{\alpha} \\ u_{\alpha}\rho\mathbf{F}^{\mathrm{T}}\mathbf{e}_2 - u_2\rho\mathbf{F}^{\mathrm{T}}\mathbf{e}_{\alpha} \\ u_{\alpha}\rho\mathbf{F}^{\mathrm{T}}\mathbf{e}_3 - u_3\rho\mathbf{F}^{\mathrm{T}}\mathbf{e}_{\alpha} \\ u_{\alpha}\rho E - \mathbf{e}_{\alpha}^{\mathrm{T}} \cdot (\sigma\mathbf{u}) \end{pmatrix}.$$

$$\mathbf{S}^{\mathrm{C}} := \begin{pmatrix} 0 \\ u_1\nabla\cdot(\rho\mathbf{F}) \\ u_2\nabla\cdot(\rho\mathbf{F}) \\ u_3\nabla\cdot(\rho\mathbf{F}) \\ 0 \end{pmatrix}, \qquad \mathbf{S}^{\mathrm{P}} := \frac{\rho}{2G\tau}\begin{pmatrix} 0 \\ (\sigma'\mathbf{F})^{\mathrm{T}}\mathbf{e}_1 \\ (\sigma'\mathbf{F})^{\mathrm{T}}\mathbf{e}_2 \\ (\sigma'\mathbf{F})^{\mathrm{T}}\mathbf{e}_3 \\ 0 \end{pmatrix},$$

where $\mathbf{e}_{\alpha}$ are the Cartesian unit vectors

This particular formulation is a result of the work in [62] where it is shown how to properly include the source terms associated with inelasticity to yield a thermodynamically compatible system of equations, i.e. its solutions satisfy thermodynamic laws.

3.3 Characteristic analysis: 3-dimensional

In the ensuing computational method the convective flux terms in Eq. (3.7) are, in the same way as Chapter 2, discretised using the well known method of Godunov and also using the previously derived characteristic based Riemann solver. It will be shown in § 3.4 that solutions are required of the augmented one-dimensional system in each of the coordinate directions. Whilst in general the method in § 2.5.1 requires no further modification in each case, the eigenvectors employed do of course change.

Considering now the three-dimensional system for elastoplastic materials, Eq. (3.7) can be rewritten as a quasi-linear system:

$$\frac{\partial \mathbf{W}}{\partial t} + \mathscr{A}^{\alpha}\frac{\partial \mathbf{W}}{\partial x_{\alpha}} = -\mathbf{S}^{\mathrm{P,QL}}. \tag{3.8}$$

The Jacobian appearing in Eq. (3.8) is

$$\mathscr{A}^{\alpha} := \begin{pmatrix} u_\alpha \mathbf{I} & -\mathbf{A}^{\alpha 1} & -\mathbf{A}^{\alpha 2} & -\mathbf{A}^{\alpha 3} & -\mathbf{b}^{\alpha} \\ -\mathbf{F}^{\mathrm{T}}\mathbf{D}_{\alpha 1} & u_\alpha \mathbf{I} & 0 & 0 & 0 \\ -\mathbf{F}^{\mathrm{T}}\mathbf{D}_{\alpha 2} & 0 & u_\alpha \mathbf{I} & 0 & 0 \\ -\mathbf{F}^{\mathrm{T}}\mathbf{D}_{\alpha 3} & 0 & 0 & u_\alpha \mathbf{I} & 0 \\ 0 & 0 & 0 & 0 & u_\alpha \end{pmatrix}, \tag{3.9}$$

where the coefficients are given by

$$\mathbf{A}^{\alpha\beta} = [A_{ij}^{\alpha\beta}] := \frac{1}{\rho}\frac{\partial \sigma_{\alpha i}}{\partial F_{\beta j}}, \qquad \mathbf{b}^{\alpha} = [b_i^{\alpha}] := \frac{1}{\rho}\frac{\partial \sigma_{\alpha i}}{\partial \mathscr{S}}. \tag{3.10}$$

The vector of source terms is

$$\mathbf{S}^{\mathrm{P,QL}} := \frac{1}{2G\tau} \begin{pmatrix} 0 \\ (\sigma'\mathbf{F})^{\mathrm{T}}\mathbf{e}_1 \\ (\sigma'\mathbf{F})^{\mathrm{T}}\mathbf{e}_2 \\ (\sigma'\mathbf{F})^{\mathrm{T}}\mathbf{e}_3 \\ -\frac{1}{\rho T}\sum\limits_{i,k=1}^{3} \sigma'_{ik}\sigma_{ik} \end{pmatrix}. \tag{3.11}$$

It is necessary when evaluating the three-dimensional system to consider the eigenvalues defined for fluxes aligned with the general x_η spatial axis. In which case the characteristic polynomial for Eq. (3.9) ($|A^\eta - \lambda\mathbf{I}| = 0$) has the form

$$(u_\eta - \lambda)^7 \det\left|\mathbf{\Omega} - (u_\eta - \lambda)^2\mathbf{I}\right| = 0, \tag{3.12}$$

where $\mathbf{\Omega}$ is defined specific to the x_η-direction

$$\Omega_{ij} := (\mathbf{e}_i^{\mathrm{T}}\mathbf{A}_{\eta j}) \cdot (\mathbf{F}^{\mathrm{T}}\mathbf{e}_\eta)\,. \tag{3.13}$$

Note that, subject to other employed indices, repeated indices η in Eq. (3.13) does not denote summation, rather simply the direction. The diagonal matrix of eigenvalues is thus given by

$$\mathbf{\Lambda} = \mathrm{diag}\,(u_\eta\mathbf{I} - \mathscr{D},\ u_\eta\mathbf{I},\ u_\eta\mathbf{I},\ u_\eta,\ u_\eta\mathbf{I} + \pi\mathscr{D}\pi)\,, \tag{3.14}$$

where the permutation matrix Eq. (2.31) has been used.

Whilst it would be straightforward to generalise the eigenvectors for the x_1–direction, Eq. (2.32) and Eq.(2.33), to the Jacobians of the fluxes aligned with the other coordinate directions (x_2, x_3), it was found in the course of computation that these do not lend themselves to a formulation convenient for numerical computation. This is because the ratios of components of the deformation gradient appearing in the

left eigenvectors could, in some special cases lead to a divide by zero. For example, in the case of a uniaxial deformation all non-diagonal elements of the deformation tensor will be equal to zero. Using the above structure on the other coordinate directions results in some of these components appearing as a denominator in the left eigenvectors. It is mentioned that this problem does not arise in the two-dimensional formulation (see [72]). To overcome this problem small modifications can be made to the eigenvectors for each of the coordinate directions.

In the x_2–direction the left eigenvectors are

$$\mathbf{L} = \begin{pmatrix} \mathscr{D}\mathbf{Q} & \mathbf{Q}\mathbf{A}^{21} & \mathbf{Q}\mathbf{A}^{22} \\ 0 & \frac{1}{F_{22}}(F_{21}\mathbf{D}^{12} + F_{23}\mathbf{D}^{22}) - \mathbf{D}^{11} - \mathbf{D}^{23} & \frac{1}{F_{22}}(F_{21}\mathbf{D}^{32}) - \mathbf{D}^{31} \\ 0 & 0 & \frac{1}{F_{22}}(F_{23}\mathbf{D}^{12}) - \mathbf{D}^{13} \\ 0 & 0 & 0 \\ \pi\mathscr{D}\mathbf{Q} & -\pi\mathbf{Q}\mathbf{A}^{21} & -\pi\mathbf{Q}\mathbf{A}^{22} \end{pmatrix} \begin{pmatrix} \mathbf{Q}\mathbf{A}^{23} & \mathbf{Q}\mathbf{b}^2 \\ 0 & 0 \\ \frac{1}{F_{22}}(F_{21}\mathbf{D}^{22} + F_{23}\mathbf{D}^{32}) - \mathbf{D}^{21} - \mathbf{D}^{33} & 0 \\ 0 & 1 \\ -\pi\mathbf{Q}\mathbf{A}^{23} & -\pi\mathbf{Q}\mathbf{b}^2 \end{pmatrix}, \tag{3.15}$$

and the corresponding right eigenvectors

$$\mathbf{R} = \begin{pmatrix} \frac{1}{2}(\mathscr{D}\mathbf{Q})^{-1} & 0 \\ \frac{1}{2}\left(\mathbf{F}^{\mathrm{T}}\mathbf{e}_2\right) \otimes \left(\mathbf{e}_1^{\mathrm{T}}\mathbf{Q}^{-1}\mathscr{D}^{-2}\right) & \left(\mathbf{F}^{\mathrm{T}}\mathbf{e}_2\right) \otimes \left(\mathbf{e}_1^{\mathrm{T}}\mathbf{T}^1\right) - \mathbf{D}^{11} - \mathbf{D}^{32} \\ \frac{1}{2}\left(\mathbf{F}^{\mathrm{T}}\mathbf{e}_2\right) \otimes \left(\mathbf{e}_2^{\mathrm{T}}\mathbf{Q}^{-1}\mathscr{D}^{-2}\right) & \left(\mathbf{F}^{\mathrm{T}}\mathbf{e}_2\right) \otimes \left(\mathbf{e}_2^{\mathrm{T}}\mathbf{T}^1\right) - \mathbf{D}^{13} \\ \frac{1}{2}\left(\mathbf{F}^{\mathrm{T}}\mathbf{e}_2\right) \otimes \left(\mathbf{e}_3^{\mathrm{T}}\mathbf{Q}^{-1}\mathscr{D}^{-2}\right) & \left(\mathbf{F}^{\mathrm{T}}\mathbf{e}_2\right) \otimes \left(\mathbf{e}_3^{\mathrm{T}}\mathbf{T}^1\right) \\ 0 & 0 \end{pmatrix} \begin{pmatrix} 0 & 0 \\ \left(\mathbf{F}^{\mathrm{T}}\mathbf{e}_2\right) \otimes \left(\mathbf{e}_1^{\mathrm{T}}\mathbf{T}^2\right) & -\left(\mathbf{e}_1^{\mathrm{T}}\mathbf{\Omega}^{-1}\mathbf{b}^2\right)\mathbf{F}^{\mathrm{T}}\mathbf{e}_2 \\ \left(\mathbf{F}^{\mathrm{T}}\mathbf{e}_2\right) \otimes \left(\mathbf{e}_2^{\mathrm{T}}\mathbf{T}^2\right) - \mathbf{D}^{31} & -\left(\mathbf{e}_2^{\mathrm{T}}\mathbf{\Omega}^{-1}\mathbf{b}^2\right)\mathbf{F}^{\mathrm{T}}\mathbf{e}_2 \\ \left(\mathbf{F}^{\mathrm{T}}\mathbf{e}_2\right) \otimes \left(\mathbf{e}_3^{\mathrm{T}}\mathbf{T}^2\right) - \mathbf{D}^{12} - \mathbf{D}^{33} & -\left(\mathbf{e}_3^{\mathrm{T}}\mathbf{\Omega}^{-1}\mathbf{b}^2\right)\mathbf{F}^{\mathrm{T}}\mathbf{e}_2 \\ 0 & 1 \end{pmatrix} \begin{pmatrix} \frac{1}{2}(\mathscr{D}\mathbf{Q})^{-1}\pi \\ -\frac{1}{2}\left(\left(\mathbf{F}^{\mathrm{T}}\mathbf{e}_2\right) \otimes \left(\mathbf{e}_1^{\mathrm{T}}\mathbf{Q}^{-1}\mathscr{D}^{-2}\right)\right)\pi \\ -\frac{1}{2}\left(\left(\mathbf{F}^{\mathrm{T}}\mathbf{e}_2\right) \otimes \left(\mathbf{e}_2^{\mathrm{T}}\mathbf{Q}^{-1}\mathscr{D}^{-2}\right)\right)\pi \\ -\frac{1}{2}\left(\left(\mathbf{F}^{\mathrm{T}}\mathbf{e}_2\right) \otimes \left(\mathbf{e}_3^{\mathrm{T}}\mathbf{Q}^{-1}\mathscr{D}^{-2}\right)\right)\pi \\ 0 \end{pmatrix}, \tag{3.16}$$

where the following coefficients have been redefined

$$\mathbf{T}_1 := \mathbf{\Omega}^{-1}\left(\mathbf{A}^{21}\mathbf{D}^{11} + \mathbf{A}^{21}\mathbf{D}^{32} + \mathbf{A}^{22}\mathbf{D}^{13}\right),$$
$$\mathbf{T}_2 := \mathbf{\Omega}^{-1}\left(\mathbf{A}^{22}\mathbf{D}^{31} + \mathbf{A}^{23}\mathbf{D}^{12} + \mathbf{A}^{23}\mathbf{D}^{33}\right).$$

Similarly for the x_3–direction the left eigenvectors are

$$\mathbf{L} = \begin{pmatrix} \mathscr{D}\mathbf{Q} & \mathbf{Q}\mathbf{A}^{31} & \mathbf{Q}\mathbf{A}^{32} & \mathbf{Q}\mathbf{A}^{33} & \mathbf{Q}\mathbf{b}^3 \\ 0 & \frac{1}{F_{33}}(F_{31}\mathbf{D}^{13} + F_{32}\mathbf{D}^{23}) - \mathbf{D}^{11} - \mathbf{D}^{22} & \frac{1}{F_{33}}(F_{31}\mathbf{D}^{33}) - \mathbf{D}^{31} & 0 & 0 \\ 0 & 0 & \frac{1}{F_{33}}(F_{32}\mathbf{D}^{13}) - \mathbf{D}^{12} & \frac{1}{F_{33}}(F_{31}\mathbf{D}^{23} + F_{32}\mathbf{D}^{33}) - \mathbf{D}^{21} - \mathbf{D}^{32} & 0 \\ 0 & 0 & 0 & 0 & 1 \\ \pi\mathscr{D}\mathbf{Q} & -\pi\mathbf{Q}\mathbf{A}^{31} & -\pi\mathbf{Q}\mathbf{A}^{32} & -\pi\mathbf{Q}\mathbf{A}^{33} & -\pi\mathbf{Q}\mathbf{b}^3 \end{pmatrix}, \tag{3.17}$$

and the corresponding right eigenvectors

$$\mathbf{R} = \begin{pmatrix} \frac{1}{2}(\mathscr{D}\mathbf{Q})^{-1} & 0 & 0 & 0 & 0 \\ \frac{1}{2}\left(\mathbf{F}^{\mathrm{T}}\mathbf{e}_3\right) \otimes \left(\mathbf{e}_1^{\mathrm{T}}\mathbf{Q}^{-1}\mathscr{D}^{-2}\right) & \left(\mathbf{F}^{\mathrm{T}}\mathbf{e}_3\right) \otimes \left(\mathbf{e}_1^{\mathrm{T}}\mathbf{T}^1\right) - \mathbf{D}^{11} - \mathbf{D}^{22} & \left(\mathbf{F}^{\mathrm{T}}\mathbf{e}_3\right) \otimes \left(\mathbf{e}_1^{\mathrm{T}}\mathbf{T}^2\right) & -\left(\mathbf{e}_1^{\mathrm{T}}\mathbf{\Omega}^{-1}\mathbf{b}^3\right)\mathbf{F}^{\mathrm{T}}\mathbf{e}_3 & 0 \\ \frac{1}{2}\left(\mathbf{F}^{\mathrm{T}}\mathbf{e}_3\right) \otimes \left(\mathbf{e}_2^{\mathrm{T}}\mathbf{Q}^{-1}\mathscr{D}^{-2}\right) & \left(\mathbf{F}^{\mathrm{T}}\mathbf{e}_3\right) \otimes \left(\mathbf{e}_2^{\mathrm{T}}\mathbf{T}^1\right) - \mathbf{D}^{13} & \left(\mathbf{F}^{\mathrm{T}}\mathbf{e}_3\right) \otimes \left(\mathbf{e}_2^{\mathrm{T}}\mathbf{T}^2\right) - \mathbf{D}^{21} & -\left(\mathbf{e}_2^{\mathrm{T}}\mathbf{\Omega}^{-1}\mathbf{b}^3\right)\mathbf{F}^{\mathrm{T}}\mathbf{e}_3 & 0 \\ \frac{1}{2}\left(\mathbf{F}^{\mathrm{T}}\mathbf{e}_3\right) \otimes \left(\mathbf{e}_3^{\mathrm{T}}\mathbf{Q}^{-1}\mathscr{D}^{-2}\right) & \left(\mathbf{F}^{\mathrm{T}}\mathbf{e}_3\right) \otimes \left(\mathbf{e}_3^{\mathrm{T}}\mathbf{T}^1\right) & \left(\mathbf{F}^{\mathrm{T}}\mathbf{e}_3\right) \otimes \left(\mathbf{e}_3^{\mathrm{T}}\mathbf{T}^2\right) - \mathbf{D}^{12} - \mathbf{D}^{23} & -\left(\mathbf{e}_3^{\mathrm{T}}\mathbf{\Omega}^{-1}\mathbf{b}^3\right)\mathbf{F}^{\mathrm{T}}\mathbf{e}_3 & 1 \\ 0 & 0 & 0 & 1 & \frac{1}{2}(\mathscr{D}\mathbf{Q})^{-1}\pi \\ & & & & -\frac{1}{2}\left(\left(\mathbf{F}^{\mathrm{T}}\mathbf{e}_3\right) \otimes \left(\mathbf{e}_1^{\mathrm{T}}\mathbf{Q}^{-1}\mathscr{D}^{-2}\right)\right)\pi \\ & & & & -\frac{1}{2}\left(\left(\mathbf{F}^{\mathrm{T}}\mathbf{e}_3\right) \otimes \left(\mathbf{e}_2^{\mathrm{T}}\mathbf{Q}^{-1}\mathscr{D}^{-2}\right)\right)\pi \\ & & & & -\frac{1}{2}\left(\left(\mathbf{F}^{\mathrm{T}}\mathbf{e}_3\right) \otimes \left(\mathbf{e}_3^{\mathrm{T}}\mathbf{Q}^{-1}\mathscr{D}^{-2}\right)\right)\pi \\ & & & & 0 \end{pmatrix}, \tag{3.18}$$

with

$$\mathbf{T}_1 := \mathbf{\Omega}^{-1}\left(\mathbf{A}^{31}\mathbf{D}^{11} + \mathbf{A}^{31}\mathbf{D}^{22} + \mathbf{A}^{32}\mathbf{D}^{13}\right),$$
$$\mathbf{T}_1 := \mathbf{\Omega}^{-1}\left(\mathbf{A}^{32}\mathbf{D}^{21} + \mathbf{A}^{33}\mathbf{D}^{12} + \mathbf{A}^{33}\mathbf{D}^{23}\right).$$

The differences between the eigenvectors for each coordinate direction are subtle, and thus only minor changes are required in the programming. A detailed derivation of these is provided in Appendix D.

3.4 Numerical scheme

The conservative system of equations, Eq. (3.7), is solved over a fixed, structured computational grid consisting of quadrilateral cells denoted by $I_{i,j,k}$, where cell cen-

tres are denoted by the indices i, j, k. Each cell has the dimensions $\Delta x_{1_{i,j,k}} = x_{1_{i+1/2,j,k}} - x_{1_{i-1/2,j,k}}$, $\Delta x_{2_{i,j,k}} = x_{2_{i,j+1/2,k}} - x_{2_{i,j-1/2,k}}$, $\Delta x_{3_{i,j,k}} = x_{3_{i,j,k+1/2}} - x_{3_{i,j,k-1/2}}$, thus forming the control volumes $\mathscr{V}_{i,j,k} = \Delta x_{1_{i,j,k}} \Delta x_{2_{i,j,k}} \Delta x_{3_{i,j,k}}$. Integrating Eq. (3.7) over $\mathscr{V}_{i,j,k}$ yields the following system of ordinary-differential-equations

$$\frac{\mathrm{d}}{\mathrm{d}t}\mathbf{U}_{i,j,k} = -\Delta t \left(\mathscr{L}_{i,j,k} + \mathbf{S}^{\mathrm{P}}_{i,j,k} \right), \tag{3.19}$$

where $\mathbf{U}_{i,j,k}$ is the vector of volume averaged conserved variables stored at the cell centres, and the unsplit spatial discretisation operator is expressed as

$$\begin{aligned} \mathscr{L}_{i,j,k} \quad := \quad & \left\{ \frac{\mathscr{F}^1_{i+1/2,j,k} - \mathscr{F}^1_{i-1/2,j,k}}{\Delta x_{1_{i,j,k}}} + \frac{\mathscr{F}^2_{i,j+1/2,k} - \mathscr{F}^2_{i,j-1/2,k}}{\Delta x_{2_{i,j,k}}} \right. \\ & \left. + \frac{\mathscr{F}^3_{i,j,k+1/2} - \mathscr{F}^3_{i,j,k-1/2}}{\Delta x_{3_{i,j,k}}} + \mathbf{S}^{\mathrm{C}}_{i,j,k} \right\}, \end{aligned} \tag{3.20}$$

where $\mathscr{F}^1_{i\pm1/2,j,k}$, $\mathscr{F}^2_{i,j\pm1/2,k}$, $\mathscr{F}^3_{i,j,k\pm1/2}$, are the numerical fluxes evaluated at the cell boundaries. To solve the multi-dimensional problem Eqs. (3.19)-(3.20) an unsplit dimension-by-dimension approach is used. For this, each numerical flux function is calculated via solution of a one-dimensional Riemann problem orientated normal to the respective boundary. Specifically, the high-order characteristics based approximate Riemann problem solver presented in Chapter 2 is used in conjunction with the fifth-order MPWENO scheme, since this proved to be the most practical for the equations of non-linear elasticity, based upon accuracy and cost. For $\mathscr{F}^2_{i,j\pm1/2,k}$ then, the solution is found for the augmented one-dimensional system in the x_2-direction using data in the j-direction only. Eq. (3.20) is therefore constructed using the solutions of six one-dimensional Riemann problems, one across each cell boundary, for each cell in a three dimensional calculation. Only once all the numerical fluxes are summed according to Eq. (3.20) is the solution advanced in time.

3.4.1 Evaluation of the compatibility vector

For each cell, the source term $\mathbf{S}^{\mathrm{C}}$ is computed according to

$$\mathbf{S}^{\mathrm{C}}_{i,j,k} = \begin{pmatrix} 0 \\ u^n_{1_{i,j,k}} \beta_{i,j,k} \\ u^n_{2_{i,j,k}} \beta_{i,j,k} \\ u^n_{3_{i,j,k}} \beta_{i,j,k} \\ 0 \end{pmatrix}. \tag{3.21}$$

Here $u^n_{\alpha_{i,j,k}}$ denotes the volume averaged velocity components at the centre of cell $I_{i,j,k}$, evaluated at the last timestep or sub-step in the case of multilevel time

integration. The vector β contains additional derivatives requiring discretisation. In the same way as the spatial operator Eq. (3.20), β can be evaluated by taking differences across each cell volume

$$\beta_{i,j,k} = \frac{(\rho\mathbf{F}^{\mathrm{T}})_{i+1/2,j,k}\mathbf{e}_1 - (\rho\mathbf{F}^{\mathrm{T}})_{i-1/2,j,k}\mathbf{e}_1}{\Delta x_{1_{i,j,k}}} + \frac{(\rho\mathbf{F}^{\mathrm{T}})_{i,j+1/2,k}\mathbf{e}_2 - (\rho\mathbf{F}^{\mathrm{T}})_{i,j-1/2,k}\mathbf{e}_2}{\Delta x_{2_{i,j,k}}} + \frac{(\rho\mathbf{F}^{\mathrm{T}})_{i,j,k+1/2}\mathbf{e}_3 - (\rho\mathbf{F}^{\mathrm{T}})_{i,j,k-1/2}\mathbf{e}_3}{\Delta x_{3_{i,j,k}}}. \tag{3.22}$$

Following [48], values of those terms evaluated at the cell boundaries are taken from the high–order Riemann problem solution for the corresponding cell edge. In this approach the term $\mathbf{S}^{\mathrm{C}}$ carries little overhead to the overall scheme; the necessary terms are simply added at the end of each convective flux evaluation.

3.4.2 Time integration

Devising a numerical scheme to solve Eq. (3.19) is challenging as a result of the terms in $\mathbf{S}^{\mathrm{P}}$ governing the onset of inelastic deformations. The relaxation time, τ, of a metal could, under dynamic loading, vary over a large range of order of magnitudes. Consideration of the limits of τ provides a better understanding of the difficulties, and scope for devising adequate numerical algorithms:

- the elastic limit, $\tau \to \infty$
- the hydrodynamic limit, $\tau \to 0$

In the elastic limit, $\mathbf{S}^{\mathrm{P}} \to 0$ in Eq. (3.7), i.e. the system approaches the governing equations of non-linear elasticity. For a solid material the hydrodynamic limit, so called because the material will behave like a fluid, is reached under very high strain rates. In this regime solids can be approximated well by the compressible Euler equations:

$$\frac{\partial \mathbf{U}^{\mathrm{E}}}{\partial t} + \frac{\partial \mathscr{F}^{\mathrm{E}^\alpha}}{\partial x_\alpha} = 0, \tag{3.23}$$

with

$$\mathbf{U}^{\mathrm{E}} := \begin{pmatrix} \rho\mathbf{u} \\ \rho \\ \rho E \end{pmatrix}, \qquad \mathscr{F}^{\mathrm{E}^\alpha} := \begin{pmatrix} u_\alpha \rho\mathbf{u} - p\mathbf{e}_\alpha \\ \rho u_\alpha \\ u_\alpha(\rho E - p) \end{pmatrix}, \tag{3.24}$$

where p is hydrostatic pressure; and an appropriate equation of state of the form $\mathscr{E} = \mathscr{E}(\rho, \mathscr{S})$.

It is desirable to use for computations a global timestep dictated by the grid sizes and elastic wave speeds

$$\Delta t = \mathscr{C} \times \min_{i,j,k} \left(\frac{\Delta x_1}{|u_1| + \sqrt{\lambda^1_{\mathrm{ac}_{\max}}}}, \frac{\Delta x_2}{|u_2| + \sqrt{\lambda^2_{\mathrm{ac}_{\max}}}}, \frac{\Delta x_3}{|u_3| + \sqrt{\lambda^3_{\mathrm{ac}_{\max}}}} \right), \tag{3.25}$$

where $\sqrt{\lambda^{\alpha}_{\mathrm{ac}_{\max}}}$ denotes the maximum wavespeed of the acoustic tensor, Eq. (3.13), in the direction α, and $0 < \mathscr{C} \leq 1$ is the CFL number [cf. Eq. (2.58)]. However based upon the above limits the timescales associated with the relaxation operator can be small in comparison, hence the system of ODEs Eq. (3.19) will become stiff. Since in most circumstances one cannot forecast zones in which either stiff or non-stiff regimes will be apparent, it is necessary to solve the complete system of equations throughout the domain with an appropriate time integration method that overcomes the problem of stiff ODEs.

Since high–order methods have already been established for the homogeneous equations of non-linear elasticity ($\mathbf{S}^{\mathrm{P}} = 0$ in Eq. (3.7)), a natural extension for solving Eq. (3.19) would be to use temporal splitting:

$$\mathbf{U}^{*} = \mathbf{U}^{n} - \Delta t\, \mathscr{L}(\mathbf{U}^{n}), \tag{3.26a}$$

$$\mathbf{U}^{n+1} = \mathbf{U}^{*} - \Delta t\, \mathbf{S}^{\mathrm{P}}(\mathbf{U}^{n+1}). \tag{3.26b}$$

That is, the homogeneous system of non-linear elasticity is updated explicitly using the forward Euler method, Eq. (3.26a), whilst the (possibly stiff) source terms are updated implicitly using Eq. (3.26b). The latter can then be solved using an *L*-stable implicit integration technique, eliminating any influence of the relaxation time on the CFL condition. Jin [34] discusses the use of splitting schemes applied to hyperbolic conservation laws with stiff relaxation operators. Here it is shown that solutions via temporal splitting is sufficient provided that the numerical algorithm has the correct *asymptotic limit*: in the hydrodynamic limit the scheme is a stable and consistent evaluation of the *equilibrium system*, Eq. (3.23), for fixed spatial and temporal step sizes. Violating this property can result in spurious solutions.

To ensure that in the asymptotic limit the numerical method leads to an explicit integration of the *equilibrium system*, small modifications need to be made to the formulation of governing theory, Eq. (3.7). As stated in § 2.2, in conjunction with the equations for $\mathbf{F}$ one has the mass continuity equation, Eq. (2.6). As a result, Eq. (2.6) can be used in place of one equation for the deformation gradient tensor whilst maintaining a fully determined system. One choice would be to replace the equation for ρF_{11} in Eq. (3.7), thus the vectors in Eq. (3.2) are replaced with

$$\mathbf{U} := \begin{pmatrix} \rho\mathbf{u} \\ \rho \\ \rho F_{12} \\ \vdots \\ \rho F_{33} \\ \rho E \end{pmatrix}, \qquad \mathscr{F}^{\alpha} := \begin{pmatrix} u_{\alpha}\rho\mathbf{u} - \sigma\mathbf{e}_{\alpha} \\ \rho u_{\alpha} \\ \rho u_{\alpha} F_{12} - \rho u_{1} F_{\alpha 2} \\ \vdots \\ \rho u_{\alpha} F_{33} - \rho u_{3} F_{\alpha 3} \\ u_{\alpha}\rho E - \mathbf{u}^{\mathrm{T}} \cdot (\sigma\mathbf{e}_{\alpha}) \end{pmatrix}, \tag{3.27}$$

and the vector of source terms adjusted accordingly for the zero right-hand side of Eq. (2.6). For computations, Eq. (2.3) can be rearranged to recover F_{11} in terms of

$\rho_0, \rho, F_{12}, \ldots, F_{33}$. Following [10], there now exists a constant 5×13 matrix

$$\mathcal{Q} = \begin{pmatrix} 1 & 0 & 0 & 0 & 0 & 0 & 0 & 0 & 0 & 0 & 0 & 0 & 0 \\ 0 & 1 & 0 & 0 & 0 & 0 & 0 & 0 & 0 & 0 & 0 & 0 & 0 \\ 0 & 0 & 1 & 0 & 0 & 0 & 0 & 0 & 0 & 0 & 0 & 0 & 0 \\ 0 & 0 & 0 & 1 & 0 & 0 & 0 & 0 & 0 & 0 & 0 & 0 & 0 \\ 0 & 0 & 0 & 0 & 0 & 0 & 0 & 0 & 0 & 0 & 0 & 0 & 1 \end{pmatrix}, \tag{3.28}$$

that satisfies $\mathcal{Q}\mathbf{S}^{\mathrm{P}} = 0$ and gives $\mathbf{U}^{\mathrm{E}} = \mathcal{Q}\mathbf{U}$, i.e. recovers the conserved variables of the Euler equations. Furthermore it is assumed that $\mathbf{S}^{\mathrm{P}}(\mathbf{U}) = 0$ can be solved uniquely in terms of $\mathbf{U}^{\mathrm{E}}$: assuming a function $\mathcal{E}$, giving $\mathbf{U} = \mathcal{E}(\mathbf{U}^{\mathrm{E}})$, then $\mathbf{S}^{\mathrm{P}}(\mathcal{E}(\mathbf{U}^{\mathrm{E}})) = 0$ [10]. This is apparent since for the Euler equations the deviatoric stress tensor is zero, thus giving the required result. Using these results the analysis in § 3.2 of [55] can be applied to Eqs. (3.26a)-(3.26b), to prove that in the limit $\tau \to 0$ the scheme is an explicit evaluation of the compressible Euler equations.

The accuracy of the explicit update, Eq. (3.26a), has been improved by instead using the third order TVD Runge-Kutta method Eq. (2.57). This is consistent with the TVD requirements of the WENO reconstruction scheme used in the evaluation of convective flux terms. Since stress can be expressed as functions of the state parameters the implicit part Eq. (3.26a) is solved using the iterative Newton-Raphson method. In this study only first-order of accuracy of the implicit part shall be considered. It is mentioned however that using diagonally implicit Runge-Kutta (DIRK) methods (see for example [1])or perhaps implicit-explicit Runge-Kutta (IMEX) schemes (see for example [55]) the overall accuracy could be raised to match that of the explicit part.

3.5 Examples

Before proceeding with the presentation of example testcases the closure relations Eq. (2.15) and Eq. (3.6) must be specified. In this chapter, two expressions for the internal energy are considered. The first was presented in [48], and is an isentropic hyperelastic equation of state in terms of the invariants of the elastic Greens tensor, $\mathbf{C}$, (see Eq. (2.10)):

$$\mathscr{E}(\mathcal{I}_1, \mathcal{I}_3) = -\int_{V_0}^{V} p(V)\mathrm{d}V + \frac{G}{2\rho_0}\left(\mathcal{I}_1 - 3\mathcal{I}_3^{1/3}\right), \tag{3.29}$$

where $V = 1/\rho$ is the specific volume, with the function for cold pressure $p(V)$ taken from [86]:

$$p(V) = p_{01}(\eta - 1) + p_{02}(\eta - 1)^2 + p_{03}(\eta - 1)^3 \text{ GPa}, \qquad \eta = V_0/V. \tag{3.30}$$

The second formulation considered is the isotropic hyperelastic equation of state used in the previous chapter: Eq. (2.82)-(2.83).

One function for the relaxation time capable of modelling sufficiently the physical loading behaviour of metals is the power law function [47]

$$\tau = \tau_0 \left(\frac{\sigma_0}{\sigma_{\text{EQ}}} \right)^n , \tag{3.31}$$

where σ_0, τ_0 and n are material specific constants, and the shear stress intensity is given by

$$\sigma_{\text{EQ}} := \sqrt{[(\sigma_{11} - \sigma_{22})^2 + (\sigma_{22} - \sigma_{33})^2 + (\sigma_{33} - \sigma_{11})^2 + 6(\sigma_{12}^2 + \sigma_{13}^2 + \sigma_{23}^2)]/2.} \tag{3.32}$$

Determination of the parameters entering into Eq. (3.31) can be achieved by performing a series of numerical experiments [46, 60]. Specifically, the system of equations Eq. (3.7) can be reduced for the special case of uniaxial strain of a thin rod (see [28] for a detailed derivation). Simulations can then be performed where the sample is deformed in one coordinate direction at a constant strain rate thus providing stress versus strain data. These numerical tests are analogous to the Split Hopkinson Pressure Bar (SHPB) test [60] commonly employed to investigate high strain rate loading behaviour. Therefore any function minimisation method can be used to determine accurate constants by comparison of the numerical and available experimental data. It is noted that using this technique it is possible to develop models that take into account microscopic phenomena such as dislocation motion, with the necessary constants, not readily available for all metals, being determined via the numerical tests [46, 60]. The model Eq. (3.31) represents a simple empirical model and admits strain rate dependency of the flow stress. Figure 3.1 illustrates the yield stress against strain rate for different values of n. Note that in general the parameters σ_0, τ_0 and n will depend on the state of the material [27] to realise influences such as temperature on the yield stress.

In some cases inelastic deformations are required to satisfy idealised plasticity theory, or at least some approximation of it, in order to provide comparison with certain well known numerical experiments of previous studies. That is, the rate of change of stress is equivalently zero under further loading once the stress intensity reaches the material specific yield stress. Furthermore, the yield surface is required to be independent of strain-rate effects. There are different approaches one can take to achieve ideal plasticity with the present governing model. One would be to use a modified version of the radial return algorithm, see for example [58, 48]. Another might be to use the modified potential function proposed in [39]. However a different approach is proposed here based upon the model Eq. (3.31).

In ideal plasticity theory, the flow stress $\sigma = \sigma_y$ is taken to be the value at which the rate of change of stress goes to zero: $\partial\sigma/\partial t = 0$. Substituting this into Eq. (3.3)

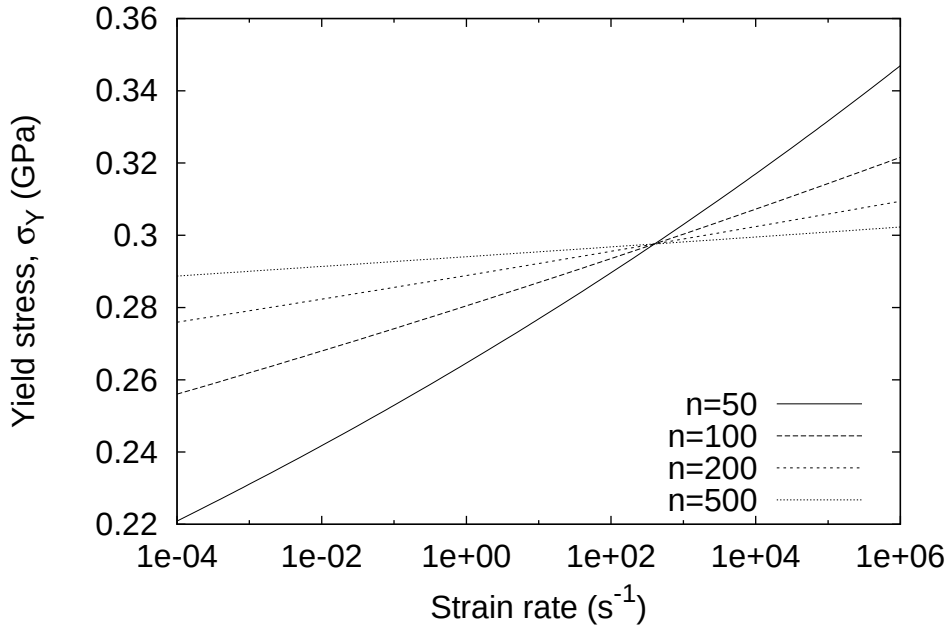

Figure 3.1: Yield stress plotted against strain rate showing the influence of the parameter n in Eq. (3.31). Results were obtained using the bar theory in [28], with the isentropic equation of state from § 2.6. The material was aluminium, with constants equal to those in § 3.5.1. Values of the constants in Eq. (3.31) were $\sigma_0 = 0.2976\,\text{GPa}$ and $\tau_0 = 1 \cdot 10^{-5}\,\text{s}$.

gives

$$\tau = \frac{\sigma_y}{2G\dot{\epsilon}} \tag{3.33}$$

By further substituting in the analytic model for τ, and after some algebraic manipulation an expression can be obtained for the stress on the yield surface:

$$\sigma_y = \sigma_0 \left(\tau_0 \sigma_0^{-1} G\dot{\epsilon}\right)^{1/(n+1)} . \tag{3.34}$$

From this result it is clear that strain rate effects entering into the governing model vanish in the limit $n \to \infty$, such that $\sigma_y \to \sigma_0$, where σ_0 will represent the required yield stress (Figure 3.1). Of course this can not be achieved in reality, but n can instead be taken large enough such that strain rate effects are decreased. Furthermore in doing so a rigorous test is provided for the time integrator. It is seen (Figure 3.1) that even at values of $n = 500$ strain-rate effects remain apparent, and therefore the model is used for illustrative purposes only, rather than as a suggested method if one requires strict idealised plasticity.

3.5.1 One-dimensional testcases

For a test in one-dimension the plate impact problem of Wilkins [86] is considered. The problem consists of an 0.5 cm aluminium flyer plate impacting a semi-infinite aluminium target. These tests were conducted using a similar Eulerian model in [48], using the isentropic hyperelastic equation of state Eq. (3.29). In both [86, 48] the material is assumed to obey ideal plasticity. This is approximated here using the model Eq. (3.31). Constants used for the constitutive equations correspond to Aluminium: $G = 24.8$ GPa, $\rho_0 = 2.7\,\mathrm{kg\,m^{-3}}$, $p_{01} = 73$ GPa, $p_{02} = 172$ GPa, $p_{03} = 40$ GPa, $\sigma_0 = 0.2976$ GPa, $n = 100$, $\tau_0 = 1$.

Two impact velocities are investigated, $u_1 = 0.8\,\mathrm{km\,s^{-1}}$ and $u_1 = 2.0\,\mathrm{km\,s^{-1}}$. In both cases the grid consists of 500 cells in the interval [0:5] cm, with the interface initially located at $x_0 = 0.5$ cm, and $\mathscr{C} = 0.6$. The simulation starts with the flyer plate in contact with the target.

The numerical algorithm for this problem was modified to accommodate the unconstrained free boundary of the flyer plate. A detailed description of these algorithms shall be left to the next chapter and only a brief summary is given here. The interface location is tracked via a level-set field which identifies those cells within the material and designates cells in the void region as *ghost cells* whose state is determined via solution of a Riemann problem [44]. In this case a solid-vacuum Riemann problem is solved using a method similar to that proposed in [49].

For the lower of the two impact velocities the time series in Figures 3.2-3.3 shows that the impact results in shock waves propagating into both the flyer plate and the target. The left travelling wave eventually reaches the free surface and is subsequently reflected resulting in a right travelling rarefaction wave. At later times elastic plastic flow is clearly distinguishable from the characteristic splitting of waves; the so called elastic precursor travelling faster than the plastic wave. Unfortunately no analytic solution exists for this problem, but both the wave speeds and the respective jump in properties are in good qualitative agreement with [86, 48]. It is noted that taking $n = 100$ in Eq. (3.31) does not provide strain-rate independent flow stress (Figure 3.1), and indeed it can be expected that strain rate effects manifest within the results, hence no more than a qualitative analysis could be made regardless of the availability of analytic solutions for idealised plasticity.

Despite this, the use of the model Eq. (3.31) provides a rigorous test on the robustness of the time integration scheme since the large power n results in sharp changes between non-stiff and stiff regimes. Furthermore, the form of Eq. (3.31) is representative of the types of models one would like to employ for obtaining physically realistic solutions. The higher velocity impact further illustrates the robustness of the numerical techniques. The higher peak stresses mean that the plastic wave travels faster and no splitting of the elastic and plastic parts can be distinguished (Figures 3.4-3.5). These behaviours indicate that the hydrodynamic limit

is approached, yet the scheme predicts correct wavespeeds and high wave resolution using underresolved discretisation parameters.

3.5.2 A two-dimensional testcase

For a two-dimensional example consider a plane of material, with the origin located at ($\mathbf{x} = 0$). The region $r > 2$ cm (where $r = |\mathbf{x}|$) is raised to a pressure $p = 10$ GPa (where $p = -\rho^2(\partial \mathscr{U}/\partial\rho)$) and temperature $T = 500\,K$, whilst the inner cylinder, $r \leq 2$ cm, is initiated at ambient conditions, $\mathbf{F} = \mathbf{I}$, $T = 300$ K. Both regions are initially at rest. The test is chosen on the basis that the resulting behaviours should be cylindrically symmetric, thus allowing comparison with one-dimensional polar calculations. The hyperelastic equation of state Eq. (2.82)-(2.83) is used, with the material constants taken for copper provided in Table 2.1. For the relaxation model, Eq. (3.31) is used with the following constants for copper taken from [47]: $\tau_0 = 0.92$ s, $\sigma_0 = 0.045$ GPa, $n = 10.1$. These were found in [47] on the basis of producing a best match with experimental data. Solutions were found using a computational domain $[0:10,\ 0:10]$ cm, where the axis are modelled as symmetric boundaries (see Appendix J). The grid was uniform, with $\Delta x_1 = \Delta x_2 = 1/25$ cm, and the timestep was restricted using $\mathscr{C} = 0.6$. For comparison, one-dimensional cylindrical polar results were obtained (see Appendix C for the relevant formulation), using $\Delta r = 1/50$ cm and $\mathscr{C} = 0.6$.

The initial conditions result in a cylindrical shock converging on the origin through the central ambient material, which subsequently reflects from the origin. Inspired by the presentation of cylindrically symmetric examples in [48], the Cartesian results are plotted as a scatter graph in Figure 3.6 so as to examine the extent to which cylindrical symmetry is preserved. Results are shown at time $t = 10\,\mu$s, after the shock has reflected from the origin. Overall agreement is good for both the wavespeeds and profiles. The preservation of cylindrical symmetry is also good.

3.5.3 A three-dimensional testcase

For a three dimensional testcase initial conditions are taken similar to the previous two-dimensional case. Consider a volume of material, with the origin ocated at ($\mathbf{x} = 0$). The region $r > 2$cm (where $r = |\mathbf{x}|$), is raised to a pressure $p = 10$GPa and temperature $T = 500$ K, whilst the inner sphere, $r \leq 2$ cm, is initiated at ambient conditions, $\mathbf{F} = \mathbf{I}$, $T = 300$ K. Again both regions are initially at rest. The material is again assumed to be copper, with the constitutive equations and respective constants equal to those before. Solutions were found using a computational domain $[0:10,\ 0:10,\ 0:10]$ cm, where the $x_1 = 0, x_2 = 0, x_3 = 0$ planes were modelled as symmetric boundaries. The grid was uniform, with $\Delta x_1 = \Delta x_2 = \Delta x_3 = 1/10$ cm, and the timestep was restricted using $\mathscr{C} = 0.6$. Similarly, one-dimensional spherical

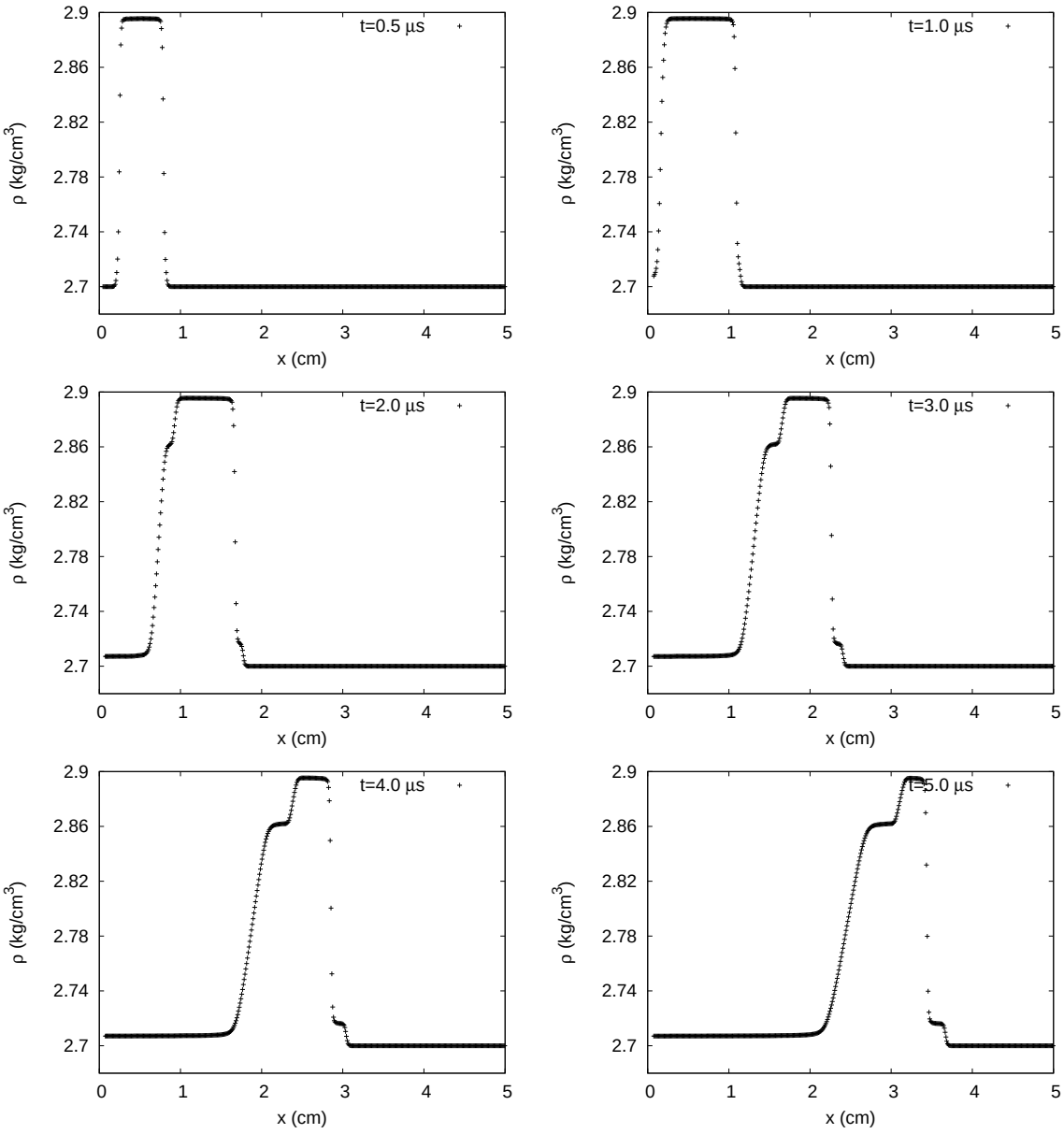

Figure 3.2: Time sequence of density profiles for an aluminium flyer plate impacting an aluminium target at $0.8\,\mathrm{km\,s^{-1}}$ (§ 3.5.1). Results were obtained with a uniform grid spacing $\Delta x = 1/100\,\mathrm{cm}$ and using $\mathscr{C} = 0.6$.

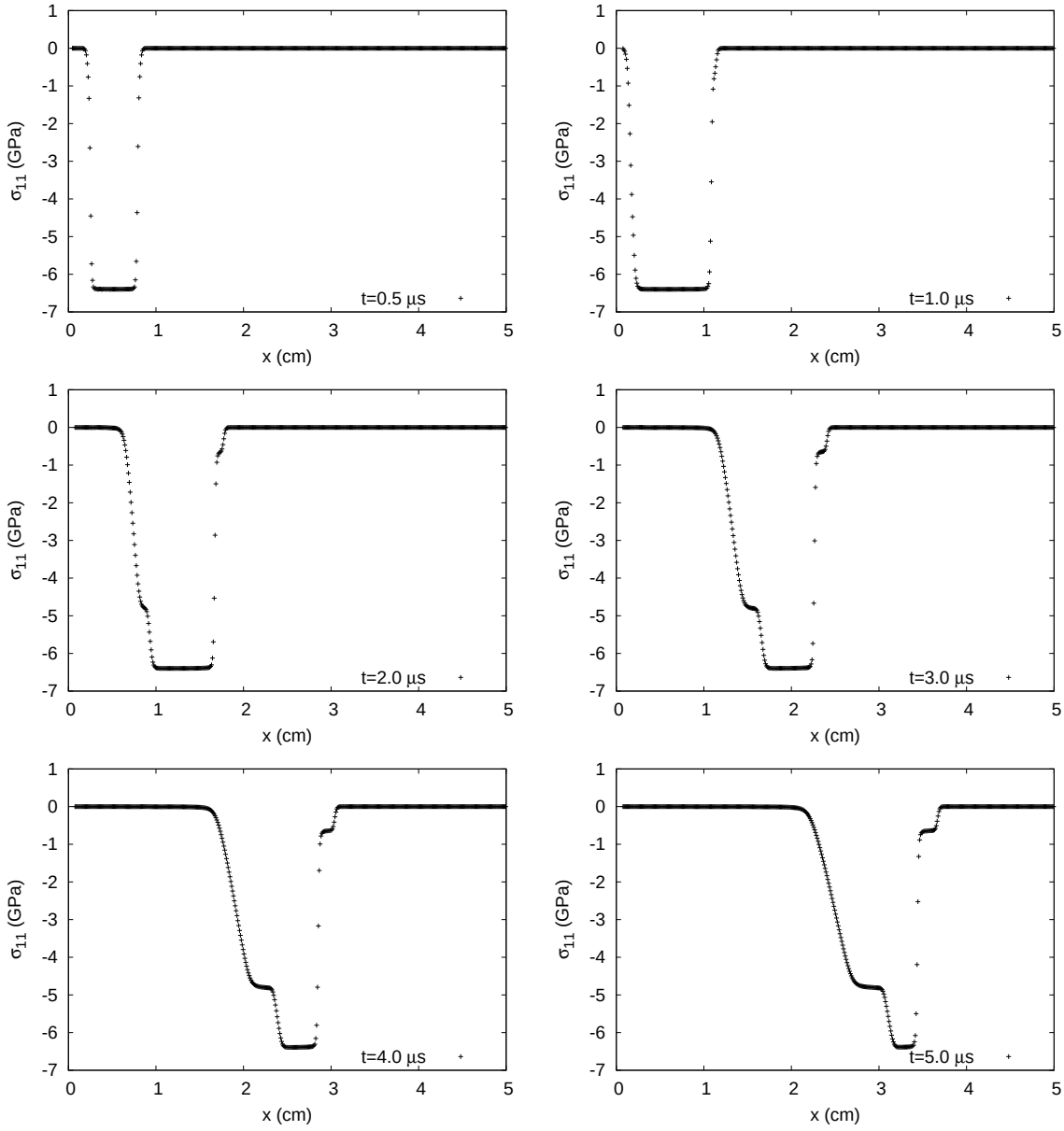

Figure 3.3: Time sequence of normal stress profiles for an aluminium flyer plate impacting an aluminium target at $0.8\,\mathrm{km\,s^{-1}}$ (§ 3.5.1). Results were obtained with a uniform grid spacing $\Delta x = 1/100\,\mathrm{cm}$ and using $\mathscr{C} = 0.6$.

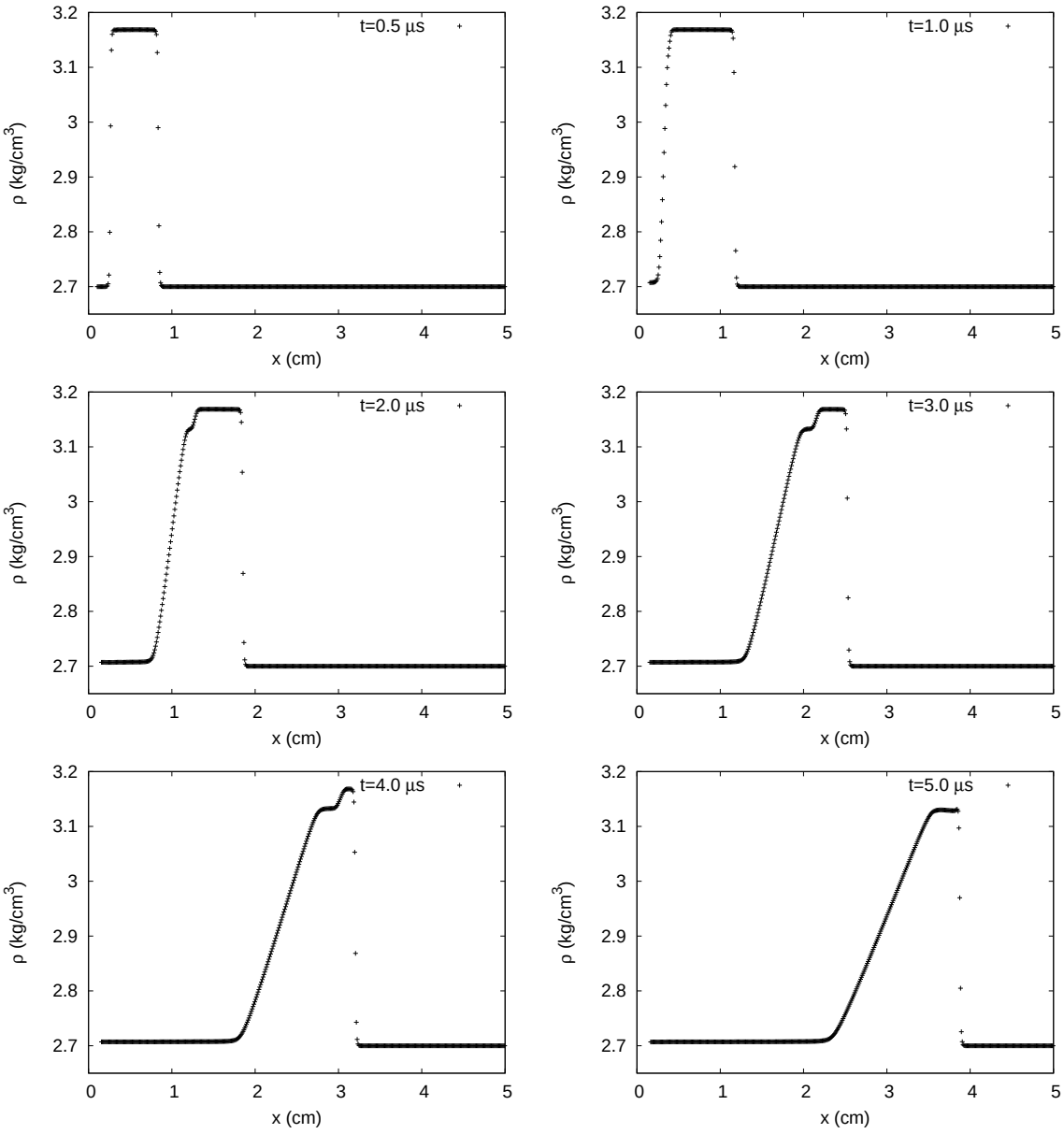

Figure 3.4: Time sequence of density profiles for an aluminium flyer plate impacting an aluminium target at $2.0\,\mathrm{km\,s^{-1}}$ (§ 3.5.1). Results were obtained with a uniform grid spacing $\Delta x = 1/100\,\mathrm{cm}$ and using $\mathscr{C} = 0.6$.

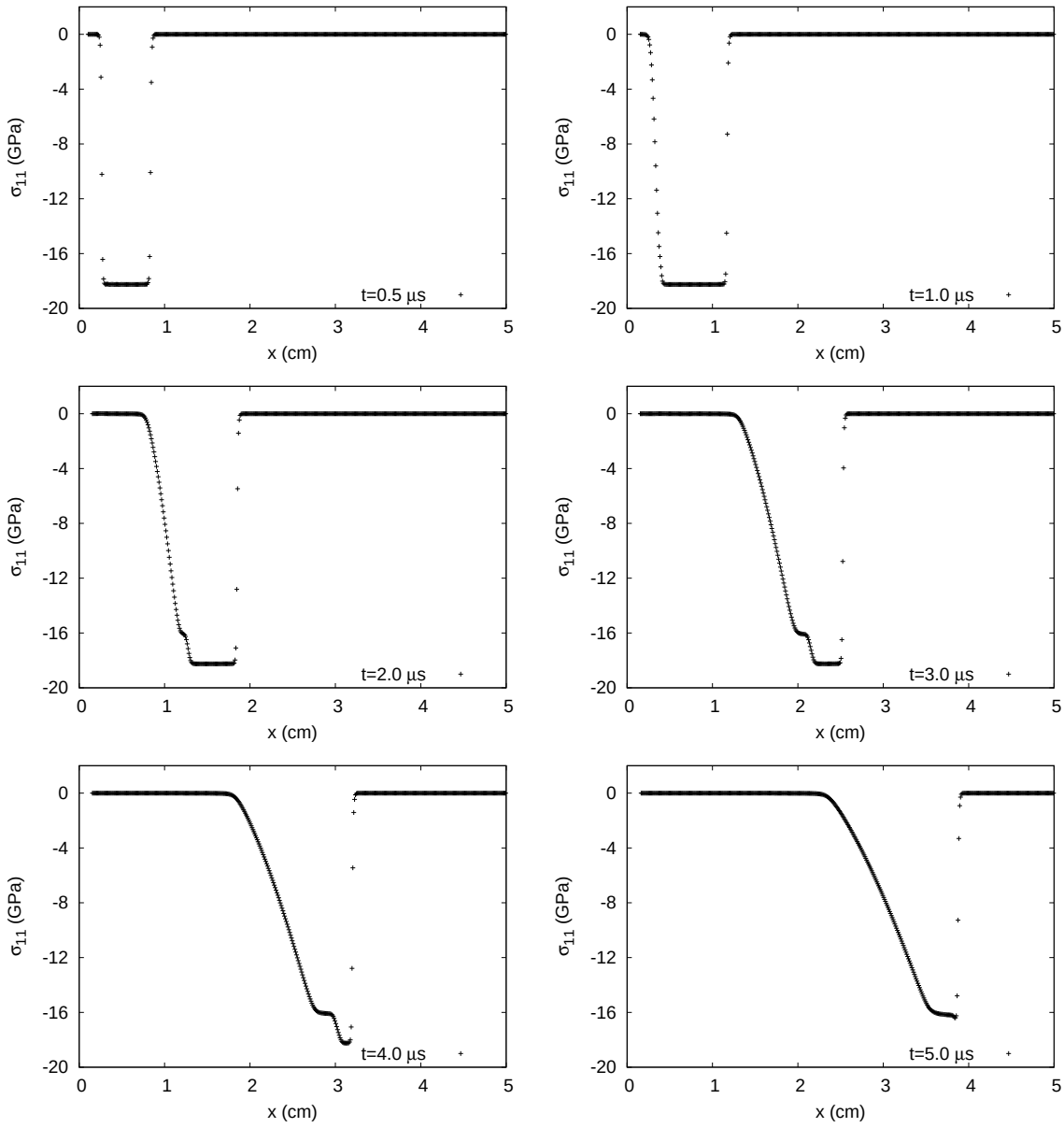

Figure 3.5: Time sequence of normal stress profiles for an aluminium flyer plate impacting an aluminium target at $2.0\,\mathrm{km\,s^{-1}}$ (§ 3.5.1). Results were obtained with a uniform grid spacing $\Delta x = 1/100\,\mathrm{cm}$ and using $\mathscr{C} = 0.6$.

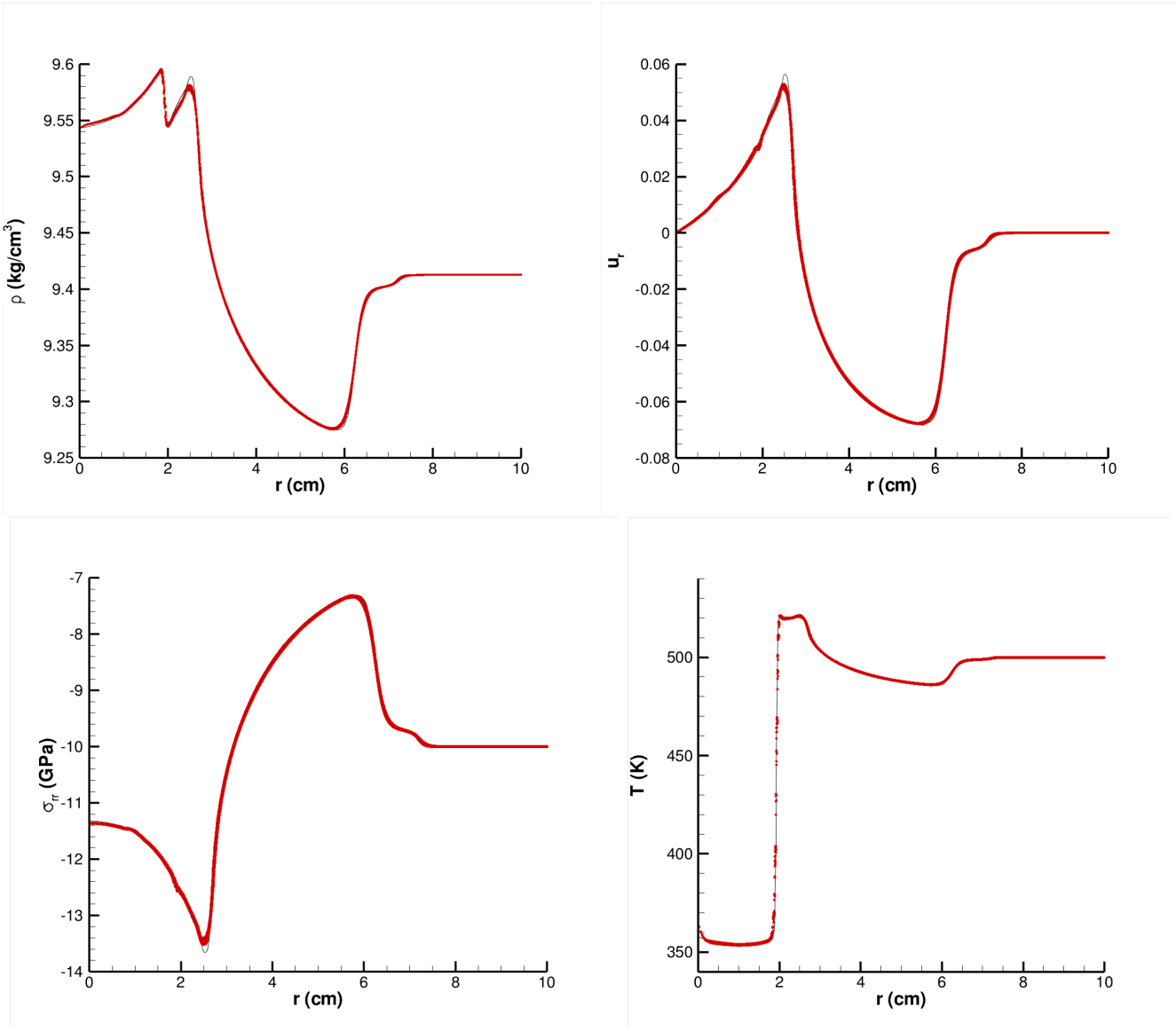

Figure 3.6: Scatter graph comparison of two-dimensional cartesian (points) and one-dimensional cylindrical (solid line) solutions of the testcase in § 3.5.2 at a time $t = 10\,\mu s$. Cartesian results were obtained with a uniform grid spacing $\Delta x = \Delta y = 1/25$ cm and using $\mathscr{C} = 0.6$.

polar results were obtained for reference (see Appendix C for the relevant formulation), using $\Delta r = 1/50$ cm and $\mathscr{C} = 0.6$.

Both the wavespeeds and profiles are again in good agreement with the one-dimensional results (Figure 3.7), despite the lower resolution. Spherical symmetry is also seen to be preserved to a good degree.

3.6 Conclusions

In this chapter a high-order shock capturing method was proposed for simulating elastoplastically deforming solid media. The methods were based upon a governing model cast in the Eulerian reference frame, thus allowing the use of fixed Cartesian grids. In the previous chapter the reduced system of non-linear elasticity was investigated and high-order approximations of the Riemann problem for the augmented one-dimensional system were developed and tested. The extension of these to three-dimensions proved straightforward requiring only small modifications to the eigenstructure to avoid divisions by zero.

The extension to model plasticity required additional terms to be evaluated. These pose a difficulty to the existing algorithm since the relaxation terms can vary from zero to infinity. However analysis of the model revealed that in the latter limit the system can be approximated well by the simpler compressible Euler equations, and that a simple reformulation yields a mapping between both systems. Application of straightforward temporal splitting is valid in this case as a result of these modifications. Thus the existing methods developed for the homogeneous reduced system of non-linear elasticity needed no further modification and are solved as before using explicit time integration. The addition therefore due to plasticity is a subsequent time integration of the relaxation terms. In this second step the relaxation terms are updated implicitly to overcome numerical stiffness when the relaxation time becomes small in comparison to the employed global timestep dictated by the characteristic speeds.

Simple functions for the relaxation time were taken that result in strain-rate dependency of the flow stress. The form chosen is representative of the types of models that can be used to obtain physically realistic results. In addition, the particular form, a power law function, provided a rigorous test of the time integration methods. This strain on the methods was further amplified by using the model to approximate ideal plasticity. Using this assumption one-dimensional test were conducted simulating plate impact experiments. The processes involved moderate to high strain-rates. In the numerical calculations the discretisation parameters were underresolved, yet the scheme successfully provided results qualitatively comparable to other results reported in the literature. The scheme was also applied to examples in two- and three-dimensions. In these cases the constants entering into the consti-

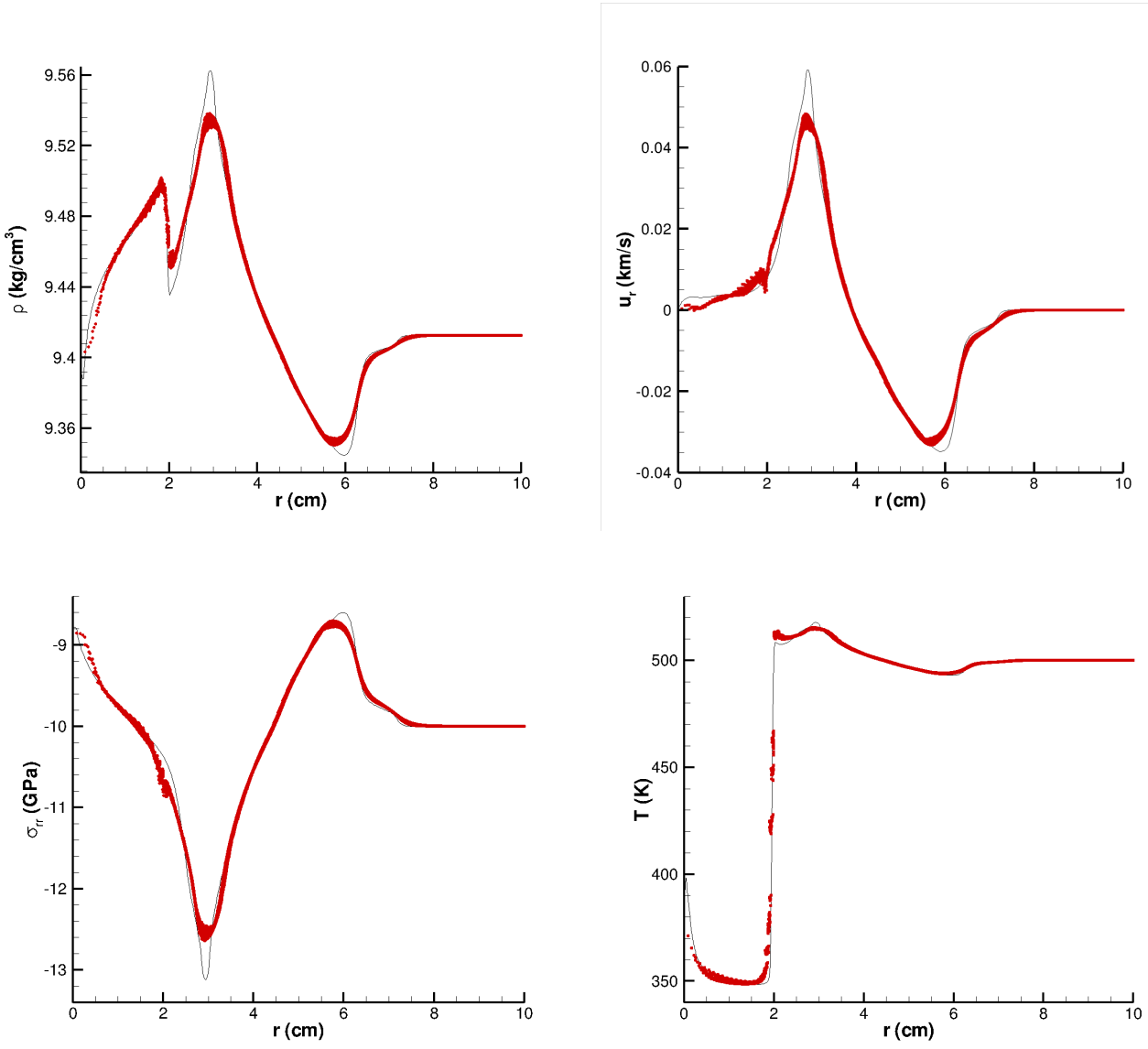

Figure 3.7: Scatter graph comparison of three-dimensional cartesian (points) and one-dimensional spherical (solid line) solutions of the testcase in § 3.5.3 at a time $t = 10\,\mu s$. Cartesian results were obtained with a uniform grid spacing $\Delta x = \Delta y = \Delta z = 1/10$ cm and using $\mathscr{C} = 0.6$.

tutive equations were taken from the literature where they were derived based upon best match with experimental data. The tests were cylindrically and spherically symmetric respectively, and in both cases symmetry was preserved by the Cartesian solver when compared to one-dimensional polar calculations.

4

An Eulerian method for multi-component problems with sliding interfaces[†]

Synopsis

This chapter is devoted to developing a multimaterial numerical scheme for non-linear elastic solids, with emphasis on the inclusion of interfacial boundary conditions. In particular for colliding solid objects it is desirable to allow large deformations and relative slide, whilst employing fixed grids and maintaining sharp interfaces. This is achieved by extending interface tracking methods for gas dynamics to solid mechanics, by using the model for elastic materials in conservative form. Interface interactions are captured using the solution of a multi-material Riemann problem which is derived in detail. Several different boundary conditions are considered including solid/solid and solid/vacuum contact problems. The underlying single material numerical method includes the characterstic based Riemann solver and high-order WENO reconstruction previously detailed. Numerical solutions of example multi-material problems are provided in comparison to exact solutions for the one-dimensional augmented system, and for a two-dimensional friction experiment.

4.1 Introduction

In the previous chapters a high–order shock capturing scheme was proposed for solid dynamics where Godunov's method was applied to an Eulerian model [28] in conservative form using fixed Cartesian grids. It is the purpose of this chapter to explore certain methods to be used in conjunction with these schemes to enable the solution of systems comprising multiple components.

Recall from Chapter 1 that when interfaces of two solid materials come into contact two limits can be identified for the resulting behaviour: *stick* where both the traction and velocity vectors of each material normal to the common interface are equal; *slip* where tangential components of the traction normal to the interface are

[†]Much of the work in this chapter was presented in [5]: **P.T. Barton** & D. Drikakis, An Eulerian method for multi-component problems in non-linear elasticity with sliding interfaces, *under review* (2009).

zero and the components slide freely over one another. In reality, for high velocity impacts the behaviour will lie somewhere in between these two limits [88], with the tangential motion a complex non-linear function of the interfacial state. An accurate numerical scheme for modelling such processes must incorporate an interface tracking method where the boundary evolution reflects the motion dictated by the physics. That is it allows unconstrained sliding between components. From the various interface tracking methods, these requirements single out the level-set, marker particle, and moving grid methods. VOF methods on the other hand require a common velocity vector between interacting components within mixed cells. The next question then is how to incorporate these within the established numerical scheme and more importantly how to account for the interaction between components.

In the moving grid method the governing equations are recast into a moving generalised coordinate system and, since the new form remains conservative, requires little modifications to the established single component numerical methods. The method assumes that for all time the interface location coincides with the grid cell edges at the limits of the computational mesh. In general then each material will be solved on an independent grid. When two materials or grids are in contact, or at free surfaces, a multi-material Riemann problem can be solved for each boundary edge, the solution of which is used not only to determine the numerical fluxes across that boundary, but also to prescribe the interface motion. For interior cells the edge velocities are taken as an extrapolation of the values at the boundaries. Doing so ensures grid quality is maintained. The use of a moving computational grid in this way is similar to simplified arbitrary Lagrangian Eulerian (SALE) methods, but differs in the use of an underlying cell centred Godunov method. Moving grid methods of these specifics are comparably less commonly used, but have been used in conjunction with an alternative formulation for elastoplastic solid materials on quadrilateral grids in [80] for the study of impacting solids.

Another interesting approach is that classed as the ghost fluid method (GFM), proposed in the pioneering work in [19], as a means of treating interface interactions. The method assumes that one can identify, using for example level-set functions, those cells directly adjacent to and enclosing the interface. For each time iteration, the interface location is used to distinguish cells within each material's domain and those that are not; the latter are termed *ghost cells*. The ghost cells are then prescribed a state in such a way that, when each material is advanced to the next time level using an independent single component solver, the presence and resulting behaviour of material interfaces and their interactions are then captured. In [19] the ghost cell states are defined based upon the overlying state of the adjacent fluid and the boundary extrapolated entropy. In [44] it was proposed that solutions to the resulting multi-material Riemann problem at interfaces could be used to define the ghost cell states in what has become known as the modified ghost fluid method (MGFM). An immediate advantage of the ghost cell approach in general

is that no additional terms enter into the governing physical equations and for the most part each material is treated independently. Furthermore, the integral form of the governing equations need not be limited to the time dependent domain for each material; thus one need only consider flux functions for cell boundaries as per a single component solver. Ghost fluid type methods have been used in conjunction with an alternative formulation for solid materials in [75] for the study of impacting solids; in conjunction with a Lagrangian solid mechanics method in [20] to form a coupled solid/fluid scheme; and for solid/fluid problems in [45] utilising the compressible Euler equations with equations of state that enable simplified elastic-plastic response. Ghost fluid type methods have yet to be applied to any of the aforemention models for solid dynamics in conservative form.

The ghost fluid type methods are contrary to conservative methods such as in [49, 32] where the integral form of the governing equations is solved for each material's (time dependent) region. The resulting finite volume numerical scheme thus requires reconstruction of the interface for calculation of cell apertures and volume fractions within mixed cells. Such methods have been successfully applied to the aforementioned models in conservative form, including in [49] where the VOF method is used in a coupled solid/fluid scheme, and in [83, 84, 85] where marker particles are used to track boundaries in the simulation of impacting solid materials. Although conservation is a desirable property it is recalled that only the level-set or marker particle method would accommodate the requirements for sliding material interfaces. Between these, extension of the level-set methods to multiple space dimensions is more straightforward, but are non-conservative by default. Using level-set functions to track interfaces in a conservative scheme such as in [32] could lead to difficulties in solid dynamics problems on account of mass loss, but is nonetheless worth considering as continuous improvements are made in mass conservation through improving the employed numerical tools for solving the level-set fields.

The purpose of this chapter is, by using the conservative model of non-linear elasticity, to modify the single component numerical scheme to incorporate each of the following multi-material methods:

- the moving grid method,
- the modified ghost fluid method,
- a conservative level-set method.

In Chapter 3 it was shown that the inhomogeneous system of elastoplastic solids can be solved using time operator splitting, thus requiring no change to the underlying solution of the equations for non-linear elasticity. Furthermore, since plastic deformations are volume preserving, the plastic update has no influence on the boundary evolution in this approach. Hence only the equations for elasticity need be considered.

The rest of the chapter proceeds as follows. In § 4.2 the necessary theory is presented for non-linear elastic materials in a new moving coordinate system for and the moving grid scheme for the model is detailed; § 4.3 presents the MGFM for solid materials; in § 4.4 a conservative level-set scheme is proposed. In each of these sections emphasis is placed on the modifications to the numerical scheme and method of boundary evolution. § 4.5 is devoted to a detailed derivation of the Riemann problem solution for multi-materials, with focus on the characteristic relations and the applicable boundary conditions. The numerical schemes are compared to exact solutions in § 4.6 for a series of tests using different interfacial boundary conditions and/or materials; furthermore the MGFM method is applied to a two-dimensional dynamic-friction testcase. Finally conclusions are drawn in § 4.7.

4.2 The moving grid method

The model for elastoplastic materials in a generalised moving coordinate system $\xi_i = \xi_i(x_k, t)$ can be written in the following matrix form (see Appendix C):

$$\frac{\partial \overline{\mathbf{U}}}{\partial t} + \frac{\partial \overline{\mathscr{F}}^i}{\partial \xi_i} = -\overline{\mathbf{S}}^{\mathrm{C}} - \overline{\mathbf{S}}^{\mathrm{P}} \tag{4.1}$$

where

$$\overline{\mathbf{U}} := J \begin{pmatrix} \rho \mathbf{u} \\ \rho \mathbf{F}^{\mathrm{T}} \mathbf{e}_1 \\ \rho \mathbf{F}^{\mathrm{T}} \mathbf{e}_2 \\ \rho \mathbf{F}^{\mathrm{T}} \mathbf{e}_3 \\ \rho E \end{pmatrix}, \qquad \overline{\mathscr{F}}^i := J \begin{pmatrix} \rho \mathbf{u} \widehat{u}_k - \widehat{\sigma} \mathbf{e}_k \\ \rho \mathbf{F}^{\mathrm{T}} \mathbf{e}_1 \widehat{u}_k - u_1 \rho \widehat{\mathbf{F}}^{\mathrm{T}} \mathbf{e}_k \\ \rho \mathbf{F}^{\mathrm{T}} \mathbf{e}_2 \widehat{u}_k - u_2 \rho \widehat{\mathbf{F}}^{\mathrm{T}} \mathbf{e}_k \\ \rho \mathbf{F}^{\mathrm{T}} \mathbf{e}_3 \widehat{u}_k - u_3 \rho \widehat{\mathbf{F}}^{\mathrm{T}} \mathbf{e}_k \\ \rho E \widehat{u}_k - \mathbf{e}_k^{\mathrm{T}} \cdot (\widehat{\sigma} \mathbf{u}) \end{pmatrix},$$

with

$$\widehat{u}_i := \frac{\partial \xi_i}{\partial x_k}(u_k - \mu_k), \qquad \widehat{\sigma}_{ij} := \sigma_{jk} \frac{\partial \xi_i}{\partial x_k}, \qquad \widehat{F}_{ji} := F_{kj} \frac{\partial \xi_i}{\partial x_k}. \tag{4.2}$$

Here $\mu_k := \partial x_k / \partial \tau$ is the grid velocity vector.

The relative changes in the eigenvalues and eigenvectors from § 3.3 shall not be repeated here and instead are left to Appendix D.

The governing model is solved over a time-dependent, structured computational grid, where cell centred quantities are denoted by the indices i and cell boundary values by $i \pm 1/2$. Each cell can be defined as $I_i(t) := [x_{i+1/2}(t), x_{i-1/2}(t)]$ with the dimensions $(\Delta x)_i(t) = x_{i+1/2}(t) - x_{i-1/2}(t)$. The strategy is employed whereby each material or component occupies a different grid. For each grid, spatially averaged states of the respective material are stored at cell centres [cf. Eq. (2.56)]. It is noted that only grid coordinates are stored at cell nodes.

The system Eq. (4.1) is solved numerically for each material, denoted by α, according to the following finite-volume discretisation:

$$\frac{\mathrm{d}}{\mathrm{d}t}\overline{\mathbf{U}}_i^{\alpha}(t) = \frac{\overline{\mathscr{F}}\left(\widetilde{\mathbf{U}}_{i+1/2}^{\alpha}\right) - \overline{\mathscr{F}}\left(\widetilde{\mathbf{U}}_{i-1/2}^{\alpha}\right)}{(\Delta\xi)_i}. \tag{4.3}$$

The numerical fluxes are predicted using the approximate solution of a local Riemann problem at each cell edge. The Riemann problem solution is found using the characteristics based method proposed in Chapter 2.

For each time step the required intercell velocity at the grid boundaries is taken to be the normal velocity predicted by the multi-material Riemann problem solution. In a multi-dimensional problem the interior cell edge velocities can be determined by redistributing the nodes using as boundary conditions the new boundary node locations and solving a suitable grid generation algorithm (see [22]). In one dimension however, the determination of interior intercell velocities is greatly simplified, and instead these are taken to be a linear extrapolation of the CM/MD boundary values. It will be assumed that only one boundary, that which is in contact with another material in the two material problems to be considered, will move. The other shall remain fixed. Thus the extrapolated inter-cell velocities for interior cells is taken to be:

$$\mu_{i\pm1/2} = u_{\mathrm{B}}\frac{|x_{\mathrm{E}} - x_{i\pm1/2}|}{|x_{\mathrm{E}} - x_{\mathrm{B}}|}, \tag{4.4}$$

where x_{E} is the node at the opposite end of the grid to the multi-material boundary denoted by x_{B}. In this way the grid for each material is assumed to be anchored at that end opposite the multi-material boundary, with the latter allowed to move freely at the prescribed velocity. At the end of each time step each cell is then moved at the velocity Eq. (4.4) according to:

$$\frac{\mathrm{d}x_{i\pm1/2}}{\mathrm{d}t} = \mu_{i\pm1/2}. \tag{4.5}$$

Note that increased accuracy in time integration of Eq. (4.3) and Eq. (4.5) is achieved using the third-order TVD RK method Eq. (2.57).

4.3 The modified ghost fluid method

Although the ghost fluid type methods employed for multiple interacting materials are applicable to any of the interface tracking techniques, for the reasons mentioned in § 4.1 level-set functions are used. For a system comprising multiple materials, each component, denoted by α, is assumed to occupy the region $\Gamma^{\alpha}(t)$. In the course of the computation each region is identifyable by defining a level-set function, $\phi^{\alpha}(x,t)$, that

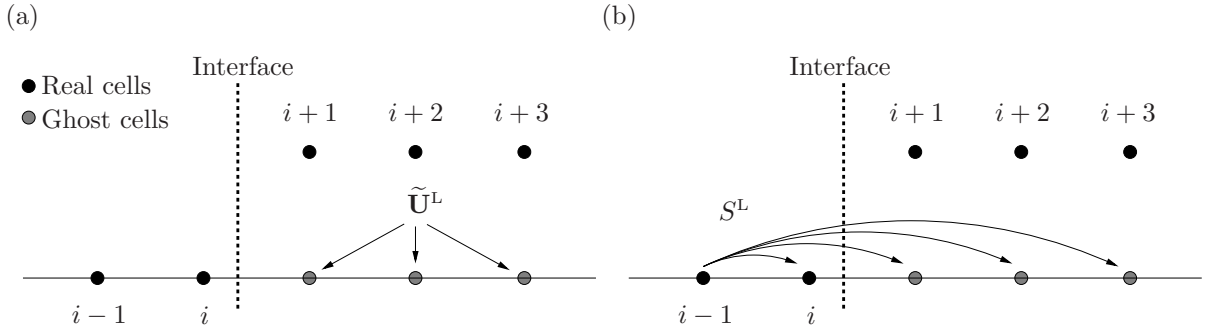

Figure 4.1: Illustration of the modified ghost fluid method; (a) the prescription of ghost cell states for a material to the left of the interface using the solution $\widetilde{\mathbf{U}}^{\mathrm{L}}$ of the multimaterial Riemann problem; (b) the entropy fix.

at every point in space and time represents the signed Euclidean distance from the interface. Thus the zero isocontour of ϕ^α marks the location of a material interface, $\partial\Gamma^\alpha(t) = \{x : \phi^\alpha(x) = 0\}$, while a positive value distinguishes those regions occupied by the corresponding medium, and a negative value those that are not. For each material then

$$\phi^\alpha\,(x,\,t)\begin{cases} > 0,\ x \in \Gamma^\alpha(t), \\ = 0,\ x \in \partial\Gamma^\alpha(t), \\ < 0,\ x \notin \Gamma^\alpha(t). \end{cases} \tag{4.6}$$

In fact, one need only employ $N-1$ level-set functions for a system of N materials.

It is assumed a computational mesh is employed where cell centred quantities are denoted by the indices i and cell boundaries by $i \pm 1/2$; thus each cell is denoted $I_i := [x_{i-1/2}, x_{i+1/2}]$ and has the size $(\Delta x)_i = x_{i+1/2} - x_{i-1/2}$. Space averages of the state variables, and values of the level-set functions at the current time level t^n, are stored at cell centres. For an interface located between grid points i and $i+1$ (Figure 4.1(a)), identifiable by $\phi_i \cdot \phi_{i+1} > 0$, the material to the left of the interface has the set of ghost cells $\{I_{i+1}, I_{i+2}, \ldots, I_{i+N_f+1}\}$ where N_f denotes the number of fictitious points required by the numerical stencil for the employed single component solver. The known states $\mathbf{U}^{\mathrm{L}} = \mathbf{U}(x_i, t^n)$ and $\mathbf{U}^{\mathrm{R}} = \mathbf{U}(x_{i+1}, t^n)$ at the current time level for the left and right materials respectively can be used to pose a multimaterial Riemann problem across the interface. The solutions $\widetilde{\mathbf{U}}^{\mathrm{L/R}}$, found using the proceedure to be explained in detail next, are used to define the state of the respective material's ghost cell immediately adjacent to the boundary. In fact all other ghost cells are also taken to have the extrapolated predicted state. Thus, for every cell designated as a ghost cell for either material the real material and ghost material states are stored.

Having defined the ghost cell states the governing equations for each material are solved independently for the next time level. For each material a solution is sought only for real cells and the ghost cells immediately adjacent to boundaries. Using the method-of-lines approach for the governing transport equations Eq. (2.22) the discretised system for the material α reads:

$$\frac{\mathrm{d}}{\mathrm{d}t}\mathbf{U}_i^\alpha(t) = -\frac{\mathscr{F}\left(\widetilde{\mathbf{U}}^\alpha(x_{i+1/2})\right) - \mathscr{F}\left(\widetilde{\mathbf{U}}^\alpha(x_{i-1/2})\right)}{(\Delta x)_i}. \tag{4.7}$$

For each solid component the method presented in Chapter 2 is used for predicting the numerical flux functions; the 5th-order monotonicity preserving weighted essentially non-oscillatory (MPWENO-5) method is used to reconstruct characteristic variables.

The interface evolves according to the level-set convection equation

$$\frac{\partial \phi^\alpha}{\partial t} + u_\eta \frac{\partial \phi^\alpha}{\partial x} = 0, \tag{4.8}$$

which is also solved using the method-of-lines; spatial derivatives are discretised using the 5th-order central scheme in [54] and time integration is performed using the same 3rd-order TVD RK method as for the material equations.

In both the computations of the material equations and the boundary evolution equation the temporal updates using the RK method are performed harmoniously for each sub-stage. The reason being is that the interface interaction calculation is carried out for each sub-stage for those cells that enclose the interface and from which the time-local interface velocity can be used in Eq. (4.8) for a more accurate overall boundary advection. For the considered one-dimensional cases, away from the interface, where velocities for the coresponding iso-contours are unknown, the interface velocity can be extrapolated to all cells. This ensures that the level-set function at each point satisfies the Eikonal equation $\mid \nabla\varphi \mid = 1$, that is it remains a signed distance function.

It is mentioned that level-set methods are by default non-conservative and spurious conservation errors can occur, in particular for multi-dimensional problems. One cause is that for multi-dimensional problems the boundary extrapolated velocity does not necessarily correspond exactly to the velocities for each isocontour paramount to ensuring that ϕ remains a signed-distance function. Reinitialisation algorithms (see for example [70, 54]) are thus required incrementally to reinstate this property. Problems also arise where the described geometry develops thin ligaments or has corners where characteristics converge (see for example [17]). However for the one-dimensional examples considered here mass conservation errors are found to be negligible on account of using the above described numerical methods.

An anomaly observed in gas-dynamics that can degrade the resolution of problems with interfaces is the so called 'heating' errors. These errors appear as deviations from the true solution in certain state variables, such as density and entropy, in the vicinity of the interface. In [19] a simple and effective fix was proposed for this problem in conjunction with the original ghost fluid method: for a material to the left of an interface located between cells I_i and I_{i+1}, the real cell I_i immediately adjacent to the boundary takes the value of entropy from the cell I_{i-1}. The fix applied to the right material follows by symmetry. With the fix carried out prior to the interface interaction computation the value of entropy from cell I_{i-1} is also prescribed to the ghost cells since $\partial\mathscr{S} = 0$ at the boundary. This concept is illustrated in Figure 4.1(b). In the examples to follow, the extent to which the entropy fix supresses heating errors shall be investigated for problems in solid mechanics.

4.3.1 Multi-dimensional implementation

The order of proceedings for the MGFM implemented in multidimensions does not depart from the one-dimensional case, rather certain components of the method become slightly more involved. In the first instance, boundary cells can be identified by checking for sign changes in the level-set functions as with the one-dimensional approach, only now this check is performed in each coordinate direction. The main difficulty one faces in implementing the MGFM in multi-dimensions is how to define the left and right states for the Riemann problem initial conditions. Whereas in one-dimension the interface lies normal to the Cartesian axis along which the solution is sought, and intersects some point between two adjacent cell centres, in multi-dimensions it is quite likely that the interface may lie at some arbitrary angle to these axis. Consider the case where a ghost cell state is sought for Solid 1 that is in contact with Solid 2. Ideally, when solving the Riemann problem in a given ghost cell immediately adjacent to the boundary (from hereon named *boundary ghost cells*) for Solid 1, one would like to have knowledge of the state extrapolated in a sensible way from the neighbouring real cells (from hereon named *boundary real cells*). In order to facilitate this approach, any state quantity q of Solid 1 can be extrapolated from the boundary real cells along the interface normal trajectory by solving to steady state the following PDE [19]:

$$\frac{\partial q}{\partial \tau} \pm n_k \frac{\partial q}{\partial x_k} = 0, \tag{4.9}$$

where τ is fictitious time, the $\pm$ operator is used to define the direction of extrapolation, and $\mathbf{n}$ is the unit normal to the level-set isocontour:

$$\mathbf{n} = \frac{\nabla\phi}{|\nabla\phi|}. \tag{4.10}$$

Thus, within the boundary ghost cells of Solid 1, one can obtain the extrapolated state of Solid 1, $\mathbf{U}^{\mathrm{S1,\,EXT}}$, and has the underlying real state of Solid 2, $\mathbf{U}^{\mathrm{S2}}$. To account for the arbitrary angle of the interface with respect to the Cartesian axis, the state variables for both materials within the boundary ghost cells must be rotated onto the coordinate system defined by the interface normal. This can be easily achieved by using the local interface normal computed from the level-set field (using Eq. (4.10)) to define a rotation matrix $\mathbf{R}^{\mathrm{ROT}} = \mathbf{R}^{\mathrm{ROT}}(\mathbf{n})$ (see [49]) and subsequently rotating the velocity and deformation tensor as follows:

$$\begin{pmatrix} \mathbf{u} \\ \mathbf{F} \\ S \end{pmatrix}^{\mathrm{ROT}} = \begin{pmatrix} \mathbf{R}^{\mathrm{ROT}}\mathbf{u} \\ \mathbf{R}^{\mathrm{ROT}}\mathbf{F}\mathbf{R}^{\mathrm{ROT^T}} \\ S \end{pmatrix} \tag{4.11}$$

The initial conditions for the Riemann problem thus become: $\mathbf{U}^{\mathrm{L}} = (\mathbf{U}^{\mathrm{S1,\,EXT}})^{\mathrm{ROT}}$ and $\mathbf{U}^{\mathrm{R}} = (\mathbf{U}^{\mathrm{S2}})^{\mathrm{ROT}}$. The subsequent components of the method then follow the one-dimensional proceedure. Once the solution has been computed one need only rotate the resultant state back to the Cartesian coordinate system using the inverse of Eq. (4.11).

The implementation of the MGFM in multi-dimensions can be summarised as follows:

Step 1: Using the level-set field(s) at the current timelevel, all real cells and those cells that can be classified as ghost cells, based upon the previously described criteria, are distinguished for computation.

Step 2: For each material, the state of boundary real cells is extrapolated along the interface normal trajectory to all boundary ghost cells. Also, if the entropy fix is being used this can be incorporated into the same extrapolation routine at this stage.

Step 3: A multi-material Riemann problem is solved within all boundary ghost cells using the extrapolated states and, for the case of solid/solid contact problems, the underlying real state of the adjacent material, rotated normal to the interface. The solution (rotated back to the Cartesian coordinate system) is subsequently extrapolated to all other ghost cells.

Step 4: One is then free to use the chosen numerical scheme for single component problems to update each material independently to the next timelevel. In general this involves solving for each cell within the computational domain regardless of whether it is a real cell or a ghost cell. In practice however one need only solve for those real cells and a narrow band of boundary ghost cells surrounding the material.

Step 5: The level-set field(s) are then updated to the next timelevel using as the velocity vector at each point the extrapolated interface velocities determined from solution of the boundary Riemann problems. After the updated level-set field(s) have been obtained, each is reinitialised to ensure compliance with the Eikonal condition.

Steps 1-5 are repeated for each timelevel in the computation.

4.4 The conservative level-set method

It is assumed that each component, denoted α, in a multi-component system is governed by an individual system of conservation laws, which in matrix form can be written:

$$\frac{\partial \mathbf{U}^\alpha}{\partial t} + \frac{\partial \mathscr{F}^{k^\alpha}}{\partial x_k} = 0, \tag{4.12}$$

where $\mathbf{U}^\alpha$ is the vector of conserved variables, $\mathscr{F}^{k^\alpha}$ the convective fluxes functions. In the same way as Eq. (4.6) the region $\Gamma^\alpha(t)$ can be defined for each component that is occupied by that material, using level-set functions. In the numerical scheme Eq. (4.12) is solved on a fixed, structured computational grid with cell centres denoted by i. Each cell has the dimensions $(\Delta x_1)_i = x_{1_{i+1/2}} - x_{1_{i-1/2}}$, where $i \pm 1/2$ denote the cell boundaries. Within each cell a control volume can be formed, the volume, $\mathscr{V}_i^\alpha$, of which will depend upon $\Gamma^\alpha(t)$; for full cells $\mathscr{V}_i^\alpha = (\Delta x_1)_i$. Integrating Eq. (4.12) over the region $\Gamma^\alpha(t)$ on the computational grid and applying Gauss's theorem gives:

$$\left(\frac{\partial \mathscr{V}\mathbf{U}}{\partial t}\right)_i^\alpha + \mathscr{F}_{i+1/2}^\alpha - \mathscr{F}_{i-1/2}^\alpha + \mathscr{F}_i^{\mathrm{B}^\alpha} = 0. \tag{4.13}$$

The numerical fluxes across the interface

$$\mathscr{F}^{\mathrm{B}} := -N_1 \begin{pmatrix} \sigma \mathbf{e}_1 \\ u_1 \mathbf{F}^{\mathrm{T}} \mathbf{e}_1 \\ u_2 \mathbf{F}^{\mathrm{T}} \mathbf{e}_2 \\ u_3 \mathbf{F}^{\mathrm{T}} \mathbf{e}_3 \\ \mathbf{u}^{\mathrm{T}}(\sigma \mathbf{e}_1) \end{pmatrix}, \tag{4.14}$$

where N_1 is the interface normal computed from the level-set field: $\mathbf{N} = \nabla\phi/|\nabla\phi|$, are computed only in mixed cells from the solution of a multi-material Riemann problem to be described next.

A difficulty faced by any conservative tracking method on fixed grids is the possibility of small cut cell regions occurring and thus limiting the timestep in accordance with the CFL condition. One solution is to merge the data in these cells with neighbouring full cells. In [32] a clever means of achieving this was proposed: all cells

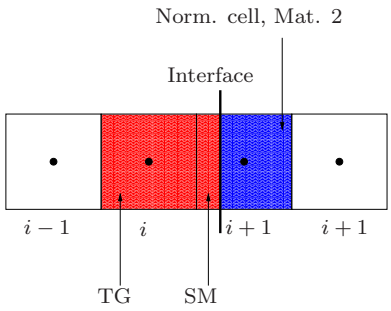

Figure 4.2: Illustration the conservative method; merging of small cells with adjacent normal cells for left material (red) and right material (blue).

are updated as normal regardless of their volume fraction; at the end of each time update, for each material, the solution in the nearest full cell to the boundary, called the target cell (Figure 4.2), is subjected to the following correction:

$$(\mathscr{V}\mathbf{U})^{n+1}_{\mathrm{TG}} = (\mathscr{V}\mathbf{U})^{*}_{\mathrm{TG}} - \frac{(\mathscr{V}\mathbf{U})^{*}_{\mathrm{TG}}\mathscr{V}^{n+1}_{\mathrm{SM}} - (\mathscr{V}\mathbf{U})^{*}_{\mathrm{SM}}\mathscr{V}^{n+1}_{\mathrm{TG}}}{\mathscr{V}^{n+1}_{\mathrm{TG}} + \mathscr{V}^{n+1}_{\mathrm{SM}}}, \tag{4.15}$$

where $(\mathscr{V}\mathbf{U})_{\mathrm{TG}}$ and $(\mathscr{V}\mathbf{U})_{\mathrm{SM}}$ denote the solutions in target and small/empty cells respectively; and $(\mathscr{V}\mathbf{U})^{*}$ is the solution at the end of the timestep (or sub-step) prior to the correction. Following this, the updated state in target cells, $\mathbf{U}^{n+1}_{\mathrm{TG}}$, is extrapolated to the adjacent small cells. It is mentioned that for each material, 'small' cell actually refers to any cell with a volume fraction of less than half, or empty cells that may be occupied after the next time update. The generation of material within, or emptying of cells is thus accommodated automatically.

Similar to the modified ghost fluid method discussed in the previous section, in order to facilitate the use of the high-order scheme throughout the domain occupied by each component, all cells outside and not treated in some way already according to the above are given a state so as to complete the stencil of the reconstruction method when solving near the boundary. This is taken to be the state of the full cell immediately inside the boundary.

The level-set equation Eq. (4.8) is again used to advect the material boundaries as in the MGFM, and in harmony with temporal updates of the physical equations. For the conservative method, each sub step is slightly more involved since one must also compute new values of the volume fractions after the level-set functions are updated, and carry out the mass correction proceedure.

4.5 Multi-material Riemann problems

The multi-material Riemann problem details depend on the materials on either side of the interface, which could be solid or vacuum, and the orientation with respect

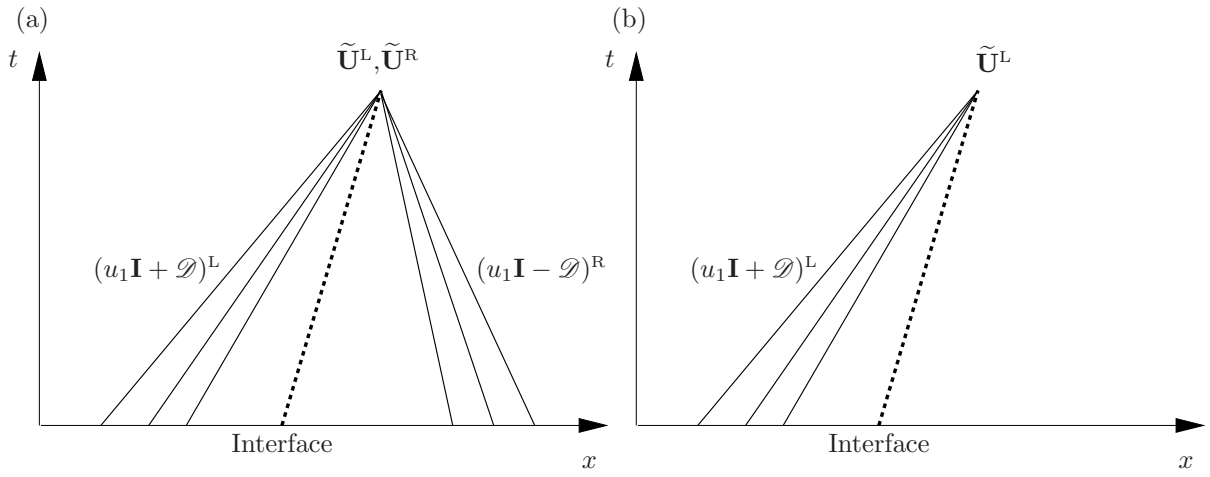

Figure 4.3: x-t plots of example multi-material Riemann problem solutions for (a) solid on left in contact with another solid on right and (b) solid on left in contact with a vacuum.

to the interface of the material for which the solution is sought. Sample solutions are depicted in Figure 4.3. Where appropriate, any corresponding state quantity shall be identifiable by superscript L or R for left and right materials respectively. Emphasis shall be placed on the solution for the left hand material, but it is found that the solution for the converse differs only by sign on certain terms and these shall be identified clearly.

For each solid material, the following thirteen invariant relations can be written:

$$\mathbf{\Phi}^{\mathrm{L/R}} := \mathbf{L}^{\mathrm{L/R}} \cdot \partial \mathbf{W}^{\mathrm{L/R}} = 0. \tag{4.16}$$

Recall that the rows of $\mathbf{L}^{\mathrm{L/R}}$ are the left eigenvectors of the linearised Jacobian matrix Eq. (3.9) and correspond to the wavespeeds with canonical ordering. For the left material of the multi-material Riemann problem one can utilise the invariants corresponding to the three non-linear waves with speeds $u_1\mathbf{I}+\mathscr{D}$ and contact: $\mathbf{\Phi}_j,\ 4 \leq j \leq 13$. Partial derivatives in each of these relations can be replaced with differences according to

$$\partial \mathbf{W}^{\mathrm{L}} \approx \Delta \mathbf{W}^{\mathrm{L}} := \widetilde{\mathbf{W}}^{\mathrm{L}} - \mathbf{W}^{\mathrm{L}}, \tag{4.17}$$

where $\widetilde{\mathbf{W}}^{\mathrm{L}}$ denotes the primitive state of the left hand material at the interace, and $\mathbf{W}^{\mathrm{L}}$ is the state at the current time level just inside the boundary. For the moving grid method $\mathbf{W}^{\mathrm{L}}$ would be taken as the state in the respective boundary cell; for the MGFM method for an interface located between cells I_i and I_{i+1} can be taken to be $\mathbf{W}^{\mathrm{L}} = \mathbf{W}(\mathbf{U}_i)$ (and $\mathbf{W}^{\mathrm{R}} = \mathbf{W}(\mathbf{U}_{i+1})$); for the conservative level-set method

will be the state within the mixed cell. The linearised coefficients are also taken to be evaluated from these states for each respective material. Thus, for each solid at the boundary one has ten relations for the thirteen unknowns; consideration of the boundary conditions is required to yield the additional relations.

It is usual in solid mechanics problems to prescribe the interfacial boundary conditions in terms of restrictions on the interface velocities $\widetilde{\mathbf{u}}$, and/or the traction $\widetilde{\sigma}\mathbf{e}_n$, where $\mathbf{e}_n$ is the normal to the interface ($\mathbf{e}_n = \mathbf{e}_\eta$ for the one-dimensional case in the η-direction). It will be seen that the number of boundary conditions must necessarily coincide with the number of non-linear waves. From Eq. (2.5) and since $\mathscr{E} = \mathscr{E}(\mathbf{F}, \mathscr{S})$ stress is a function of $\mathbf{F}$ and $\mathscr{S}$. The traction at the boundary can be approximated by a power series around the state $(\mathbf{F}^{\mathrm{L/R}},\ \mathscr{S}^{\mathrm{L/R}})$ inside the boundary:

$$\begin{aligned}\sigma_{\eta i}(\widetilde{\mathbf{F}}^{\mathrm{L/R}},\ \widetilde{\mathscr{S}}^{\mathrm{L/R}}) \ =\ & \sigma_{\eta i}(\mathbf{F}^{\mathrm{L/R}},\ \mathscr{S}^{\mathrm{L/R}}) + \frac{\partial \sigma_{\eta i}}{\partial F_{jk}}(\mathbf{F}^{\mathrm{L/R}},\ \mathscr{S}^{\mathrm{L/R}})\left[\widetilde{F}_{jk}^{\mathrm{L/R}} - F_{jk}^{\mathrm{L/R}}\right] + \\ & \frac{\partial \sigma_{\eta i}}{\partial \mathscr{S}}(\mathbf{F}^{\mathrm{L/R}},\ \mathscr{S}^{\mathrm{L/R}})\left[\widetilde{\mathscr{S}}^{\mathrm{L/R}} - \mathscr{S}^{\mathrm{L/R}}\right] + \dots \end{aligned} \tag{4.18}$$

Neglecting higher order terms and using the definitions of the coefficients in Eq. (3.10), Eq. (4.18) can be rewritten as

$$\begin{aligned}\widetilde{\sigma}_{\eta i}^{\mathrm{L/R}} \ =\ & \sigma_{\eta i}^{\mathrm{L/R}} + \rho^{\mathrm{L/R}}\left[A_{ik}^{\eta 1}\left(\widetilde{\mathbf{F}} - \mathbf{F}\right)_{1k} + A_{ik}^{\eta 2}\left(\widetilde{\mathbf{F}} - \mathbf{F}\right)_{2k} + \right. \\ & \left. A_{ik}^{\eta 3}\left(\widetilde{\mathbf{F}} - \mathbf{F}\right)_{3k} + b_i^{\eta}\left(\widetilde{\mathscr{S}} - \mathscr{S}\right)\right]^{\mathrm{L/R}}. \end{aligned} \tag{4.19}$$

Thus combining Eq. (4.19) with the applicable invariants gives thirteen equations for sixteen unknowns:

$$\hat{\mathbf{L}}^{\mathrm{L/R}}\left[\begin{pmatrix} \widetilde{\mathbf{u}} \\ \widetilde{\mathbf{F}}^{\mathrm{T}}\mathbf{e}_1 \\ \widetilde{\mathbf{F}}^{\mathrm{T}}\mathbf{e}_2 \\ \widetilde{\mathbf{F}}^{\mathrm{T}}\mathbf{e}_3 \\ \widetilde{\mathscr{S}} \end{pmatrix}^{\mathrm{L/R}} - \begin{pmatrix} \mathbf{u} \\ \mathbf{F}^{\mathrm{T}}\mathbf{e}_1 \\ \mathbf{F}^{\mathrm{T}}\mathbf{e}_2 \\ \mathbf{F}^{\mathrm{T}}\mathbf{e}_3 \\ \mathscr{S} \end{pmatrix}^{\mathrm{L/R}}\right] - \frac{1}{\rho^{\mathrm{L/R}}}\begin{pmatrix} 0 \\ 0 \\ 0 \\ 0 \\ (\widetilde{\sigma}^{\mathrm{L/R}} - \sigma^{\mathrm{L/R}})\mathbf{e}_\eta \end{pmatrix} = 0 \tag{4.20}$$

where

$$\hat{\mathbf{L}} = (\hat{\mathrm{l}}_1,\ \hat{\mathrm{l}}_2,\ \hat{\mathrm{l}}_3,\ \hat{\mathrm{l}}_4,\ \hat{\mathrm{l}}_5,\ \hat{\mathrm{l}}_6,\ \hat{\mathrm{l}}_7,\ \hat{\mathrm{l}}_8,\ \hat{\mathrm{l}}_9,\ \hat{\mathrm{l}}_{10},\ \hat{\mathrm{l}}_{11},\ \hat{\mathrm{l}}_{12},\ \hat{\mathrm{l}}_{13})^{\mathrm{T}}, \tag{4.21}$$

with

$$\begin{aligned}\hat{\mathrm{l}}_1 =& ((\mathscr{D}\mathbf{Q})_{11},\ (\mathscr{D}\mathbf{Q})_{12},\ (\mathscr{D}\mathbf{Q})_{13},\ \xi Q_{1i}A_{i1}^{\eta 1},\ \xi Q_{1i}A_{i2}^{\eta 1},\ \xi Q_{1i}A_{i3}^{\eta 1},\\ & \xi Q_{1i}A_{i1}^{\eta 2},\ \xi Q_{1i}A_{i2}^{\eta 2},\ \xi Q_{1i}A_{i3}^{\eta 2},\ \xi Q_{1i}A_{i1}^{\eta 3},\ \xi Q_{1i}A_{i2}^{\eta 3},\ \xi Q_{1i}A_{i3}^{\eta 3},\ \xi Q_{1i}B_i^{\eta}),\\ \hat{\mathrm{l}}_2 =& ((\mathscr{D}\mathbf{Q})_{21},\ (\mathscr{D}\mathbf{Q})_{22},\ (\mathscr{D}\mathbf{Q})_{23},\ \xi Q_{2i}A_{i1}^{\eta 1},\ \xi Q_{2i}A_{i2}^{\eta 1},\ \xi Q_{2i}A_{i3}^{\eta 1},\\ & \xi Q_{2i}A_{i1}^{\eta 2},\ \xi Q_{2i}A_{i2}^{\eta 2},\ \xi Q_{2i}A_{i3}^{\eta 2},\ \xi Q_{2i}A_{i1}^{\eta 3},\ \xi Q_{2i}A_{i2}^{\eta 3},\ \xi Q_{2i}A_{i3}^{\eta 3},\ \xi Q_{2i}B_i^{\eta}),\end{aligned}$$

$$
\begin{aligned}
\hat{\mathbf{l}}_3 =&((\mathscr{D}\mathbf{Q})_{31},\ (\mathscr{D}\mathbf{Q})_{32},\ (\mathscr{D}\mathbf{Q})_{33},\ \xi Q_{3i}A^{\eta 1}_{i1},\ \xi Q_{3i}A^{\eta 1}_{i2},\ \xi Q_{3i}A^{\eta 1}_{i3},\\
&\xi Q_{3i}A^{\eta 2}_{i1},\ \xi Q_{3i}A^{\eta 2}_{i2},\ \xi Q_{3i}A^{\eta 2}_{i3},\ \xi Q_{3i}A^{\eta 3}_{i1},\ \xi Q_{3i}A^{\eta 3}_{i2},\ \xi Q_{3i}A^{\eta 3}_{i3},\ \xi Q_{3i}B^{\eta}_{i}),\\
\hat{\mathbf{l}}_4 =&\mathbf{l}_4, \qquad \hat{\mathbf{l}}_5 =\mathbf{l}_5, \qquad \hat{\mathbf{l}}_6 =\mathbf{l}_6, \qquad \hat{\mathbf{l}}_7 =\mathbf{l}_7,\\
\hat{\mathbf{l}}_8 =&\mathbf{l}_8, \qquad \hat{\mathbf{l}}_9 =\mathbf{l}_9, \qquad \hat{\mathbf{l}}_{10} =\mathbf{l}_{10},\\
\hat{\mathbf{l}}_{11} =&(0,\ 0,\ 0,\ A^{\eta 1}_{11},\ A^{\eta 1}_{12},\ A^{\eta 1}_{13},\ A^{\eta 2}_{11},\ A^{\eta 2}_{12},\ A^{\eta 2}_{13},\ A^{\eta 3}_{11},\ A^{\eta 3}_{12},\ A^{\eta 3}_{13},\ B^{\eta}_{1}),\\
\hat{\mathbf{l}}_{12} =&(0,\ 0,\ 0,\ A^{\eta 1}_{21},\ A^{\eta 1}_{22},\ A^{\eta 1}_{23},\ A^{\eta 2}_{21},\ A^{\eta 2}_{22},\ A^{\eta 2}_{23},\ A^{\eta 3}_{21},\ A^{\eta 3}_{22},\ A^{\eta 3}_{23},\ B^{\eta}_{2}),\\
\hat{\mathbf{l}}_{13} =&(0,\ 0,\ 0,\ A^{\eta 1}_{31},\ A^{\eta 1}_{32},\ A^{\eta 1}_{i3},\ A^{\eta 2}_{31},\ A^{\eta 2}_{32},\ A^{\eta 2}_{33},\ A^{\eta 3}_{31},\ A^{\eta 3}_{32},\ A^{\eta 3}_{33},\ B^{\eta}_{3}).
\end{aligned}
$$

Here $\mathbf{l}_k$ is the k-th left eigenvector of the system in Cartesian coordinates in the η-direction. The parameter $\xi = \pm 1$ has been included in Eq. (4.21) to distinguish the direction of the non-linear waves: $\xi = +1$ if the material is on the left, $\xi = -1$ if on the right. The inverse of Eq. (4.21) is

$$
\hat{\mathbf{R}} = (\hat{\mathbf{r}}_1,\ \hat{\mathbf{r}}_2,\ \hat{\mathbf{r}}_3,\ \hat{\mathbf{r}}_4,\ \hat{\mathbf{r}}_5,\ \hat{\mathbf{r}}_6,\ \hat{\mathbf{r}}_7,\ \hat{\mathbf{r}}_8,\ \hat{\mathbf{r}}_9,\ \hat{\mathbf{r}}_{10},\ \hat{\mathbf{r}}_{11},\ \hat{\mathbf{r}}_{12},\ \hat{\mathbf{r}}_{13}), \tag{4.22}
$$

where

$$
\begin{aligned}
\hat{\mathbf{r}}_1 =&((\mathscr{D}\mathbf{Q})^{-1}_{11},\ (\mathscr{D}\mathbf{Q})^{-1}_{21},\ (\mathscr{D}\mathbf{Q})^{-1}_{31},\ 0,\ 0,0,\ 0,\ 0,\ 0,0,\ 0,\ 0,\ 0)^{\mathrm{T}},\\
\hat{\mathbf{r}}_2 =&((\mathscr{D}\mathbf{Q})^{-1}_{12},\ (\mathscr{D}\mathbf{Q})^{-1}_{22},\ (\mathscr{D}\mathbf{Q})^{-1}_{32},\ 0,\ 0,0,\ 0,\ 0,\ 0,0,\ 0,\ 0,\ 0)^{\mathrm{T}},\\
\hat{\mathbf{r}}_3 =&((\mathscr{D}\mathbf{Q})^{-1}_{13},\ (\mathscr{D}\mathbf{Q})^{-1}_{23},\ (\mathscr{D}\mathbf{Q})^{-1}_{33},\ 0,\ 0,0,\ 0,\ 0,\ 0,0,\ 0,\ 0,\ 0)^{\mathrm{T}},\\
\hat{\mathbf{r}}_4 =&\mathbf{r}_4, \qquad \hat{\mathbf{r}}_5 =\mathbf{r}_5, \qquad \hat{\mathbf{r}}_6 =\mathbf{r}_6, \qquad \hat{\mathbf{r}}_7 =\mathbf{r}_7,\\
\hat{\mathbf{r}}_8 =&\mathbf{r}_8, \qquad \hat{\mathbf{r}}_9 =\mathbf{r}_9, \qquad \hat{\mathbf{r}}_{10} =\mathbf{r}_{10},\\
\hat{\mathbf{r}}_{11} =&(\xi(\mathbf{Q}^{-1}\mathscr{D}\mathbf{Q})^{-1}_{11},\ \xi(\mathbf{Q}^{-1}\mathscr{D}\mathbf{Q})^{-1}_{21},\ \xi(\mathbf{Q}^{-1}\mathscr{D}\mathbf{Q})^{-1}_{31},\ F_{\eta 1}\Omega^{-1}_{11},\ F_{\eta 2}\Omega^{-1}_{11},\\
&F_{\eta 3}\Omega^{-1}_{11},\ F_{\eta 1}\Omega^{-1}_{21},\ F_{\eta 2}\Omega^{-1}_{21},\ F_{\eta 3}\Omega^{-1}_{21},\ F_{\eta 1}\Omega^{-1}_{31},\ F_{\eta 2}\Omega^{-1}_{31},\ F_{\eta 3}\Omega^{-1}_{31},\ 0)^{\mathrm{T}},\\
\hat{\mathbf{r}}_{12} =&(\xi(\mathbf{Q}^{-1}\mathscr{D}\mathbf{Q})^{-1}_{12},\ \xi(\mathbf{Q}^{-1}\mathscr{D}\mathbf{Q})^{-1}_{22},\ \xi(\mathbf{Q}^{-1}\mathscr{D}\mathbf{Q})^{-1}_{32},\ F_{\eta 1}\Omega^{-1}_{12},\ F_{\eta 2}\Omega^{-1}_{12},\\
&F_{\eta 3}\Omega^{-1}_{12},\ F_{\eta 1}\Omega^{-1}_{22},\ F_{\eta 2}\Omega^{-1}_{22},\ F_{\eta 3}\Omega^{-1}_{22},\ F_{\eta 1}\Omega^{-1}_{32},\ F_{\eta 2}\Omega^{-1}_{32},\ F_{\eta 3}\Omega^{-1}_{32},\ 0)^{\mathrm{T}},\\
\hat{\mathbf{r}}_{13} =&(\xi(\mathbf{Q}^{-1}\mathscr{D}\mathbf{Q})^{-1}_{13},\ \xi(\mathbf{Q}^{-1}\mathscr{D}\mathbf{Q})^{-1}_{23},\ \xi(\mathbf{Q}^{-1}\mathscr{D}\mathbf{Q})^{-1}_{33},\ F_{\eta 1}\Omega^{-1}_{13},\ F_{\eta 2}\Omega^{-1}_{13},\\
&F_{\eta 3}\Omega^{-1}_{13},\ F_{\eta 1}\Omega^{-1}_{23},\ F_{\eta 2}\Omega^{-1}_{23},\ F_{\eta 3}\Omega^{-1}_{23},\ F_{\eta 1}\Omega^{-1}_{33},\ F_{\eta 2}\Omega^{-1}_{33},\ F_{\eta 3}\Omega^{-1}_{33},\ 0)^{\mathrm{T}}.
\end{aligned}
$$

Here $\mathbf{r}_k$ is the k-th right eigenvector of the system in Cartesian coordinates in the η-direction. Thus Eq. (4.20) can be rewritten

$$
\widetilde{\mathbf{W}}^{\mathrm{L/R}} = \mathbf{W}^{\mathrm{L/R}} + \frac{1}{\rho^{\mathrm{L/R}}}\left[\hat{\mathbf{r}}_{11}(\widetilde{\sigma}_{\eta 1} - \sigma_{\eta 1}) + \hat{\mathbf{r}}_{12}(\widetilde{\sigma}_{\eta 2} - \sigma_{\eta 2}) + \hat{\mathbf{r}}_{13}(\widetilde{\sigma}_{\eta 3} - \sigma_{\eta 3})\right]^{\mathrm{L/R}}. \tag{4.23}
$$

It remains then to specify values of the traction at the boundary $\widetilde{\sigma}^{\mathrm{L/R}}\mathbf{e}_\eta$. It turns out that this depends entirely on the problem and the boundary conditions one wishes to apply. There are a number of scenarios that can occur in solid mechanics, depending on whether the solid is in contact with a vacuum or another solid. Selected idealised conditions shall be considered separately.

- *Solid in contact with another solid: 'stick' conditions*

  The 'stick' boundary conditions for two solid materials in contact is an idealised condition where at the interface the traction and velocity vectors are equal:

$$\widetilde{\sigma}^{\mathrm{L}}\mathbf{e}_\eta = \widetilde{\sigma}^{\mathrm{R}}\mathbf{e}_\eta, \qquad \widetilde{\mathbf{u}}^{\mathrm{L}} = \widetilde{\mathbf{u}}^{\mathrm{R}}. \tag{4.24}$$

  The solution at the boundary for each material is given by Eq. (4.23), with ξ differing in sign for each component depending on the position in relation to the contact. The first three equations provide relations for $\widetilde{\mathbf{u}}^{\mathrm{L/R}}$ in terms of the state $\mathbf{U}^{\mathrm{L/R}}$ (or coefficients deduced from it) and $\widetilde{\sigma}^{\mathrm{L/R}}\mathbf{e}_\eta$ for each component

$$\widetilde{\mathbf{u}}^{\mathrm{L}} = \mathbf{u}^{\mathrm{L}} + \frac{1}{\rho^{\mathrm{L}}}\left(\mathbf{Q}^{-1}\mathscr{D}^{-1}\mathbf{Q}\right)^{\mathrm{L}}\left(\widetilde{\sigma}^{\mathrm{L}} - \sigma^{\mathrm{L}}\right)\mathbf{e}_\eta, \tag{4.25a}$$

$$\widetilde{\mathbf{u}}^{\mathrm{R}} = \mathbf{u}^{\mathrm{R}} - \frac{1}{\rho^{\mathrm{R}}}\left(\mathbf{Q}^{-1}\mathscr{D}^{-1}\mathbf{Q}\right)^{\mathrm{R}}\left(\widetilde{\sigma}^{\mathrm{R}} - \sigma^{\mathrm{R}}\right)\mathbf{e}_\eta. \tag{4.25b}$$

  Substituting the conditions in Eq. (4.24) in Eq. (4.25) and rearranging gives

$$\begin{aligned}\widetilde{\sigma}^{\mathrm{L/R}}\mathbf{e}_\eta = &\left[\frac{1}{\rho^{\mathrm{L}}}\left(\mathbf{Q}^{-1}\mathscr{D}^{-1}\mathbf{Q}\right)^{\mathrm{L}} + \frac{1}{\rho^{\mathrm{R}}}\left(\mathbf{Q}^{-1}\mathscr{D}^{-1}\mathbf{Q}\right)^{\mathrm{R}}\right]^{-1} \\ &\left[\frac{1}{\rho^{\mathrm{L}}}\left(\mathbf{Q}^{-1}\mathscr{D}^{-1}\mathbf{Q}\right)^{\mathrm{L}}\sigma^{\mathrm{L}}\mathbf{e}_\eta + \frac{1}{\rho^{\mathrm{R}}}\left(\mathbf{Q}^{-1}\mathscr{D}^{-1}\mathbf{Q}\right)^{\mathrm{R}}\sigma^{\mathrm{R}}\mathbf{e}_\eta + \mathbf{u}^{\mathrm{R}} - \mathbf{u}^{\mathrm{L}}\right]\end{aligned} \tag{4.26}$$

- *Solid in contact with another solid: 'slip' conditions*

  Another idealised interfacial condition for two solids in contact is the 'slip' condition where the normal stress and normal velocities are equal, whilst the tangential components of the traction vectors are zero. It is more convenient in terms of notation for this example to consider the case of $\eta = 1$:

$$\widetilde{\sigma}^{\mathrm{L}}_{11} = \widetilde{\sigma}^{\mathrm{R}}_{11}, \qquad \widetilde{\sigma}^{\mathrm{L}}_{12} = \widetilde{\sigma}^{\mathrm{L}}_{13} = \widetilde{\sigma}^{\mathrm{R}}_{12} = \widetilde{\sigma}^{\mathrm{R}}_{13} = 0, \qquad \widetilde{u}^{\mathrm{L}}_1 = \widetilde{u}^{\mathrm{R}}_1. \tag{4.27}$$

  In the same way as with the 'stick' boundary conditions, one starts with Eq. (4.25) defined for both materials. In this case only the expressions for $\widetilde{u}^{\mathrm{L}}_1$ and $\widetilde{u}^{\mathrm{R}}_1$ are required since the only unknowns are $\widetilde{\sigma}^{\mathrm{L}}_{11}$ and $\widetilde{\sigma}^{\mathrm{R}}_{11}$:

$$\widetilde{u}^{\mathrm{L}}_1 = u^{\mathrm{L}}_1 + \frac{1}{\rho^{\mathrm{L}}}\left(\mathbf{Q}^{-1}\mathscr{D}^{-1}\mathbf{Q}\right)^{\mathrm{L}}_{1i}\left(\widetilde{\sigma}^{\mathrm{L}}_{1i} - \sigma^{\mathrm{L}}_{1i}\right), \tag{4.28a}$$

$$\widetilde{u}^{\mathrm{R}}_1 = u^{\mathrm{R}}_1 - \frac{1}{\rho^{\mathrm{R}}}\left(\mathbf{Q}^{-1}\mathscr{D}^{-1}\mathbf{Q}\right)^{\mathrm{R}}_{1i}\left(\widetilde{\sigma}^{\mathrm{R}}_{1i} - \sigma^{\mathrm{R}}_{1i}\right). \tag{4.28b}$$

  Setting the tangential components of the traction to zero and rearranging Eq. (4.28) gives

$$\begin{aligned}\widetilde{\sigma}^{\mathrm{L/R}}_{11} = &\left[\tfrac{1}{\rho^{\mathrm{L}}}\left(\mathbf{Q}^{-1}\mathscr{D}^{-1}\mathbf{Q}\right)^{\mathrm{L}}_{11} + \tfrac{1}{\rho^{\mathrm{R}}}\left(\mathbf{Q}^{-1}\mathscr{D}^{-1}\mathbf{Q}\right)^{\mathrm{R}}_{11}\right]^{-1} \\ &\left[\tfrac{1}{\rho^{\mathrm{L}}}\left(\mathbf{Q}^{-1}\mathscr{D}^{-1}\mathbf{Q}\right)^{\mathrm{L}}_{1i}\sigma^{\mathrm{L}}_{1i} + \tfrac{1}{\rho^{\mathrm{R}}}\left(\mathbf{Q}^{-1}\mathscr{D}^{-1}\mathbf{Q}\right)^{\mathrm{R}}_{1i}\sigma^{\mathrm{R}}_{1i} + u^{\mathrm{R}}_1 - u^{\mathrm{L}}_1\right].\end{aligned} \tag{4.29}$$

- *Solid in contact with a vacuum*

  A solid in contact with a vacuum is the simplest of the scenarios. This case requires that the traction is zero. Thus the boundary conditions are the required result:

$$\widetilde{\sigma}^{\mathrm{L/R}}\mathbf{e}_\eta = 0. \tag{4.30}$$

This completes the approximate solution of the Riemann problem for a solid in contact with either another solid or vacuum, one need only insert the computed traction vector found from one of the above into Eq. (4.23) to give the solution at the boundary, $\widetilde{\mathbf{W}}^{\mathrm{L/R}}$.

A final consideration is that the value of stress taken at the boundary is only a first order approximation. Thus one evaluation of Eq. (4.23) does not necessarily enforce, for example, $\widetilde{\sigma}^{\mathrm{L/R}}\mathbf{e}_\eta = 0$ for the solid/vacuum case. It is simple to evaluate Eq. (4.23) a small number of times to achieve the required result, for each iteration taking the value of $\mathbf{W}^{\mathrm{L/R}}$ inside the boundary to be the last known value of $\widetilde{\mathbf{W}}^{\mathrm{L/R}}$. Experience shows that doing so has only a small influence on the final result, but then makes little impact on the overall cost of the scheme since these solutions are sought in the small number of boundary cells.

4.6 Examples

To assess the performance of the numerical methods initial value problems are chosen that involve three-dimensional deformations. Each case differs not only in perhaps initial conditions, but in the materials invloved and the boundary conditions that are applied at the interface. All computations are performed in the x_1-direction ($\eta = 1$). Each case uses a uniform grid in the range [0:1] cm with a grid spacing $\Delta x = 1/500$ cm. The interface is initially located at $x_0 = 0.5$ cm.

To access the performance of the numerical schemes for these problems, exact solutions have been found using the method proposed in Chapter 2. The exact solution to a Riemann problem is uniquely determined from the (known) initial left and right states, and (unknown) wavespeeds. The residual error, $\mathscr{R}$, in continuity of, for example, the traction and velocities across the central contact as determined from the Rankine-Hugonoit and required boundary conditions, gives a measure of the error in the wavespeeds. The exact solution method follows an iterative proceedure which given the initial left and right states seeks the exact wave speeds so as to minimise $\mathscr{R}$. The residuals are found by systematically evaluating the solution across each wave to obtain the inner most states either side of the contact. These states then provide the required measures. An initial guess of the wavespeeds, and of course wave types, is taken from an estimate of the inner states between waves

Table 4.1: Equation of state parameters

Parameter	Value			Units
	Cu	Al	Steel	
ρ_0	8.93	2.71	8.03	$\mathrm{g\,cm^{-3}}$
c_0	4.6	6.22	5.68	$\mathrm{km\,s^{-1}}$
c_v	$3.9 \cdot 10^{-4}$	$9.0 \cdot 10^{-4}$	$5.0 \cdot 10^{-4}$	$\mathrm{kJ\,g^{-1}\,K^{-1}}$
T_0	300	300	300	K
b_0	2.1	3.16	3.1	$\mathrm{km\,s^{-1}}$
α	1.0	1.0	0.596	–
β	3.0	3.577	2.437	–
γ	2.0	2.088	1.563	–

using the linearised solver. The exact wavespeeds are then found by solving the non-linear system $\mathscr{R}(\mathfrak{S}_1, \mathfrak{S}_2, \ldots, \mathfrak{S}_6) = 0$ for $\mathfrak{S}_j$, $1 \leq j \leq 6$, using the Newton-Raphson method. The way in which the solution is sought, by evaluating first the waves on the left side of the contact, and then for the right, make it straightforward to solve systems where the left and right materials differ, or in the case of solid/vacuum where material on one side does not exist.

4.6.1 IVP 2

In this first testcase both materials are considered to be copper with the parameters in the equation of state, Eq. (2.82)-(2.83), given in Table 4.1.

The initial left and right velocities, deformation gradients, and entropies are taken to be:

$$\mathbf{U}^{\mathrm{L}} \left\{ \quad \mathbf{u} = \begin{pmatrix} 2 \\ 0 \\ 0.1 \end{pmatrix} \mathrm{km\,s^{-1}}, \qquad \mathbf{F} = \begin{pmatrix} 1 & 0 & 0 \\ -0.01 & 0.95 & 0.02 \\ -0.015 & 0 & 0.9 \end{pmatrix}, \quad \mathscr{S} = 0\,\mathrm{kJ\,g^{-1}\,K^{-1}} \right.$$

$$\mathbf{U}^{\mathrm{R}} \left\{ \quad \mathbf{u} = \begin{pmatrix} 0 \\ -0.03 \\ -0.01 \end{pmatrix} \mathrm{km\,s^{-1}}, \quad \mathbf{F} = \begin{pmatrix} 1 & 0 & 0 \\ 0.015 & 0.95 & 0 \\ -0.01 & 0 & 0.9 \end{pmatrix}, \qquad \mathscr{S} = 0\,\mathrm{kJ\,g^{-1}\,K^{-1}} \right.$$

These are the initial conditions used in IVP 2 of § 2.6, which were a modification of the testcase in [50]. The stick interfacial boundary conditions are used. This configuration is equivalent to a single material problem and thus provides an opportunity to assess the performance of the interface tracked schemes with a single material computation. The solution comprises a left travelling longitudinal shock, tranverse rarefaction, and transverse shock; the right travelling wavetypes are symmetric to

the left. As is expected the single material method (SMM) resolves the contact wave across a finite number of grid points (Figure 4.4). Small errors are noticeable in the density and entropy, occurrences which are synonymous to the so called 'heating' errors observed in gas dynamics problems.

The moving grid method improves on these errors, as does the MGFM but not to the same degree, the conservative method producing worsened heating errors (Figures 4.5-4.7). The heating errors are largely reduced by applying the entropy fix in the MGFM (Figure 4.8). The resolution of non-linear wave profiles differs very little between each of the methods and all demonstrate excellent agreement with the exact solution.

4.6.2 IVP 1

In this second example both materials are again considered to be copper with equation of state parameters taken to be the same as in the previous testcase. The following initial conditions are taken from IVP 1 in § 2.6:

$$\mathbf{U}^{\mathrm{L}} \left\{ \begin{array}{l} \mathbf{u} = \begin{pmatrix} 0 \\ 0.5 \\ 1 \end{pmatrix} \mathrm{km\,s^{-1}}, \quad \mathbf{F} = \begin{pmatrix} 0.98 & 0 & 0 \\ 0.02 & 1 & 0.1 \\ 0 & 0 & 1 \end{pmatrix}, \quad \mathscr{S} = 1 \cdot 10^{-3}\,\mathrm{kJ\,g^{-1}\,K^{-1}} \end{array} \right.$$

$$\mathbf{U}^{\mathrm{R}} \left\{ \begin{array}{l} \mathbf{u} = \begin{pmatrix} 0 \\ 0 \\ 0 \end{pmatrix} \mathrm{km\,s^{-1}}, \quad \mathbf{F} = \begin{pmatrix} 1 & 0 & 0 \\ 0 & 1 & 0.1 \\ 0 & 0 & 1 \end{pmatrix}, \quad \mathscr{S} = 0\,\mathrm{kJ\,g^{-1}\,K^{-1}} \end{array} \right.$$

The stick interfacial boundary conditions are again used, thus resulting in an alternative single material problem. This time, the resultant jump in density across the contact wave is larger and facilitates a further investigation of the heating errors. The solution comprises three left travelling rarefaction waves, a right travelling contact, and two right travelling rarefactions led by a right travelling shock wave. The single material computations are shown for reference (Figure 4.9). All of the multi-material schemes, as expected, maintain a sharp jump in variables across the contact (Figures 4.10-4.12) and also lend an improvement to the small undershoots/overshoots observed at the tail of some rarefaction waves using the SMM. The heating errors are quite significant in the density profile using the MGFM, but are again much improved by applying the entropy fix (Figure 4.13). Overall comparison with the exact solutions is very good and each successfully realises the desired interfacial boundary conditions.

4.6.3 IVP 3

In this example the left hand material is taken to be aluminium, whilst the right is copper. The necessary constants for both materials are given in Table 4.1. The initial

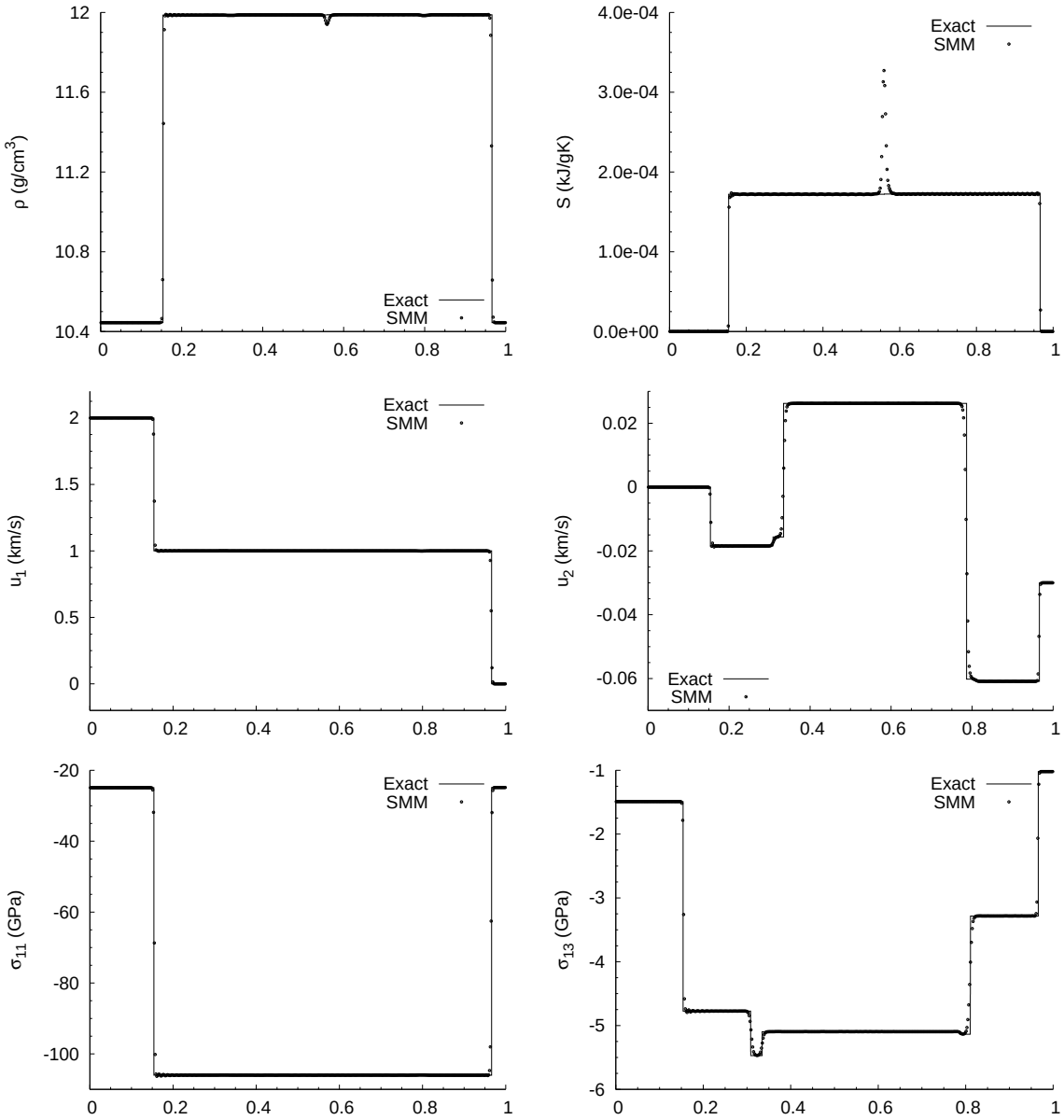

Figure 4.4: Comparison of exact (solid line) and numerical (points) solutions of IVP 2 at the time $t = 0.6\,\mu$s using the single material method (SMM), with $\mathscr{C} = 0.6$, and $\Delta x = 1/500$ cm.

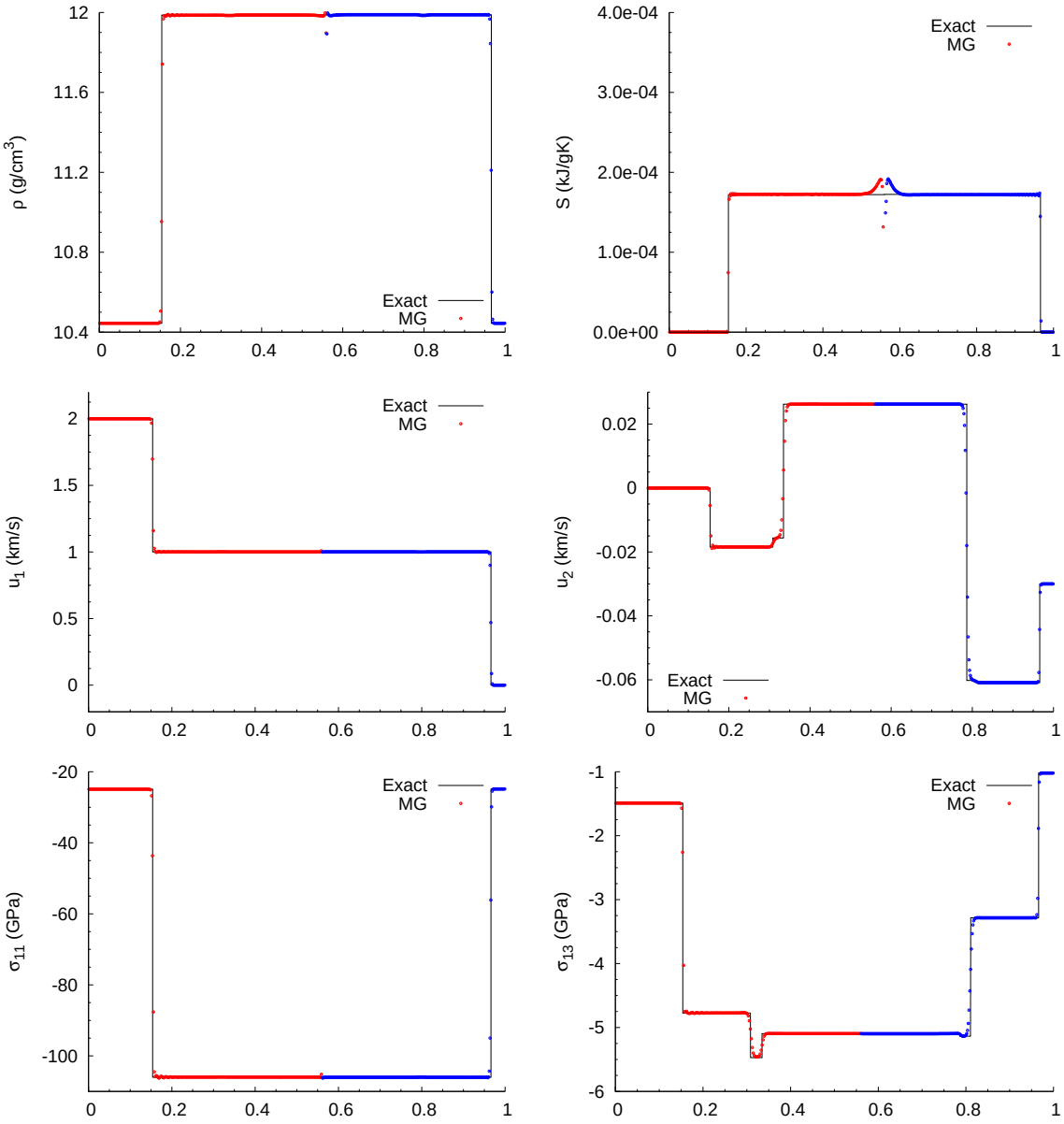

Figure 4.5: Comparison of exact (solid line) and numerical (points) solutions of IVP 2 at the time $t = 0.6\,\mu$s using the moving grid (MG) method, with $\mathscr{C} = 0.6$, and $\Delta x = 1/500$ cm.

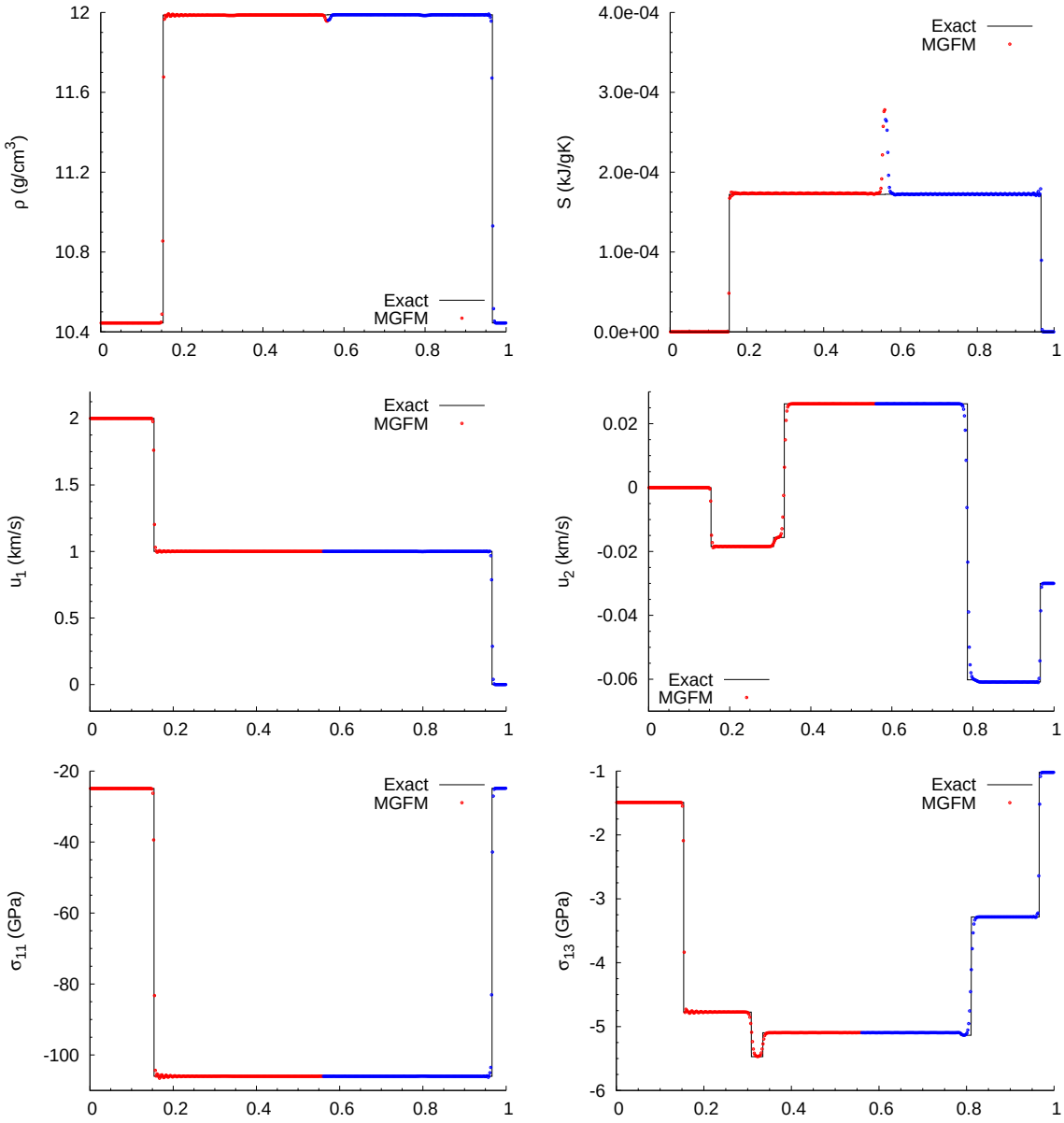

Figure 4.6: Comparison of exact (solid line) and numerical (points) solutions of IVP 2 at the time $t = 0.6\,\mu$s using the modified ghost fluid method (MGFM), with $\mathscr{C} = 0.6$, and $\Delta x = 1/500\,$cm.

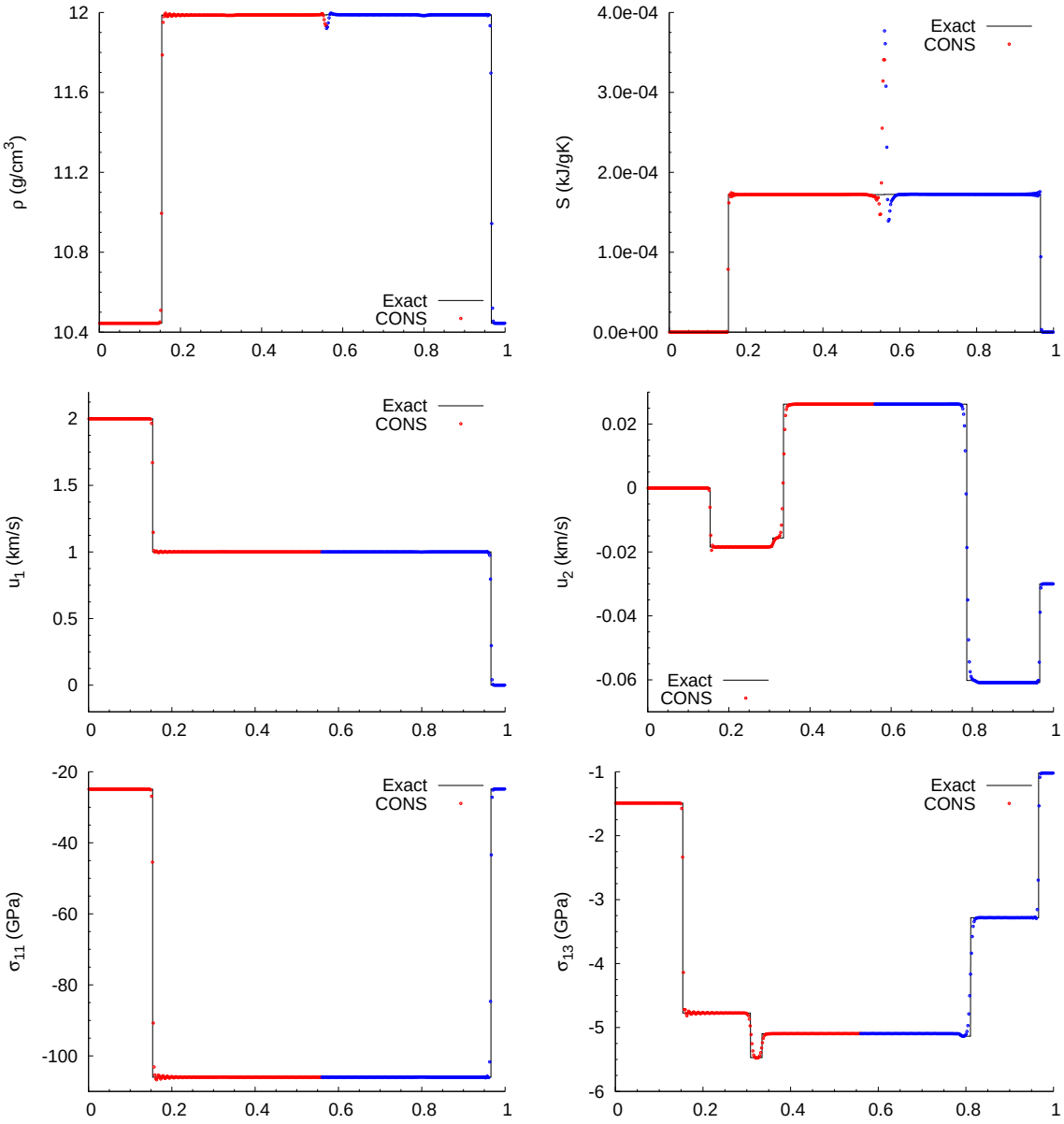

Figure 4.7: Comparison of exact (solid line) and numerical (points) solutions of IVP 2 at the time $t = 0.6\,\mu$s using the conservative level-set method (CONS), with $\mathscr{C} = 0.6$, and $\Delta x = 1/500$ cm.

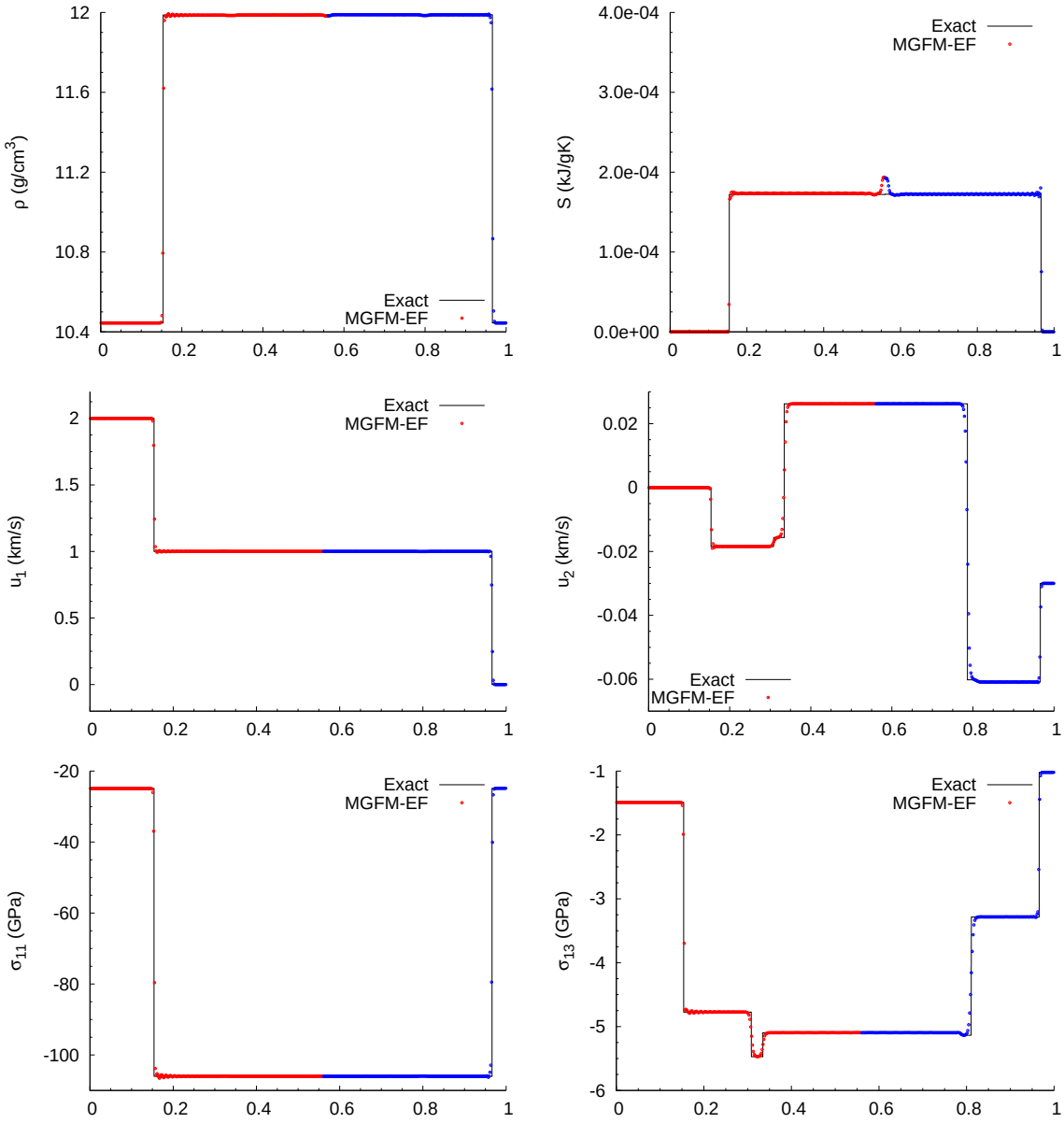

Figure 4.8: Comparison of exact (solid line) and numerical (points) solutions of IVP 2 at the time $t = 0.6\,\mu$s using the modified ghost fluid method with entropy fix (MGFM-EF), with $\mathscr{C} = 0.6$, and $\Delta x = 1/500$ cm.

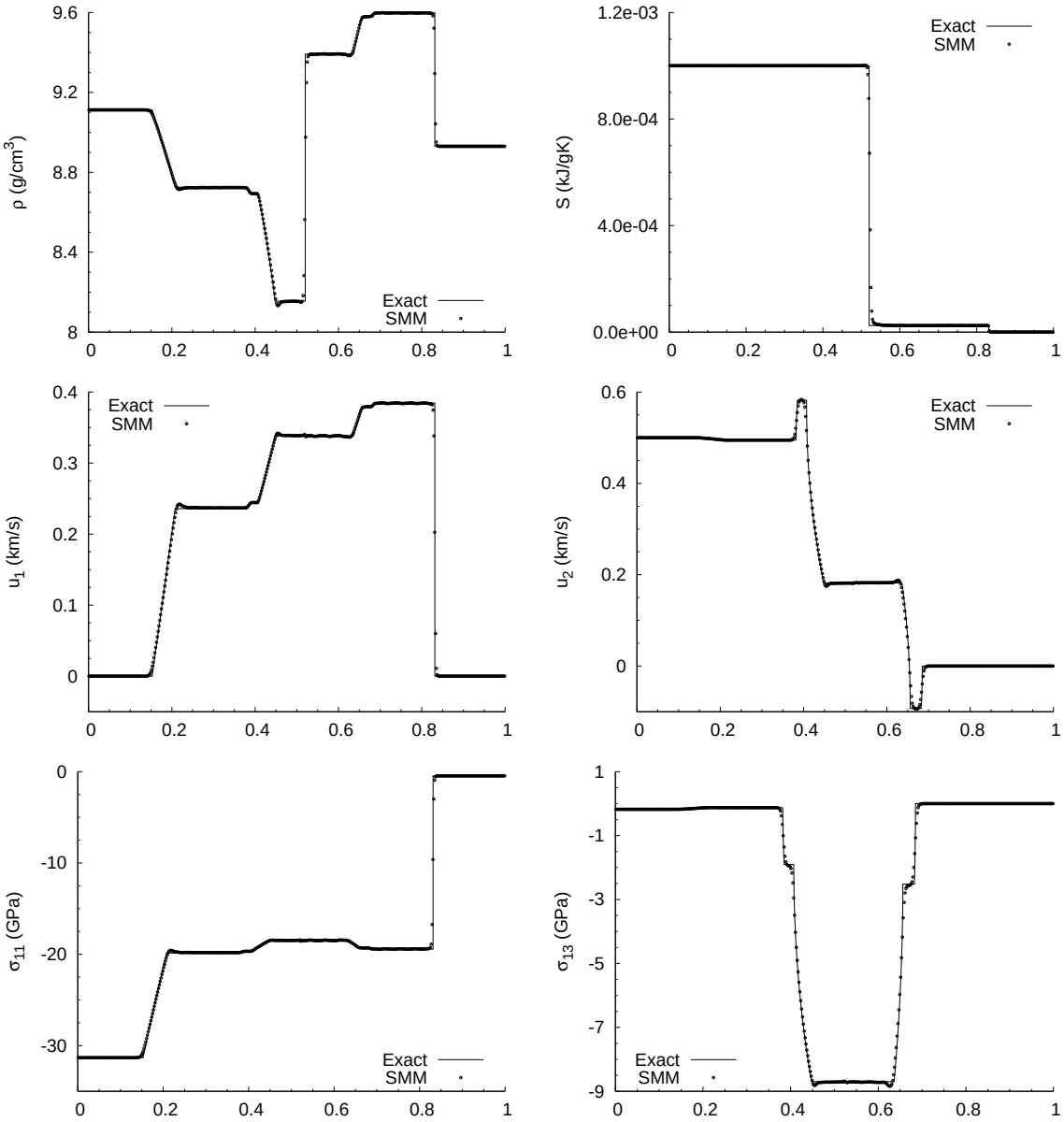

Figure 4.9: Comparison of exact (solid line) and numerical (points) solutions of IVP 1 at a time $t = 0.6\,\mu$s, with $\mathscr{C} = 0.6$, and $\Delta x = 1/500$ cm using the single material method (SMM).

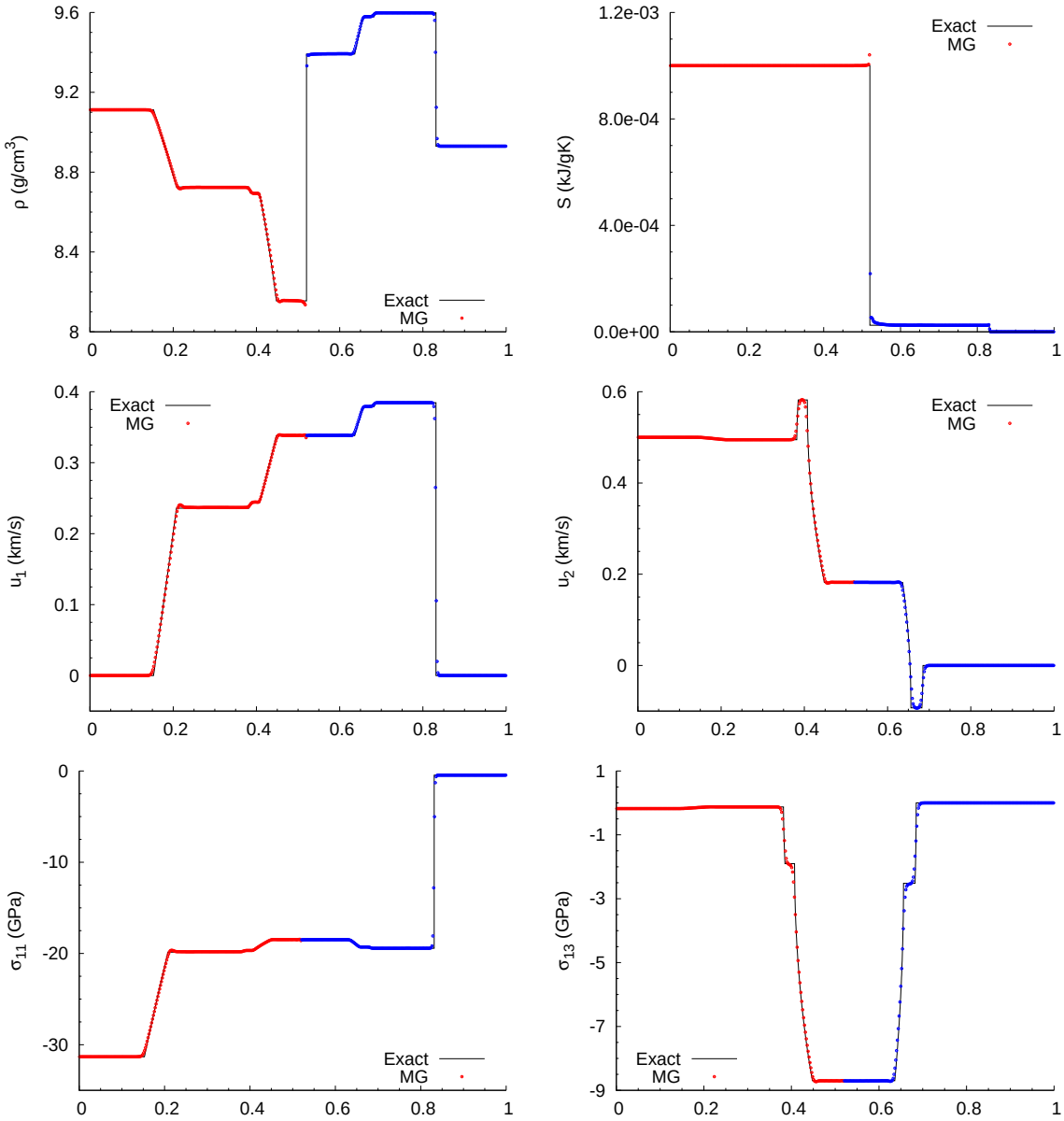

Figure 4.10: Comparison of exact (solid line) and numerical (points) solutions of IVP 1 at the time $t = 0.6\,\mu$s using the moving grid (MG) method, with $\mathscr{C} = 0.6$, and $\Delta x = 1/500$ cm.

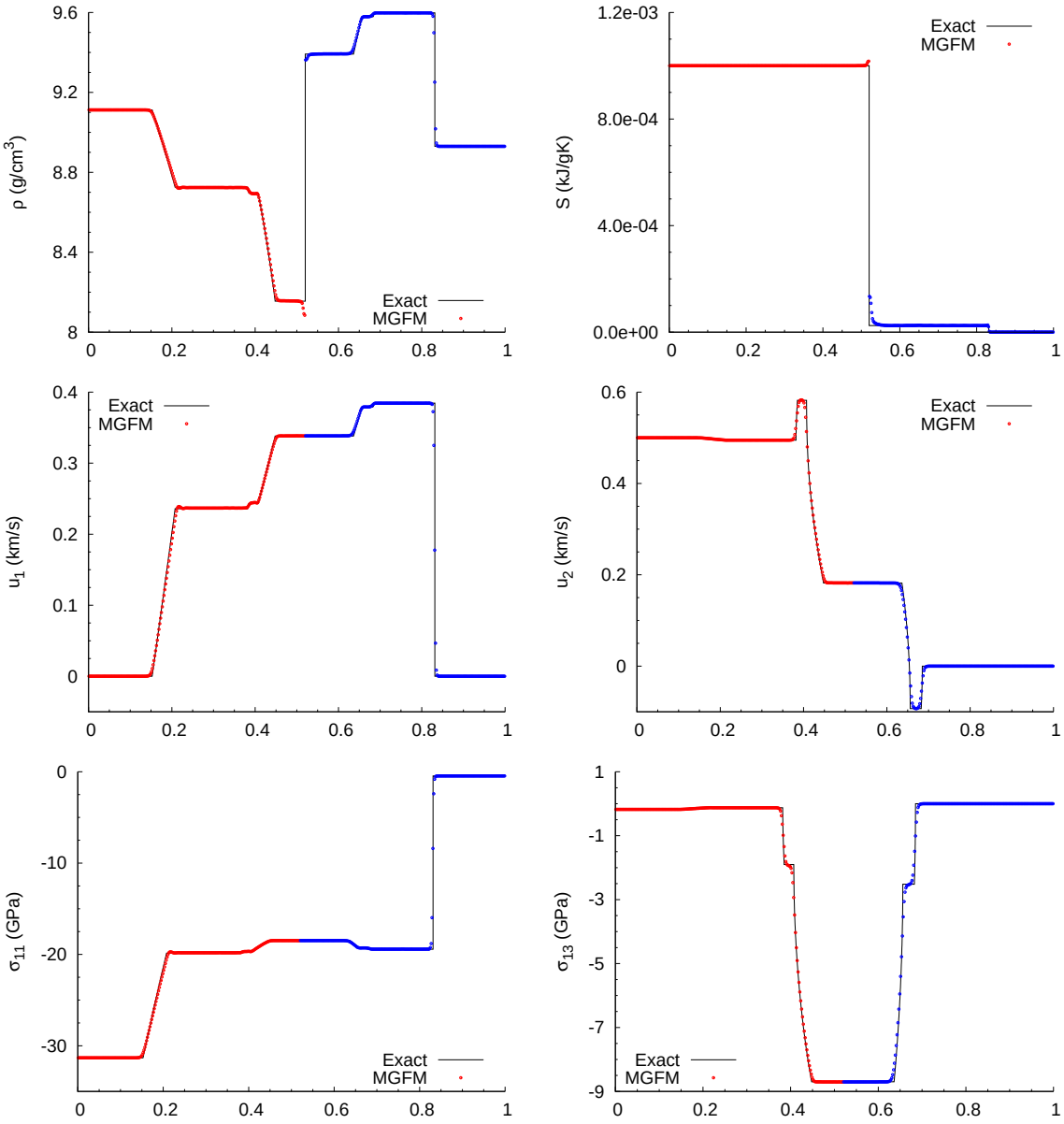

Figure 4.11: Comparison of exact (solid line) and numerical (points) solutions of IVP 1 at the time $t = 0.6\,\mu$s using the modified ghost fluid method (MGFM), with $\mathscr{C} = 0.6$, and $\Delta x = 1/500\,$cm.

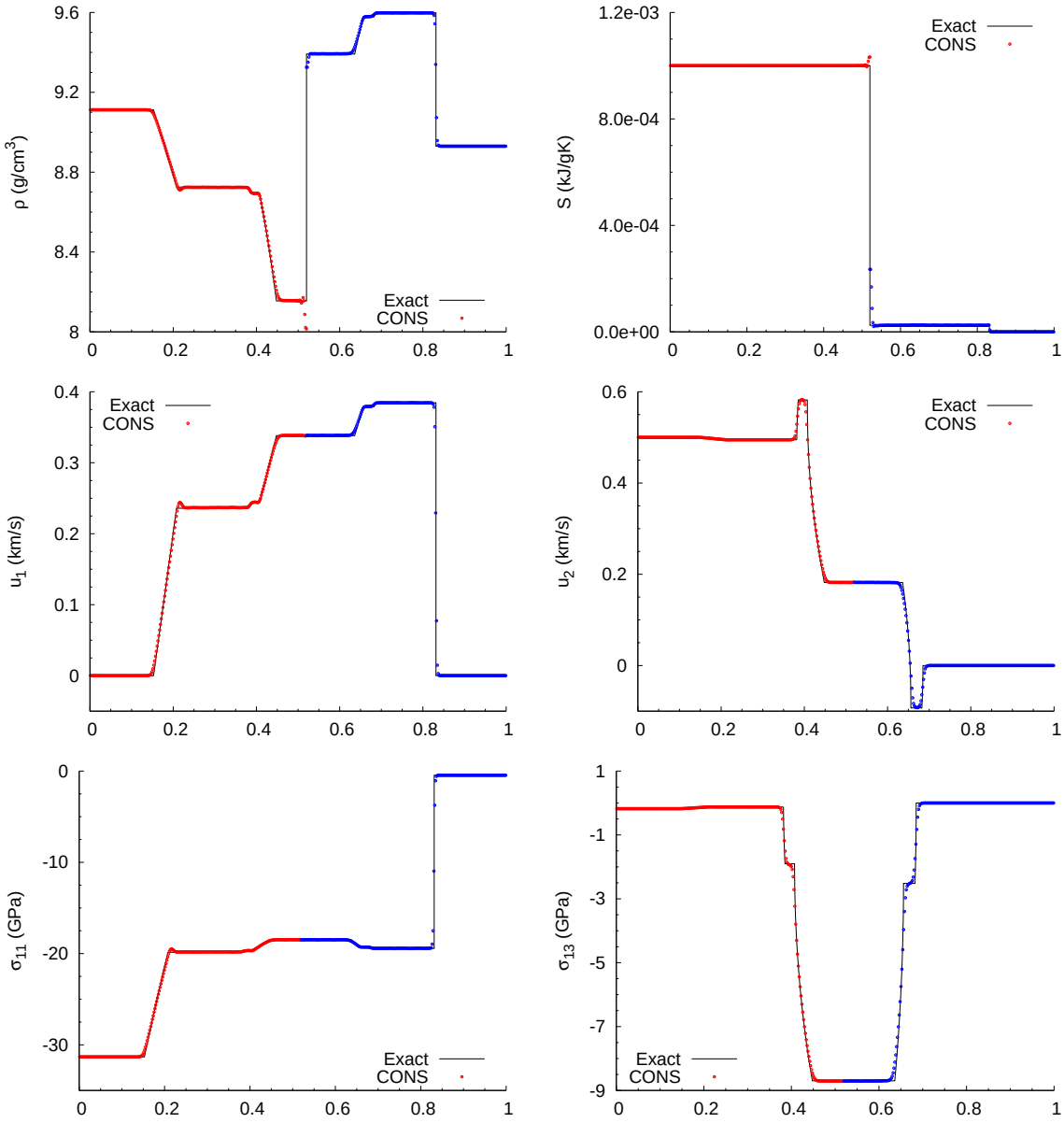

Figure 4.12: Comparison of exact (solid line) and numerical (points) solutions of IVP 1 at the time $t = 0.6\,\mu$s using the conservative level-set method (CONS), with $\mathscr{C} = 0.6$, and $\Delta x = 1/500$ cm.

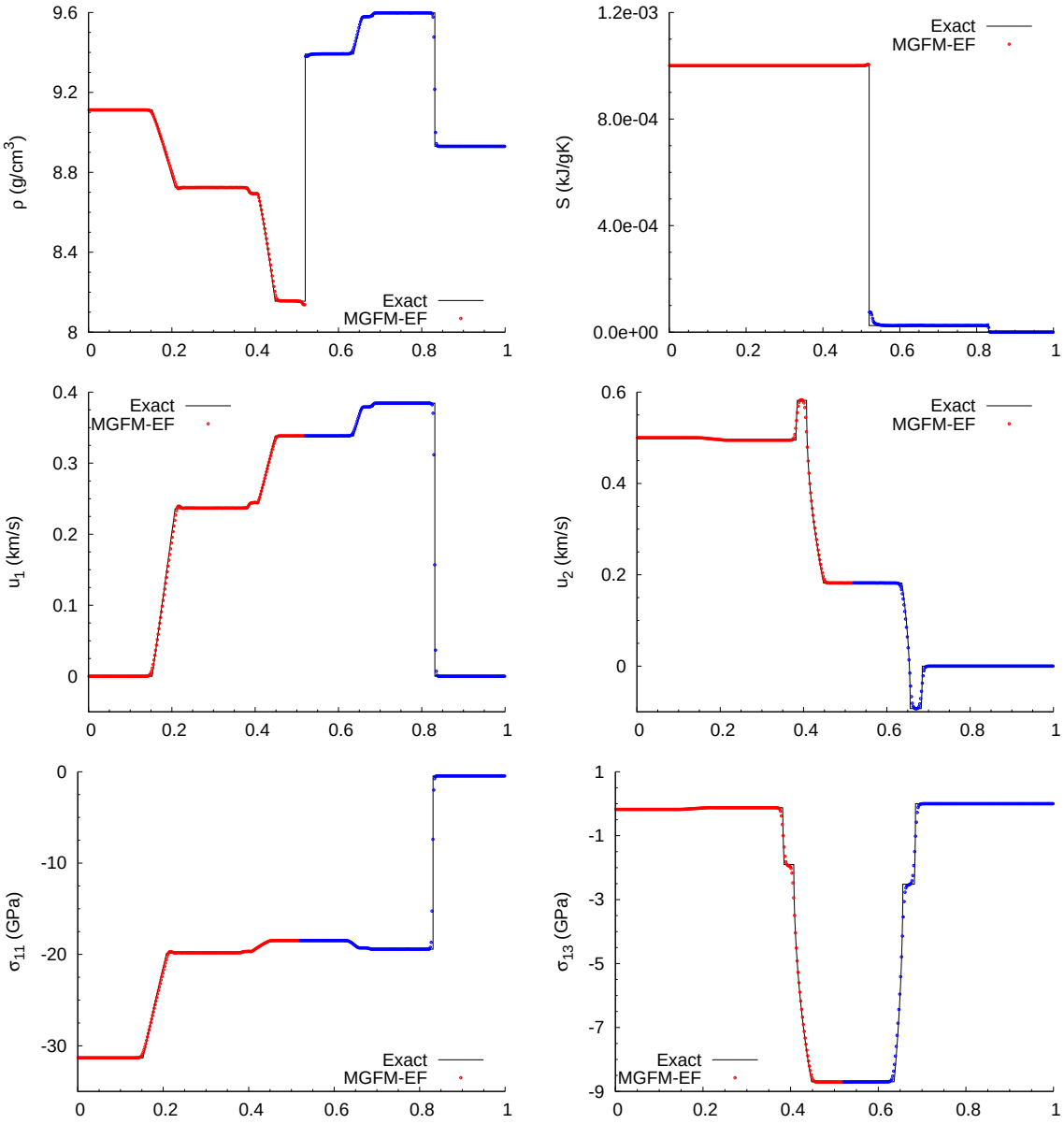

Figure 4.13: Comparison of exact (solid line) and numerical (points) solutions of IVP 1 at the time $t = 0.6\,\mu$s using the modified ghost fluid method with entropy fix (MGFM-EF), with $\mathscr{C} = 0.6$, and $\Delta x = 1/500$ cm.

states for the aluminium and copper are taken to be the same as the left and right states respectively for IVP 2. The slip boundary conditions were used in the interface calculation. All non-linear waves in the solution are shocks with a right travelling contact wave. The heating errors observed previously still manifest in the interface region for each method (Figures 4.14-4.16), the MGFM and conservative level-set methods performing most poorly in these regions, although not as discernible as a result of the large density difference of the two materials. The entropy fix again proves effective in reducing these anomalies for the MGFM (Figure 4.17). In all cases the slip boundary conditions are accurately enforced; the tangential velocity gradients are discontinuous and the tangential components of the traction go to zero across the contact wave. Overall the agreement with the exact solution is very good.

4.6.4 IVP 4

This final one-dimensional example assumes only the left hand material is solid; the initial contact is a free surface of the semi-infinite solid and the right hand region taken to be a vacuum. The solid material is aluminium with the same constants used in the previous testcase and initial conditions for the left material of IVP 2. The solution comprises a longitudinal rarefaction wave followed by two transverse shock waves all propagating to the left of the initial contact. The initial state of the solid results in an acceleration of the free surface (contact) to the right.

Similar behaviour as in the previous testcases are observed of heating errors using each of the methods (Figures 4.18-4.21), although the conservative method does not perform as poorly in comparison. All methods are successfull in achieving the zero traction boundary condition and predicting accurate locations of the non-linear waves and free surface.

4.6.5 2-d example

In the final example the MGFM scheme is demonstrated in two-dimensions by simulating the experimental setup from [36] of a copper flyer plate impacting a aluminium cone encased within a steel shroud (Fig. 4.22). Although only non-linear elastic solids are considered in the present study, and indeed in reality inelastic deformations will play a role, this testcase provides an opportunity to assess the ability to allow for sliding in two-dimensions. Material properties for all components are tabulated in Table 4.1. The problem is cylindrically symmetric, hence the governing laws are augmented by the geometric source terms presented in Appendix C. Each material is identifiable by a dedicated level-set function, with the surrounding space taken to be a vacuum. The use of multiple level-set fields within a void calls for the inclusion of some form of collision criteria, such that the contact between each material is identifiable within each cell. Here the approach proposed in [75] is

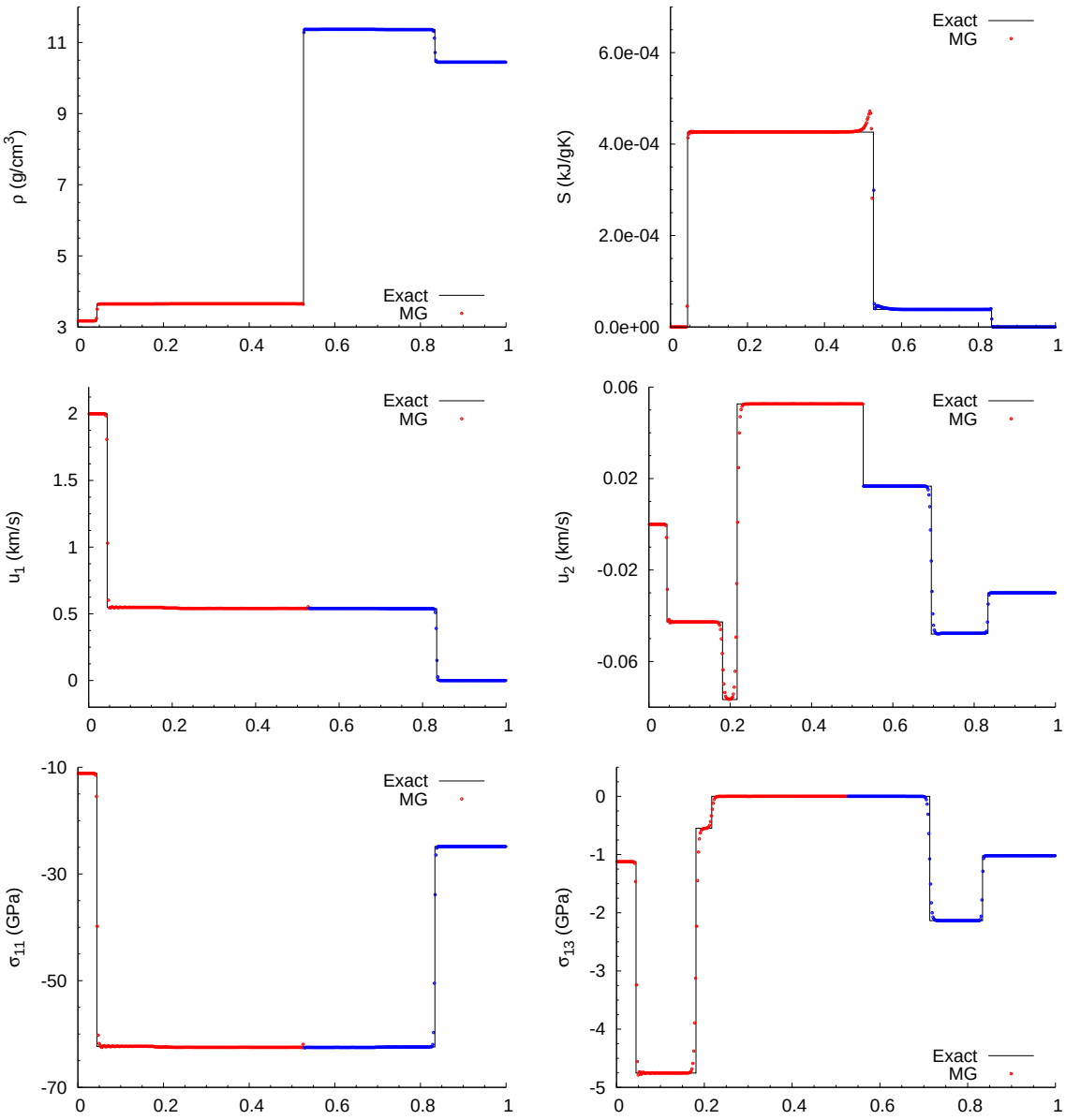

Figure 4.14: Comparison of exact (solid line) and numerical (points) solutions of IVP 3 at the time $t = 0.5\,\mu$s using the moving grid (MG) method, with $\mathscr{C} = 0.6$, and $\Delta x = 1/500$ cm.

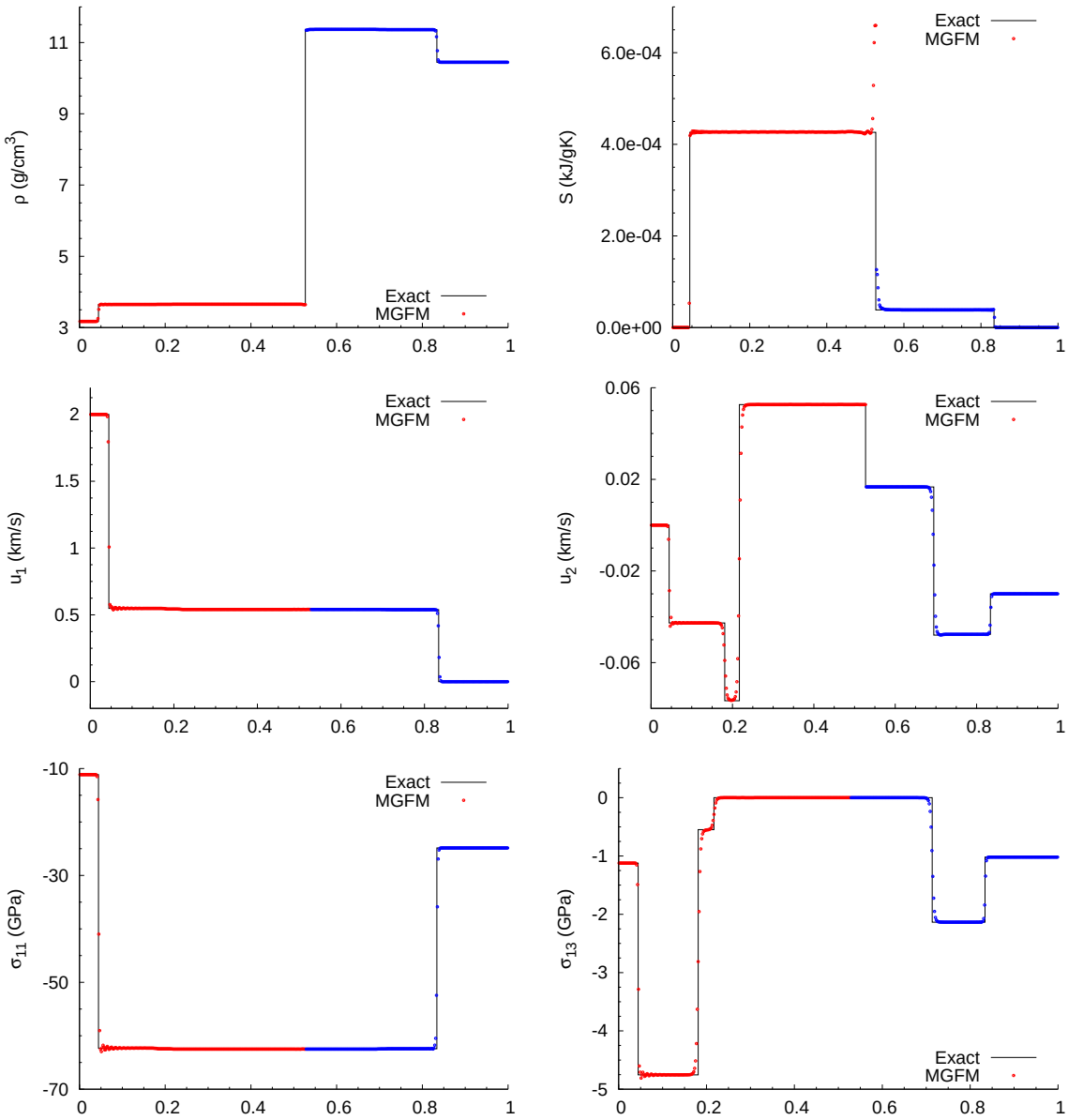

Figure 4.15: Comparison of exact (solid line) and numerical (points) solutions of IVP 3 at the time $t = 0.5\,\mu$s using the modified ghost fluid method (MGFM), with $\mathscr{C} = 0.6$, and $\Delta x = 1/500\,$cm.

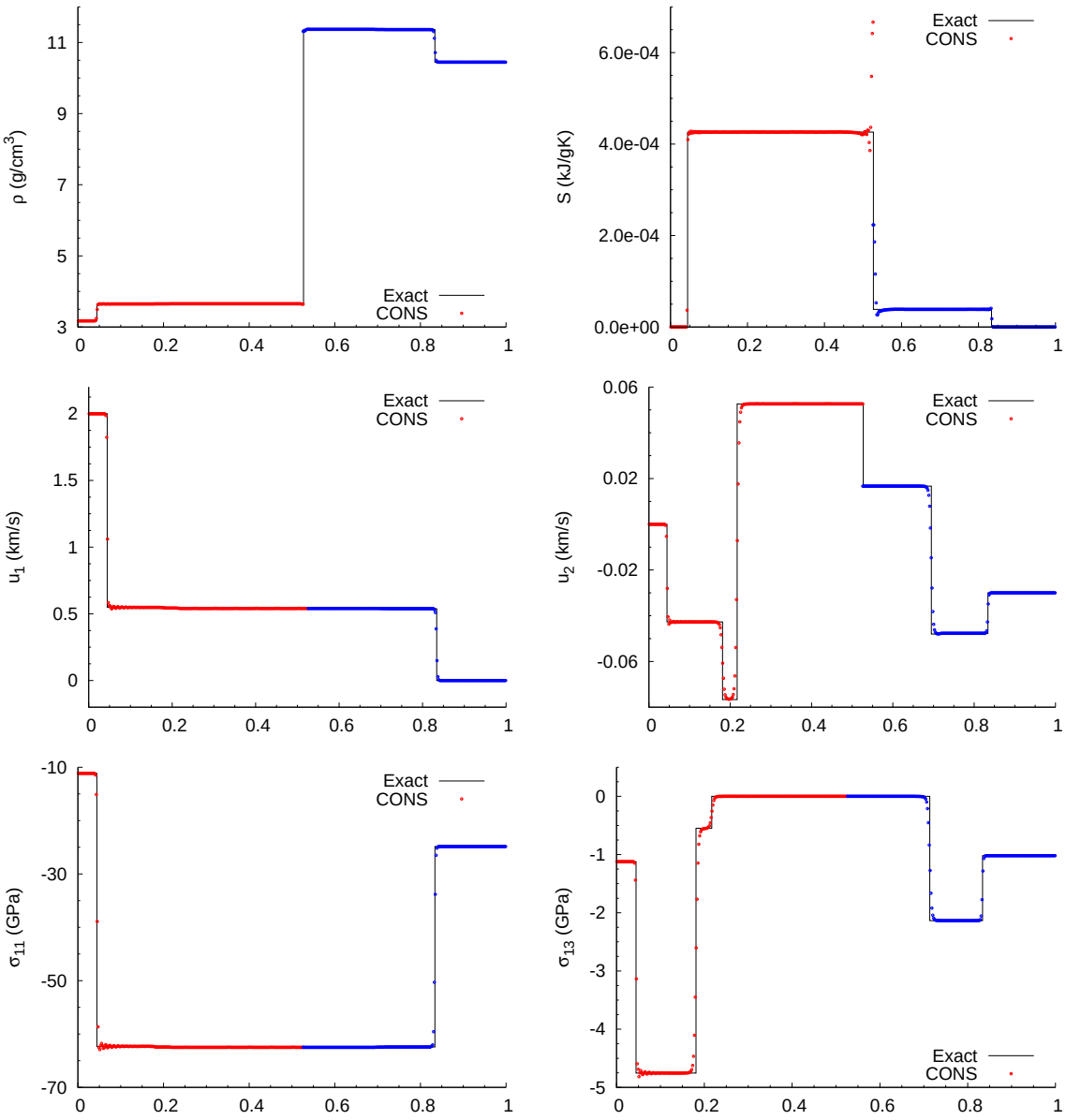

Figure 4.16: Comparison of exact (solid line) and numerical (points) solutions of IVP 3 at the time $t = 0.5\,\mu$s using the conservative level-set method (CONS), with $\mathscr{C} = 0.6$, and $\Delta x = 1/500\,$cm.

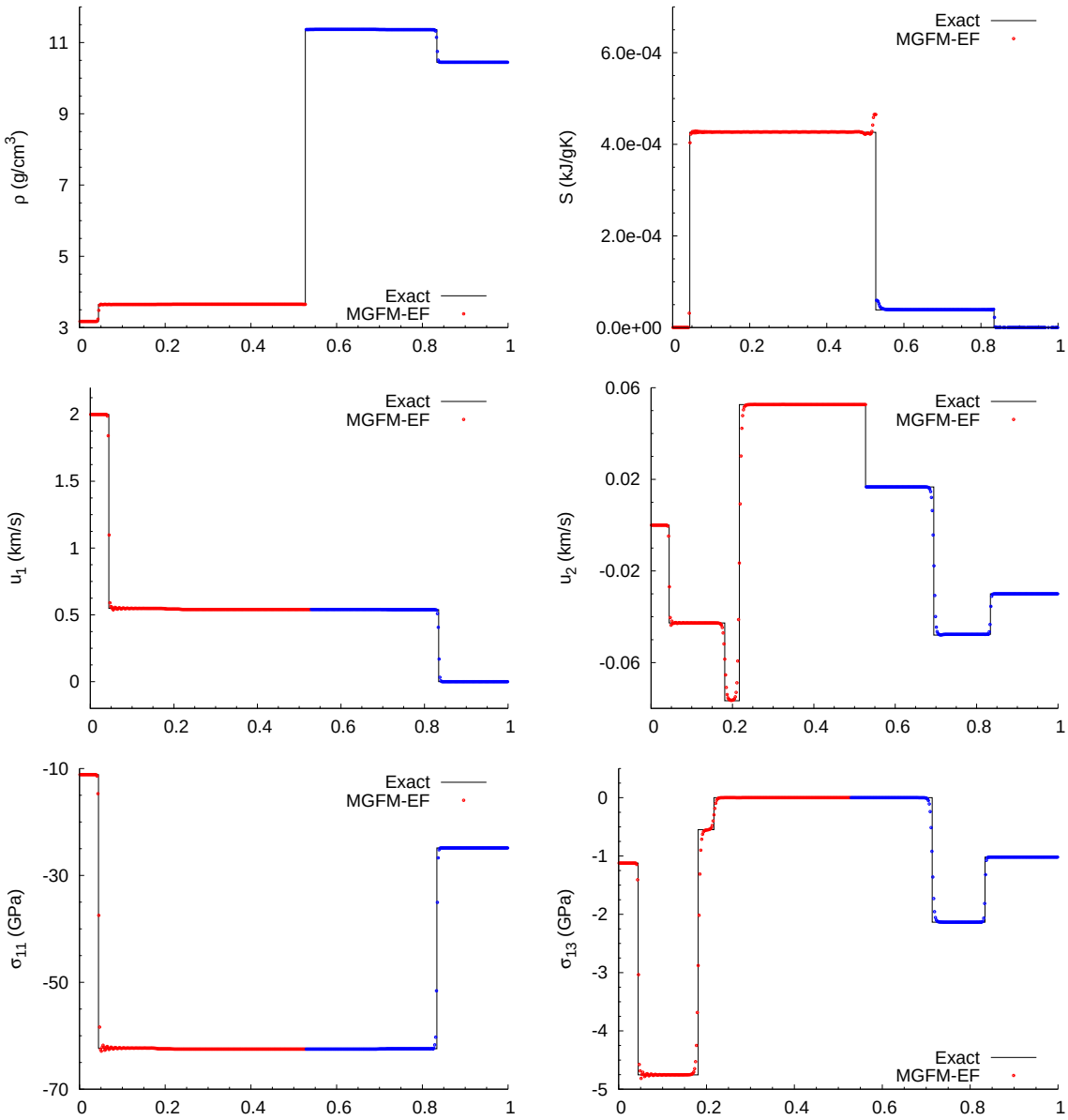

Figure 4.17: Comparison of exact (solid line) and numerical (points) solutions of IVP 3 at the time $t = 0.5\,\mu$s using the modified ghost fluid method with entropy fix (MGFM-EF), with $\mathscr{C} = 0.6$, and $\Delta x = 1/500$ cm.

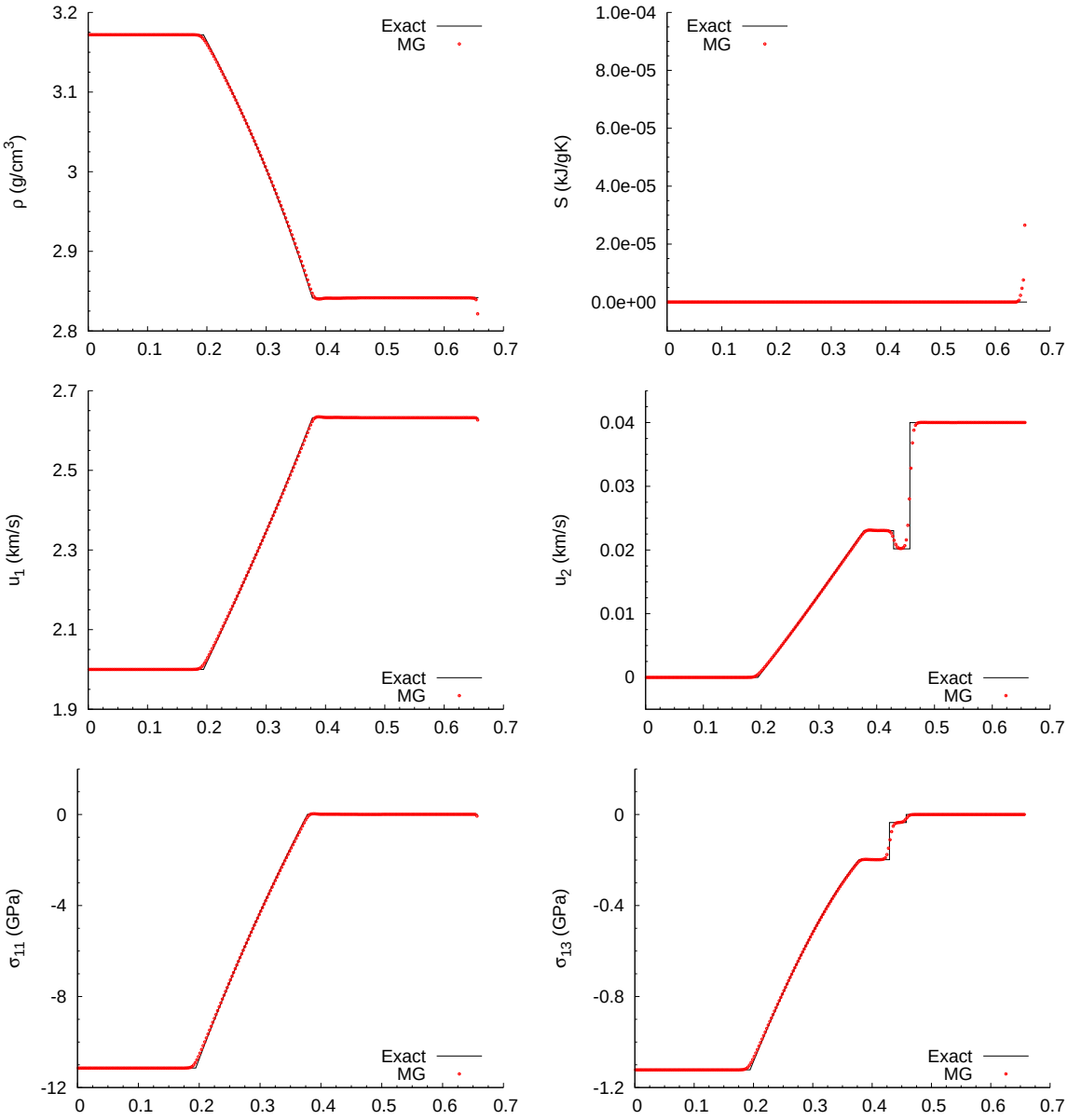

Figure 4.18: Comparison of exact (solid line) and numerical (points) solutions of IVP 4 at the time $t = 0.6\,\mu$s using the moving grid method (MG), with $\mathscr{C} = 0.6$, and $\Delta x = 1/500$ cm.

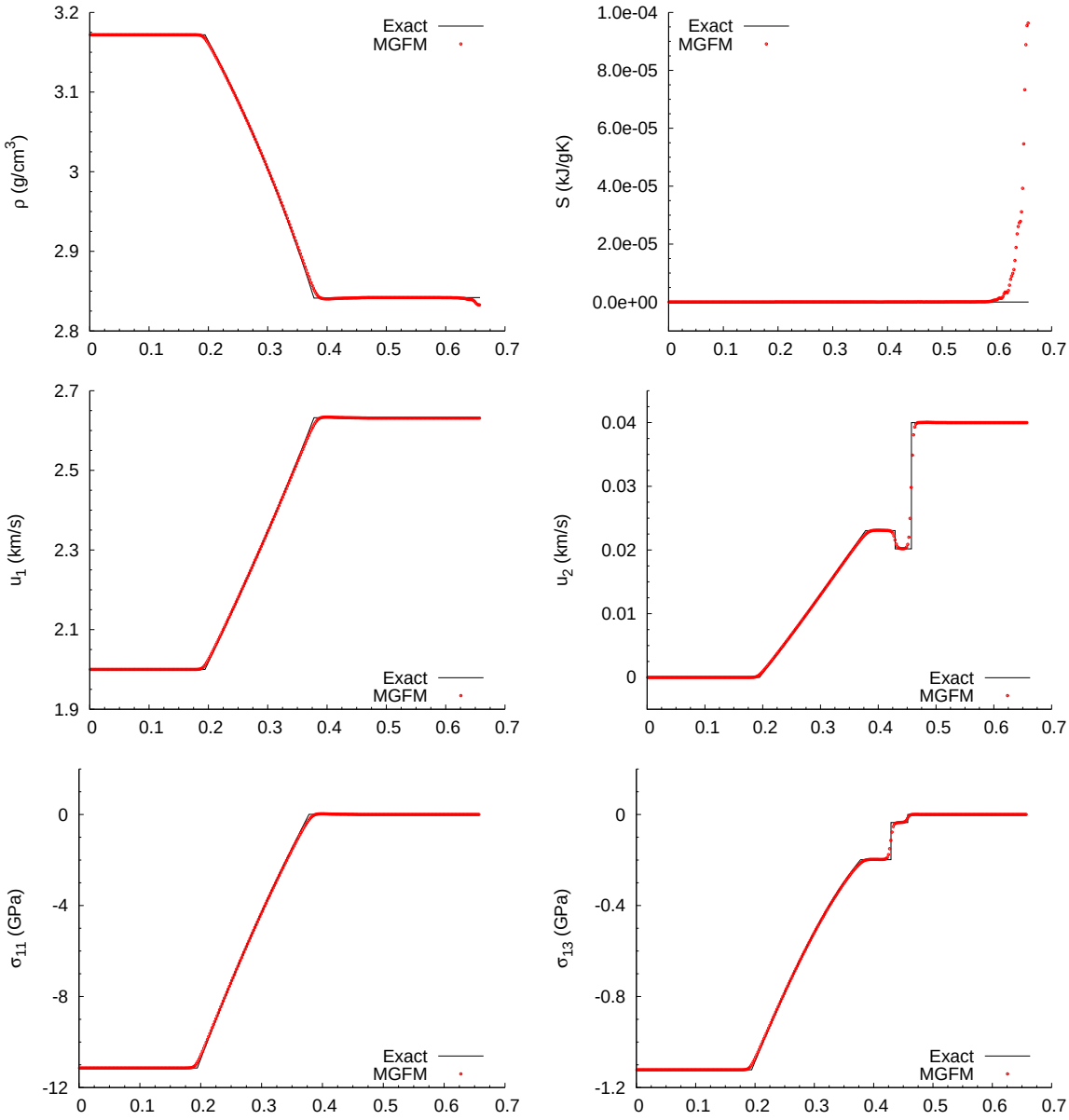

Figure 4.19: Comparison of exact (solid line) and numerical (points) solutions of IVP 4 at the time $t = 0.6\,\mu$s using the modified ghost fluid method (MGFM), with $\mathscr{C} = 0.6$, and $\Delta x = 1/500$ cm.

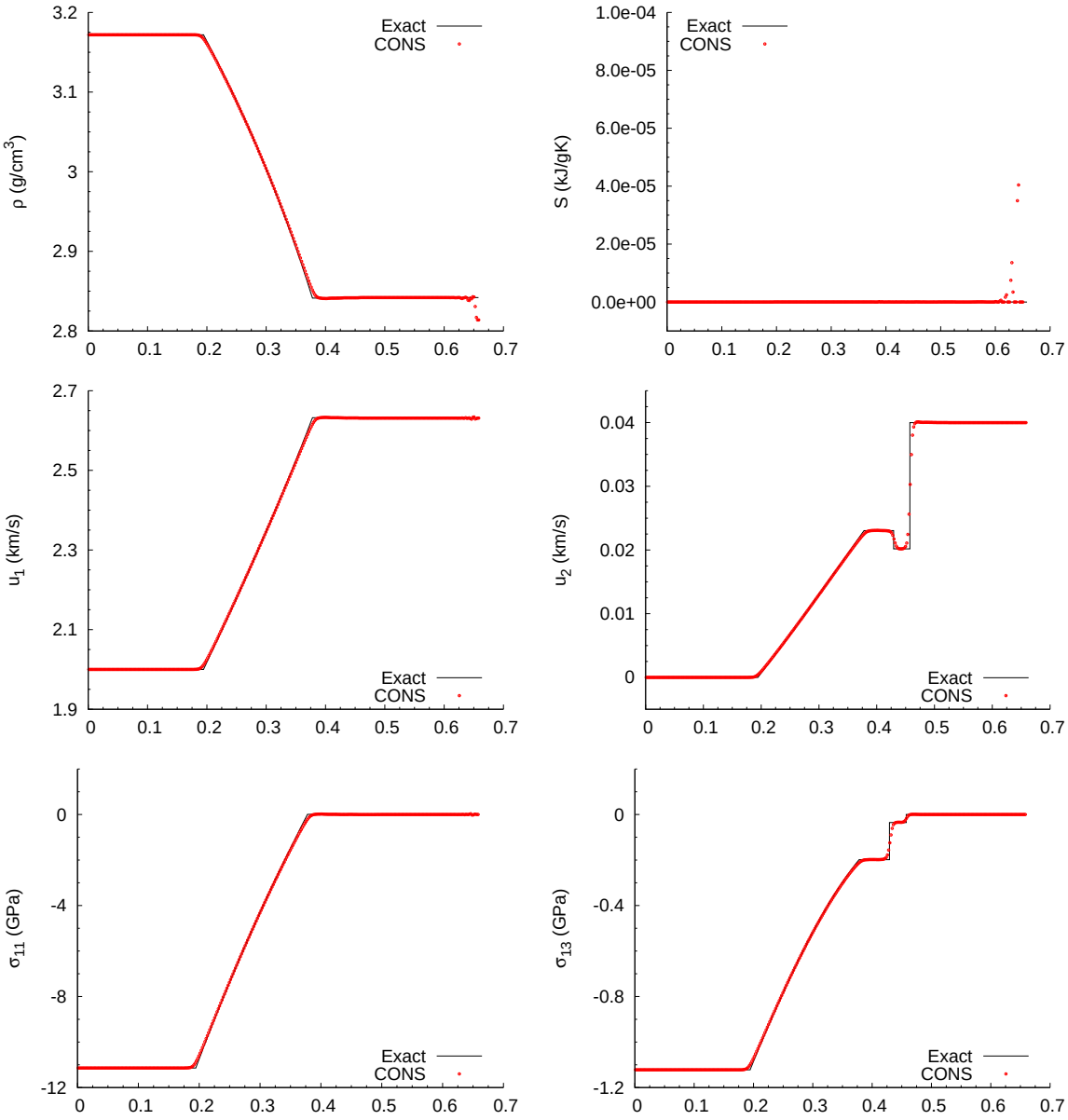

Figure 4.20: Comparison of exact (solid line) and numerical (points) solutions of IVP 4 at the time $t = 0.6\,\mu$s using the conservative level-set method (CONS), with $\mathscr{C} = 0.6$, and $\Delta x = 1/500$ cm.

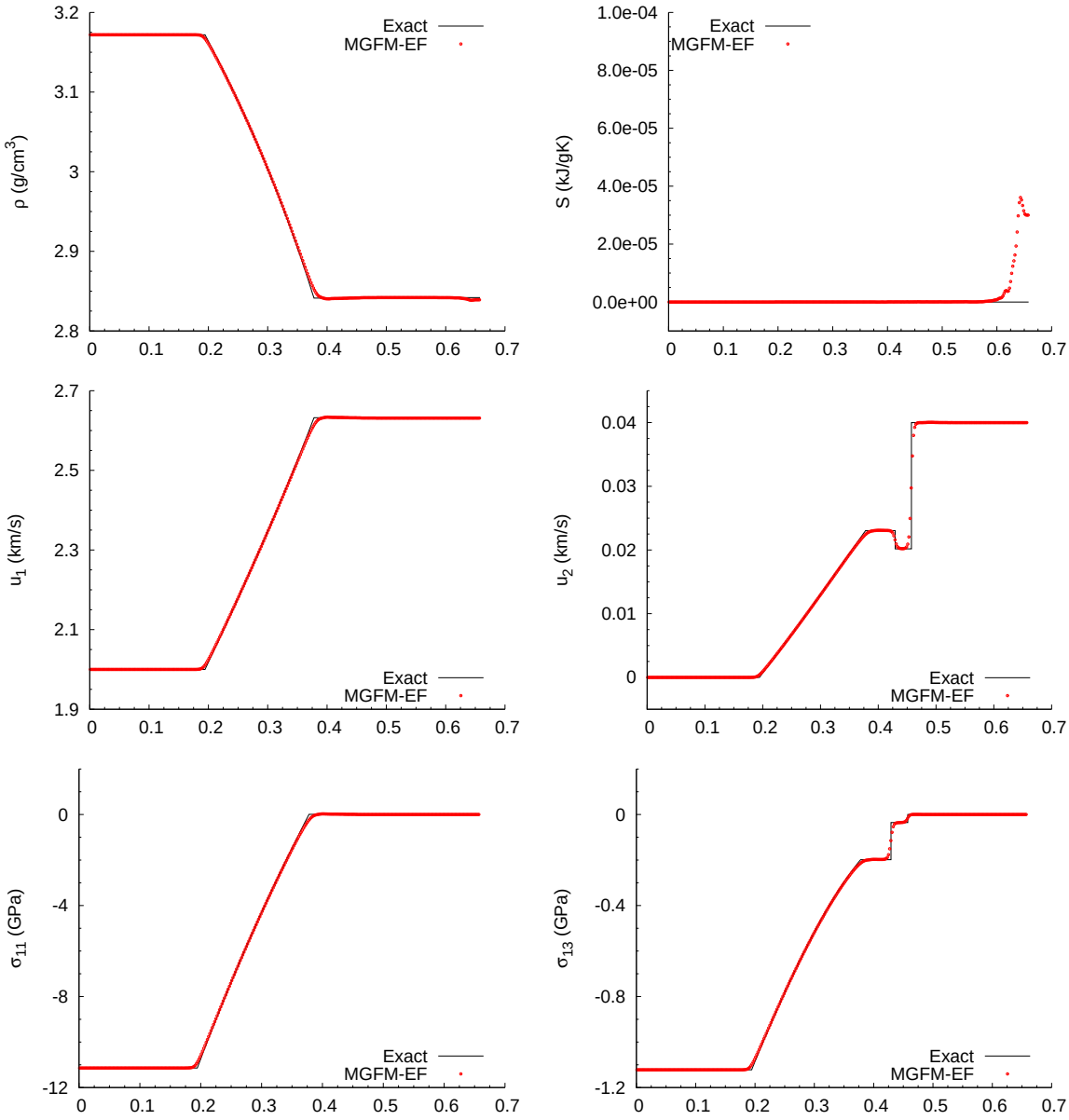

Figure 4.21: Comparison of exact (solid line) and numerical (points) solutions of IVP 4 at the time $t = 0.6\,\mu$s using the modified ghost fluid method with entropy fix (MGFM-EF), with $\mathscr{C} = 0.6$, and $\Delta x = 1/500$ cm.

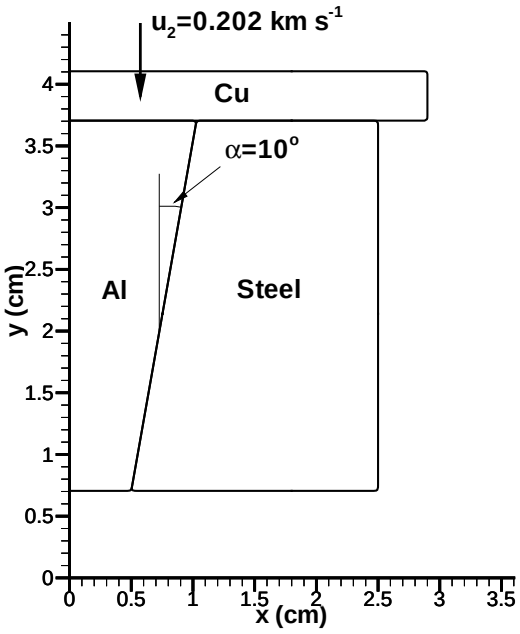

Figure 4.22: Illustration of the friction experiment setup.

used where contact between a Solid 1 and Solid 2 is assumed whenever the difference in level set fields between the two materials is less than 10% of the cell size: $|\phi^{S1} + \phi^{S2}| < 0.1\Delta x \rightarrow$ contact. The computational grid covered the domain [0:3.6, 0:4.28] cm, with uniform quadrilateral cells of size $\Delta\mathbf{x} = 1/50$ cm. The CFL number was taken to be $C = 1/3$. For the initial conditions all materials are assumed to be in a stress free configuration: $\mathbf{F} = \mathbf{I}$ and $S = 0$. The cone and steel casing were taken to be at rest, whilst the copper flyer plate was initialised with a non-zero velocity component: $u_2 = 0.202\,\mathrm{km\,s^{-1}}$ for solutions sought in x_1x_2-domain. Solutions were computed for both the slip and stick boundary conditions. For the former this experiment proves to be a rigorous test on account of the interface between the aluminium cone and steel casing lying at an oblique angle to the Cartesian coordinate system; thus the experiment provides analysis of the ability to allow for sliding in higher-dimensions.

The impact of the copper plate results in a shock wave propagating into the cone and case wave travels obliquely to the interface (Fig. 4.23). Likewise a shock propagates into the flyer plate, which, upon reaching the upper free surface, results in a downwards moving elastic release wave. The fact that the waves propagate at an angle to the interface between the cone and case means a discontinuous change occurs in the component of velocity tangential to the boundary, and hence sliding

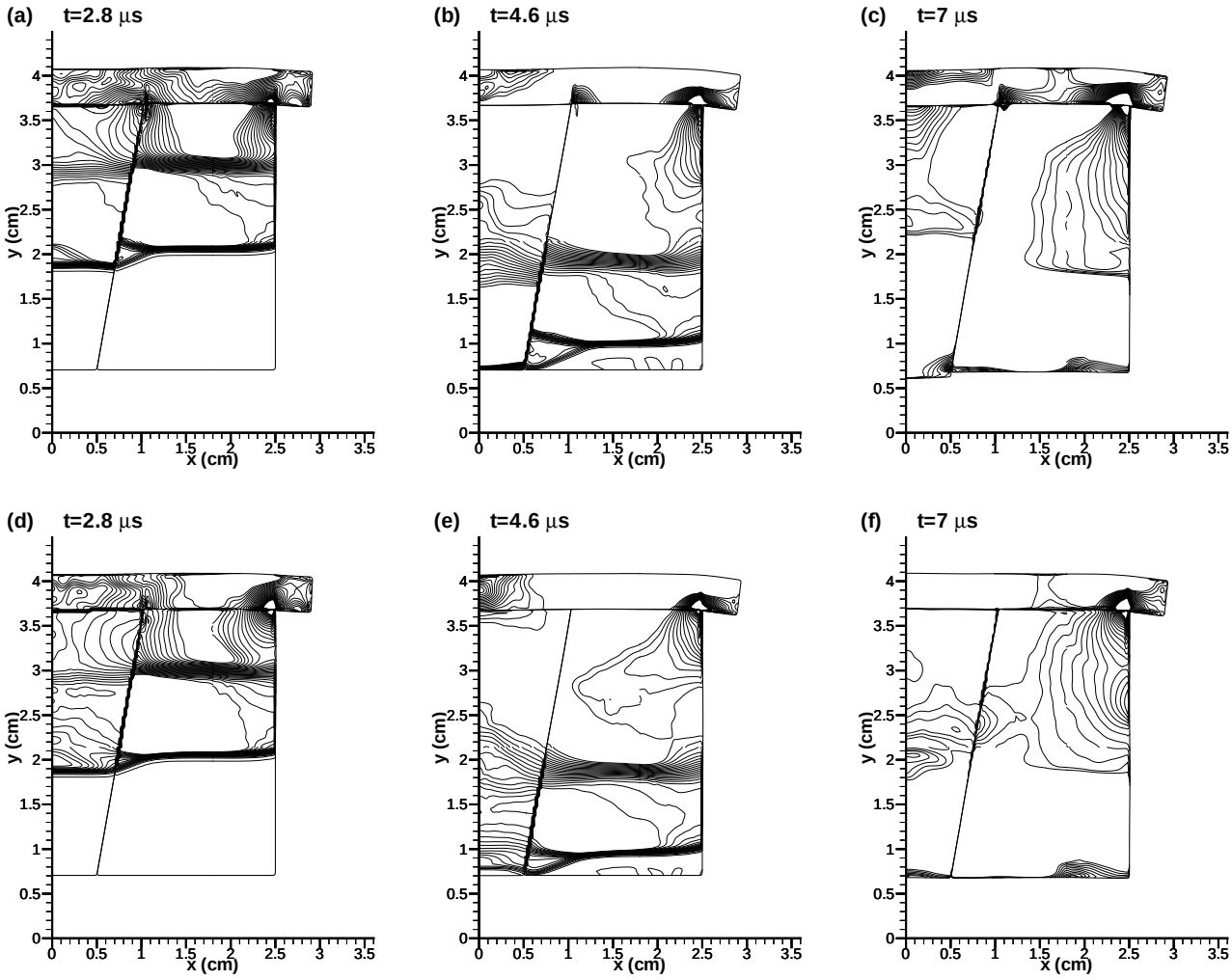

Figure 4.23: Contour plots of the pressure, $p = -\mathrm{Tr}(\sigma)/3$, at different indicated times for the friction experiment using (a)-(c) the slip boundary conditions, and (d)-(f) the stick boundary conditions.

between the two components, in the case of slip conditions. Upon reaching the bottom free surface of the cone in this case, the initial shock wave forces the cone to petrude from the confining case. The stick boundary conditions on-the-other-hand result in no sliding and thus the bottom free surface of the cone and case move simultaneously following the arrival of the first wave. The prominant influence of the chosen interfacial boundary conditions is illustrated by the markedly different time-histories of free-surface velocity of the central cone and casing (Fig. 4.24). Due to the difference in material properties, the waves travel faster in the aluminium cone

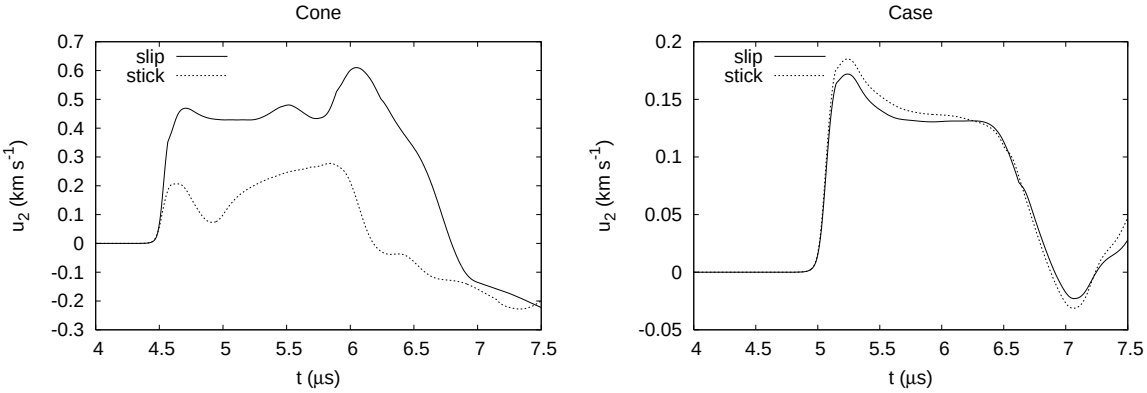

Figure 4.24: Time evolution of free surface velocities for the aluminium cone and steel case showing the effects of using the stick and slip interfacial boundary conditions. Measurements were taken at the radial locations $x = 0$ cm and $x = 1.5$ cm of the free-surfaces for the cone and case respectively.

than the steel case. Thus, the initial shock reaches the free-surface of the cone some time before reaching the free-surface of the case. For the slip boundary conditions the shock accelerates the free-surface of the cone which subsequently maintains a constant velocity until arrival of the release wave. For the stick conditions, the free-surface of the case is initially accelerated but quickly decelerates due to the the binding to the (at that point in time) stationary case. Only once the loading shock has reached the case free-surface does the cone begin again to accelerate further. Referring back to § 1, in reality one would expect that the interfacial friction would dictate that the behaviour lie somewhere between these two results. It is thus encouraging that the present method successfully realises both the bounding limits of interfacial motion.

4.7 Conclusions

The moving grid method, modified ghost fluid method, and a conservative level-set based methid originally applied to the the equations of gas-dynamics have been extended to non-linear elastic materials in one-dimension. Each scheme is a straightforward extension of the existing single material scheme. The required solution of multi-material Riemann problems has been derived for different interfacial boundary conditions including a solid in contact with another solid, and a solid in contact with a vacuum. The modified ghost fluid, and conservative level-set based methods boast the use of fixed Cartesian grids and high-order shock capturing methods whilst maintaining sharp interfaces and are simple means to employ existing single compo-

nent solvers to capture interface interactions. Here level-set functions are employed to allow the possibility of relative sliding between solid components.

Numerical solutions of various multi-material problems demonstrates an accurate incorporation of each boundary condition in each method. A particularly favourable achievement is the ability to allow perfect sliding. An entropy fix proved to reduce the observed 'heating' errors for the MGFM method; it is mentioned that this fix could indeed be applied to either of the other methods, but that doing so would violate the strict conservation. Since the methods have been derived based upon the augmented one-dimensional system extension of the schemes to multi-dimensions should be straightforward and is the subject of ongoing work.

5

A hybrid molecular–continuum method for solid materials[†]

Synopsis

For many problems in solid dynamics singularities exist where constitutive equations in continuum models remain outstanding due to a lack of comprehensive understanding of the physical behaviour. In these circumstances one would like to employ atomistic studies, but face limitations on the maximum possible domain sizes. Hybrid approaches which seek to flawlessly combine molecular dynamics and continuum mechanics methods can be designed to overcome these difficulties. This chapter is devoted to proposing one such method based upon a domain decomposition framework using a combination of flux and state coupling. Examples are presented for strong shear waves in metals modelled by the EAM potential within the molecular dynamics region.

5.1 Introduction

Multiscale modelling strategies target limitations on the range of applicability of one or a number of methodologies by linking models applicable at different length scales. The use of such an approach is justified where singularities exist in the modelling of a particular system such that adequate constitutive models for continuum mechanics (CM) are not available in these regions, and atomistic studies using molecular dynamics (MD) are limited by the current computational resources. The objective here is to achieve an atomistic study of a singularity in a solid material by targeting limitations on the range of applicability of MD simulations. In turn it will be shown how such an approach can eliminate the reliance on particular constitutive models used in the CM methods. In this way the simulation domain can be decomposed into regions Γ^{MD} where MD is applied, and regions Γ^{CM} where CM models are sufficient (Fig. 5.1).

The purpose of this chapter is to establish a computational technique that has

[†]Much of the work in this chapter was presented in [38]: M. Kalweit, **P.T. Barton** & D. Drikakis, Hybrid molecular dynamics - continuum mechanics method for solid materials, *under review* (2009).

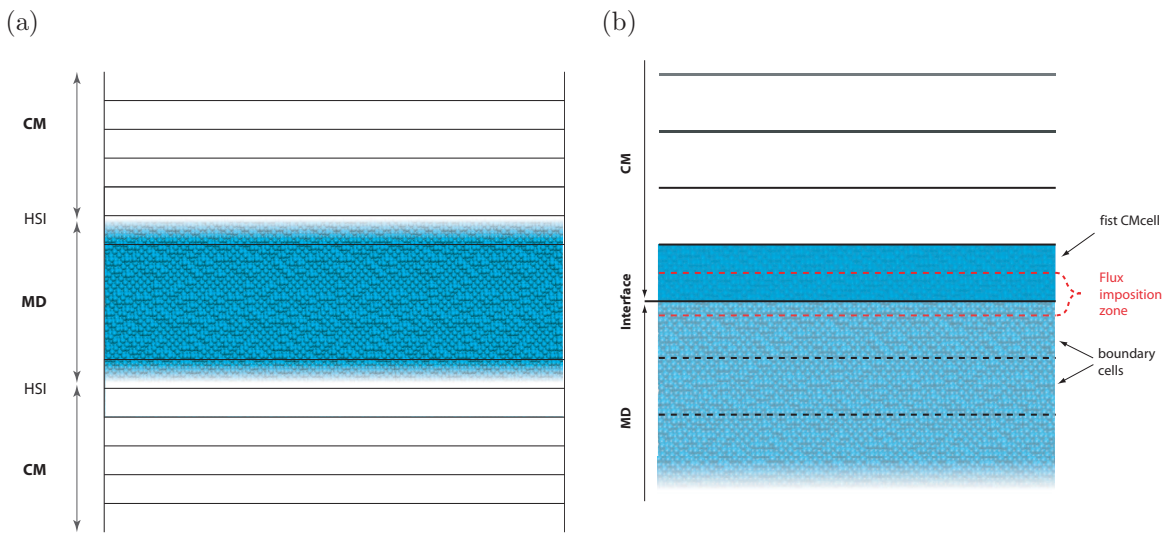

Figure 5.1: Illustration of the domain-decomposition multiscale modelling strategy in one-dimension: (a) Geometrical division where the MD domain is enclosed by two CM domains; (b) Magnified dissection of the HSI at the CM/MD boundary.

the ability to resolve simultaneously micro- and macro-scale phenomena in solid materials via a concurrent coupling of continuum mechanics and molecular dynamics methods. The hybrid domain-decomposition framework, whereby information is passed via a HSI, is adopted to provide the dynamic feedback mechanism required between an Eulerian continuum method for solid materials and MD solver. The continuum solver employed was presented in Chapter 2 using high-order solutions to Riemann problems at cell edges to predict numerical flux functions for the augmented one-dimensional analogue of the governing system from [28]. In this chapter problems shall be considered where the bulk behaviour on the macro-scale is assumed to be one-dimensional. At the micro-scale, three-dimensional MD simulations of the material can be conducted. It is mentioned that the employed coupling by fluxes for the CM to MD direction, and by state for the MD to CM direction, represents a specific combination that is most suitable for the investigated problem. The choice here is made on the basis that for MD this is the unambiguous combination: it is relatively straightforward to deduce macroscale quantities from a defined region within the atomistic simulation domain, but the converse, changing the state of a group of atoms in response to a macroscale measure, is somewhat difficult as one would have to reconstruct the microscopic state from a few macroscopic variables.

The rest of this chapter proceeds as follows. In §5.2 details of the HSI are discussed along with a summary of the implementation of the scheme. In §5.3 an overview is given of the employed MD solver, while §5.4 presents the CM numerical methods. An analysis of the multiscale scheme using example test cases is presented in §5.5 and finally conclusions are drawn in §5.6.

(a) (b)

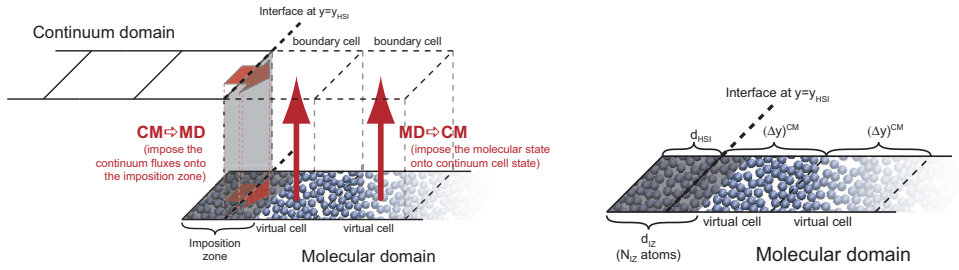

Figure 5.2: Illustration of the HSI setup for the one-dimensional case distinguishing the required zones for both the MD and CM solvers and their relation: (a) CM and MD side of the HSI including the indicated transfer for information; (b) MD side of the HSI showing the geometrical positions and relations. (from [38])

5.2 Coupling of MD with CM

5.2.1 Communication and the HSI

From the viewpoint of the individual simulation method, either based on CM or MD theory, the HSI should provide applicable boundary conditions such that physical information can pass between each domain with minimal numerical artifacts. The HSI must thus strictly conserve mass, momentum and energy; and should not be distinguishable from any deduced results.

Considering first the MD perspective, at the limits of the domain where the CM/MD boundaries reside, reservoirs containing N_{IZ} of the outermost atoms are singled out to be subject to the CM predicted fluxes across the HSI to ensure the application of physically consistent boundary conditions on the MD simulation (Fig. 5.2). Named the *imposition zone* (IZ), these atoms extend a depth d_{IZ}, as measured normal to the CM/MD boundary, into the MD simulation box. For the CM solver, the edge of a computational cell is placed to coincide with the CM/MD boundary a distance d_{HSI}, as measured normal to the CM/MD boundary and from the outermost atoms, into the MD simulation box. Boundary cells, assumed to be of equal size $(\Delta y)^{\mathrm{CM}}$ to the adjacent real cells and the number of which dictated by the stencil employed by the CM numerical methods, are superimposed on the MD domain. The state within these boundary cells is computed by the MD from an ensemble average of the atoms that reside within these cells at the time instant of measurement. It is emphasised that these cells are solely to impose the necessary

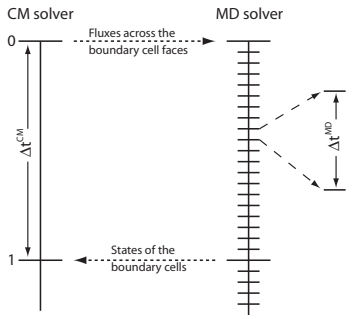

Figure 5.3: Illustration of the time wise synchronisation between the CM and MD solver. (from [38])

boundary conditions on the continuum solver and do not influence in any way the MD solution. It is from the state of these boundary cells and the cells immediately adjacent to the boundary that the CM solver can predict the fluxes to impose on the MD.

For the experiments to be considered the following simplifying assumptions have been made:

- zero mass transfer across the HSI
- material in the continuum domain remains elastic

The implication of the first assumption on the numerical scheme is that the flux functions that apply to the HSI as provided by the CM simulation correspond to the Lagrangian system and thus contain contributions due to traction acting on the boundary only. The second assumption simplifies the CM simulation since inelastic deformations must be accounted for through constitutive laws for the relaxation time of tangential stresses requiring the knowledge of material dependent parameters which, for the single crystal materials that will be investigated, remain undetermined. It is noted that for setups where the MD materials are equilibrated to assume a polycrystalline structure material constants are readily obtained.

5.2.2 Timing

The CM and MD solutions are advanced concurrently in time. A predetermined fixed timestep $(\Delta t)^{\mathrm{MD}}$ is employed in the MD simulations which gives a predefined fixed global timestep for the CM solver of $(\Delta t)^{\mathrm{CM}} = f_{\mathrm{C}} \times (\Delta t)^{\mathrm{MD}}$, where f_{C} is the ratio of time steps (Fig. 5.3). It is necessary in the first instance and the start of each

CM timestep to ensure that $(\Delta t)^{\mathrm{CM}}$ does not violate the CFL condition dictated by the material's state and the employed numerical methods:

$$0 < (\Delta t)^{\mathrm{CM}} \times \max_i \left(\frac{|u_2| + \sqrt{\lambda_{\mathrm{ac}_{\max}}}}{\Delta y} \right) < \mathscr{C} \ , \tag{5.1}$$

[cf. Eq. (2.58)] where for the chosen numerical methods $\mathscr{C} = 1$. It is noted that Eq. (5.1) corresponds to a one-dimensional CM calculation performed in the x_2-direction, which is denoted by $y := x_2$.

5.2.3 Coupling procedure

For coupling in the MD $\rightarrow$ CM direction, at the coincident time for information transfer for each boundary cell of the CM solver, the MD solver passes the following vector of state parameters:

$$\mathbf{U}^{\mathrm{MD}} = (\mathbf{u}, \sigma_{11}, \sigma_{12}, \ldots, \sigma_{33}, T) \ , \tag{5.2}$$

from which it is necessary to deduce the corresponding vector of state variables for the continuum description.

For the opposite direction, CM $\rightarrow$ MD, consider a volume of material where the bounding surface moves with the motion of the material it contains. The vectors of momentum and energy fluxes, $\mathscr{F}_{\mathrm{P}}$ and $\mathscr{F}_{\mathrm{E}} = \mathscr{F}_{\mathrm{ES}}$ respectively, transferred at each point on the surface are:

$$\mathscr{F}_{\mathrm{P}} = (-\sigma \mathbf{n}) \ , \qquad \mathscr{F}_{\mathrm{ES}} = (-\mathbf{n}^{\mathrm{T}} \cdot (\sigma \mathbf{u})) \ , \tag{5.3}$$

where σ is the Cauchy stress tensor, $\mathbf{u}$ the velocity vector, Q the energy flux due to heat conductivity, and $\mathbf{n}$ is the outward pointing unit vector normal to the surface. The MD simulation therefore receives the prescription of stresses at the CM/MD boundary.

Within the multiscale modelling strategy the solution procedure from the MD perspective can be summarised as follows:

Step 1: At each instance of information transfer the MD waits to receive the fluxes across the HSI predicted by the CM solver.

Step 2: The MD solver iterates the molecular system for f_{C} timesteps. During the iteration, the CM predicted fluxes are imposed onto the atoms inside the IZ. The states in the boundary cells may be measured intermittently across this period of time such that an average can be determined in the next instance of information transfer.

Step 3: On reaching the instance of information transfer, the averaged boundary cell states are passed to the CM solver.

Similarly, the solution procedure for the continuum method can be summarised as follows:

Step 1: At the start of each timestep the CM seeks the state of the boundary cells predicted by the MD. This data can then be manipulated according to the requirements of the CM model. If the MD is yet to reach the coincident timelevel then the CM solver waits until this is the case.

Step 2: For the cell edge separating the CM and MD regions the fluxes are predicted using as initial conditions the left and right boundary adjacent states (which may be deduced through reconstruction of data across a larger stencil) and sends these to the awaiting MD.

Step 3: The fluxes are then computed for all other interior cell edges and used in the finite volume discretisation. The solution is then advanced to the next timelevel $t^{n+1} = t^n + (\Delta t)^{\text{CM}}$.

Steps 1-3 are repeated in both solvers until the required simulation time is reached.

5.3 MD solver

Only a summary of the MD solver shall be given here and the reader is instead referred to [38] for a detailed description of the necessary algorithms. The MD method is a deterministic simulation technique based on the classical molecular model [14]. Each atom is modelled as a point mass and the motion governed by Newton's law: $\mathrm{d}^2(m_i\mathbf{r}_i)/\mathrm{d}t^2 = \mathbf{f}_i$, where $\mathbf{r}_i$ is the position of an atom i with the mass m_i and $\mathbf{f}_i$ is the force acting on it. The potential energy of the system, $\mathcal{V}$, is the sum of the potential energies of all atoms: $\mathcal{V} = \sum_i \mathcal{V}_i$ and the force on an atom i is $\mathbf{f}_i = -\nabla_{\mathbf{r}_i}\mathcal{V}_i$. The total energy of the system is given by $E_{\text{tot}} = \mathcal{V} + \sum_i \frac{1}{2} m_i \mathbf{v}_i^2$. The MD code used for the investigation is LAMMPS (Large-scale Atomic/Molecular Massively Parallel Simulator), which was developed at Sandia laboratories [56]. LAMMPS was extended in [38] to incorporate the MD part of the HSI.

Coupling in the MD $\rightarrow$ CM direction requires the translation of the microscopic information within the prescribed boundary cell regions into macroscopic variables. The relevant variables are calculated from the properties of atoms located inside these specified regions.

5.4 CM solver

For a continuum description of solid media the one-dimensional augmented system from Chapter 2 is used. Since mass transfer is omitted across the HSI, the CM/MD boundary will move with any motion predicted between the two domains. For the one-dimensional system here the most straightforward means of accommodating this behaviour in a conservative manner is to employ the moving mesh strategy of Chapter 4. This allows the computational boundaries to have motion governed by the material flow such that the boundary of the cell adjacent to the HSI remains coincident with the CM/MD boundary. The CM governing model is thus solved over a time-dependent, structured computational grid; and the strategy is employed whereby each material or component occupies a different grid. The finite volume Godunov flux approach is then employed. It is noted that, since the spatial order of accuracy is restricted to either first or second, the Riemann solver is formulated in terms of primitive variables, rather than the more lengthy solver formulated in terms of conserved variables. For second order spatial accuracy primitive variables are reconstructed using the MUSCL scheme in [74], in conjunction with the van Leer slope limiter. Where the numerical scheme differs from those employed/proposed in the previous chapters is in the solution at the HSIs.

5.4.0.1 Solution at the CM/MD boundary

At the start of each timestep the CM solver receives from the MD solver values of the stress tensor, the velocity vector, and temperature for each of the boundary cells. It is necessary to deduce from this information the thirteen components of the vector of primitive variables $\mathbf{W} := (\mathbf{u}, \mathbf{F}^{\mathrm{T}}\mathbf{e}_1, \mathbf{F}^{\mathrm{T}}\mathbf{e}_2, \mathbf{F}^{\mathrm{T}}\mathbf{e}_3, \mathscr{S})$. Whereas the velocities comply directly it remains to determine values for $\mathbf{F}$ and $\mathscr{S}$. The constitutive equations Eq. (2.4)-(2.5) can be used to express σ and T as functions of $\mathbf{F}$ and $\mathscr{S}$, but this poses a difficulty since one has ten unknowns and only seven relations. It is possible to overcome this difficulty if special solution procedures are taken for the determination of the inter-cell flux functions at the CM/MD boundary.

Start by considering the following non-linear system of equations:

$$\mathscr{R} := \begin{pmatrix} \sigma^{\mathrm{CM}}\mathbf{e}_1 - \sigma^{\mathrm{MD}}\mathbf{e}_1 \\ \sigma^{\mathrm{CM}}\mathbf{e}_2 - \sigma^{\mathrm{MD}}\mathbf{e}_2 \\ \sigma^{\mathrm{CM}}\mathbf{e}_3 - \sigma^{\mathrm{MD}}\mathbf{e}_3 \\ T^{\mathrm{CM}} - T^{\mathrm{MD}} \end{pmatrix} = 0 \, . \tag{5.4}$$

Since the stress tensor is symmetric the problem in fact reduces to seven equations. For isotropic hyperelastic materials the internal energy density, $\mathscr{E}$, can be formulated in terms of the invariants of any symmetric strain tensor; here the Finger strain tensor $\mathbf{G}$ is assumed, such that $\mathscr{E} = \mathscr{E}(\mathbf{G}, \mathscr{S})$, and it is thus convenient to reconsider

the formulation of the stress tensor using the following Murnaghan formula:

$$\sigma_{ij} = -2\rho G_{ik} \frac{\partial \mathscr{E}}{\partial G_{kj}} \, . \tag{5.5}$$

By substituting the constitutive equation for temperature Eq. (2.4)-(2.5) and Eq. (2.9) into Eq. (5.4) the latter becomes a function of $\mathbf{G}$ and $\mathscr{S}$:

$$\mathscr{R} = \mathscr{R}(G_{11}, G_{12}, G_{13}, G_{22}, G_{23}, G_{33}, \mathscr{S}) \tag{5.6}$$

(recall $\mathbf{G}$ is symmetric). Thus Eqs. (5.4) can be solved using Newtons method to obtain $\mathbf{G}$ and $\mathscr{S}$.

In order to deduce from $\mathbf{G}$ the components of the deformation tensor consider the strain tensor in the following diagonal form:

$$\mathbf{G} = \mathbf{U}^{-1}\mathbf{K}^{-2}\mathbf{U} \, , \tag{5.7}$$

where $\mathbf{U}$ is an orthogonal matrix ($\mathbf{U}^{-1}\mathbf{U} = \mathbf{I}$) and $\mathbf{K}$ is a diagonal tensor who's components represent the principle stretches. Given $\mathbf{G}$, both $\mathbf{U}$ and $\mathbf{K}$ can be found easily using the method in [69]. With these values known the attention is turned to $\mathbf{F}$, which can be decomposed as

$$\mathbf{F} = \mathbf{U}\mathbf{K}\mathbf{U}^{-1}\mathbf{V} \, , \tag{5.8}$$

where the tensor $\mathbf{V}$ is orthogonal. Finally then everything is known except $\mathbf{V}$. One choice would be to simply take $\mathbf{V} = \mathbf{I}$, however the approximate solution method for the Riemann problems posed at the cell boundaries is dependent on $\mathbf{V}$ and it is insufficient to assume any orthogonal matrix unless further special modifications are made to the solution procedure.

It can be shown (see Chapter 4) that the approximate solution of the Riemann problem across the CM/MD interface cell can be explicitly stated as:

$$\begin{pmatrix} \widetilde{\mathbf{u}} \\ \widetilde{\mathbf{F}}^{\mathrm{T}}\mathbf{e}_1 \\ \widetilde{\mathbf{F}}^{\mathrm{T}}\mathbf{e}_2 \\ \widetilde{\mathbf{F}}^{\mathrm{T}}\mathbf{e}_3 \\ \widetilde{\mathscr{S}} \end{pmatrix} = \begin{pmatrix} \mathbf{u} \\ \mathbf{F}^{\mathrm{T}}\mathbf{e}_1 \\ \mathbf{F}^{\mathrm{T}}\mathbf{e}_2 \\ \mathbf{F}^{\mathrm{T}}\mathbf{e}_3 \\ \mathscr{S} \end{pmatrix} + \frac{1}{\rho} \begin{pmatrix} \zeta \mathbf{Q}^{-1}\mathscr{D}^{-1}\mathbf{Q}\left(\widetilde{\sigma}\mathbf{e}_2 - \sigma\mathbf{e}_2\right) \\ \left(\mathbf{F}^{\mathrm{T}}\mathbf{e}_2\right) \otimes \left(\mathbf{e}_1^{\mathrm{T}}\mathbf{\Omega}^{-1}\right)\left(\widetilde{\sigma}\mathbf{e}_2 - \sigma\mathbf{e}_2\right) \\ \left(\mathbf{F}^{\mathrm{T}}\mathbf{e}_2\right) \otimes \left(\mathbf{e}_2^{\mathrm{T}}\mathbf{\Omega}^{-1}\right)\left(\widetilde{\sigma}\mathbf{e}_2 - \sigma\mathbf{e}_2\right) \\ \left(\mathbf{F}^{\mathrm{T}}\mathbf{e}_2\right) \otimes \left(\mathbf{e}_3^{\mathrm{T}}\mathbf{\Omega}^{-1}\right)\left(\widetilde{\sigma}\mathbf{e}_2 - \sigma\mathbf{e}_2\right) \\ 0 \end{pmatrix} \, , \tag{5.9}$$

where

$$\begin{aligned} \widetilde{\sigma}\mathbf{e}_2 \; = \; & \left[\frac{1}{\rho^{\mathrm{CM}}}\left(\mathbf{Q}^{-1}\mathscr{D}^{-1}\mathbf{Q}\right)^{\mathrm{CM}} + \frac{1}{\rho^{\mathrm{MD}}}\left(\mathbf{Q}^{-1}\mathscr{D}^{-1}\mathbf{Q}\right)^{\mathrm{MD}}\right]^{-1} \\ & \left[\frac{1}{\rho^{\mathrm{CM}}}\left(\mathbf{Q}^{-1}\mathscr{D}^{-1}\mathbf{Q}\right)^{\mathrm{CM}}\sigma^{\mathrm{CM}}\mathbf{e}_2 + \frac{1}{\rho^{\mathrm{MD}}}\left(\mathbf{Q}^{-1}\mathscr{D}^{-1}\mathbf{Q}\right)^{\mathrm{MD}}\sigma^{\mathrm{MD}}\mathbf{e}_2 + \zeta\left(\mathbf{u}^{\mathrm{MD}} - \mathbf{u}^{\mathrm{CM}}\right)\right] \end{aligned} \tag{5.10}$$

with $\zeta = -1$ if solving for material on the right and $\zeta = +1$ for material on the left. Thus it is seen that the only information required from the MD data in order to predict the interface state is the stress vector and acoustic tensor, all of which are independent of the choice of $\mathbf{V}$.

The order of accuracy of the CM/MD boundary Riemann problem is increased to second order by using data from a four point stencil, instead of two. The MD then is required to provide the data in two boundary cells for all HSI's. The MUSCL scheme is again used, as with the CM bulk solver, with the van Leer slope limiter.

5.5 Examples

In this section example testcase are used to demonstrate the hybrid simulation method. In all examples to follow the MD simulations employ the embedded atom method (EAM) [12] for modelling the interatomic interactions; the potentials are thus defined as

$$\mathcal{V}^{\mathrm{EAM}} = \sum_{i=1}^{N} \left[F_i\left(\bar{\rho}_i\right) + \frac{1}{2} \sum_{j=1, j\neq i}^{N} U_{ij}\left(r_{ij}\right) \right] , \tag{5.11}$$

where

$$\bar{\rho}_i = \sum_{j=1, j\neq i}^{N} \rho\left(r_{ij}\right) . \tag{5.12}$$

The term $F_i\left(\bar{\rho}_i\right)$ is the required energy to embed an atom i into the electron gas at the site $\mathbf{r}_i$ with the average electron density $\bar{\rho}_i$, which is the sum of the radial symmetric contributions of all other atoms $j \neq i$. The parameter $U_{ij}\left(r_{ij}\right)$ is the pair interaction potential between the atomic cores of atom i and j.

The hyperelastic equation of state from [3] is used to close the continuum model:

$$\mathscr{E}(\mathcal{I}_1, \mathcal{I}_2, \mathcal{I}_3, S) = \frac{K_0}{2\alpha^2}(\mathcal{I}_3^{\alpha/2} - 1)^2 + c_{\mathrm{V}} T_0 \mathcal{I}_3^{\gamma/2} \left[\exp(\mathscr{S}/c_{\mathrm{V}}) - 1\right] + \frac{B}{2}\mathcal{I}_3^{-2/3}(\mathcal{I}_1^2/3 - \mathcal{I}_2). \tag{5.13}$$

where $\mathcal{I}_1 := \mathrm{tr}\ \mathbf{G}$, $\mathcal{I}_2 := \frac{1}{2}\left[(\mathrm{tr}\ \mathbf{G})^2 - \mathrm{tr}\ \mathbf{G}^2\right]$, $\mathcal{I}_3 := \det|\mathbf{G}|$, are the invariants of the elastic Finger tensor $\mathbf{G} = \mathbf{F}^{-\mathrm{T}}\mathbf{F}^{-1}$. The reference squared bulk speed of sound K_0 and constant α in the first term are found from hydrostatic compression curves deduced from MD simulations for each of the materials employed below. The same results then provide the Gruneisen constant [90]: $\gamma = -2/3 - (V/2)\left[\left(\mathrm{d}^2 p(V)/\mathrm{d}V^2\right)/\left(\mathrm{d}p(V)/\mathrm{d}V\right)\right]$ where $V = 1/\rho$ is the specific volume. The squared speed of shear waves $B(\rho)$ is taken to be the constant value obtained from shear tests performed using MD at the employed pressures. The material parameters are given in Table 5.1 for all examples to follow.

In both of the following examples the MD domain ranges from $-y_{\mathrm{HSI}}$ to y_{HSI} and is equilibrised in the same manner. All simulations are performed assuming globally

Table 5.1: Material constants for the internal energy density described by Eq. (5.13).

Parameter	Material			Units
	Cu[a]	Cu[b]	Al[b]	
ρ_0	8.80	8.79	2.63	$\mathrm{g\,cm^{-3}}$
K_0	14.67	14.53	24.57	$\mathrm{km^2\,s^{-2}}$
c_v	$3.93 \cdot 10^{-4}$	$3.93 \cdot 10^{-4}$	$9.24 \cdot 10^{-4}$	$\mathrm{kJ\,g^{-1}\,K^{-1}}$
T_0	300	300	300	K
B	8.65	10.18	17.41	$\mathrm{km^2\,s^{-2}}$
α	0.76	0.979	1.05	–
γ	1.88	2.35	2.45	–

[a] Constants derived from MD experiments using the EAM potential of [21].
[b] Constants derived from MD experiments using the EAM potential in [9].

one-dimensional problems although the MD simulations are three-dimensional. To simulate an infinite material in the x_1- and x_3-directions, periodic boundary conditions are applied to the bounding plane in these dimensions; the HSI's are located at $-y_\mathrm{HSI}$ (top) and $-y_\mathrm{HSI}$ (bottom). After generating the atomic positions, the MD domain is equilibrated to a static pressure p, a temperature T and zero velocity. During the equilibration, the stress in the x_2-direction is maintained by applying a constant flux boundary condition as described with a momentum flux vector: $\mathscr{F}_\mathrm{P} = (0, p, 0)$. The size of the simulation domain in the x_1- and x_3-directions is adjusted by using a Berendsen barostat [7] to converge the systems towards a diagonal stress tensor ($\sigma_{xx} = \sigma_{yy} = \sigma_{zz} = p$) with zero deviatoric components: $\sigma' = \sigma - p\mathbf{I} = 0$. In practice the deviatoric stress components do tend to zero throughout equilibrisation , but will retain a small non-zero value.

In order to maintain a consistent initial state for both continuum and molecular regions, the continuum simulation is initialised to a state where the deformation and entropy correspond to the temperature and diagonal components of stress of the first boundary cell in the MD domain resulting from equilibrisation. This is achieved by solving the non-linear system Eq. (5.4) neglecting off-diagonal stress terms and solving only for the principal strains and entropy.

5.5.1 Example 1

In this first example the motion of strong non-linear shear waves is considered in copper. The decomposition of the simulation domain is such that an MD region is bounded at the top and bottom by CM domains. The MD simulation domain

had the approximate range $[0:50, -250:250, 0:50]$ Å. Shear waves, travelling in opposite directions, are generated in the lower CM domain by imposing a tangential velocity $\mathbf{u}_{\text{INI}}^{\text{Cu}} = (0, 0.5, 0)$ km s^{-1} on the region $y < -750$ Å, with the rest of the domain taken to be at rest. The upwards travelling wave should thus propagate out of the first CM region, into the MD, and subsequently into the upper CM domain, unperturbed. The initial static pressure $p = 5.1$ GPa and temperature $T = 300$ K were assumed throughout. The EAM parameters of [21] for the Cu atoms was used.

At first, the effect of CM cell size was examined, whilst the HSI variables were maintained at constant values: N_{IZ} taken to be a predetermined value based upon the imposition zone volume for $d_{\text{IZ}} = 2.5$Å and number density corresponding to a pressure of 5.1 GPa; $d_{\text{HSI}} = 2.5$Å. The ratio of timesteps was taken to be $f_{\text{C}} = 10$ with $(\Delta t)^{\text{MD}} = 0.0025$ ps.

The results of the hybrid MD-CM method show that a prominent numerical artifact is a peak in the shear stress, which is an artifact of a wave that is generated when the original shear wave is partially reflected while passing through the HSIs (Figure 5.4). It is observed that the wave reflections are more profound as the wave propagates from the MD domain into the CM domain, which can be expected if the grid resolution of the CM is not on the order of the lattice parameter [73]. Furthermore, due to the inherent regularisation, the CM solver smears the waves over a finite number of grid points decreasing the resolution. It is not surprising that using a smaller CM cell size yields improved solutions and the solution is seen to converge (Figure 5.5). Overall agreement is good for CM cell sizes of $(\Delta y)^{\text{CM}} \leq 20$Å; in all these cases the MD solution is in good agreement with the pure CM.

Subsequent investigations of the HSI variables indicated little influence on the solution as compared to changing the CM cell size, rather effecting the stability of the scheme, and are thus omitted. The values employed represent optimum values found through lengthy parameteric analysis of the HSI variables alone.

5.5.2 Example 2

Here results are presented using the multi-scale scheme for simulations of dry sliding between two semi-infinite tribo-pair materials, using an experimental setup similar to that employed in [29, 88, 18]. The system comprises an interface between the materials representing a (0,1,0) plane with MD used to simulate the regions immediately adjacent to the interface in both materials and CM for the remaining bulk material. For these tests the MD simulation domain had the approximate range $[0:72, -250:250, 0:72]$ Å, with the interface plane separating the two materials at $y_0 = 0$ Å. The upper region $y > y_0$ is assumed to be copper (Cu) whilst the lower region $y < y_0$ is assumed to aluminium (Al). The CM cell size was taken to be $(\Delta y)^{\text{CM}} = 20$Å. The sample is assumed to have been preloaded by the passage of an oblique shock wave such that the bulk pressure and relative tangential velocities are

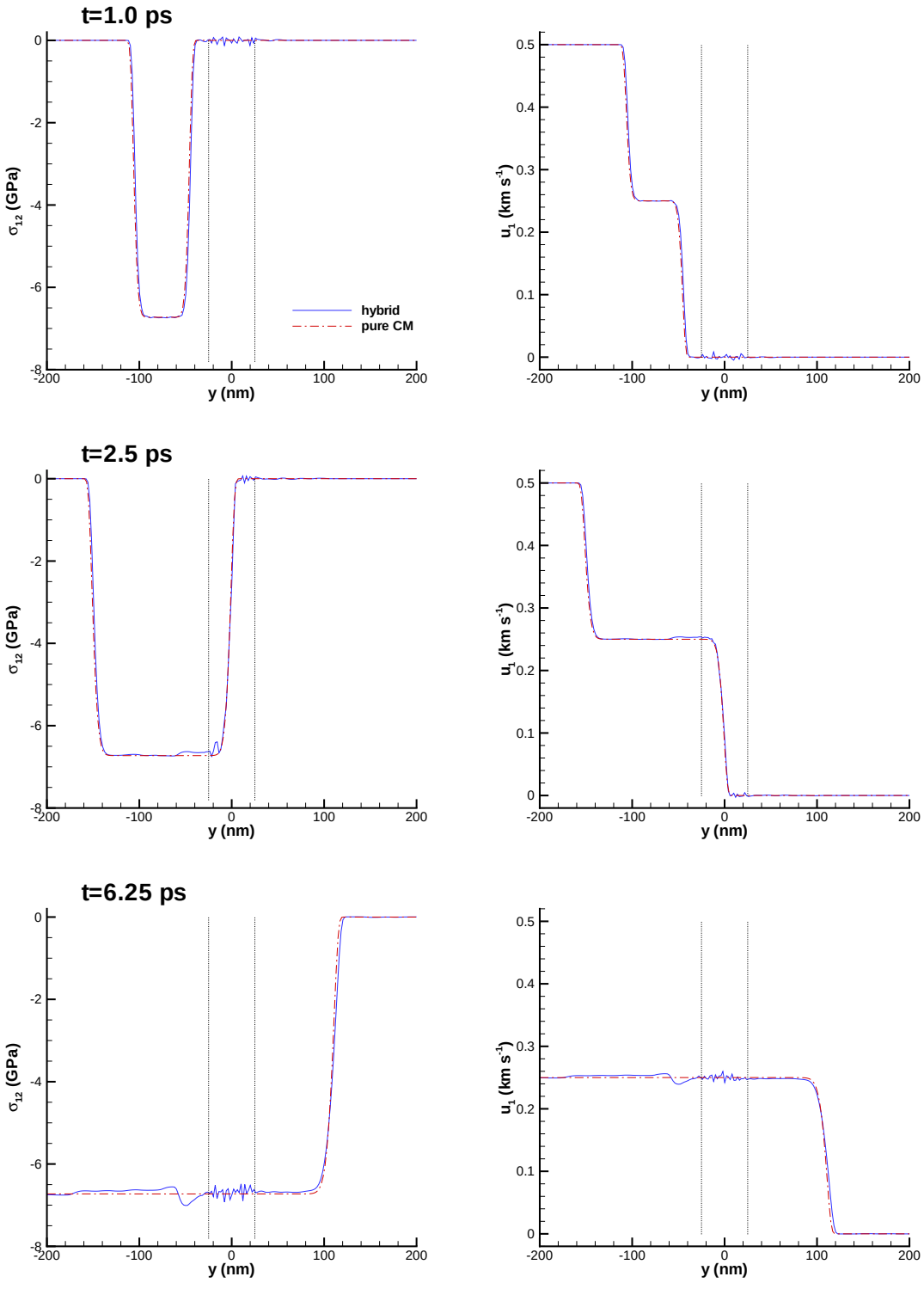

Figure 5.4: Profiles of shear stress and tangential velocity at different time instances using pure CM and the hybrid method with a CM cell size of $\Delta y = 20$Å for Example 1. The lines at $y = \pm 25$Å mark the locations of the HSI's in the hybrid solution.

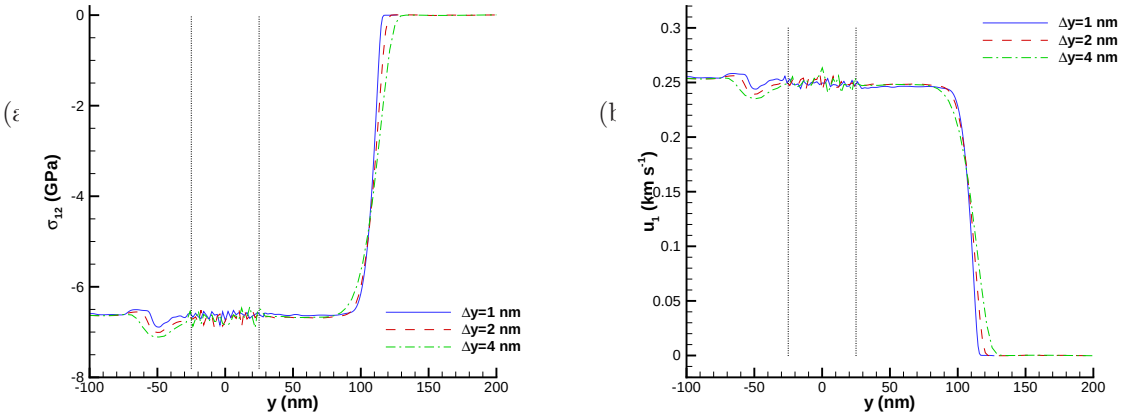

Figure 5.5: Profiles of shear stress and tangential velocity at different using the hybrid method with different CM cell sizes Δy for Example 1. The lines at $y = \pm 25$Å mark the locations of the HSI's in the hybrid solution.

non-zero. The EAM parameters of Cai and Ye [9] for the system of Cu and Al atoms have been used. The initial static pressure $p = 11.2\,\mathrm{GPa}$ and temperature $T = 300\,\mathrm{K}$ is assumed throughout both materials. At the start of each multiscale simulation the initial desired bulk sliding velocity $\mathbf{u}^{\alpha}_{\mathrm{INI}}$ for each material α is added to the velocity $\mathbf{u}^{\alpha}_{i}(t=0)$ for each atom i in the MD and throughout the CM. For the experiments conducted here the relative sliding velocity was $\Delta\mathbf{u} = (0, 0.2, 0)\,\mathrm{km\,s^{-1}}$ and achieved using the initial velocities $\mathbf{u}^{\mathrm{Al}}_{\mathrm{INI}} = (0, -0.1, 0)\,\mathrm{km\,s^{-1}}$ and $\mathbf{u}^{\mathrm{Cu}}_{\mathrm{INI}} = (0, 0.1, 0)\,\mathrm{km\,s^{-1}}$. The interface in all cases was assumed to be atomically smooth. The conditions result in two strong shear waves being generated within the MD region at the interface which subsequently propagate into the bulk material.

Overall agreement is good between the results using the hybrid method and with calculations from a larger pure MD domain with the size $[0:72, -500:500, 0:72]$ Å (Figure 5.6). Again due to partial reflection of the shear waves when reaching the HSIs numerical artifacts can be observed in the MD solution. After the waves have passed through into the CM domains they become slightly diffused artificially as expected, but the speed of propagation and transmitted loads remain in good agreement with the pure MD. Note that small differences remain apparent as a result of differences in the equilibration of the two MD samples, which can clearly be seen in the profiles prior even to the shear waves reaching the HSIs.

5.6 Conclusions

A Coupled MD-CM method for simulating solids subject to large tangential deformations has been proposed. The method allows the simulation of macroscale

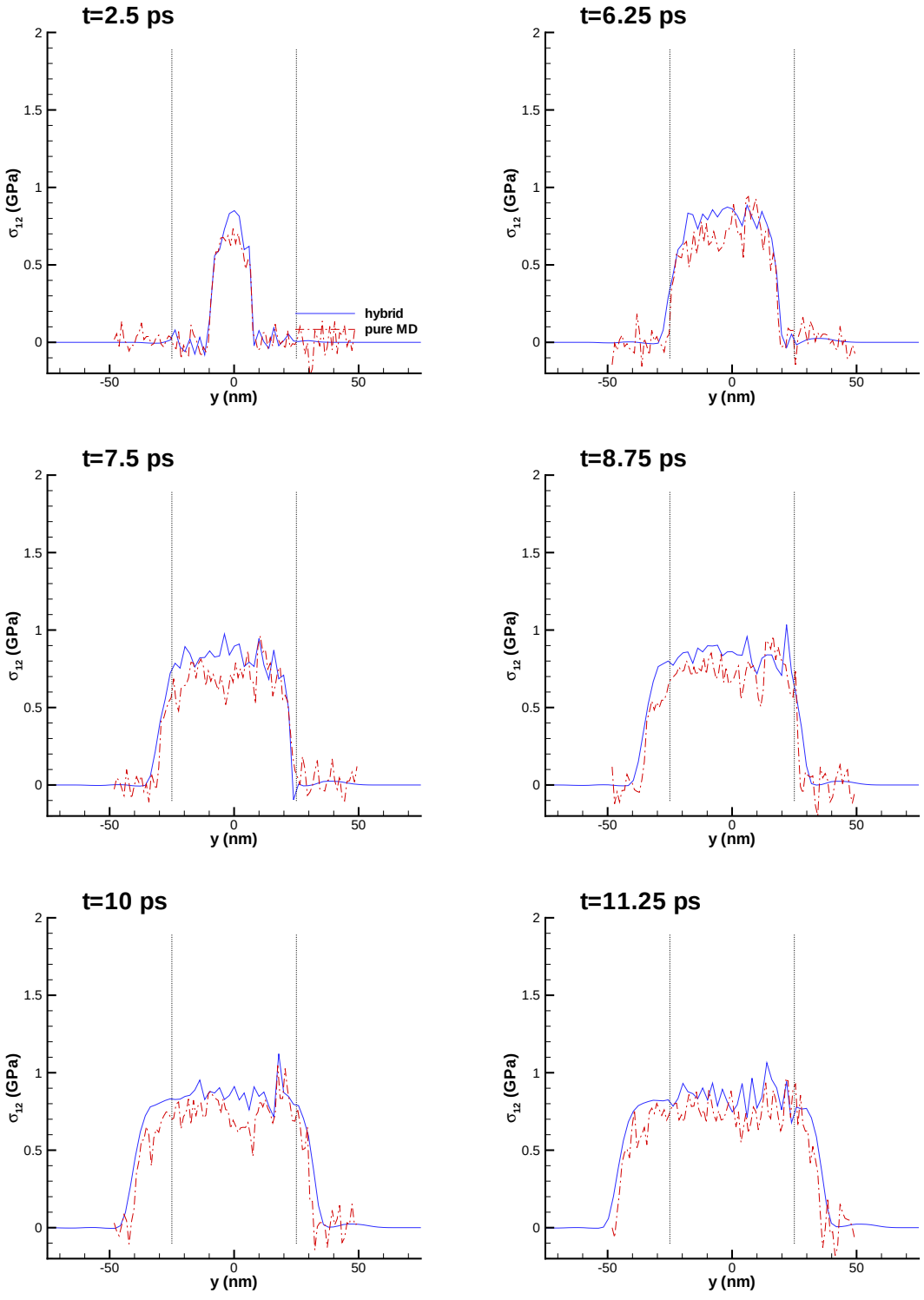

Figure 5.6: Profiles of shear stress at different time instances using pure MD and the multi-scale method with a CM cell size of $\Delta y = 20$Å for Example 2. The lines at $y = \pm 25$Å mark the locations of the HSI's in the hybrid solution.

simulation domains, while still resolving the atomistic details at a desired region in the materials. The numerical parameters of the method have been investigated for their influence on the quality of the coupling. In particular, the production of any numerical artifacts, such as the partial reflection of shear waves passing through the CM-MD interface. It has been shown that the cell size of the continuum grid is the most important parameter, and a cell size of ≤ 20Å gives acceptable results.

Examples showed a case where waves are generated outside of the MD simulation box and which can be investigated as they subsequently pass through the atomistic domain. Another case considered waves that are generated in the MD domain and subsequently travel into the CM domains. The former demonstrates the potential use of the hybrid method for studying wave physics. The latter is an example of where a singularity exists in CM constitutive equations (friction models) and requires pure atomistic studies, which faces difficulties as a result of limited domain sizes which the hybrid approach overcomes.

6

Conclusions and future work

6.1 Conclusions

The work in this thesis has focused on establishing numerical schemes for compressible solid materials that allow the simulation of multi-component systems. Initially these methods were developed and validated in a pure continuum framework for single materials. The focus of the extension to multi-solid systems comprised two investigations: the proposal and examination of certian interface tracking methods on the basis of established requirements; and the proposal and use of a new multiscale modelling strategy to study the interfacial behaviour between contacting materials.

A continuum model for solid dynamics has been used throughout where the governing laws are written as first order partial differentials in conservative form. The choice of this model was made on the basis that an Eulerian finite volume shock capturing method could thus be developed for solid mechanics. Owing to the great wealth of numerical tools proposed in the open litrature for solving partial differential equations, there exist many possibilities of achieving these goals. In the first instance the special case of non-linear elasticity was considered in one space dimension. The method of lines was adopted and the Godunov flux approach, where Riemann problems are solved locally at cell edges, was used in the discretisation of convective terms. State-of-the-art reconstruction methods were incorporated to achieve higher order spatial discretisations. These were selected on the basis of similarities between the model and the models on which the methods were established (such as MHD); or on a percieved potential of applying certain methods within the new setting. Reconstruction was carried out for characteristic variables; a necessary approach to achieve monotonic solutions.

Validating such methodologies is not trivial: unlike the equations of gas-dynamics for example, testcases in solid materials require the resolution of free-surfaces and boundaries, hence the need for an interface tracking method. This challenge was circumvented by deriving exact solutions to Riemann problems in non-linear elasticity.

Again due to the lack of available interenal flow problems for problems in solid dynamics, numerical solutions using fine grids were sought for one-dimensional polar

monologues of the governing model for particular polar symmetric multi-dimensional problems.

The MPWENO method proved most effective at resolving the complex wave systems for selected initial value problems involving three-dimensional deformations. Specifically the fifth-order MPWENO method proved to be the best balance between accuracy and cost. The same was true for multi-dimensional problems involving elastoplastic deformations.

Effort was devoted to establishing methods that remain sufficiently general, i.e. neglecting basing derivations on specific equations of state so that the methods were not limited to any one solid material.

It is mentioned that using level-set functions to track interfaces in a conservative scheme such as in [32] could lead to difficulties in solid dynamics problems on account of mass loss. To exemplify this point consider a geometry with corners which would be typical to many problems in solid mechanics. Translating this through a grid using the level-set advection equation to evolve the boundaries will result in mass loss in the corner regions where characteristics converge and the inherent regularisation deletes the unresolved information (see [17]). Whilst modifications of the necessary numerical algorithms have been proposed that successfully suppress these errors, they are not entirely eliminated. Thus one can expect an error in the change in volume fraction in these regions across each time level. The result would be an erroneous computation of state variables potentially compromising numerical stability. From these considerations it is thus justified that if one is to employ level-set functions then a ghost fluid method should provide better stability.

Later these methods were adapted to form a multiscale physics solver in conjunction with molecular dynamics; however it was the continuum mechanics solver that remained the focul point.

6.2 Future work

Much of the work represents the foundations of a more vast capability and there remains much further work to establish a general three-dimensional modelling technique that covers all physical behaviours within multiple solid materials.

Referring back to the summarised historically observed behaviours of solid materials undergoing dynamic deformations in Chapter 1, one can identify a number of outstanding phenomena achievable within the framework of the model employed for this work. Many of these can be accounted for by including additional constitutive equations, or indeed through modifications of those that are already employed. Some of the more primary behaviours and strategies for inclduing them are as follows:

- **Fracture mechanics:** Incorporation of damage kinetics within the current model can be achieved using additional equations for the evolution of a scalar

damage measure [63] or pore volume per unit volume [8, 80, 23, 81] (both exhibit similar form). Implications on the existing constitutive models manifest as additional terms in the closure model for internal energy density; specifically an additional energy function in terms of the chosen scalar parameter for the damage kinetics.

- **Work hardening:** One means of including work hardening is to add to the list of state variables the equivelent plastic strain [40, 58]. Transport equations can thus be derived and added to the governing system where the mechanism for production of plastic strain is a function of the equivelent plastic strain rate, many models for which are available in the open litrature. Note also that in [49] the inclusion of an additional equation for the work hardeing parameter was accompanied by a modification of the closure model for internal energy density to include a contribution due to strain hardening.

- **Thermal softening and melting:** The inclusion of thermal softening and melting within the proposed scheme need not require modifications of the bulk algorithms. In this work the mechanism for inelastic deformations was governed by the relaxation time of tangential stresses, which here was considered merely as a function of the stress tensor components. In reality the relaxation time would be a complex non-linear function not only the stress but also the temperature [27]. It is possible to formulate common constitutive models for flow stress that include thermal influenecs, such as the Johnson-Cook model [35] using the derivation presented in [8].

The proposed interface tracking schemes on fixed grids, namely the level-set based approaches, have shown excellent implementation of the desired interfacial boundary conditions in one-dimension. This implies that the use of these methods would be invaluable in higher space dimensions if this property holds; hence extension to high space dimensions can be designated as an important further task. One reason level-set methods were originally chosen was that extension of the related boundary advection algorithms are relatively straightforward to extend to multi-dimensions. It is necessary then to simply solve the same one-dimensional multi-material Riemann problems orientated normal to the boundary in the respective boundary cells. Extrapolation of state quantities to surrounding ghost cells can be achieved by using the PDE based method in [19]. The MGFM and conservative level-set methods will of course differ in specifics but the principle tasks of solving boundary Riemann problems and extrapolating variables will be the same.

A profound numerical artifact observed in the multiscale simulations was partial reflection of waves as they pass through HSIs. The main influencial parameter on this behaviour was found to be the continuum cell size; with artifacts reducing as the cell size converged to the order of the lattice parameter. Whilst one could apply

an adaptive mesh refinement strategy to the continuum solver in the vicinity of the HSIs, it is desirable to maintain a cellsize as large as possible. This is especially true when considering extension to multiple space dimensions. Recognising similar reasonings in the CGMD class of methods, in [73] a 'perfectly matched layer' algorithm was proposed as a remedial modification of the underlying schemes. Of course this method was derived on the basis of employing finite-element analysis of the continuum theory and it is not immediately clear how this could be adapted to suit the current framework. Nonetheless, since the desired results of zero reflections is achieved in this way without resorting to small cell sizes, it warrants investigation in further work.

References

[1] U. M. Ascher & L. R. Petzold, *Computer methods for ordinary differential equations and differential-algebraic equations*, (SIAM, 1998).

[2] D. S. Balsara & C. Shu, Monotonicity preserving weighted essentially non-oscillatory schemes with increasingly high order accuracy, *J. Comp. Phys.*, **160**, 405 (2000).

[3] P. T. Barton, D. Drikakis, E. Romenski & V. A. Titarev, Exact and approximate solutions of Riemann problems in non-linear elasticity, *J. Comp. Phys.*, **228** 7046 (2009).

[4] P. T. Barton, D. Drikakis & E. Romenski, An Eulerian finite-volume scheme for large elastoplastic deformations in solids, *Int. J. Num. Meth. Eng.* DOI: 10.1002/nme.2695 (2009).

[5] P. T. Barton & D. Drikakis, An Eulerian method for multi-component problems in non-linear elasticity with sliding interfaces, *under review* (2009).

[6] D. J. Benson, Computational methods in Lagrangian and Eulerian hydrocodes, *Comp. Meth. Appl. Mech. Eng.*, **99** 235 (1992).

[7] H. J. C. Berendsen, J. P. M. Postma, W. F. van Gunsteren, A. DiNola & J. R. Haak, Molecular dynamics with coupling to an external bath, *J. Chem. Phys.*, **81** 3684 (1984).

[8] A. V. Bushman, *Intense Dynamic Loading Of Condensed Matter*, (CRC, 1992).

[9] J. Cai & Y. Y. Ye, Simple analytical embedded-atom-potential model including a long-range force for fcc metals and their alloys, *Phys. Rev. B* **54** 8398 (1996).

[10] G.-Q. Chen, C. D. Levermore & T.-P. Liu, Hyperbolic Conservation Laws with Stiff Relaxation Terms and Entropy, *Comm. Pure Appl. Math.*, **47** 787 (1994).

[11] F. Dambakizi, P. Le Tallec & J. P. Perlat, Multiscale thermomechanical modeling of shock-driven dry friction, *J. Comp. Phys.*, **198** 1701 (2009).

[12] M. S. Daw, S. M. Foiles & M. I. Baskes, The Embedded Atom Method: a review of theory and applications, Materials Science Reports, *Mater. Sci. Rep.*, **9** 251 (1993).

[13] D. Drikakis & W. Rider, *High-Resolution Methods for Incompressible and Low-Speed Flows*, (Springer, 2005).

[14] D. Drikakis & M. Kalweit, Computational Modelling of Flow and Mass Transport Processes in Nano-technology, *Handbook of Computational Nano–technology*, M. Rieth & W. Schommers (editors), (American Scientific Publishers, Stevenson Ranch, CA, USA 2006).

[15] W. E, W. Ren & E. Vanden-Eijinden, A general strategy for designing seamless multiscale methods, *J. Comp. Phys.*, **228** 5437 (2009).

[16] A. Eberle, Characteristic Flux Averaging Approach to the Solution of Euler's Equations, in *VKI Lecture Series, Computational Fluid Dynamics* (1987).

[17] D. Enright, R. Fedkiw, J. Ferziger & I. Mitchell, A Hybrid particle Level Set Method for Improved Interface Capturing, *J. Comp. Phys.*, **183**, 83 (2002).

[18] N. Epiphaniou, M. Kalweit, D. Drikakis, G. Ball & N. Park, Molecular dynamics simulations of dynamic friction and mixing at rapidly moving material interfaces, *J. Phys. D*, in press (2009).

[19] R. P. Fedkiw, T. Aslam, B. Merriman & S. Osher, A Non-oscillatory Eulerian Approach to Interfaces in Multimaterial Flows (the Ghost Fluid Method), *J. Comp. Phys.*, **152**, 457 (1999).

[20] R. P. Fedkiw, Coupling an Eulerian Fluid Calculation to a Lagrangian Solid Calculation with the Ghost Fluid Method, *J. Comp. Phys.*, **175**, 200 (2002).

[21] S. M. Foiles, M. I. Baskes & M. S. Daw, Embedded-atom-method functions for the fcc metals Cu, Ag, Au, Ni, Pd, Pt, and their alloys, *Phys. Rev. B*, **33** 8983 (1986).

[22] V. E. Fortov, B. Goel, C.-D. Munz, A. L. Ni, A. V. Shutov & O. Yu. Vorobiev, Numerical simulations of nonstationary fronts and interfaces by the godunov method in moving grids, *Nuclear Sci. Eng.*, **123**, 169 (1996).

[23] V. Fortov, V. Kondaurov & I. Lomov, Investigation of the nuclear explosion effect on asteroids, *Int. J. Impact Eng.*, **20**, 265 (1997).

[24] X. Garaizar, The small anisotropy formulation of elastic deformation, *Acta Applicandae Mathematicae*, **14**, 259 (1989).

[25] X. Garaizar, Solution of a Riemann problem for elasticity, *J. Elasticity*, **26**, 43 (1991).

[26] S. K. Godunov & E. I. Romenskii, Nonstationary Equations of Nonlinear Elasticity Theory in Eulerian Coordinates, *J. App. Mech. Tech. Phys.*, **13**, 868 (1972).

[27] S. K. Godunov, A. F. Demchuk, N. S. Kozin & V. I. Mali, Interpolation formulas for maxwell viscosity of certain metals as a function of shear-strain intensity and temperature, *J. Appl. Mech. Tech. Phys.*, **15** 526 (1974).

[28] S. K. Godunov & E. I. Romenskii, *Elements of Continuum Mechanics and Conservation Laws*, (Kluwer Academic/Plenum Publishers, 2003).

[29] J. E. Hammerberg, T. C. Germann, B. L. Holian & R. Ravelo, Nanoscale structure and high velocity sliding at Cu/Ag interfaces, *Mat. Res. Soc. Symp. Proc*, **821** 103 (2004).

[30] C. W. Hirt, A. A. Amsden& J. L. Cook, An arbitrary Lagrangian-Eulerian computing method for all flow speeds, *J. Comp. Phys.*, **135**, 203 (1997).

[31] B. P. Howell & G. J. Ball, A Free-Lagrange augmented Godunov method for the simulation of elastic-plastic solids, *J. Comp. Phys.*, **175**, 128 (2002).

[32] X. Y. Hu, B. C. Khoo, N. A. Adams & F. L. Huang, A conservative interface method for compressible flows, *J. Comp. Phys.*, **219**, 553 (2006).

[33] G. S. Jiang & C. W. Shu, Efficient implementation of weighted ENO schemes, *J. Comp. Phys.*, **126**, 202 (1996).

[34] S. Jin, Runge-Kutta methods for hyperbolic conservation laws with stiff relaxation, *J. Comp. Phys.*, **122** 51 (1995).

[35] G. R. Johnson & W. H. Cook, A constitutive model and data for metals subjected to large strains, high strain rates and high temperatures, in *Proceedings of the Seventh International Symposium on Ballistics, Hague*, (1983).

[36] A. Juanicotena, Experimental investigation of dynamic friction at high contact pressure applied to an aluminium/stainless steel tribo pair, *J. Phys. IV*, **134** 559 (2006).

[37] M. Kalweit & D. Drikakis, Multiscale Methods for Micro/Nano Flows and Materials, *J. Comp. Theo. Nanosci.*, **5** 1923 (2008).

[38] M. Kalweit, P. T. Barton & D. Drikakis, Hybrid molecular dynamics - continuum mechanics method for solid materials, *under review*, (2009).

[39] G. Kluth & B. Després, Perfect plasticity and hyperelastic models for isotropic materials, *Continuum Mech. Thermodyn.*, **20**, 173 (2008).

[40] V. I. Kondaurov, Equations of elastoviscoplastic medium with finite deformations, *J. App. Mech. Tech. Phys.*, **23**, 584 (1982).

[41] A. G. Kulikovskii & N.V. Pogorelov, Mathematical Aspects of Numerical Solution of Hyperbolic Systems, (CRC Press, 2001).

[42] P. G. LeFloch & F. Olsson, A second-order Godunov method for the conservation laws of nonlinear elastodynamics, *Impact Comp. Sci. Eng*, **2**, 318 (1990).

[43] P. G. LeFloch, Hyperbolic systems of conservation laws: The theory of classical and nonclassical shock waves, (Berkhäuser Varlag, 2002).

[44] T. G. Liu, B. C. Khoo & K. S. Yeo, Ghost fluid method for strong shock impacting on material interface, *J. Comp. Phys.*, **190**, 651 (2003).

[45] T. G. Liu, W. F. Xie & B. C. Khoo, The modified ghost fluid method for coupling of fluid and structure constituted with hydro-elasto-plastic equation of state, *SIAM J. Sci. Comp.*, **30**, 1105 (2008).

[46] L. A. Merzhievskii & S. A. Samonin, Construction of the time dependence of the relaxation of tangential stresses on the state parameters of a medium, *J. Appl. Mech. Tech. Phys.*, **21** 716 (1980).

[47] L. A. Merzhievsky & A. V. Tyagel'sky, Relation of dislocation kinetics with dynamic characteristics in modelling mechanical behaviour of materials, *J. de Phys.* C3, **49** 457 (1988).

[48] G. H. Miller & P. Colella, A High-Order Eulerian Godunov Method for Elastic-Plastic Flow in Solids, *J. Comp. Phys.*, **167**, 131 (2001).

[49] G. H. Miller & P. Colella, A Conservative Three-Dimensional Eulerian Method for Coupled Solid-Fluid Shock Capturing, *J. Comp. Phys.*, **183**, 26 (2002).

[50] G. H. Miller, An iterative Riemann solver for systems of hyperbolic conservation laws, with application to hyperelastic solid mechanics, *J. Comp. Phys.*, **193**, 198 (2003).

[51] G. H. Miller, Minimal rotationally invariant bases for hyperelasticity, *SIAM J. Appl. Math.*, **64**, 2050 (2004).

[52] R. E. Miller and E. B. Tadmor, A unified framework and performance benchmark of fourteen multiscale atomistic/continuum coupling methods, *Modelling Simul. Mater. Sci. Eng.*, **17** 055009 (2009).

[53] N. I. Muskhelishvili, Some basic problems of the mathematical theory of elasticity, 3rd Edition, (P. Noorddhoff, 1953).

[54] R. R. Nourgaliev & T. G. Theofanous, High-fidelity interface tracking in compressible flows: Unlimited anchored adaptive level set, *J. Comp. Phys.*, **224**, 836 (2007).

[55] L. Pareschi & G. Russo, Implicit-Explicit Runge-Kutta Schemes and Applications to Hyperbolic Systems with Relaxation, *J. Sci. Comp.*, **25** 129 (2005).

[56] S. J. Plimpton, Fast Parallel Algorithms for Short-Range Molecular Dynamics, *J. Comp. Phys.*, **117** 1 (1995).

[57] B. J. Plohr & D. H. Sharp, A conservative Eulerian formulation of the equations for elastic flow, *Adv. Appl. Math.*, **9**, 418 (1988).

[58] B. J. Plohr & D. H. Sharp, A Conservative Formulation for Plasticity, *Adv. Appl. Math.*, **13**, 462 (1992).

[59] J. Qiu & C. Shu, On the construction, comparison, and local characteristic decomposition for high-order central WENO schemes, *J. Comp. Phys.*, **183**, 187 (2002).

[60] A. D. Resnyanky, DYNA-modelling of the high-velocity impact problems with a split-element algorithm, *Int. J. Impact Eng.*, **27** 709 (2002).

[61] W. J. Rider & D. B. Kothe, Stretching and tearing interface tracking methods, AIAA-95-1717-CP (1995).

[62] E. I. Romensky, Thermodynamics and Hyperbolic Systems of Balance Laws in Continuum Mechanics, in *Godunov Methods: Theory and Applications*, edited by E. F. Toro (Kluwer Academic/Plenum Publishers, 2001).

[63] E. I. Romenskii, Deformation model for brittle materials and the structure of failure waves, *J. App. Mech. Tech. Phys.*, **48**, 437 (2007).

[64] E. I. Romensky, private communication, (2006).

[65] M. Scheidler, On the coupling of pressure and deviatoric stress in inotropic hyperelastic materials, Army Research Laboratory Technical Report, ARL–TR–954 (1996).

[66] E. Shapiro, Step-by-Step Eberles scheme derivation. Technical report, Cranfield University, (2006).

[67] C. Shu & S. Osher, Efficient Implementation of Essentially Non-oscillatory Shock-Capturing Schemes, *J. Comp. Phys.*, **77**, 439 (1988).

[68] J. C. Simo & M. Ortiz, A unified approach to finite deformation elastoplastic analysis based on the use of hyperelastic constitutive equations, *Comp. Meth. Appl. Mech. Eng.*, **49**, 221 (1985).

[69] B. T. Smith, B. S. Garbow, J. J. Dongarra, J. M. Boyle & Y. Ikebe, Matrix Eigensystem Routines - EISPACK Guide, 2nd Edition, in *Lecture Notes in Computer Science, Volume 6* (Springer-Verlag, 1976)

[70] M. Sussman, P. Smereka & S. Osher, A level set approach for computing solutions to incompressible two-phase flow, *J. Comp. Phys.*, **114**, 146 (1994).

[71] P. D. Thomas & C. K. Lombard, Geometric conservation law and its application to flow computations on moving grids, *AIAA J.*, **17** 1030 (1979).

[72] V. A. Titarev, E. Romenski & E. F. Toro, MUSTA-type upwind fluxes for non-linear elasticity, *Int. J. Numer. Meth. Eng.*, **73** 897 (2008).

[73] A. C. To & S. Li, Perfectly matched multiscale simulations, *Phys. Rev. B*, **72** 035414 (2005).

[74] E. F. Toro, Riemann Solvers and Numerical Methods for Fluid Dynamics: A Practical Introduction, 2nd Edition, (Springer, 1999).

[75] L. B. Tran & H. S. Udaykumar, A particle-level set-based sharp interface cartesian grid method for impact, penetration, and void collapse, *J. Comp. Phys.*, **193**, 469 (2004).

[76] J. A. Trangenstein & P. Colella, A Higher-Order Godunov Method for Modelling Finite Deformation in Elastic-Plastic Solids, *Comm. Pure App. Math.*, **44**, 41 (1991).

[77] J. A. Trangenstein & R. B. Pember, Numerical algorithms for strong discontinuities in elastic-plastic solids, *J. Comp. Phys.*, **103**, 63 (1992).

[78] J. A. Trangenstein, A second-order Godunov algorithm for two-dimensional solid mechanics, *Comp. Mech.*, **13**, 343 (1994).

[79] J. A. Trangenstein, Adaptive mesh refinement for wave propagation in nonlinear solids, *SIAM J. Sci. Comp.*, **16**, 819 (1995).

[80] O. Y. Vorobiev, I. N. Lomov, A. V. Shutov, V. I. Kondaurov, A.L. Ni & V. E. Fortov, Application of schemes on moving grids for numerical simulation of hypervelocity impact problems, *Int. J. Impact Eng.*, **17** 891 (1995).

[81] O. Vorobiev, A. Shutov, I. N. Lomov, D. A. Shishov, S. A. Medin & V. E. Fortov, Comparative analysis of computer codes for hypervelocity impact problems with large deformations, *Int. J. Impact Eng.*, **20** 805 (1997).

[82] D. H. Wagner, Conservation Laws, Coordinate Transformations, and Differential Forms, in *Hyperbolic Problems: Theory, Numerics, Applications*, edited by J. Glimm, J. W. Grove, M. J. Graham & B. J. Plohr 471 (World Scientific, 1996).

[83] J. Walter, J. Glimm, J. Grove, H. Hwang, X. Lin, B. J. Plohr, D. H. Sharp & D. D. Yu, Eulerian Front Tracking For Solid Dynamics, http://citeseer.ist.psu.edu/walter99eulerian.html, (2009).

[84] J. Walter, D. Yu , B. J. Plohr, J. Grove & J. Glimm, An algorithm for Eulerian front tracking for solid deformation, Stony Brook AMS Preprint; SUNYSB-AMS-00-24 (2000).

[85] F. Wang, J. G. Glimm, J. W. Grove & B. J. Plohr, A conservative Eulerian numerical scheme for elastoplasticity and application to plate impact problems, *Impact Comp. Sci. Eng.*, **5** 285 (1993).

[86] M. L. Wilkins, Calculation of Elastic-Plastic Flow, UCRL Technical Report, UCRL–7322 (1963).

[87] M. L. Wilkins, Computer simulation of dynamic phenomena, (Springer, 1999).

[88] R. E. Winter, G. J. Ball & P.T. Keightley, Mechanisms of shock-induced dynamic friction, *J. Phys. D*, **39** 5043 (2006).

[89] N. N. Yanenko, E. A. Kroshko, V. V. Liseikin, V. M. Fomin, V. P. Shapeev & Yu. A. Shitov, Methods for the construction of moving grids for problems of fluid dynamics with big deformations, Lecture notes in Physics: Proceedings of the 5th International conference on numerical methods in fluid dynamics, Twente University (1976).

[90] Y. B. Zel'dovich & Y. P. Raizer, Physics of Shock Waves and High-Temperature Hydrodynamic Phenomena, v 2 Academic Press (1967).

[91] J. A. Zukas, Introduction to Hydrocodes, Studies in Applied Mechanics 49 (Elsevier, 2004).

A

Vector and tensor notation

Here, some of the vector and tensor notation used throughout this thesis is elaborated on. Unless specified otherwise all indices, using for example i, are assumed to have values in the range $1 \leq i \leq 3$. The following examples are provided for clarity.

Assume two vectors:

$$\mathbf{a} = \begin{pmatrix} a_1 \\ a_2 \\ a_3 \end{pmatrix}, \qquad \mathbf{b} = \begin{pmatrix} b_1 \\ b_2 \\ b_3 \end{pmatrix}.$$

The transpose of $\mathbf{b}$ is:

$$\mathbf{b}^{\mathrm{T}} = (b_1,\ b_2\ b_3). \tag{A.1}$$

The vector product of $\mathbf{a}$ and $\mathbf{b}$ is:

$$\mathbf{a} \otimes \mathbf{b}^{\mathrm{T}} = \begin{pmatrix} a_1b_1 & a_1b_2 & a_1b_3 \\ a_2b_1 & a_2b_2 & a_2b_3 \\ a_3b_1 & a_3b_2 & a_3b_3 \end{pmatrix}. \tag{A.2}$$

The dot product of $\mathbf{a}$ and $\mathbf{b}$ is:

$$\mathbf{a} \cdot \mathbf{b} = a_ib_i = a_1b_1 + a_2b_2 + a_3b_3. \tag{A.3}$$

Assume two three-by-three matrices:

$$\mathbf{A} = \begin{pmatrix} A_{11} & A_{12} & A_{13} \\ A_{21} & A_{22} & A_{23} \\ A_{31} & A_{32} & A_{33} \end{pmatrix}, \qquad \mathbf{B} = \begin{pmatrix} B_{11} & B_{12} & B_{13} \\ B_{21} & B_{22} & B_{23} \\ B_{31} & B_{32} & B_{33} \end{pmatrix}.$$

The product of the two matrices gives the following result:

$$\mathbf{AB} = A_{ik}B_{kj} = A_{i1}B_{1j} + A_{i2}B_{2j} + A_{i3}B_{3j}, \tag{A.4}$$

where summation is assumed over repeated indices as in Eq. (A.3). For clarity where summation occurs for more than one indices for two matrices the following notation is adopted:

$$\sum_{i,j=1}^{3} A_{ij}B_{ij} = A_{11}B_{11} + A_{12}B_{12} + A_{13}B_{13} + \ldots + A_{33}B_{33}. \tag{A.5}$$

Example

Some quite complex terms appear in the right eigenvalues written in compact form in Eq. (2.33) and provide a good example of the use of much of the notation detailed above. Although these are provided in expanded form in Appendix D it is intuitive to look at one of these terms in detail. Take the following term:

$$\left(\mathbf{F}^{\mathrm{T}}\mathbf{e}_1\right) \otimes \left(\mathbf{e}_2^{\mathrm{T}}\mathbf{T}^1\right) - \mathbf{D}^{23}, \tag{A.6}$$

with

$$\mathbf{T}^1 := \mathbf{\Omega}^{-1}\left(\mathbf{A}^{11}\mathbf{D}^{21} + \mathbf{A}^{11}\mathbf{D}^{32} + \mathbf{A}^{12}\mathbf{D}^{23}\right). \tag{A.7}$$

Consider first the expansion of the second term, Eq. (A.7):

$$\begin{aligned}
\mathbf{T}^1 &= \mathbf{\Omega}^{-1}\left\{\begin{pmatrix} A_{11}^{11} & A_{12}^{11} & A_{13}^{11} \\ A_{21}^{11} & A_{22}^{11} & A_{23}^{11} \\ A_{31}^{11} & A_{32}^{11} & A_{33}^{11} \end{pmatrix}\left[\begin{pmatrix} 0 & 0 & 0 \\ 1 & 0 & 0 \\ 0 & 0 & 0 \end{pmatrix} + \begin{pmatrix} 0 & 0 & 0 \\ 0 & 0 & 0 \\ 0 & 1 & 0 \end{pmatrix}\right]\right. \\
&\quad \left. + \begin{pmatrix} A_{11}^{12} & A_{12}^{12} & A_{13}^{12} \\ A_{21}^{12} & A_{22}^{12} & A_{23}^{12} \\ A_{31}^{12} & A_{32}^{12} & A_{33}^{12} \end{pmatrix}\begin{pmatrix} 0 & 0 & 0 \\ 0 & 0 & 1 \\ 0 & 0 & 0 \end{pmatrix}\right\} && \text{(A.8)} \\
&= \mathbf{\Omega}^{-1}\left[\begin{pmatrix} A_{12}^{11} & 0 & 0 \\ A_{22}^{11} & 0 & 0 \\ A_{32}^{11} & 0 & 0 \end{pmatrix} + \begin{pmatrix} 0 & A_{13}^{11} & 0 \\ 0 & A_{23}^{11} & 0 \\ 0 & A_{33}^{11} & 0 \end{pmatrix} + \begin{pmatrix} 0 & 0 & A_{12}^{12} \\ 0 & 0 & A_{22}^{12} \\ 0 & 0 & A_{32}^{12} \end{pmatrix}\right] && \text{(A.9)} \\
&= \mathbf{\Omega}^{-1}\begin{pmatrix} A_{12}^{11} & A_{13}^{11} & A_{12}^{12} \\ A_{22}^{11} & A_{23}^{11} & A_{22}^{12} \\ A_{32}^{11} & A_{33}^{11} & A_{32}^{12} \end{pmatrix} && \text{(A.10)} \\
&= \begin{pmatrix} \Omega_{11}^{-1}A_{12}^{11} + \Omega_{12}^{-1}A_{22}^{11} + \Omega_{13}^{-1}A_{32}^{11} & \Omega_{11}^{-1}A_{13}^{11} + \Omega_{12}^{-1}A_{23}^{11} + \Omega_{13}^{-1}A_{33}^{11} \\ \Omega_{21}^{-1}A_{12}^{11} + \Omega_{22}^{-1}A_{22}^{11} + \Omega_{23}^{-1}A_{32}^{11} & \Omega_{21}^{-1}A_{13}^{11} + \Omega_{22}^{-1}A_{23}^{11} + \Omega_{23}^{-1}A_{33}^{11} \\ \Omega_{31}^{-1}A_{12}^{11} + \Omega_{32}^{-1}A_{22}^{11} + \Omega_{33}^{-1}A_{32}^{11} & \Omega_{31}^{-1}A_{13}^{11} + \Omega_{32}^{-1}A_{23}^{11} + \Omega_{33}^{-1}A_{33}^{11} \end{pmatrix} \\
&\quad \begin{pmatrix} \Omega_{11}^{-1}A_{12}^{12} + \Omega_{12}^{-1}A_{22}^{12} + \Omega_{13}^{-1}A_{32}^{12} \\ \Omega_{21}^{-1}A_{12}^{12} + \Omega_{22}^{-1}A_{22}^{12} + \Omega_{23}^{-1}A_{32}^{12} \\ \Omega_{31}^{-1}A_{12}^{12} + \Omega_{32}^{-1}A_{22}^{12} + \Omega_{33}^{-1}A_{32}^{12} \end{pmatrix} && \text{(A.11)}
\end{aligned}$$

Using this result the following equalities are found for the first term, Eq. (A.6):

$$
\begin{aligned}
\left(\mathbf{F}^{\mathrm{T}}\mathbf{e}_1\right) \otimes \left(\mathbf{e}_2^{\mathrm{T}}\mathbf{T}^1\right) - \mathbf{D}^{23} \;=\; & \left[\begin{pmatrix} F_{11} & F_{21} & F_{31} \\ F_{12} & F_{22} & F_{32} \\ F_{13} & F_{23} & F_{33} \end{pmatrix} \begin{pmatrix} 1 \\ 0 \\ 0 \end{pmatrix} \right] \otimes && \text{(A.12)} \\
& \left[(0,\ 1\ 0) \begin{pmatrix} T_{11} & T_{12} & T_{13} \\ T_{21} & T_{22} & T_{23} \\ T_{31} & T_{32} & T_{33} \end{pmatrix} \right] - && \text{(A.13)} \\
& \begin{pmatrix} 0 & 0 & 0 \\ 0 & 0 & 1 \\ 0 & 0 & 0 \end{pmatrix} && \text{(A.14)} \\
= \; & \begin{pmatrix} F_{11} \\ F_{12} \\ F_{13} \end{pmatrix} \otimes (T_{21},\ T_{22}\ T_{23}) - \begin{pmatrix} 0 & 0 & 0 \\ 0 & 0 & 1 \\ 0 & 0 & 0 \end{pmatrix} && \text{(A.15)} \\
& && \text{(A.16)} \\
= \; & \begin{pmatrix} F_{11}T_{21} & F_{11}T_{22} & F_{11}T_{23} \\ F_{12}T_{21} & F_{12}T_{22} & F_{12}T_{23} - 1 \\ F_{13}T_{21} & F_{13}T_{22} & F_{13}T_{23} \end{pmatrix} && \text{(A.17)} \\
= \; & \begin{pmatrix} F_{11}(\Omega_{21}^{-1}A_{12}^{11} + \Omega_{22}^{-1}A_{22}^{11} + \Omega_{23}^{-1}A_{32}^{11}) \\ F_{12}(\Omega_{21}^{-1}A_{12}^{11} + \Omega_{22}^{-1}A_{22}^{11} + \Omega_{23}^{-1}A_{32}^{11}) \\ F_{13}(\Omega_{21}^{-1}A_{12}^{11} + \Omega_{22}^{-1}A_{22}^{11} + \Omega_{23}^{-1}A_{32}^{11}) \\ F_{11}(\Omega_{21}^{-1}A_{13}^{11} + \Omega_{22}^{-1}A_{23}^{11} + \Omega_{23}^{-1}A_{33}^{11}) \\ F_{12}(\Omega_{21}^{-1}A_{13}^{11} + \Omega_{22}^{-1}A_{23}^{11} + \Omega_{23}^{-1}A_{33}^{11}) \\ F_{13}(\Omega_{21}^{-1}A_{13}^{11} + \Omega_{22}^{-1}A_{23}^{11} + \Omega_{23}^{-1}A_{33}^{11}) \\ F_{11}(\Omega_{21}^{-1}A_{12}^{12} + \Omega_{22}^{-1}A_{22}^{12} + \Omega_{23}^{-1}A_{32}^{12}) \\ F_{12}(\Omega_{21}^{-1}A_{12}^{12} + \Omega_{22}^{-1}A_{22}^{12} + \Omega_{23}^{-1}A_{32}^{12}) - 1 \\ F_{13}(\Omega_{21}^{-1}A_{12}^{12} + \Omega_{22}^{-1}A_{22}^{12} + \Omega_{23}^{-1}A_{32}^{12}) \end{pmatrix} && \text{(A.18)}
\end{aligned}
$$

B

Proof of continuity

For completeness consider the conservation laws for the elastic deformation gradients of an elastoplastic material in quasi-linear form and Cartesian coordinates:

$$\frac{\partial F_{ij}}{\partial t} + u_k \frac{\partial F_{ij}}{\partial x_k} - F_{kj} \frac{\partial u_i}{\partial x_k} = \varphi_{ij}, \tag{B.1}$$

$$= -\frac{1}{2G\tau} \sigma'_{im} F_{mj}. \tag{B.2}$$

Adopting the proceedure presented in [28] for proving continuity of the equivalent conservation laws written for the Finger strain tensor, the following equalities can be found:

$$D_t \rho = \frac{\partial \rho}{\partial F_{ij}} D_t F_{ij} := \frac{\partial \rho}{\partial F_{ij}} \left(\frac{\partial F_{ij}}{\partial t} + u_k \frac{\partial F_{ij}}{\partial x_k} \right),$$
$$= \frac{\partial \rho}{\partial F_{ij}} \left(F_{kj} \frac{\partial u_i}{\partial x_k} - \frac{1}{2G\tau} \sigma'_{im} F_{mj} \right), \tag{B.3}$$

where $D_t := \frac{\partial}{\partial t} + u_k \frac{\partial}{\partial x_k}$ denotes the substantial derivative. Using $\rho = \rho_0 / \det|F|$, the derivatives of density with respect to deformation in (B.3) are

$$\frac{\partial \rho}{\partial F_{ij}} = -\frac{\rho_0}{\det|F|^2} \frac{\partial \det|F|}{\partial F_{ij}},$$
$$= -\frac{\rho_0}{\det|F|} F_{ij}^{-\mathrm{T}} = -\rho F_{ij}^{-\mathrm{T}}. \tag{B.4}$$

Thus

$$\frac{\partial \rho}{\partial F_{ij}} F_{kj} \frac{\partial u_i}{\partial x_k} = -\rho F_{ij}^{-\mathrm{T}} F_{jk}^{\mathrm{T}} \frac{\partial u_i}{\partial x_k},$$
$$= -\rho \delta_{ik} \frac{\partial u_i}{\partial x_k} = -\rho \frac{\partial u_k}{\partial x_k}. \tag{B.5}$$

Using these results and expanding Eq. (B.3) gives

$$\frac{\partial \rho}{\partial t} + u_k \frac{\partial \rho}{\partial x_k} = \frac{\partial \rho}{\partial F_{ij}} \left(F_{kj} \frac{\partial u_i}{\partial x_k} - \frac{1}{2G\tau} \sigma'_{im} F_{mj} \right), \tag{B.6}$$

$$= -\rho \frac{\partial u_k}{\partial x_k} + \frac{\rho}{2G\tau} \delta_{im} \sigma'_{im}, \tag{B.7}$$

$$= -\rho \frac{\partial u_k}{\partial x_k}, \tag{B.8}$$

which is the non-conservative form of the continuity equation. It is easily found that for the special case of non-linear elasticity the same result is obtained since $\varphi_{ij} = 0$.

C

Transformation of coordinate systems

C.1 Generalised moving coordinates

Consider the time-dependent curvilinear coordinate system $\xi_i = \xi_i(x_k, t),\ \tau = \tau(t)$. The transformation from Cartesian coordinates is achieved by using the following identities:

$$\mathrm{d}x_k = \frac{\partial x_k}{\partial \xi_i}\mathrm{d}\xi_i + \frac{\partial x_k}{\partial \tau}\mathrm{d}\tau. \tag{C.1}$$

Rather than consider each of the conservation laws independently, it is possible to transform instead the complete system written in vector form:

$$\frac{\partial \mathbf{U}}{\partial t} + \frac{\partial \mathscr{F}^k}{\partial x_k} = \mathbf{S}, \tag{C.2}$$

where $\mathbf{U}$, $\mathscr{F}$, $\mathbf{S}$ are the vectors of conserved variables, flux functions, and source terms respectively [cf. Eq. (3.7)-(3.2)]. Transformed into the new coordinate system, Eq. (C.2) becomes (see for example [13])

$$\frac{\partial \mathbf{U}}{\partial \tau} + \frac{\partial \xi_i}{\partial \tau}\frac{\partial \mathbf{U}}{\partial \xi_i} + \frac{\partial \xi_i}{\partial x_k}\frac{\partial \mathscr{F}^k}{\partial \xi_i} \ = \ \mathbf{S}. \tag{C.3}$$

Multiplying through by the Jacobian $J = |\partial x_k/\partial \xi_i|$ gives

$$J\frac{\partial \mathbf{U}}{\partial \tau} + J\frac{\partial \xi_i}{\partial \tau}\frac{\partial \mathbf{U}}{\partial \xi_i} + J\frac{\partial \xi_i}{\partial x_k}\frac{\partial \mathscr{F}^k}{\partial \xi_i} \ = \ J\mathbf{S}, \tag{C.4}$$

which by defining $\mu_k := \partial x_k/\partial \tau$ to be the grid velocity vector can be written

$$J\frac{\partial \mathbf{U}}{\partial \tau} - J\mu_k\frac{\partial \xi_i}{\partial x_k}\frac{\partial \mathbf{U}}{\partial \xi_i} + J\frac{\partial \xi_i}{\partial x_k}\frac{\partial \mathscr{F}^k}{\partial \xi_i} \ = \ J\mathbf{S}. \tag{C.5}$$

The last result can be rearranged to give the following equalities:

$$\frac{\partial J\mathbf{U}}{\partial \tau} + \frac{\partial J\left(\widehat{\mathscr{F}^i} - \widehat{\mu}_i\mathbf{U}\right)}{\partial \xi_i} \ = \ J\mathbf{S} + \mathbf{U}\left[\frac{\partial J}{\partial \tau} - \frac{\partial J\widehat{\mu}_k}{\partial \xi_i}\right] + \mathscr{F}^k\frac{\partial}{\partial \xi_i}\left(J\frac{\partial \xi_i}{\partial x_k}\right) \tag{C.6}$$

$$= \ J\mathbf{S}, \tag{C.7}$$

where $\widehat{\mu}_i = \mu_k \left(\partial \xi_i / \partial x_k\right)$ is the grid velocity vector in curvilinear coordinates, and $\widehat{\mathscr{F}^i} = \mathscr{F}^k \left(\partial \xi_i / \partial x_k\right)$ is the flux vector in curvilinear coordinates. Proof of the elimination of the last term on the right hand side of Eq. (C.6) is given in detail in [13] and shall not be repeated; the second from last term is equal to zero as a result of the geometric conservation law [71]

$$\frac{\partial J}{\partial \tau} - \frac{\partial J \widehat{\mu}_k}{\partial \xi_i} = 0. \tag{C.8}$$

For an elastoplastic material the governing model in moving curvilinear coordinates can thus be written

$$\frac{\partial \overline{\mathbf{U}}}{\partial t} + \frac{\partial \overline{\mathscr{F}}^i}{\partial \xi_i} = \overline{\mathbf{S}}, \tag{C.9}$$

where

$$\overline{\mathbf{U}} := J \begin{pmatrix} \rho \mathbf{u} \\ \rho \mathbf{F}^{\mathrm{T}} \mathbf{e}_1 \\ \rho \mathbf{F}^{\mathrm{T}} \mathbf{e}_2 \\ \rho \mathbf{F}^{\mathrm{T}} \mathbf{e}_3 \\ \rho E \end{pmatrix}, \qquad \overline{\mathscr{F}}^i := J \begin{pmatrix} \rho \mathbf{u} \widehat{u}_k - \widehat{\sigma} \mathbf{e}_k \\ \rho \mathbf{F}^{\mathrm{T}} \mathbf{e}_1 \widehat{u}_k - u_1 \rho \widehat{\mathbf{F}}^{\mathrm{T}} \mathbf{e}_k \\ \rho \mathbf{F}^{\mathrm{T}} \mathbf{e}_2 \widehat{u}_k - u_2 \rho \widehat{\mathbf{F}}^{\mathrm{T}} \mathbf{e}_k \\ \rho \mathbf{F}^{\mathrm{T}} \mathbf{e}_3 \widehat{u}_k - u_3 \rho \widehat{\mathbf{F}}^{\mathrm{T}} \mathbf{e}_k \\ \rho E \widehat{u}_k - \mathbf{e}_k^{\mathrm{T}} \cdot (\widehat{\sigma} \mathbf{u}) \end{pmatrix},$$

with

$$\widehat{u}_i := \frac{\partial \xi_i}{\partial x_k}(u_k - \mu_k), \qquad \widehat{\sigma}_{ij} := \sigma_{jk} \frac{\partial \xi_i}{\partial x_k}, \qquad \widehat{F}_{ji} := F_{kj} \frac{\partial \xi_i}{\partial x_k}. \tag{C.10}$$

The source term in Eq. (C.9) can be decomposed into the vector of terms associated with the compatibility constraints, $\overline{\mathbf{S}}^{\mathrm{C}}$, and those terms governing the onset of inelastic deformations, $\overline{\mathbf{S}}^{\mathrm{P}}$:

$$\overline{\mathbf{S}} := -\overline{\mathbf{S}}^{\mathrm{C}} - \overline{\mathbf{S}}^{\mathrm{P}}, \tag{C.11}$$

where

$$\overline{\mathbf{S}}^{\mathrm{C}} := \begin{pmatrix} 0 \\ u_1 \nabla_\xi \cdot \left(J \rho \widehat{\mathbf{F}} \right) \\ u_2 \nabla_\xi \cdot \left(J \rho \widehat{\mathbf{F}} \right) \\ u_3 \nabla_\xi \cdot \left(J \rho \widehat{\mathbf{F}} \right) \\ 0 \end{pmatrix}, \qquad \overline{\mathbf{S}}^{\mathrm{P}} := J \mathbf{S}^{\mathrm{P}}. \tag{C.12}$$

In the form Eq. (C.9) the system resembles that expressed in Cartesian coordinates; thus converting numerical methods derived for the equations in curvilinear coordinates simplifies easily to Cartesian through elimination of the metrics.

C.2 Cylindrical polar coordinates

Let the generalised coordinate system ξ employed in the previous section now denote the non-moving cylindrical polar coordinates $\xi = (r, \theta, z)$. Partial derivatives in Cartesian coordinates can be transformed into cylindrical polar coordinates using the following identities

$$x_1 = r\cos\theta \tag{C.13}$$
$$x_2 = r\sin\theta \tag{C.14}$$
$$x_3 = z \tag{C.15}$$

thus

$$r = \sqrt{x_1^2 + x_2^2} \tag{C.16}$$
$$\theta = \arctan\left(x_2/x_1\right) \tag{C.17}$$
$$z = x_3 \tag{C.18}$$

giving the metrics

$$\frac{\partial r}{\partial x_1} = \cos\theta, \tag{C.19}$$
$$\frac{\partial r}{\partial x_2} = \sin\theta, \tag{C.20}$$
$$\frac{\partial \theta}{\partial x_1} = \frac{1}{r}\cos\theta, \tag{C.21}$$
$$\frac{\partial \theta}{\partial x_2} = -\frac{1}{r}\sin\theta. \tag{C.22}$$

Vectors and tensors are rotated via the rotation matrix

$$\mathbf{R}^{\mathrm{CYL}} = \begin{pmatrix} \cos\theta & \sin\theta & 0 \\ -\sin\theta & \cos\theta & 0 \\ 0 & 0 & 1 \end{pmatrix} \tag{C.23}$$

giving for example the velocity vector $\mathbf{u}^{\mathrm{CYL}} = \mathbf{R}^{\mathrm{CYL}}\mathbf{u}$ and deformation tensor $\mathbf{F}^{\mathrm{CYL}} = \mathbf{R}^{\mathrm{CYL}}\mathbf{F}\mathbf{R}^{\mathrm{CYL}}$ [48]. Thus the governing system, (3.7), in cylindrical coordinates becomes

$$\frac{\partial \mathbf{U}}{\partial t} + \frac{1}{r}\frac{\partial r\mathscr{F}^r}{\partial r} + \frac{1}{r}\frac{\partial \mathscr{F}^\theta}{\partial \theta} + \frac{\partial \mathscr{F}^z}{\partial z} = \mathbf{S}^{\mathrm{G}} - \mathbf{S}^{\mathrm{C}} - \mathbf{S}^{\mathrm{P}} \tag{C.24}$$

where the vector of conserved variables is now

$$\mathbf{U} := \left(\rho\mathbf{u}^{\mathrm{CYL}},\ \rho\mathbf{F}^{\mathrm{CYL}^{\mathrm{T}}}\mathbf{e}_1,\ \rho\mathbf{F}^{\mathrm{CYL}^{\mathrm{T}}}\mathbf{e}_2,\ \rho\mathbf{F}^{\mathrm{CYL}^{\mathrm{T}}}\mathbf{e}_3, \rho E\right)^{\mathrm{T}} \tag{C.25}$$

and the flux vectors $\mathscr{F}^{\alpha}$, and inelastic source terms $\mathbf{S}^{\mathrm{P}}$ maintain the same form as before only the state variables are replaced with those rotated into the new coordinate system. The source term $\mathbf{S}^{\mathrm{C}}$ and resultant geometric source term $\mathbf{S}^{\mathrm{G}}$ are given by

$$\mathbf{S}^{\mathrm{C}} := \frac{1}{r}\begin{pmatrix} 0 \\ 0 \\ 0 \\ u_r\left(r\frac{\partial \rho F_{rr}}{\partial r} + \frac{\partial \rho F_{\theta r}}{\partial \theta} + r\frac{\partial \rho F_{zr}}{\partial z}\right) + u_r\left(\rho F_{rr} - \rho F_{\theta\theta}\right) \\ u_r\left(r\frac{\partial \rho F_{r\theta}}{\partial r} + \frac{\partial \rho F_{\theta\theta}}{\partial \theta} + r\frac{\partial \rho F_{z\theta}}{\partial z}\right) + u_r\left(\rho F_{r\theta} + \rho F_{\theta r}\right) \\ u_r\left(r\frac{\partial \rho F_{rz}}{\partial r} + \frac{\partial \rho F_{\theta z}}{\partial \theta} + r\frac{\partial \rho F_{zz}}{\partial z}\right) + u_r\rho F_{rz} \\ u_\theta\left(r\frac{\partial \rho F_{rr}}{\partial r} + \frac{\partial \rho F_{r\theta}}{\partial \theta} + r\frac{\partial \rho F_{zr}}{\partial z}\right) + u_\theta\left(\rho F_{rr} - \rho F_{\theta\theta}\right) \\ u_\theta\left(r\frac{\partial \rho F_{r\theta}}{\partial r} + \frac{\partial \rho F_{\theta\theta}}{\partial \theta} + r\frac{\partial \rho F_{z\theta}}{\partial z}\right) + u_\theta\left(\rho F_{r\theta} + \rho F_{\theta r}\right) \\ u_\theta\left(r\frac{\partial \rho F_{rz}}{\partial r} + \frac{\partial \rho F_{\theta z}}{\partial \theta} + r\frac{\partial \rho F_{zz}}{\partial z}\right) + u_\theta\rho F_{rz} \\ u_z\left(r\frac{\partial \rho F_{rr}}{\partial r} + \frac{\partial \rho F_{\theta r}}{\partial \theta} + r\frac{\partial \rho F_{zr}}{\partial z}\right) + u_z\left(\rho F_{rr} - \rho F_{\theta\theta}\right) \\ u_z\left(r\frac{\partial \rho F_{r\theta}}{\partial r} + \frac{\partial \rho F_{\theta\theta}}{\partial \theta} + r\frac{\partial \rho F_{z\theta}}{\partial z}\right) + u_z\left(\rho F_{r\theta} + \rho F_{\theta r}\right) \\ u_z\left(r\frac{\partial \rho F_{rz}}{\partial r} + \frac{\partial \rho F_{\theta z}}{\partial \theta} + r\frac{\partial \rho F_{zz}}{\partial z}\right) + u_z\rho F_{rz} \\ 0 \end{pmatrix}$$

$$\mathbf{S}^{\mathrm{G}} := \frac{1}{r}\begin{pmatrix} \rho u_\theta^2 - \sigma_{\theta\theta} \\ -\rho u_r u_\theta + \sigma_{r\theta} \\ 0 \\ \rho F_{r\theta}u_\theta - \rho F_{\theta\theta}u_r \\ \rho F_{\theta r}u_r - \rho F_{rr}u_\theta \\ 0 \\ \rho F_{\theta r}u_r - \rho F_{rr}u_\theta \\ \rho F_{\theta\theta}u_r - \rho F_{r\theta}u_\theta \\ \rho F_{\theta z}u_r - \rho F_{rz}u_\theta \\ \rho F_{z\theta}u_\theta - \rho F_{\theta\theta}u_z \\ \rho F_{\theta r}u_z - \rho F_{zr}u_\theta \\ 0 \\ 0 \end{pmatrix}$$

C.3 Spherical polar coordinates

Let the generalised coordinate system ξ employed in the previous section now denote the non-moving spherical polar coordinates (r, θ, ϕ). Partial derivatives in Cartesian coordinates can be transformed into cylindrical polar coordinates using the following

identities

$$x_1 = r\sin\theta\cos\phi \tag{C.26}$$
$$x_2 = r\sin\theta\sin\phi \tag{C.27}$$
$$x_3 = r\cos\theta \tag{C.28}$$

thus

$$r = \sqrt{x_1^2 + x_2^2 + x_3^2} \tag{C.29}$$
$$\theta = \arccos(x_3/r) \tag{C.30}$$
$$\phi = \arctan(x_2/x_1) \tag{C.31}$$

giving

$$\frac{\partial r}{\partial x_1} = \sin\theta\cos\phi, \tag{C.32}$$
$$\frac{\partial r}{\partial x_2} = \sin\theta\sin\phi, \tag{C.33}$$
$$\frac{\partial r}{\partial x_3} = \cos\theta, \tag{C.34}$$
$$\frac{\partial \theta}{\partial x_1} = \frac{1}{r}\cos\theta\cos\phi, \tag{C.35}$$
$$\frac{\partial \theta}{\partial x_2} = \frac{1}{r}\cos\theta\sin\phi, \tag{C.36}$$
$$\frac{\partial \theta}{\partial x_3} = -\frac{1}{r}\sin\theta, \tag{C.37}$$
$$\frac{\partial \phi}{\partial x_1} = -\frac{\sin\phi}{r\sin\theta}, \tag{C.38}$$
$$\frac{\partial \phi}{\partial x_2} = \frac{\cos\phi}{r\sin\theta}, \tag{C.39}$$
$$\frac{\partial \phi}{\partial x_3} = 0. \tag{C.40}$$

Vectors and tensors are rotated in the same way as with the cylindrical coordinate transformation, via the rotation matrix

$$\mathbf{R}^{\mathrm{SPH}} = \begin{pmatrix} \sin\theta\cos\phi & \cos\theta\cos\phi & -\sin\phi \\ \sin\theta\sin\phi & \cos\theta\sin\phi & \cos\phi \\ \cos\theta & -\sin\theta & 0 \end{pmatrix}. \tag{C.41}$$

Thus the system of conservation laws, (3.7) can be rewritten in spherical coordinates

$$\frac{\partial \mathbf{U}}{\partial t} + \frac{1}{r^2}\frac{\partial r^2 \mathscr{F}^r}{\partial r} + \frac{1}{r\sin\theta}\frac{\partial \sin\theta \mathscr{F}^\theta}{\partial \theta} + \frac{1}{r\sin\theta}\frac{\partial \mathscr{F}^\phi}{\partial \phi} = \mathbf{S}^{\mathrm{G}} - \mathbf{S}^{\mathrm{C}} - \mathbf{S}^{\mathrm{P}} \tag{C.42}$$

where the vector of conserved variables is now

$$\mathbf{U} := \left(\rho\mathbf{u}^{\text{SPH}},\ \rho\mathbf{F}^{\text{SPH}^{\text{T}}}\mathbf{e}_1,\ \rho\mathbf{F}^{\text{SPH}^{\text{T}}}\mathbf{e}_2,\ \rho\mathbf{F}^{\text{SPH}^{\text{T}}}\mathbf{e}_3, \rho E\right)^{\text{T}} \tag{C.43}$$

and the flux vectors $\mathscr{F}^{\alpha}$, and inelastic source terms $\mathbf{S}^{\text{P}}$ again maintain the same form as for the Cartesian system, only the state variables are replaced with those rotated into the spherical coordinate system. The source term $\mathbf{S}^{\text{C}}$ and geometric source term $\mathbf{S}^{\text{G}}$ are given by

$$\mathbf{S}^{\text{G}} := \frac{1}{r}\begin{pmatrix} \rho u_\theta^2 - \sigma_{\theta\theta} + \rho u_\phi^2 - \sigma_{\phi\phi} \\ -\rho u_r u_\theta + \sigma_{\theta r} + \cot\theta(\rho u_\phi^2 - \sigma_{\phi\phi}) \\ -\cot\theta(\rho u_\phi u_\theta - \sigma_{\theta\phi}) - \rho u_\phi u_r + \sigma_{r\phi} \\ \rho u_\theta F_{r\theta} - \rho u_r F_{\theta\theta} - \rho u_r F_{\phi\phi} + \rho u_\phi F_{r\phi} \\ \rho F_{\theta r} u_r - \rho F_{rr} u_\theta - \cot\theta(\rho u_r F_{\phi\phi} - \rho u_\phi F_{r\phi}) \\ \cot\theta(\rho u_r F_{\phi\theta} - \rho u_\phi F_{r\theta}) + \rho u_r F_{\phi r} - \rho u_\phi F_{rr} \\ \rho u_r F_{\theta r} - \rho u_\theta F_{rr} - \rho u_\theta F_{\phi\phi} + \rho u_\phi F_{\theta\phi} \\ \rho u_r F_{\theta\theta} + \rho u_\theta F_{r\theta} + \cot\theta(-\rho u_\theta F_{\phi\phi} + \rho u_\phi F_{\theta\phi}) \\ \rho u_r F_{\theta\phi} + \rho u_\theta F_{r\phi} + \cot\theta(\rho u_r F_{\phi\theta} - \rho u_\phi F_{\theta\theta}) + \rho u_\theta F_{\phi r} - \rho u_\phi F_{\theta r} \\ \rho u_\theta F_{\phi\theta} - \rho u_\phi F_{\theta\theta} + \cot\theta(\rho u_\theta F_{\phi r} - \rho u_\phi F_{\theta r}) + \rho u_r F_{\phi r} - \rho u_\phi F_{rr} \\ \rho u_\phi F_{\theta r} - \rho u_\theta F_{\phi r} + \cot\theta(\rho u_\theta F_{\phi\theta} - \rho u_\phi F_{\theta\theta}) + \rho u_r F_{\phi\theta} - \rho u_\phi F_{r\theta} \\ \cot\theta(\rho u_\theta F_{\phi\phi} - \rho u_\phi F_{\theta\phi}) + \rho u_r F_{\phi\phi} - \rho u_\phi F_{r\phi} \\ 0 \end{pmatrix}$$

$$
\mathbf{S}^{\mathrm{C}} := \begin{pmatrix}
0 \\
0 \\
0 \\
u_r \left(\frac{\partial \rho F_{rr}}{\partial r} + \frac{\partial \rho F_{\theta r}}{r \partial \theta} + \frac{\partial \rho F_{\phi r}}{r \sin\theta \partial \phi} \right) \\
u_r \left(\frac{\partial \rho F_{r\theta}}{\partial r} + \frac{\partial \rho F_{\theta\theta}}{r \partial \theta} + \frac{\partial \rho F_{\phi\theta}}{r \sin\theta \partial \phi} \right) \\
u_r \left(\frac{\partial \rho F_{r\phi}}{\partial r} + \frac{\partial \rho F_{\theta\phi}}{r \partial \theta} + \frac{\partial \rho F_{\phi\phi}}{r \sin\theta \partial \phi} \right) \\
u_\theta \left(\frac{\partial \rho F_{rr}}{\partial r} + \frac{\partial \rho F_{\theta r}}{r \partial \theta} + \frac{\partial \rho F_{\phi r}}{r \sin\theta \partial \phi} \right) \\
u_\theta \left(\frac{\partial \rho F_{r\theta}}{\partial r} + \frac{\partial \rho F_{\theta\theta}}{r \partial \theta} + \frac{\partial \rho F_{\phi\theta}}{r \sin\theta \partial \phi} \right) \\
u_\theta \left(\frac{\partial \rho F_{r\phi}}{\partial r} + \frac{\partial \rho F_{\theta\phi}}{r \partial \theta} + \frac{\partial \rho F_{\phi\phi}}{r \sin\theta \partial \phi} \right) \\
u_\phi \left(\frac{\partial \rho F_{rr}}{\partial r} + \frac{\partial \rho F_{\theta r}}{r \partial \theta} + \frac{\partial \rho F_{\phi r}}{r \sin\theta \partial \phi} \right) \\
u_\phi \left(\frac{\partial \rho F_{r\theta}}{\partial r} + \frac{\partial \rho F_{\theta\theta}}{r \partial \theta} + \frac{\partial \rho F_{\phi\theta}}{r \sin\theta \partial \phi} \right) \\
u_\phi \left(\frac{\partial \rho F_{r\phi}}{\partial r} + \frac{\partial \rho F_{\theta\phi}}{r \partial \theta} + \frac{\partial \rho F_{\phi\phi}}{r \sin\theta \partial \phi} \right) \\
0
\end{pmatrix} +
$$

$$
\frac{\rho}{r} \begin{pmatrix}
0 \\
0 \\
0 \\
u_r \left(F_{rr} - F_{\theta\theta} \right) + u_r \left(\cot\theta F_{\theta r} + F_{rr} - F_{\phi\phi} \right) \\
u_r \left(F_{r\theta} + F_{\theta r} \right) + u_r \left(\cot\theta (F_{\theta\theta} - F_{\phi\phi}) + F_{r\theta} \right) \\
u_r F_{r\phi} + u_r \left(\cot\theta (F_{\theta\phi} + F_{\phi\theta}) + F_{r\phi} + F_{\phi r} \right) \\
u_\theta \left(F_{rr} - F_{\theta\theta} \right) + u_\theta \left(\cot\theta F_{\theta r} + F_{rr} - F_{\phi\phi} \right) \\
u_\theta \left(F_{r\theta} + F_{\theta r} \right) + u_\theta \left(\cot\theta (F_{\theta\theta} - F_{\phi\phi}) + F_{r\theta} \right) \\
u_\theta F_{r\phi} + u_\theta \left(\cot\theta (F_{\theta\phi} + F_{\phi\theta}) + F_{r\phi} + F_{\phi r} \right) \\
u_\phi \left(F_{rr} - F_{\theta\theta} \right) + u_\phi \left(\cot\theta F_{\theta r} + F_{rr} - F_{\phi\phi} \right) \\
u_\phi \left(F_{r\theta} + F_{\theta r} \right) + u_\phi \left(\cot\theta (F_{\theta\theta} - F_{\phi\phi}) + F_{r\theta} \right) \\
u_\phi F_{\phi r} + u_\phi \left(\cot\theta (F_{\theta\phi} + F_{\phi\theta}) + F_{r\phi} + F_{\phi r} \right) \\
0
\end{pmatrix}
$$

D

Characteristic analysis

D.1 Transformation from conservative to non-conservative form

Since the characteristic analysis is fundamental to the derivation of an approximate solution of Riemann problems employed within the numerical schemes, this is conducted in this appendix for the system of equations transformed into moving, generalised coordinates. This way it is possible to deduce from the resulting eigenvalues and eigenvectors the approximate solution algorithms when employing the moving grid scheme, but which also simplify easily to those for Cartesian coordinates through the elimination of metrics.

Starting with the continuity equation, which in conservative form is given by

$$\frac{\partial J\rho}{\partial t} + \frac{\partial J\rho\overline{u}_k}{\partial \xi_k} = 0, \tag{D.1}$$

and expanding the partial derivatives gives the following non-conservative formulation:

$$\frac{\partial J\rho}{\partial t} + \overline{u}_k \frac{\partial J\rho}{\partial \xi_k} + J\rho \frac{\partial \overline{u}_k}{\partial \xi_k} = 0. \tag{D.2}$$

In conservative form the momentum conservation laws are given by Eq. (2.1a). Expanding the partial derivatives gives

$$J\rho\left(\frac{\partial u_i}{\partial t} + \overline{u}_k \frac{\partial u_i}{\partial \xi_k} - \frac{1}{J\rho}\frac{\partial J\widehat{\sigma}_{ik}}{\partial \xi_k}\right) + u_i\left(\frac{\partial J\rho}{\partial t} + \frac{\partial J\rho\overline{u}_k}{\partial \xi_k}\right) = 0. \tag{D.3}$$

As a consequence of Eq. (D.2) this reduces to non-conservative form:

$$\frac{\partial u_i}{\partial t} + \overline{u}_k \frac{\partial u_i}{\partial \xi_k} - \frac{1}{J\rho}\frac{\partial J\widehat{\sigma}_{ik}}{\partial \xi_k} = 0. \tag{D.4}$$

Similarly the strain conservation laws, Eq. (3.1), expand to give

$$J\rho\left(\frac{\partial F_{ij}}{\partial t} + \overline{u}_k \frac{\partial F_{ij}}{\partial \xi_k} - \frac{1}{J\rho}u_i \frac{\partial J\rho\widehat{F}_{kj}}{\partial \xi_k} - \widehat{F}_{kj}\frac{\partial u_i}{\partial \xi_k}\right) +$$
$$F_{ij}\left(\frac{\partial J\rho}{\partial t} + \frac{\partial J\rho\overline{u}_k}{\partial \xi_k}\right) = -u_i \frac{\partial J\rho\widehat{F}_{kj}}{\partial \xi_k} - J\varphi_{ij}, \tag{D.5}$$

and again using Eq. (D.2) these reduce to non-conservative form:

$$\frac{\partial F_{ij}}{\partial t} + u_k \frac{\partial F_{ij}}{\partial \xi_k} - \widehat{F}_{kj} \frac{\partial u_i}{\partial \xi_k} = -\frac{1}{\rho} \varphi_{ij}. \tag{D.6}$$

Lastly, consider the the energy conservation law in conservative form for a heat-conducting material. Expanding the partial derivatives gives

$$J\rho \left(\frac{\partial E}{\partial t} + \overline{u}_k \frac{\partial E}{\partial \xi_k} - \frac{1}{J\rho} u_i \frac{\partial J \widehat{\sigma}_{ik}}{\partial \xi_k} - \frac{1}{\rho} \widehat{\sigma}_{ik} \frac{\partial u_i}{\partial \xi_k} \right) + E \left(\frac{\partial J\rho}{\partial t} + \frac{\partial J\rho \overline{u}_k}{\partial \xi_k} \right) = JQ. \tag{D.7}$$

As a consequence of Eq. (D.2) this reduces to

$$\frac{\partial E}{\partial t} + \overline{u}_k \frac{\partial E}{\partial \xi_k} - \frac{1}{J\rho} u_i \frac{\partial J \widehat{\sigma}_{ik}}{\partial \xi_k} - \frac{1}{\rho} \widehat{\sigma}_{ik} \frac{\partial u_i}{\partial \xi_k} = \frac{1}{\rho} Q. \tag{D.8}$$

Using the definition of total energy, $E = \mathscr{E} + (u_1 + u_2 + u_3)/2$, Eq. (D.8) becomes

$$\frac{\partial \mathscr{E}}{\partial t} + \overline{u}_k \frac{\partial \mathscr{E}}{\partial \xi_k} - \frac{1}{\rho} \widehat{\sigma}_{ik} \frac{\partial u_i}{\partial \xi_k} + u_i \left(\frac{\partial u_i}{\partial t} + \overline{u}_k \frac{\partial u_i}{\partial \xi_k} - \frac{1}{J\rho} \frac{\partial J \widehat{\sigma}_{ik}}{\partial \xi_k} \right) = \frac{1}{\rho} Q. \tag{D.9}$$

As a consequence of Eq. (D.4) this reduces to

$$\frac{\partial \mathscr{E}}{\partial t} + \overline{u}_k \frac{\partial \mathscr{E}}{\partial \xi_k} - \frac{1}{\rho} \widehat{\sigma}_{ik} \frac{\partial u_i}{\partial \xi_k} = \frac{1}{\rho} Q. \tag{D.10}$$

Recall the dependence of the internal energy density on the state parameters: $\mathcal{E} = \mathcal{E}(\mathbf{F}, \mathscr{S})$. Derivatives of $\mathcal{E}$ with respect to any variable ϕ can be written

$$\frac{\partial \mathscr{E}}{\partial \phi} = \frac{\mathrm{d}\mathscr{E}}{\mathrm{d}F_{ij}} \frac{\partial F_{ij}}{\partial \phi} + \frac{\mathrm{d}\mathscr{E}}{\mathrm{d}\mathscr{S}} \frac{\partial \mathscr{S}}{\partial \phi}, \tag{D.11}$$

which can be substituted into Eq. (D.10) where ϕ represents either t or ξ_k; in addition $\widehat{\sigma}_{ik}$ can be replaced with the Murnaghan formula, Eq. (2.5), giving

$$\frac{\mathrm{d}\mathscr{E}}{\mathrm{d}\mathscr{S}} \left(\frac{\partial \mathscr{S}}{\partial t} + \overline{u}_k \frac{\partial \mathscr{S}}{\partial \xi_k} \right) + \frac{\mathrm{d}\mathscr{E}}{\mathrm{d}F_{ij}} \left(\frac{\partial F_{ij}}{\partial t} + \overline{u}_k \frac{\partial F_{ij}}{\partial \xi_k} - \widehat{F}_{kj} \frac{\partial u_i}{\partial \xi_k} \right) = \frac{1}{\rho} Q. \tag{D.12}$$

Using the equations for deformation gradient in non-conservative form, Eq. (D.6), yields

$$\frac{\mathrm{d}\mathscr{E}}{\mathrm{d}\mathscr{S}} \left(\frac{\partial \mathscr{S}}{\partial t} + \overline{u}_k \frac{\partial \mathscr{S}}{\partial \xi_k} \right) + \frac{\mathrm{d}\mathscr{E}}{\mathrm{d}F_{ij}} \left(-\frac{1}{\rho} \varphi_{ij} \right) = \frac{1}{\rho} Q. \tag{D.13}$$

Finally, by rearranging Eq. (D.13) the evolution equation for entropy is obtained (recall $T = \partial \mathscr{E} / \mathscr{S}$):

$$\frac{\partial \mathscr{S}}{\partial t} + \overline{u}_k \frac{\partial \mathscr{S}}{\partial \xi_k} = \frac{1}{T} \left[\frac{\mathrm{d}\mathscr{S}}{\mathrm{d}F_{ij}} \left(\frac{1}{\rho} \varphi_{ij} \right) + \frac{1}{\rho} Q \right]. \tag{D.14}$$

By introducing the vector of primitive variables

$$\mathbf{W} := (u_1,\ u_2,\ u_3,\ F_{11},\ F_{12},\ \ldots,\ F_{33},\ \mathscr{S})^{\mathrm{T}}\,, \tag{D.15}$$

the quasi-linear system can be written

$$\frac{\partial \mathbf{W}}{\partial t} + \mathscr{A}^k \frac{\partial \mathbf{W}}{\partial \xi_k} = \mathbf{S}, \tag{D.16}$$

where the Jacobian is given by

$$\mathscr{A}^k := \left(\begin{array}{cccccccc}
\overline{u}_k & 0 & 0 & -A^{k1}_{11} & -A^{k1}_{12} & -A^{k1}_{13} & -A^{k2}_{11} \\
0 & \overline{u}_k & 0 & -A^{k1}_{21} & -A^{k1}_{22} & -A^{k1}_{23} & -A^{k2}_{21} \\
0 & 0 & \overline{u}_k & -A^{k1}_{31} & -A^{k1}_{32} & -A^{k1}_{33} & -A^{k2}_{31} \\
-\widehat{F}_{k1} & 0 & 0 & \overline{u}_k & 0 & 0 & 0 \\
-\widehat{F}_{k2} & 0 & 0 & 0 & \overline{u}_k & 0 & 0 \\
-\widehat{F}_{k3} & 0 & 0 & 0 & 0 & \overline{u}_k & 0 \\
0 & -\widehat{F}_{k1} & 0 & 0 & 0 & 0 & \overline{u}_k \\
0 & -\widehat{F}_{k2} & 0 & 0 & 0 & 0 & 0 \\
0 & -\widehat{F}_{k3} & 0 & 0 & 0 & 0 & 0 \\
0 & 0 & -\widehat{F}_{k1} & 0 & 0 & 0 & 0 \\
0 & 0 & -\widehat{F}_{k2} & 0 & 0 & 0 & 0 \\
0 & 0 & -\widehat{F}_{k3} & 0 & 0 & 0 & 0 \\
0 & 0 & 0 & 0 & 0 & 0 & 0
\end{array}\right.$$

$$\left.\begin{array}{cccccc}
-A^{k2}_{12} & -A^{k2}_{13} & -A^{k3}_{11} & -A^{k3}_{12} & -A^{k3}_{13} & -b^k_1 \\
-A^{k2}_{22} & -A^{k2}_{23} & -A^{k3}_{21} & -A^{k3}_{22} & -A^{k3}_{23} & -b^k_2 \\
-A^{k2}_{32} & -A^{k2}_{33} & -A^{k3}_{31} & -A^{k3}_{32} & -A^{k3}_{33} & -b^k_3 \\
0 & 0 & 0 & 0 & 0 & 0 \\
0 & 0 & 0 & 0 & 0 & 0 \\
0 & 0 & 0 & 0 & 0 & 0 \\
0 & 0 & 0 & 0 & 0 & 0 \\
\overline{u}_k & 0 & 0 & 0 & 0 & 0 \\
0 & \overline{u}_k & 0 & 0 & 0 & 0 \\
0 & 0 & \overline{u}_k & 0 & 0 & 0 \\
0 & 0 & 0 & \overline{u}_k & 0 & 0 \\
0 & 0 & 0 & 0 & \overline{u}_k & 0 \\
0 & 0 & 0 & 0 & 0 & \overline{u}_k
\end{array}\right), \tag{D.17}$$

with the following coefficients

$$A^{k\beta}_{ij} := \frac{1}{\rho}\frac{\partial \widehat{\sigma}_{ki}}{\partial F_{\beta j}}, \qquad b^k_i := \frac{1}{\rho}\frac{\partial \widehat{\sigma}_{ki}}{\partial \mathscr{S}}. \tag{D.18}$$

The source term in Eq. (D.16) is given by

$$\mathbf{S} := \frac{1}{\rho}\left(0,\ 0,\ 0,\ -\varphi_{11},\ -\varphi_{12},\ \ldots,\ -\varphi_{33},\ \frac{1}{T}\left(\varphi_{ij}\frac{\mathrm{d}S}{\mathrm{d}F_{ij}} + Q\right)\right)^{\mathrm{T}}. \tag{D.19}$$

D.2 Characteristic polynomial and the eigenvalues

If λ denotes the wavespeeds then the characteristic polynomial for (2.25) ($|\mathscr{A}^k - \lambda\mathbf{I}| = 0$) has the form

$$(\overline{u}_k - \lambda)^7 \det\left|\mathbf{\Omega} - (\overline{u}_k - \lambda)^2\mathbf{I}\right| = 0,$$

where $\mathbf{\Omega}$ is the *acoustic tensor* and defined in Eq. (3.13).

D.3 Transformation to canonical form

In order to reduce the equations to a canonical form the proceedure from [64] for the two-dimensional equations of non-linear elasticity is here extended to the three-dimensional equations. In what follows the augmented one-dimensional system is considered for clarity and, in the first instance, the η–direction. Only the special case of non-linear elasticity is considered, thus $\mathbf{S} = 0$ in Eq. (D.16).

In matrix form Eq. (D.4) reads as

$$\left(\frac{\partial}{\partial t} + \overline{u}_\eta\frac{\partial}{\partial \xi_\eta}\right)\mathbf{u} - \mathbf{\Psi}_\eta\frac{\partial}{\partial \xi_\eta}\begin{pmatrix}\mathbf{F}^{\mathrm{T}}\mathbf{e}_1\\ \mathbf{F}^{\mathrm{T}}\mathbf{e}_2\\ \mathbf{F}^{\mathrm{T}}\mathbf{e}_3\\ \mathscr{S}\end{pmatrix} = 0, \tag{D.20}$$

where

$$\mathbf{\Psi}_\eta := \begin{pmatrix}\mathbf{A}^{\eta 1} & \mathbf{A}^{\eta 2} & \mathbf{A}^{\eta 3} & \mathbf{B}^{\eta}\end{pmatrix}. \tag{D.21}$$

Using the Eqs. (D.6)-(D.14) and the definition of the acoustic tensor, Eq. (3.13), the following relationship can be derived

$$\mathbf{\Psi}_\eta\left(\frac{\partial}{\partial t} + \overline{u}_\eta\frac{\partial}{\partial \xi_\eta}\right)\begin{pmatrix}\mathbf{F}^{\mathrm{T}}\mathbf{e}_1\\ \mathbf{F}^{\mathrm{T}}\mathbf{e}_2\\ \mathbf{F}^{\mathrm{T}}\mathbf{e}_3\\ \mathscr{S}\end{pmatrix} - \mathbf{\Omega}\frac{\partial \mathbf{u}}{\partial \xi_\eta} = 0. \tag{D.22}$$

By multiplying Eq. (D.20) by $\mathscr{D}\mathbf{Q}$, and Eq. (D.22) by $\mathbf{Q}$, and adding the results gives

$$\mathscr{D}\mathbf{Q}\frac{\partial}{\partial t}\mathbf{u} + (\overline{u}_\eta\mathbf{I} - \mathscr{D})\,\mathscr{D}\mathbf{Q}\frac{\partial}{\partial \xi_\eta}\mathbf{u} + \mathbf{Q}\mathbf{\Psi}_\eta\frac{\partial}{\partial t}\begin{pmatrix}\mathbf{F}^{\mathrm{T}}\mathbf{e}_1\\ \mathbf{F}^{\mathrm{T}}\mathbf{e}_2\\ \mathbf{F}^{\mathrm{T}}\mathbf{e}_3\\ \mathscr{S}\end{pmatrix} + (\overline{u}_\eta\mathbf{I} - \mathscr{D})\,\mathbf{Q}\mathbf{\Psi}_\eta\frac{\partial}{\partial \xi_\eta}\begin{pmatrix}\mathbf{F}^{\mathrm{T}}\mathbf{e}_1\\ \mathbf{F}^{\mathrm{T}}\mathbf{e}_2\\ \mathbf{F}^{\mathrm{T}}\mathbf{e}_3\\ \mathscr{S}\end{pmatrix} = 0. \tag{D.23}$$

Alternatively, subtracting the results gives

$$\mathscr{D}\mathbf{Q}\frac{\partial}{\partial t}\mathbf{u} + (\overline{u}_\eta\mathbf{I} + \mathscr{D})\,\mathscr{D}\mathbf{Q}\frac{\partial}{\partial \xi_\eta}\mathbf{u} - \mathbf{Q}\mathbf{\Psi}_\eta\frac{\partial}{\partial t}\begin{pmatrix}\mathbf{F}^{\mathrm{T}}\mathbf{e}_1\\ \mathbf{F}^{\mathrm{T}}\mathbf{e}_2\\ \mathbf{F}^{\mathrm{T}}\mathbf{e}_3\\ \mathscr{S}\end{pmatrix} - (\overline{u}_\eta\mathbf{I} + \mathscr{D})\,\mathbf{Q}\mathbf{\Psi}_\eta\frac{\partial}{\partial \xi_\eta}\begin{pmatrix}\mathbf{F}^{\mathrm{T}}\mathbf{e}_1\\ \mathbf{F}^{\mathrm{T}}\mathbf{e}_2\\ \mathbf{F}^{\mathrm{T}}\mathbf{e}_3\\ \mathscr{S}\end{pmatrix} = 0. \tag{D.24}$$

Both Eq. (D.23) and Eq. (D.24) are in canonical form. An additional equation in canonical form is the entropy equation, Eq. (D.14), making a total of seven.

At this point the required additional six equations in canonical form can be derived in the general case, the η–direction, however one finds it is better to disseminate these for specific coordinate directions $\eta = 1, 2, 3$. Whilst these steps are not strictly required, subtle changes in the formulation for each direction leads to eigenfunctions that are more convenient for use in a computer code (eliminates chances of having a divide by zero [cf. § 3.3]).

D.3.1 The canonical system in the ξ_1–direction

The non-conservative equations for deformation, Eq. (D.6), in the ξ_1–direction can be combined to form a canonical system. For example taking the equations for F_{11} and F_{12} and equating gives

$$\frac{\widehat{F}_{12}}{\widehat{F}_{11}}\left(\frac{\partial F_{11}}{\partial t} + \overline{u}_1\frac{\partial F_{11}}{\partial \xi_k}\right) - \left(\frac{\partial F_{12}}{\partial t} + \overline{u}_1\frac{\partial F_{12}}{\partial \xi_k}\right) = 0. \tag{D.25}$$

Similarly, from the other equations for deformation the following relations can be found

$$\frac{\widehat{F}_{13}}{\widehat{F}_{11}}\left(\frac{\partial F_{11}}{\partial t} + \overline{u}_1\frac{\partial F_{11}}{\partial \xi_k}\right) - \left(\frac{\partial F_{13}}{\partial t} + \overline{u}_1\frac{\partial F_{13}}{\partial \xi_k}\right) = 0, \tag{D.26}$$

$$\frac{\widehat{F}_{12}}{\widehat{F}_{11}}\left(\frac{\partial F_{21}}{\partial t}+\overline{u}_1\frac{\partial F_{21}}{\partial \xi_1}\right)-\left(\frac{\partial F_{22}}{\partial t}+\overline{u}_1\frac{\partial F_{22}}{\partial \xi_1}\right)=0, \tag{D.27}$$

$$\frac{\widehat{F}_{13}}{\widehat{F}_{11}}\left(\frac{\partial F_{21}}{\partial t}+\overline{u}_1\frac{\partial F_{21}}{\partial \xi_1}\right)-\left(\frac{\partial F_{23}}{\partial t}+\overline{u}_1\frac{\partial F_{23}}{\partial \xi_1}\right)=0, \tag{D.28}$$

$$\frac{\widehat{F}_{12}}{\widehat{F}_{11}}\left(\frac{\partial F_{31}}{\partial t}+\overline{u}_1\frac{\partial F_{31}}{\partial \xi_1}\right)-\left(\frac{\partial F_{32}}{\partial t}+\overline{u}_1\frac{\partial F_{32}}{\partial \xi_1}\right)=0, \tag{D.29}$$

$$\frac{\widehat{F}_{13}}{\widehat{F}_{11}}\left(\frac{\partial F_{31}}{\partial t}+\overline{u}_1\frac{\partial F_{31}}{\partial \xi_1}\right)-\left(\frac{\partial F_{33}}{\partial t}+\overline{u}_1\frac{\partial F_{33}}{\partial \xi_1}\right)=0. \tag{D.30}$$

Each of Eqs. (D.25)-(D.30) is in canonical form, and in matrix form read as

$$\boldsymbol{\Upsilon}_1\left(\frac{\partial}{\partial t}+\overline{u}_1\frac{\partial}{\partial \xi_1}\right)\begin{pmatrix}\mathbf{F}^{\mathrm{T}}\mathbf{e}_1\\ \mathbf{F}^{\mathrm{T}}\mathbf{e}_2\\ \mathbf{F}^{\mathrm{T}}\mathbf{e}_3\end{pmatrix}=0, \tag{D.31}$$

where

$$\boldsymbol{\Upsilon}_1:=\begin{pmatrix}
\widehat{F}_{12}/\widehat{F}_{11} & -1 & 0 & 0 & 0 & 0 & 0 & 0 & 0\\
\widehat{F}_{13}/\widehat{F}_{11} & 0 & -1 & 0 & 0 & 0 & 0 & 0 & 0\\
0 & 0 & 0 & \widehat{F}_{12}/\widehat{F}_{11} & -1 & 0 & 0 & 0 & 0\\
0 & 0 & 0 & \widehat{F}_{13}/\widehat{F}_{11} & 0 & -1 & 0 & 0 & 0\\
0 & 0 & 0 & 0 & 0 & 0 & \widehat{F}_{12}/\widehat{F}_{11} & -1 & 0\\
0 & 0 & 0 & 0 & 0 & 0 & \widehat{F}_{13}/\widehat{F}_{11} & 0 & -1
\end{pmatrix} \tag{D.32}$$

Eqs. (D.14),(D.23),(D.24),(D.31) combine to form the following canonical system

$$\mathbf{L}\frac{\partial}{\partial t}\mathbf{W}+\boldsymbol{\Lambda}\mathbf{L}\frac{\partial}{\partial \xi_1}\mathbf{W}=0 \tag{D.33}$$

with the matrix of left eigenvectors

$$\mathbf{L}=(\mathbf{l}_1,\,\mathbf{l}_2,\,\mathbf{l}_3,\,\mathbf{l}_4,\,\mathbf{l}_5,\,\mathbf{l}_6,\,\mathbf{l}_7,\,\mathbf{l}_8,\,\mathbf{l}_9,\,\mathbf{l}_{10},\,\mathbf{l}_{11},\,\mathbf{l}_{12},\,\mathbf{l}_{13})^{\mathrm{T}}, \tag{D.34}$$

where

$$\begin{aligned}
\mathbf{l}_1 =\ & ((\mathscr{D}\mathbf{Q})_{11},\,(\mathscr{D}\mathbf{Q})_{12},\,(\mathscr{D}\mathbf{Q})_{13},\,Q_{1i}A^{11}_{i1},\,Q_{1i}A^{11}_{i2},\,Q_{1i}A^{11}_{i3},\\
& Q_{1i}A^{12}_{i1},\,Q_{1i}A^{12}_{i2},\,Q_{1i}A^{12}_{i3},\,Q_{1i}A^{13}_{i1},\,Q_{1i}A^{13}_{i2},\,Q_{1i}A^{13}_{i3},\,Q_{1i}B^{1}_{i}),\\
\mathbf{l}_2 =\ & ((\mathscr{D}\mathbf{Q})_{21},\,(\mathscr{D}\mathbf{Q})_{22},\,(\mathscr{D}\mathbf{Q})_{23},\,Q_{2i}A^{11}_{i1},\,Q_{2i}A^{11}_{i2},\,Q_{2i}A^{11}_{i3},\\
& Q_{2i}A^{12}_{i1},\,Q_{2i}A^{12}_{i2},\,Q_{2i}A^{12}_{i3},\,Q_{2i}A^{13}_{i1},\,Q_{2i}A^{13}_{i2},\,Q_{2i}A^{13}_{i3},\,Q_{2i}B^{1}_{i}),\\
\mathbf{l}_3 =\ & ((\mathscr{D}\mathbf{Q})_{31},\,(\mathscr{D}\mathbf{Q})_{32},\,(\mathscr{D}\mathbf{Q})_{33},\,Q_{3i}A^{11}_{i1},\,Q_{3i}A^{11}_{i2},\,Q_{3i}A^{11}_{i3},\\
& Q_{3i}A^{12}_{i1},\,Q_{3i}A^{12}_{i2},\,Q_{3i}A^{12}_{i3},\,Q_{3i}A^{13}_{i1},\,Q_{3i}A^{13}_{i2},\,Q_{3i}A^{13}_{i3},\,Q_{3i}B^{1}_{i}),
\end{aligned}$$

$$
\begin{aligned}
\mathbf{l}_4 =& \ (0,\ 0,\ 0,\ \widehat{F}_{12}/\widehat{F}_{11},\ -1,\ 0,\ 0,\ 0,\ 0,\ 0,\ 0,\ 0,\ 0),\\
\mathbf{l}_5 =& \ (0,\ 0,\ 0,\ \widehat{F}_{13}/\widehat{F}_{11},\ 0,\ -1,\ 0,\ 0,\ 0,\ 0,\ 0,\ 0,\ 0),\\
\mathbf{l}_6 =& \ (0,\ 0,\ 0,\ 0,\ 0,\ 0,\ \widehat{F}_{12}/\widehat{F}_{11},\ -1,\ 0,\ 0,\ 0,\ 0,\ 0),\\
\mathbf{l}_7 =& \ (0,\ 0,\ 0,\ 0,\ 0,\ 0,\ \widehat{F}_{13}/\widehat{F}_{11},\ 0,\ -1,\ 0,\ 0,\ 0,\ 0),\\
\mathbf{l}_8 =& \ (0,\ 0,\ 0,\ 0,\ 0,\ 0,\ 0,\ 0,\ 0,\ \widehat{F}_{12}/\widehat{F}_{11},\ -1,\ 0,\ 0),\\
\mathbf{l}_9 =& \ (0,\ 0,\ 0,\ 0,\ 0,\ 0,\ 0,\ 0,\ 0,\ \widehat{F}_{13}/\widehat{F}_{11},\ 0,\ -1,\ 0),\\
\mathbf{l}_{10} =& \ (0,\ 0,\ 0,\ 0,\ 0,\ 0,\ 0,\ 0,\ 0,\ 0,\ 0,\ 0,\ 0,\ 1),\\
\mathbf{l}_{11} =& \ ((\mathscr{D}\mathbf{Q})_{31},\ (\mathscr{D}\mathbf{Q})_{32},\ (\mathscr{D}\mathbf{Q})_{33},\ -Q_{3i}A^{11}_{i1},\ -Q_{3i}A^{11}_{i2},\ -Q_{3i}A^{11}_{i3},\\
& \ -Q_{3i}A^{12}_{i1},\ -Q_{3i}A^{12}_{i2},\ -Q_{3i}A^{12}_{i3},\ -Q_{3i}A^{13}_{i1},\ -Q_{3i}A^{13}_{i2},\ -Q_{3i}A^{13}_{i3},\ -Q_{3i}B^{1}_{i}),\\
\mathbf{l}_{12} =& \ ((\mathscr{D}\mathbf{Q})_{21},\ (\mathscr{D}\mathbf{Q})_{22},\ (\mathscr{D}\mathbf{Q})_{23},\ -Q_{2i}A^{11}_{i1},\ -Q_{2i}A^{11}_{i2},\ -Q_{2i}A^{11}_{i3},\\
& \ -Q_{2i}A^{12}_{i1},\ -Q_{2i}A^{12}_{i2},\ -Q_{2i}A^{12}_{i3},\ -Q_{2i}A^{13}_{i1},\ -Q_{2i}A^{13}_{i2},\ -Q_{2i}A^{13}_{i3},\ -Q_{2i}B^{1}_{i}),\\
\mathbf{l}_{13} =& \ ((\mathscr{D}\mathbf{Q})_{11},\ (\mathscr{D}\mathbf{Q})_{12},\ (\mathscr{D}\mathbf{Q})_{13},\ -Q_{1i}A^{11}_{i1},\ -Q_{1i}A^{11}_{i2},\ -Q_{1i}A^{11}_{i3},\\
& \ -Q_{1i}A^{12}_{i1},\ -Q_{1i}A^{12}_{i2},\ -Q_{1i}A^{12}_{i3},\ -Q_{1i}A^{13}_{i1},\ -Q_{1i}A^{13}_{i2},\ -Q_{1i}A^{13}_{i3},\ -Q_{1i}B^{1}_{i}).
\end{aligned}
$$

Using the assumption that the right eigenvectors are orthonormal to the left ($\mathbf{RL} = \mathbf{I}$)

$$
\mathbf{R} = (\mathbf{r}_1,\ \mathbf{r}_2,\ \mathbf{r}_3,\ \mathbf{r}_4,\ \mathbf{r}_5,\ \mathbf{r}_6,\ \mathbf{r}_7,\ \mathbf{r}_8,\ \mathbf{r}_9,\ \mathbf{r}_{10},\ \mathbf{r}_{11},\ \mathbf{r}_{12},\ \mathbf{r}_{13}), \tag{D.35}
$$

where

$$
\begin{aligned}
\mathbf{r}_1 =& \ \tfrac{1}{2}((\mathscr{D}\mathbf{Q})^{-1}_{11},\ (\mathscr{D}\mathbf{Q})^{-1}_{21},\ (\mathscr{D}\mathbf{Q})^{-1}_{31},\ \widehat{F}_{11}(\mathscr{D}^2\mathbf{Q})^{-1}_{11},\ \widehat{F}_{12}(\mathscr{D}^2\mathbf{Q})^{-1}_{11},\\
& \ \widehat{F}_{13}(\mathscr{D}^2\mathbf{Q})^{-1}_{11},\ \widehat{F}_{11}(\mathscr{D}^2\mathbf{Q})^{-1}_{21},\ \widehat{F}_{12}(\mathscr{D}^2\mathbf{Q})^{-1}_{21},\ \widehat{F}_{13}(\mathscr{D}^2\mathbf{Q})^{-1}_{21},\\
& \ \widehat{F}_{11}(\mathscr{D}^2\mathbf{Q})^{-1}_{31},\ \widehat{F}_{12}(\mathscr{D}^2\mathbf{Q})^{-1}_{31},\ \widehat{F}_{13}(\mathscr{D}^2\mathbf{Q})^{-1}_{31},\ 0)^{\mathrm{T}},\\
\mathbf{r}_2 =& \ \tfrac{1}{2}((\mathscr{D}\mathbf{Q})^{-1}_{12},\ (\mathscr{D}\mathbf{Q})^{-1}_{22},\ (\mathscr{D}\mathbf{Q})^{-1}_{32},\ \widehat{F}_{11}(\mathscr{D}^2\mathbf{Q})^{-1}_{12},\ \widehat{F}_{12}(\mathscr{D}^2\mathbf{Q})^{-1}_{12},\\
& \ \widehat{F}_{13}(\mathscr{D}^2\mathbf{Q})^{-1}_{12},\ \widehat{F}_{11}(\mathscr{D}^2\mathbf{Q})^{-1}_{22},\ \widehat{F}_{12}(\mathscr{D}^2\mathbf{Q})^{-1}_{22},\ \widehat{F}_{13}(\mathscr{D}^2\mathbf{Q})^{-1}_{22},\\
& \ \widehat{F}_{11}(\mathscr{D}^2\mathbf{Q})^{-1}_{32},\ \widehat{F}_{12}(\mathscr{D}^2\mathbf{Q})^{-1}_{32},\ \widehat{F}_{13}(\mathscr{D}^2\mathbf{Q})^{-1}_{32},\ 0)^{\mathrm{T}},\\
\mathbf{r}_3 =& \ \tfrac{1}{2}((\mathscr{D}\mathbf{Q})^{-1}_{13},\ (\mathscr{D}\mathbf{Q})^{-1}_{23},\ (\mathscr{D}\mathbf{Q})^{-1}_{33},\ \widehat{F}_{11}(\mathscr{D}^2\mathbf{Q})^{-1}_{13},\ \widehat{F}_{12}(\mathscr{D}^2\mathbf{Q})^{-1}_{13},\\
& \ \widehat{F}_{13}(\mathscr{D}^2\mathbf{Q})^{-1}_{13},\ \widehat{F}_{11}(\mathscr{D}^2\mathbf{Q})^{-1}_{23},\ \widehat{F}_{12}(\mathscr{D}^2\mathbf{Q})^{-1}_{23},\ \widehat{F}_{13}(\mathscr{D}^2\mathbf{Q})^{-1}_{23},\\
& \ \widehat{F}_{11}(\mathscr{D}^2\mathbf{Q})^{-1}_{33},\ \widehat{F}_{12}(\mathscr{D}^2\mathbf{Q})^{-1}_{33},\ \widehat{F}_{13}(\mathscr{D}^2\mathbf{Q})^{-1}_{33},\ 0)^{\mathrm{T}},\\
\mathbf{r}_4 =& \ (0,\ 0,\ 0,\ \widehat{F}_{11}\Omega^{-1}_{1i}A^{11}_{i2},\ \widehat{F}_{12}\Omega^{-1}_{1i}A^{11}_{i2} - 1,\ \widehat{F}_{13}\Omega^{-1}_{1i}A^{11}_{i2},\ \widehat{F}_{11}\Omega^{-1}_{2i}A^{11}_{i2}\\
& \ \widehat{F}_{12}\Omega^{-1}_{2i}A^{11}_{i2},\ \widehat{F}_{13}\Omega^{-1}_{2i}A^{11}_{i2},\ \widehat{F}_{11}\Omega^{-1}_{3i}A^{11}_{i2},\ \widehat{F}_{12}\Omega^{-1}_{3i}A^{11}_{i2},\ \widehat{F}_{13}\Omega^{-1}_{3i}A^{11}_{i2},\ 0)^{\mathrm{T}},\\
\mathbf{r}_5 =& \ (0,\ 0,\ 0,\ \widehat{F}_{11}\Omega^{-1}_{1i}A^{11}_{i3},\ \widehat{F}_{12}\Omega^{-1}_{1i}A^{11}_{i3},\ \widehat{F}_{13}\Omega^{-1}_{1i}A^{11}_{i3} - 1,\ \widehat{F}_{11}\Omega^{-1}_{2i}A^{11}_{i3}\\
& \ \widehat{F}_{12}\Omega^{-1}_{2i}A^{11}_{i3},\ \widehat{F}_{13}\Omega^{-1}_{2i}A^{11}_{i3},\ \widehat{F}_{11}\Omega^{-1}_{3i}A^{11}_{i3},\ \widehat{F}_{12}\Omega^{-1}_{3i}A^{11}_{i3},\ \widehat{F}_{13}\Omega^{-1}_{3i}A^{11}_{i3},\ 0)^{\mathrm{T}},\\
\mathbf{r}_6 =& \ (0,\ 0,\ 0,\ \widehat{F}_{11}\Omega^{-1}_{1i}A^{12}_{i2},\ \widehat{F}_{12}\Omega^{-1}_{1i}A^{12}_{i2},\ \widehat{F}_{13}\Omega^{-1}_{1i}A^{12}_{i2},\ \widehat{F}_{11}\Omega^{-1}_{2i}A^{12}_{i2}\\
& \ \widehat{F}_{12}\Omega^{-1}_{2i}A^{12}_{i2} - 1,\ \widehat{F}_{13}\Omega^{-1}_{2i}A^{12}_{i2},\ \widehat{F}_{11}\Omega^{-1}_{3i}A^{12}_{i2},\ \widehat{F}_{12}\Omega^{-1}_{3i}A^{12}_{i2},\ \widehat{F}_{13}\Omega^{-1}_{3i}A^{12}_{i2},\ 0)^{\mathrm{T}},
\end{aligned}
$$

$$
\begin{aligned}
\mathbf{r}_7 = {} & (0,\ 0,\ 0,\ \widehat{F}_{11}\Omega_{1i}^{-1}A_{i3}^{12},\ \widehat{F}_{12}\Omega_{1i}^{-1}A_{i3}^{12},\ \widehat{F}_{13}\Omega_{1i}^{-1}A_{i3}^{12},\ \widehat{F}_{11}\Omega_{2i}^{-1}A_{i3}^{12} \\
& \widehat{F}_{12}\Omega_{2i}^{-1}A_{i3}^{12},\ \widehat{F}_{13}\Omega_{2i}^{-1}A_{i3}^{12}-1,\ \widehat{F}_{11}\Omega_{3i}^{-1}A_{i3}^{12},\ \widehat{F}_{12}\Omega_{3i}^{-1}A_{i3}^{12},\ \widehat{F}_{13}\Omega_{3i}^{-1}A_{i3}^{12},\ 0)^{\mathrm{T}}, \\
\mathbf{r}_8 = {} & (0,\ 0,\ 0,\ \widehat{F}_{11}\Omega_{1i}^{-1}A_{i2}^{13},\ \widehat{F}_{12}\Omega_{1i}^{-1}A_{i2}^{13},\ \widehat{F}_{13}\Omega_{1i}^{-1}A_{i2}^{13},\ \widehat{F}_{11}\Omega_{2i}^{-1}A_{i2}^{13} \\
& \widehat{F}_{12}\Omega_{2i}^{-1}A_{i2}^{13},\ \widehat{F}_{13}\Omega_{2i}^{-1}A_{i2}^{13},\ \widehat{F}_{11}\Omega_{3i}^{-1}A_{i2}^{13},\ \widehat{F}_{12}\Omega_{3i}^{-1}A_{i2}^{13}-1,\ \widehat{F}_{13}\Omega_{3i}^{-1}A_{i2}^{13},\ 0)^{\mathrm{T}}, \\
\mathbf{r}_9 = {} & (0,\ 0,\ 0,\ \widehat{F}_{11}\Omega_{1i}^{-1}A_{i3}^{13},\ \widehat{F}_{12}\Omega_{1i}^{-1}A_{i3}^{13},\ \widehat{F}_{13}\Omega_{1i}^{-1}A_{i3}^{13},\ \widehat{F}_{11}\Omega_{2i}^{-1}A_{i3}^{13} \\
& \widehat{F}_{12}\Omega_{2i}^{-1}A_{i3}^{13},\ \widehat{F}_{13}\Omega_{2i}^{-1}A_{i3}^{13},\ \widehat{F}_{11}\Omega_{3i}^{-1}A_{i3}^{13},\ \widehat{F}_{12}\Omega_{3i}^{-1}A_{i3}^{13},\ \widehat{F}_{13}\Omega_{3i}^{-1}A_{i3}^{13}-1,\ 0)^{\mathrm{T}}, \\
\mathbf{r}_{10} = {} & (0,\ 0,\ 0,\ -\widehat{F}_{11}\Omega_{1i}^{-1}B_i^1,\ -\widehat{F}_{12}\Omega_{1i}^{-1}B_i^1,\ -\widehat{F}_{13}\Omega_{1i}^{-1}B_i^1,\ -\widehat{F}_{11}\Omega_{2i}^{-1}B_i^1 \\
& -\widehat{F}_{12}\Omega_{2i}^{-1}B_i^1,\ -\widehat{F}_{13}\Omega_{2i}^{-1}B_i^1,\ -\widehat{F}_{11}\Omega_{3i}^{-1}B_i^1,\ -\widehat{F}_{12}\Omega_{3i}^{-1}B_i^1,\ -\widehat{F}_{13}\Omega_{3i}^{-1}B_i^1,\ 1)^{\mathrm{T}}, \\
\mathbf{r}_{11} = {} & \tfrac{1}{2}((\mathscr{D}\mathbf{Q})_{13}^{-1},\ (\mathscr{D}\mathbf{Q})_{23}^{-1},\ (\mathscr{D}\mathbf{Q})_{33}^{-1},\ -\widehat{F}_{11}(\mathscr{D}^2\mathbf{Q})_{13}^{-1},\ -\widehat{F}_{12}(\mathscr{D}^2\mathbf{Q})_{13}^{-1}, \\
& -\widehat{F}_{13}(\mathscr{D}^2\mathbf{Q})_{13}^{-1},\ -\widehat{F}_{11}(\mathscr{D}^2\mathbf{Q})_{23}^{-1},\ -\widehat{F}_{12}(\mathscr{D}^2\mathbf{Q})_{23}^{-1},\ -\widehat{F}_{13}(\mathscr{D}^2\mathbf{Q})_{23}^{-1}, \\
& -\widehat{F}_{11}(\mathscr{D}^2\mathbf{Q})_{33}^{-1},\ -\widehat{F}_{12}(\mathscr{D}^2\mathbf{Q})_{33}^{-1},\ -\widehat{F}_{13}(\mathscr{D}^2\mathbf{Q})_{33}^{-1},\ 0)^{\mathrm{T}}, \\
\mathbf{r}_{12} = {} & \tfrac{1}{2}((\mathscr{D}\mathbf{Q})_{12}^{-1},\ (\mathscr{D}\mathbf{Q})_{22}^{-1},\ (\mathscr{D}\mathbf{Q})_{32}^{-1},\ -\widehat{F}_{11}(\mathscr{D}^2\mathbf{Q})_{12}^{-1},\ -\widehat{F}_{12}(\mathscr{D}^2\mathbf{Q})_{12}^{-1}, \\
& -\widehat{F}_{13}(\mathscr{D}^2\mathbf{Q})_{12}^{-1},\ -\widehat{F}_{11}(\mathscr{D}^2\mathbf{Q})_{22}^{-1},\ -\widehat{F}_{12}(\mathscr{D}^2\mathbf{Q})_{22}^{-1},\ -\widehat{F}_{13}(\mathscr{D}^2\mathbf{Q})_{22}^{-1}, \\
& -\widehat{F}_{11}(\mathscr{D}^2\mathbf{Q})_{32}^{-1},\ -\widehat{F}_{12}(\mathscr{D}^2\mathbf{Q})_{32}^{-1},\ -\widehat{F}_{13}(\mathscr{D}^2\mathbf{Q})_{32}^{-1},\ 0)^{\mathrm{T}}, \\
\mathbf{r}_{13} = {} & \tfrac{1}{2}((\mathscr{D}\mathbf{Q})_{11}^{-1},\ (\mathscr{D}\mathbf{Q})_{21}^{-1},\ (\mathscr{D}\mathbf{Q})_{31}^{-1},\ -\widehat{F}_{11}(\mathscr{D}^2\mathbf{Q})_{11}^{-1},\ -\widehat{F}_{12}(\mathscr{D}^2\mathbf{Q})_{11}^{-1}, \\
& -\widehat{F}_{13}(\mathscr{D}^2\mathbf{Q})_{11}^{-1},\ -\widehat{F}_{11}(\mathscr{D}^2\mathbf{Q})_{21}^{-1},\ -\widehat{F}_{12}(\mathscr{D}^2\mathbf{Q})_{21}^{-1},\ -\widehat{F}_{13}(\mathscr{D}^2\mathbf{Q})_{21}^{-1}, \\
& -\widehat{F}_{11}(\mathscr{D}^2\mathbf{Q})_{31}^{-1},\ -\widehat{F}_{12}(\mathscr{D}^2\mathbf{Q})_{31}^{-1},\ -\widehat{F}_{13}(\mathscr{D}^2\mathbf{Q})_{31}^{-1},\ 0)^{\mathrm{T}}.
\end{aligned}
$$

D.4 The canonical system in the ξ_2–direction

The non-conservative equations for deformation, Eq. (D.6), in the ξ_2–direction can be combined as follows: for example taking the equations for F_{11} and F_{12} and equating gives

$$
\frac{\widehat{F}_{21}}{\widehat{F}_{22}}\left(\frac{\partial F_{12}}{\partial t}+\overline{u}_2\frac{\partial F_{12}}{\partial \xi_k}\right)-\left(\frac{\partial F_{11}}{\partial t}+\overline{u}_2\frac{\partial F_{11}}{\partial \xi_k}\right)=0. \tag{D.36}
$$

Similarly, from the other equations for deformation the following relations can be found

$$
\frac{\widehat{F}_{23}}{\widehat{F}_{22}}\left(\frac{\partial F_{12}}{\partial t}+\overline{u}_2\frac{\partial F_{12}}{\partial \xi_k}\right)-\left(\frac{\partial F_{13}}{\partial t}+\overline{u}_2\frac{\partial F_{13}}{\partial \xi_k}\right)=0, \tag{D.37}
$$

$$
\frac{\widehat{F}_{21}}{\widehat{F}_{22}}\left(\frac{\partial F_{22}}{\partial t}+\overline{u}_2\frac{\partial F_{22}}{\partial \xi_2}\right)-\left(\frac{\partial F_{21}}{\partial t}+\overline{u}_2\frac{\partial F_{21}}{\partial \xi_2}\right)=0, \tag{D.38}
$$

$$
\frac{\widehat{F}_{23}}{\widehat{F}_{22}}\left(\frac{\partial F_{22}}{\partial t}+\overline{u}_2\frac{\partial F_{22}}{\partial \xi_2}\right)-\left(\frac{\partial F_{23}}{\partial t}+\overline{u}_2\frac{\partial F_{23}}{\partial \xi_2}\right)=0, \tag{D.39}
$$

$$\frac{\widehat{F}_{21}}{\widehat{F}_{22}}\left(\frac{\partial F_{32}}{\partial t}+\overline{u}_2\frac{\partial F_{32}}{\partial \xi_2}\right)-\left(\frac{\partial F_{31}}{\partial t}+\overline{u}_2\frac{\partial F_{31}}{\partial \xi_2}\right)=0, \tag{D.40}$$

$$\frac{\widehat{F}_{23}}{\widehat{F}_{22}}\left(\frac{\partial F_{32}}{\partial t}+\overline{u}_2\frac{\partial F_{32}}{\partial \xi_2}\right)-\left(\frac{\partial F_{33}}{\partial t}+\overline{u}_2\frac{\partial F_{33}}{\partial \xi_2}\right)=0. \tag{D.41}$$

In matrix form Eqs. (D.36)-(D.41) read as

$$\boldsymbol{\Upsilon}_2\left(\frac{\partial}{\partial t}+\overline{u}_2\frac{\partial}{\partial \xi_2}\right)\begin{pmatrix}\mathbf{F}^{\mathrm{T}}\mathbf{e}_1\\ \mathbf{F}^{\mathrm{T}}\mathbf{e}_2\\ \mathbf{F}^{\mathrm{T}}\mathbf{e}_3\end{pmatrix}=0, \tag{D.42}$$

where

$$\boldsymbol{\Upsilon}_2:=\begin{pmatrix}
-1 & \widehat{F}_{21}/\widehat{F}_{22} & 0 & 0 & 0 & 0 & 0 & 0 & 0\\
0 & \widehat{F}_{23}/\widehat{F}_{22} & -1 & 0 & 0 & 0 & 0 & 0 & 0\\
0 & 0 & 0 & -1 & \widehat{F}_{21}/\widehat{F}_{22} & 0 & 0 & 0 & 0\\
0 & 0 & 0 & 0 & \widehat{F}_{23}/\widehat{F}_{22} & -1 & 0 & 0 & 0\\
0 & 0 & 0 & 0 & 0 & 0 & -1 & \widehat{F}_{21}/\widehat{F}_{22} & 0\\
0 & 0 & 0 & 0 & 0 & 0 & 0 & \widehat{F}_{23}/\widehat{F}_{22} & -1
\end{pmatrix} \tag{D.43}$$

Eqs. (D.14),(D.23),(D.24),(D.42) combine to form the following canonical system

$$\mathbf{L}\frac{\partial}{\partial t}\mathbf{W}+\boldsymbol{\Lambda}\mathbf{L}\frac{\partial}{\partial \xi_2}\mathbf{W}=0 \tag{D.44}$$

with the matrix of left eigenvectors

$$\mathbf{L}=(\mathbf{l}_1,\,\mathbf{l}_2,\,\mathbf{l}_3,\,\mathbf{l}_4,\,\mathbf{l}_5,\,\mathbf{l}_6,\,\mathbf{l}_7,\,\mathbf{l}_8,\,\mathbf{l}_9,\,\mathbf{l}_{10},\,\mathbf{l}_{11},\,\mathbf{l}_{12},\,\mathbf{l}_{13})^{\mathrm{T}}, \tag{D.45}$$

where

$$\begin{aligned}
\mathbf{l}_1 =\;& ((\mathscr{D}\mathbf{Q})_{11},\,(\mathscr{D}\mathbf{Q})_{12},\,(\mathscr{D}\mathbf{Q})_{13},\,Q_{1i}A^{21}_{i1},\,Q_{1i}A^{21}_{i2},\,Q_{1i}A^{21}_{i3},\\
&Q_{1i}A^{22}_{i1},\,Q_{1i}A^{22}_{i2},\,Q_{1i}A^{22}_{i3},\,Q_{1i}A^{23}_{i1},\,Q_{1i}A^{23}_{i2},\,Q_{1i}A^{23}_{i3},\,Q_{1i}B^{2}_{i}),\\
\mathbf{l}_2 =\;& ((\mathscr{D}\mathbf{Q})_{21},\,(\mathscr{D}\mathbf{Q})_{22},\,(\mathscr{D}\mathbf{Q})_{23},\,Q_{2i}A^{21}_{i1},\,Q_{2i}A^{21}_{i2},\,Q_{2i}A^{21}_{i3},\\
&Q_{2i}A^{22}_{i1},\,Q_{2i}A^{22}_{i2},\,Q_{2i}A^{22}_{i3},\,Q_{2i}A^{23}_{i1},\,Q_{2i}A^{23}_{i2},\,Q_{2i}A^{23}_{i3},\,Q_{2i}B^{2}_{i}),\\
\mathbf{l}_3 =\;& ((\mathscr{D}\mathbf{Q})_{31},\,(\mathscr{D}\mathbf{Q})_{32},\,(\mathscr{D}\mathbf{Q})_{33},\,Q_{3i}A^{21}_{i1},\,Q_{3i}A^{21}_{i2},\,Q_{3i}A^{21}_{i3},\\
&Q_{3i}A^{22}_{i1},\,Q_{3i}A^{22}_{i2},\,Q_{3i}A^{22}_{i3},\,Q_{3i}A^{23}_{i1},\,Q_{3i}A^{23}_{i2},\,Q_{3i}A^{23}_{i3},\,Q_{3i}B^{2}_{i}),\\
\mathbf{l}_4 =\;& (0,\,0,\,0,\,-1,\,\widehat{F}_{21}/\widehat{F}_{22},\,0,\,0,\,0,\,0,\,0,\,0,\,0,\,0),\\
\mathbf{l}_5 =\;& (0,\,0,\,0,\,0,\,\widehat{F}_{23}/\widehat{F}_{22},\,-1,\,0,\,0,\,0,\,0,\,0,\,0,\,0),\\
\mathbf{l}_6 =\;& (0,\,0,\,0,\,0,\,0,\,0,\,-1,\,\widehat{F}_{21}/\widehat{F}_{22},\,0,\,0,\,0,\,0,\,0),\\
\mathbf{l}_7 =\;& (0,\,0,\,0,\,0,\,0,\,0,\,0,\,\widehat{F}_{23}/\widehat{F}_{22},\,-1,\,0,\,0,\,0,\,0),
\end{aligned}$$

$$
\begin{aligned}
\mathbf{l}_8 =\ & (0,\ 0,\ 0,\ 0,\ 0,\ 0,\ 0,\ 0,\ 0,\ -1,\ \widehat{F}_{21}/\widehat{F}_{22},\ 0,\ 0),\\
\mathbf{l}_9 =\ & (0,\ 0,\ 0,\ 0,\ 0,\ 0,\ 0,\ 0,\ 0,\ 0,\ \widehat{F}_{23}/\widehat{F}_{22},\ -1,\ 0),\\
\mathbf{l}_{10} =\ & (0,\ 0,\ 0,\ 0,\ 0,\ 0,\ 0,\ 0,\ 0,\ 0,\ 0,\ 0,\ 0,\ 1),\\
\mathbf{l}_{11} =\ & ((\mathscr{D}\mathbf{Q})_{31},\ (\mathscr{D}\mathbf{Q})_{32},\ (\mathscr{D}\mathbf{Q})_{33},\ -Q_{3i}A^{21}_{i1},\ -Q_{3i}A^{21}_{i2},\ -Q_{3i}A^{21}_{i3},\\
& -Q_{3i}A^{22}_{i1},\ -Q_{3i}A^{22}_{i2},\ -Q_{3i}A^{22}_{i3},\ -Q_{3i}A^{23}_{i1},\ -Q_{3i}A^{23}_{i2},\ -Q_{3i}A^{23}_{i3},\ -Q_{3i}B^{2}_{i}),\\
\mathbf{l}_{12} =\ & ((\mathscr{D}\mathbf{Q})_{21},\ (\mathscr{D}\mathbf{Q})_{22},\ (\mathscr{D}\mathbf{Q})_{23},\ -Q_{2i}A^{21}_{i1},\ -Q_{2i}A^{21}_{i2},\ -Q_{2i}A^{21}_{i3},\\
& -Q_{2i}A^{22}_{i1},\ -Q_{2i}A^{22}_{i2},\ -Q_{2i}A^{22}_{i3},\ -Q_{2i}A^{23}_{i1},\ -Q_{2i}A^{23}_{i2},\ -Q_{2i}A^{23}_{i3},\ -Q_{2i}B^{2}_{i}),\\
\mathbf{l}_{13} =\ & ((\mathscr{D}\mathbf{Q})_{11},\ (\mathscr{D}\mathbf{Q})_{12},\ (\mathscr{D}\mathbf{Q})_{13},\ -Q_{1i}A^{21}_{i1},\ -Q_{1i}A^{21}_{i2},\ -Q_{1i}A^{21}_{i3},\\
& -Q_{1i}A^{22}_{i1},\ -Q_{1i}A^{22}_{i2},\ -Q_{1i}A^{22}_{i3},\ -Q_{1i}A^{23}_{i1},\ -Q_{1i}A^{23}_{i2},\ -Q_{1i}A^{23}_{i3},\ -Q_{1i}B^{2}_{i}).
\end{aligned}
$$

Using the assumption that the right eigenvectors are orthonormal to the left ($\mathbf{RL} = \mathbf{I}$)

$$
\mathbf{R} = (\mathbf{r}_1,\ \mathbf{r}_2,\ \mathbf{r}_3,\ \mathbf{r}_4,\ \mathbf{r}_5,\ \mathbf{r}_6,\ \mathbf{r}_7,\ \mathbf{r}_8,\ \mathbf{r}_9,\ \mathbf{r}_{10},\ \mathbf{r}_{11},\ \mathbf{r}_{12},\ \mathbf{r}_{13}), \tag{D.46}
$$

where

$$
\begin{aligned}
\mathbf{r}_1 =\ & \tfrac{1}{2}((\mathscr{D}\mathbf{Q})^{-1}_{11},\ (\mathscr{D}\mathbf{Q})^{-1}_{21},\ (\mathscr{D}\mathbf{Q})^{-1}_{31},\ \widehat{F}_{21}(\mathscr{D}^2\mathbf{Q})^{-1}_{11},\ \widehat{F}_{22}(\mathscr{D}^2\mathbf{Q})^{-1}_{11},\\
& \widehat{F}_{23}(\mathscr{D}^2\mathbf{Q})^{-1}_{11},\ \widehat{F}_{21}(\mathscr{D}^2\mathbf{Q})^{-1}_{21},\ \widehat{F}_{22}(\mathscr{D}^2\mathbf{Q})^{-1}_{21},\ \widehat{F}_{23}(\mathscr{D}^2\mathbf{Q})^{-1}_{21},\\
& \widehat{F}_{21}(\mathscr{D}^2\mathbf{Q})^{-1}_{31},\ \widehat{F}_{22}(\mathscr{D}^2\mathbf{Q})^{-1}_{31},\ \widehat{F}_{23}(\mathscr{D}^2\mathbf{Q})^{-1}_{31},\ 0)^{\mathrm{T}},\\
\mathbf{r}_2 =\ & \tfrac{1}{2}((\mathscr{D}\mathbf{Q})^{-1}_{12},\ (\mathscr{D}\mathbf{Q})^{-1}_{22},\ (\mathscr{D}\mathbf{Q})^{-1}_{32},\ \widehat{F}_{21}(\mathscr{D}^2\mathbf{Q})^{-1}_{12},\ \widehat{F}_{22}(\mathscr{D}^2\mathbf{Q})^{-1}_{12},\\
& \widehat{F}_{23}(\mathscr{D}^2\mathbf{Q})^{-1}_{12},\ \widehat{F}_{21}(\mathscr{D}^2\mathbf{Q})^{-1}_{22},\ \widehat{F}_{22}(\mathscr{D}^2\mathbf{Q})^{-1}_{22},\ \widehat{F}_{23}(\mathscr{D}^2\mathbf{Q})^{-1}_{22},\\
& \widehat{F}_{21}(\mathscr{D}^2\mathbf{Q})^{-1}_{32},\ \widehat{F}_{22}(\mathscr{D}^2\mathbf{Q})^{-1}_{32},\ \widehat{F}_{23}(\mathscr{D}^2\mathbf{Q})^{-1}_{32},\ 0)^{\mathrm{T}},\\
\mathbf{r}_3 =\ & \tfrac{1}{2}((\mathscr{D}\mathbf{Q})^{-1}_{13},\ (\mathscr{D}\mathbf{Q})^{-1}_{23},\ (\mathscr{D}\mathbf{Q})^{-1}_{33},\ \widehat{F}_{21}(\mathscr{D}^2\mathbf{Q})^{-1}_{13},\ \widehat{F}_{22}(\mathscr{D}^2\mathbf{Q})^{-1}_{13},\\
& \widehat{F}_{23}(\mathscr{D}^2\mathbf{Q})^{-1}_{13},\ \widehat{F}_{21}(\mathscr{D}^2\mathbf{Q})^{-1}_{23},\ \widehat{F}_{22}(\mathscr{D}^2\mathbf{Q})^{-1}_{23},\ \widehat{F}_{23}(\mathscr{D}^2\mathbf{Q})^{-1}_{23},\\
& \widehat{F}_{21}(\mathscr{D}^2\mathbf{Q})^{-1}_{33},\ \widehat{F}_{22}(\mathscr{D}^2\mathbf{Q})^{-1}_{33},\ \widehat{F}_{23}(\mathscr{D}^2\mathbf{Q})^{-1}_{33},\ 0)^{\mathrm{T}},\\
\mathbf{r}_4 =\ & (0,\ 0,\ 0,\ \widehat{F}_{21}\Omega^{-1}_{1i}A^{21}_{i1} - 1,\ \widehat{F}_{22}\Omega^{-1}_{1i}A^{21}_{i1},\ \widehat{F}_{23}\Omega^{-1}_{1i}A^{21}_{i1},\ \widehat{F}_{21}\Omega^{-1}_{2i}A^{21}_{i1}\\
& \widehat{F}_{22}\Omega^{-1}_{2i}A^{21}_{i1},\ \widehat{F}_{23}\Omega^{-1}_{2i}A^{21}_{i1},\ \widehat{F}_{21}\Omega^{-1}_{3i}A^{21}_{i1},\ \widehat{F}_{22}\Omega^{-1}_{3i}A^{21}_{i1},\ \widehat{F}_{23}\Omega^{-1}_{3i}A^{21}_{i1},\ 0)^{\mathrm{T}},\\
\mathbf{r}_5 =\ & (0,\ 0,\ 0,\ \widehat{F}_{21}\Omega^{-1}_{1i}A^{21}_{i3},\ \widehat{F}_{22}\Omega^{-1}_{1i}A^{21}_{i3},\ \widehat{F}_{23}\Omega^{-1}_{1i}A^{21}_{i3} - 1,\ \widehat{F}_{21}\Omega^{-1}_{2i}A^{21}_{i3}\\
& \widehat{F}_{22}\Omega^{-1}_{2i}A^{21}_{i3},\ \widehat{F}_{23}\Omega^{-1}_{2i}A^{21}_{i3},\ \widehat{F}_{21}\Omega^{-1}_{3i}A^{21}_{i3},\ \widehat{F}_{22}\Omega^{-1}_{3i}A^{21}_{i3},\ \widehat{F}_{23}\Omega^{-1}_{3i}A^{21}_{i3},\ 0)^{\mathrm{T}},\\
\mathbf{r}_6 =\ & (0,\ 0,\ 0,\ \widehat{F}_{21}\Omega^{-1}_{1i}A^{22}_{i1},\ \widehat{F}_{22}\Omega^{-1}_{1i}A^{22}_{i1},\ \widehat{F}_{23}\Omega^{-1}_{1i}A^{22}_{i1},\ \widehat{F}_{21}\Omega^{-1}_{2i}A^{22}_{i1} - 1\\
& \widehat{F}_{22}\Omega^{-1}_{2i}A^{22}_{i1},\ \widehat{F}_{23}\Omega^{-1}_{2i}A^{22}_{i1},\ \widehat{F}_{21}\Omega^{-1}_{3i}A^{22}_{i1},\ \widehat{F}_{22}\Omega^{-1}_{3i}A^{22}_{i1},\ \widehat{F}_{23}\Omega^{-1}_{3i}A^{22}_{i1},\ 0)^{\mathrm{T}},\\
\mathbf{r}_7 =\ & (0,\ 0,\ 0,\ \widehat{F}_{21}\Omega^{-1}_{1i}A^{22}_{i3},\ \widehat{F}_{22}\Omega^{-1}_{1i}A^{22}_{i3},\ \widehat{F}_{23}\Omega^{-1}_{1i}A^{22}_{i3},\ \widehat{F}_{21}\Omega^{-1}_{2i}A^{22}_{i3}\\
& \widehat{F}_{22}\Omega^{-1}_{2i}A^{22}_{i3},\ \widehat{F}_{23}\Omega^{-1}_{2i}A^{22}_{i3} - 1,\ \widehat{F}_{21}\Omega^{-1}_{3i}A^{22}_{i3},\ \widehat{F}_{22}\Omega^{-1}_{3i}A^{22}_{i3},\ \widehat{F}_{23}\Omega^{-1}_{3i}A^{22}_{i3},\ 0)^{\mathrm{T}},\\
\mathbf{r}_8 =\ & (0,\ 0,\ 0,\ \widehat{F}_{21}\Omega^{-1}_{1i}A^{23}_{i1},\ \widehat{F}_{22}\Omega^{-1}_{1i}A^{23}_{i1},\ \widehat{F}_{23}\Omega^{-1}_{1i}A^{23}_{i1},\ \widehat{F}_{21}\Omega^{-1}_{2i}A^{23}_{i1}\\
& \widehat{F}_{22}\Omega^{-1}_{2i}A^{23}_{i1},\ \widehat{F}_{23}\Omega^{-1}_{2i}A^{23}_{i1},\ \widehat{F}_{21}\Omega^{-1}_{3i}A^{23}_{i1} - 1,\ \widehat{F}_{22}\Omega^{-1}_{3i}A^{23}_{i1},\ \widehat{F}_{23}\Omega^{-1}_{3i}A^{23}_{i1},\ 0)^{\mathrm{T}},\\
\mathbf{r}_9 =\ & (0,\ 0,\ 0,\ \widehat{F}_{21}\Omega^{-1}_{1i}A^{23}_{i3},\ \widehat{F}_{22}\Omega^{-1}_{1i}A^{23}_{i3},\ \widehat{F}_{23}\Omega^{-1}_{1i}A^{23}_{i3},\ \widehat{F}_{21}\Omega^{-1}_{2i}A^{23}_{i3}\\
& \widehat{F}_{22}\Omega^{-1}_{2i}A^{23}_{i3},\ \widehat{F}_{23}\Omega^{-1}_{2i}A^{23}_{i3},\ \widehat{F}_{21}\Omega^{-1}_{3i}A^{23}_{i3},\ \widehat{F}_{22}\Omega^{-1}_{3i}A^{23}_{i3},\ \widehat{F}_{23}\Omega^{-1}_{3i}A^{23}_{i3} - 1,\ 0)^{\mathrm{T}},
\end{aligned}
$$

$$
\begin{aligned}
\mathbf{r}_{10} = \; & (0,\, 0,\, 0,\, -\widehat{F}_{21}\Omega_{1i}^{-1}B_i^2,\, -\widehat{F}_{22}\Omega_{1i}^{-1}B_i^2,\, -\widehat{F}_{23}\Omega_{1i}^{-1}B_i^2,\, -\widehat{F}_{21}\Omega_{2i}^{-1}B_i^2 \\
& -\widehat{F}_{22}\Omega_{2i}^{-1}B_i^2,\, -\widehat{F}_{23}\Omega_{2i}^{-1}B_i^2,\, -\widehat{F}_{21}\Omega_{3i}^{-1}B_i^2,\, -\widehat{F}_{22}\Omega_{3i}^{-1}B_i^2,\, -\widehat{F}_{23}\Omega_{3i}^{-1}B_i^2,\, 1)^{\mathrm{T}}, \\
\mathbf{r}_{11} = \; & \tfrac{1}{2}((\mathscr{D}\mathbf{Q})_{13}^{-1},\, (\mathscr{D}\mathbf{Q})_{23}^{-1},\, (\mathscr{D}\mathbf{Q})_{33}^{-1},\, -\widehat{F}_{21}(\mathscr{D}^2\mathbf{Q})_{13}^{-1},\, -\widehat{F}_{22}(\mathscr{D}^2\mathbf{Q})_{13}^{-1}, \\
& -\widehat{F}_{23}(\mathscr{D}^2\mathbf{Q})_{13}^{-1},\, -\widehat{F}_{21}(\mathscr{D}^2\mathbf{Q})_{23}^{-1},\, -\widehat{F}_{22}(\mathscr{D}^2\mathbf{Q})_{23}^{-1},\, -\widehat{F}_{23}(\mathscr{D}^2\mathbf{Q})_{23}^{-1}, \\
& -\widehat{F}_{21}(\mathscr{D}^2\mathbf{Q})_{33}^{-1},\, -\widehat{F}_{22}(\mathscr{D}^2\mathbf{Q})_{33}^{-1},\, -\widehat{F}_{23}(\mathscr{D}^2\mathbf{Q})_{33}^{-1},\, 0)^{\mathrm{T}}, \\
\mathbf{r}_{12} = \; & \tfrac{1}{2}((\mathscr{D}\mathbf{Q})_{12}^{-1},\, (\mathscr{D}\mathbf{Q})_{22}^{-1},\, (\mathscr{D}\mathbf{Q})_{32}^{-1},\, -\widehat{F}_{21}(\mathscr{D}^2\mathbf{Q})_{12}^{-1},\, -\widehat{F}_{22}(\mathscr{D}^2\mathbf{Q})_{12}^{-1}, \\
& -\widehat{F}_{23}(\mathscr{D}^2\mathbf{Q})_{12}^{-1},\, -\widehat{F}_{21}(\mathscr{D}^2\mathbf{Q})_{22}^{-1},\, -\widehat{F}_{22}(\mathscr{D}^2\mathbf{Q})_{22}^{-1},\, -\widehat{F}_{23}(\mathscr{D}^2\mathbf{Q})_{22}^{-1}, \\
& -\widehat{F}_{21}(\mathscr{D}^2\mathbf{Q})_{32}^{-1},\, -\widehat{F}_{22}(\mathscr{D}^2\mathbf{Q})_{32}^{-1},\, -\widehat{F}_{23}(\mathscr{D}^2\mathbf{Q})_{32}^{-1},\, 0)^{\mathrm{T}}, \\
\mathbf{r}_{13} = \; & \tfrac{1}{2}((\mathscr{D}\mathbf{Q})_{11}^{-1},\, (\mathscr{D}\mathbf{Q})_{21}^{-1},\, (\mathscr{D}\mathbf{Q})_{31}^{-1},\, -\widehat{F}_{21}(\mathscr{D}^2\mathbf{Q})_{11}^{-1},\, -\widehat{F}_{22}(\mathscr{D}^2\mathbf{Q})_{11}^{-1}, \\
& -\widehat{F}_{23}(\mathscr{D}^2\mathbf{Q})_{11}^{-1},\, -\widehat{F}_{21}(\mathscr{D}^2\mathbf{Q})_{21}^{-1},\, -\widehat{F}_{22}(\mathscr{D}^2\mathbf{Q})_{21}^{-1},\, -\widehat{F}_{23}(\mathscr{D}^2\mathbf{Q})_{21}^{-1}, \\
& -\widehat{F}_{21}(\mathscr{D}^2\mathbf{Q})_{31}^{-1},\, -\widehat{F}_{22}(\mathscr{D}^2\mathbf{Q})_{31}^{-1},\, -\widehat{F}_{23}(\mathscr{D}^2\mathbf{Q})_{31}^{-1},\, 0)^{\mathrm{T}}.
\end{aligned}
$$

D.5 The canonical system in the ξ_3–direction

The non-conservative equations for deformation, Eq. (D.6), in the ξ_3–direction can be combined as follows: for example taking the equations for F_{11} and F_{12} and equating gives

$$
\frac{\widehat{F}_{31}}{\widehat{F}_{11}}\left(\frac{\partial F_{13}}{\partial t}+\overline{u}_3\frac{\partial F_{13}}{\partial \xi_k}\right)-\left(\frac{\partial F_{11}}{\partial t}+\overline{u}_3\frac{\partial F_{11}}{\partial \xi_k}\right)=0. \tag{D.47}
$$

Similarly, from the other equations for deformation the following relations can be found

$$
\frac{\widehat{F}_{32}}{\widehat{F}_{33}}\left(\frac{\partial F_{13}}{\partial t}+\overline{u}_3\frac{\partial F_{13}}{\partial \xi_k}\right)-\left(\frac{\partial F_{12}}{\partial t}+\overline{u}_3\frac{\partial F_{12}}{\partial \xi_k}\right)=0, \tag{D.48}
$$

$$
\frac{\widehat{F}_{12}}{\widehat{F}_{33}}\left(\frac{\partial F_{23}}{\partial t}+\overline{u}_3\frac{\partial F_{23}}{\partial \xi_3}\right)-\left(\frac{\partial F_{21}}{\partial t}+\overline{u}_3\frac{\partial F_{21}}{\partial \xi_3}\right)=0, \tag{D.49}
$$

$$
\frac{\widehat{F}_{31}}{\widehat{F}_{33}}\left(\frac{\partial F_{23}}{\partial t}+\overline{u}_3\frac{\partial F_{23}}{\partial \xi_3}\right)-\left(\frac{\partial F_{22}}{\partial t}+\overline{u}_3\frac{\partial F_{22}}{\partial \xi_3}\right)=0, \tag{D.50}
$$

$$
\frac{\widehat{F}_{32}}{\widehat{F}_{33}}\left(\frac{\partial F_{33}}{\partial t}+\overline{u}_3\frac{\partial F_{33}}{\partial \xi_3}\right)-\left(\frac{\partial F_{31}}{\partial t}+\overline{u}_3\frac{\partial F_{31}}{\partial \xi_3}\right)=0, \tag{D.51}
$$

$$
\frac{\widehat{F}_{31}}{\widehat{F}_{33}}\left(\frac{\partial F_{33}}{\partial t}+\overline{u}_3\frac{\partial F_{33}}{\partial \xi_3}\right)-\left(\frac{\partial F_{32}}{\partial t}+\overline{u}_3\frac{\partial F_{32}}{\partial \xi_3}\right)=0. \tag{D.52}
$$

In matrix form Eqs. (D.47)-(D.52) read as

$$
\boldsymbol{\Upsilon}_3\left(\frac{\partial}{\partial t}+\overline{u}_3\frac{\partial}{\partial \xi_3}\right)\begin{pmatrix}\mathbf{F}^{\mathrm{T}}\mathbf{e}_1\\ \mathbf{F}^{\mathrm{T}}\mathbf{e}_2\\ \mathbf{F}^{\mathrm{T}}\mathbf{e}_3\end{pmatrix}=0, \tag{D.53}
$$

where

$$\boldsymbol{\Upsilon}_3 := \begin{pmatrix} -1 & 0 & \widehat{F}_{31}/\widehat{F}_{33} & 0 & 0 & 0 & 0 & 0 & 0 \\ 0 & -1 & \widehat{F}_{32}/\widehat{F}_{33} & 0 & 0 & 0 & 0 & 0 & 0 \\ 0 & 0 & 0 & -1 & 0 & \widehat{F}_{31}/\widehat{F}_{33} & 0 & 0 & 0 \\ 0 & 0 & 0 & 0 & -1 & \widehat{F}_{32}/\widehat{F}_{33} & 0 & 0 & 0 \\ 0 & 0 & 0 & 0 & 0 & 0 & -1 & 0 & \widehat{F}_{31}/\widehat{F}_{33} \\ 0 & 0 & 0 & 0 & 0 & 0 & 0 & -1 & \widehat{F}_{32}/\widehat{F}_{33} \end{pmatrix} \tag{D.54}$$

Eqs. (D.14),(D.23),(D.24),(D.53) combine to form the following canonical system

$$\mathbf{L}\frac{\partial}{\partial t}\mathbf{W} + \boldsymbol{\Lambda}\mathbf{L}\frac{\partial}{\partial \xi_3}\mathbf{W} = 0 \tag{D.55}$$

with the matrix of left eigenvectors

$$\mathbf{L} = (\mathbf{l}_1,\, \mathbf{l}_2,\, \mathbf{l}_3,\, \mathbf{l}_4,\, \mathbf{l}_5,\, \mathbf{l}_6,\, \mathbf{l}_7,\, \mathbf{l}_8,\, \mathbf{l}_9,\, \mathbf{l}_{10},\, \mathbf{l}_{11},\, \mathbf{l}_{12},\, \mathbf{l}_{13})^{\mathrm{T}}, \tag{D.56}$$

where

$$\begin{aligned}
\mathbf{l}_1 =\ & ((\mathscr{D}\mathbf{Q})_{11},\, (\mathscr{D}\mathbf{Q})_{12},\, (\mathscr{D}\mathbf{Q})_{13},\, Q_{1i}A^{31}_{i1},\, Q_{1i}A^{31}_{i2},\, Q_{1i}A^{31}_{i3},\\
& Q_{1i}A^{32}_{i1},\, Q_{1i}A^{32}_{i2},\, Q_{1i}A^{32}_{i3},\, Q_{1i}A^{33}_{i1},\, Q_{1i}A^{33}_{i2},\, Q_{1i}A^{33}_{i3},\, Q_{1i}B^{3}_{i}),\\
\mathbf{l}_2 =\ & ((\mathscr{D}\mathbf{Q})_{21},\, (\mathscr{D}\mathbf{Q})_{22},\, (\mathscr{D}\mathbf{Q})_{23},\, Q_{2i}A^{31}_{i1},\, Q_{2i}A^{31}_{i2},\, Q_{2i}A^{31}_{i3},\\
& Q_{2i}A^{32}_{i1},\, Q_{2i}A^{32}_{i2},\, Q_{2i}A^{32}_{i3},\, Q_{2i}A^{33}_{i1},\, Q_{2i}A^{33}_{i2},\, Q_{2i}A^{33}_{i3},\, Q_{2i}B^{3}_{i}),\\
\mathbf{l}_3 =\ & ((\mathscr{D}\mathbf{Q})_{31},\, (\mathscr{D}\mathbf{Q})_{32},\, (\mathscr{D}\mathbf{Q})_{33},\, Q_{3i}A^{31}_{i1},\, Q_{3i}A^{31}_{i2},\, Q_{3i}A^{31}_{i3},\\
& Q_{3i}A^{32}_{i1},\, Q_{3i}A^{32}_{i2},\, Q_{3i}A^{32}_{i3},\, Q_{3i}A^{33}_{i1},\, Q_{3i}A^{33}_{i2},\, Q_{3i}A^{33}_{i3},\, Q_{3i}B^{3}_{i}),\\
\mathbf{l}_4 =\ & (0,\, 0,\, 0,\, -1,\, 0,\, \widehat{F}_{31}/\widehat{F}_{33},\, 0,\, 0,\, 0,\, 0,\, 0,\, 0,\, 0),\\
\mathbf{l}_5 =\ & (0,\, 0,\, 0,\, 0,\, -1,\, \widehat{F}_{32}/\widehat{F}_{33},\, 0,\, 0,\, 0,\, 0,\, 0,\, 0,\, 0),\\
\mathbf{l}_6 =\ & (0,\, 0,\, 0,\, 0,\, 0,\, 0,\, -1,\, 0,\, \widehat{F}_{31}/\widehat{F}_{33},\, 0,\, 0,\, 0,\, 0),\\
\mathbf{l}_7 =\ & (0,\, 0,\, 0,\, 0,\, 0,\, 0,\, 0,\, -1,\, \widehat{F}_{32}/\widehat{F}_{33},\, 0,\, 0,\, 0,\, 0),\\
\mathbf{l}_8 =\ & (0,\, 0,\, 0,\, 0,\, 0,\, 0,\, 0,\, 0,\, 0,\, -1,\, 0,\, \widehat{F}_{31}/\widehat{F}_{33},\, 0),\\
\mathbf{l}_9 =\ & (0,\, 0,\, 0,\, 0,\, 0,\, 0,\, 0,\, 0,\, 0,\, 0,\, -1,\, \widehat{F}_{32}/\widehat{F}_{33},\, 0),\\
\mathbf{l}_{10} =\ & (0,\, 0,\, 0,\, 0,\, 0,\, 0,\, 0,\, 0,\, 0,\, 0,\, 0,\, 0,\, 1),\\
\mathbf{l}_{11} =\ & ((\mathscr{D}\mathbf{Q})_{31},\, (\mathscr{D}\mathbf{Q})_{32},\, (\mathscr{D}\mathbf{Q})_{33},\, -Q_{3i}A^{31}_{i1},\, -Q_{3i}A^{31}_{i2},\, -Q_{3i}A^{31}_{i3},\\
& -Q_{3i}A^{32}_{i1},\, -Q_{3i}A^{32}_{i2},\, -Q_{3i}A^{32}_{i3},\, -Q_{3i}A^{33}_{i1},\, -Q_{3i}A^{33}_{i2},\, -Q_{3i}A^{33}_{i3},\, -Q_{3i}B^{3}_{i}),\\
\mathbf{l}_{12} =\ & ((\mathscr{D}\mathbf{Q})_{21},\, (\mathscr{D}\mathbf{Q})_{22},\, (\mathscr{D}\mathbf{Q})_{23},\, -Q_{2i}A^{31}_{i1},\, -Q_{2i}A^{31}_{i2},\, -Q_{2i}A^{31}_{i3},\\
& -Q_{2i}A^{32}_{i1},\, -Q_{2i}A^{32}_{i2},\, -Q_{2i}A^{32}_{i3},\, -Q_{2i}A^{33}_{i1},\, -Q_{2i}A^{33}_{i2},\, -Q_{2i}A^{33}_{i3},\, -Q_{2i}B^{3}_{i}),\\
\mathbf{l}_{13} =\ & ((\mathscr{D}\mathbf{Q})_{11},\, (\mathscr{D}\mathbf{Q})_{12},\, (\mathscr{D}\mathbf{Q})_{13},\, -Q_{1i}A^{31}_{i1},\, -Q_{1i}A^{31}_{i2},\, -Q_{1i}A^{31}_{i3},\\
& -Q_{1i}A^{32}_{i1},\, -Q_{1i}A^{32}_{i2},\, -Q_{1i}A^{32}_{i3},\, -Q_{1i}A^{33}_{i1},\, -Q_{1i}A^{33}_{i2},\, -Q_{1i}A^{33}_{i3},\, -Q_{1i}B^{3}_{i}).
\end{aligned}$$

Using the assumption that the right eigenvectors are orthonormal to the left ($\mathbf{RL} = \mathbf{I}$)

$$\mathbf{R} = (\mathbf{r}_1,\ \mathbf{r}_2,\ \mathbf{r}_3,\ \mathbf{r}_4,\ \mathbf{r}_5,\ \mathbf{r}_6,\ \mathbf{r}_7,\ \mathbf{r}_8,\ \mathbf{r}_9,\ \mathbf{r}_{10},\ \mathbf{r}_{11},\ \mathbf{r}_{12},\ \mathbf{r}_{13}), \tag{D.57}$$

where

$$\begin{aligned}
\mathbf{r}_1 = {} & \tfrac{1}{2}((\mathscr{D}\mathbf{Q})_{11}^{-1},\ (\mathscr{D}\mathbf{Q})_{21}^{-1},\ (\mathscr{D}\mathbf{Q})_{31}^{-1},\ \widehat{F}_{31}(\mathscr{D}^2\mathbf{Q})_{11}^{-1},\ \widehat{F}_{32}(\mathscr{D}^2\mathbf{Q})_{11}^{-1},\\
& \widehat{F}_{33}(\mathscr{D}^2\mathbf{Q})_{11}^{-1},\ \widehat{F}_{31}(\mathscr{D}^2\mathbf{Q})_{21}^{-1},\ \widehat{F}_{32}(\mathscr{D}^2\mathbf{Q})_{21}^{-1},\ \widehat{F}_{33}(\mathscr{D}^2\mathbf{Q})_{21}^{-1},\\
& \widehat{F}_{31}(\mathscr{D}^2\mathbf{Q})_{31}^{-1},\ \widehat{F}_{32}(\mathscr{D}^2\mathbf{Q})_{31}^{-1},\ \widehat{F}_{33}(\mathscr{D}^2\mathbf{Q})_{31}^{-1},\ 0)^{\mathrm{T}},\\
\mathbf{r}_2 = {} & \tfrac{1}{2}((\mathscr{D}\mathbf{Q})_{12}^{-1},\ (\mathscr{D}\mathbf{Q})_{22}^{-1},\ (\mathscr{D}\mathbf{Q})_{32}^{-1},\ \widehat{F}_{31}(\mathscr{D}^2\mathbf{Q})_{12}^{-1},\ \widehat{F}_{32}(\mathscr{D}^2\mathbf{Q})_{12}^{-1},\\
& \widehat{F}_{33}(\mathscr{D}^2\mathbf{Q})_{12}^{-1},\ \widehat{F}_{31}(\mathscr{D}^2\mathbf{Q})_{22}^{-1},\ \widehat{F}_{32}(\mathscr{D}^2\mathbf{Q})_{22}^{-1},\ \widehat{F}_{33}(\mathscr{D}^2\mathbf{Q})_{22}^{-1},\\
& \widehat{F}_{31}(\mathscr{D}^2\mathbf{Q})_{32}^{-1},\ \widehat{F}_{32}(\mathscr{D}^2\mathbf{Q})_{32}^{-1},\ \widehat{F}_{33}(\mathscr{D}^2\mathbf{Q})_{32}^{-1},\ 0)^{\mathrm{T}},\\
\mathbf{r}_3 = {} & \tfrac{1}{2}((\mathscr{D}\mathbf{Q})_{13}^{-1},\ (\mathscr{D}\mathbf{Q})_{23}^{-1},\ (\mathscr{D}\mathbf{Q})_{33}^{-1},\ \widehat{F}_{31}(\mathscr{D}^2\mathbf{Q})_{13}^{-1},\ \widehat{F}_{32}(\mathscr{D}^2\mathbf{Q})_{13}^{-1},\\
& \widehat{F}_{33}(\mathscr{D}^2\mathbf{Q})_{13}^{-1},\ \widehat{F}_{31}(\mathscr{D}^2\mathbf{Q})_{23}^{-1},\ \widehat{F}_{32}(\mathscr{D}^2\mathbf{Q})_{23}^{-1},\ \widehat{F}_{33}(\mathscr{D}^2\mathbf{Q})_{23}^{-1},\\
& \widehat{F}_{31}(\mathscr{D}^2\mathbf{Q})_{33}^{-1},\ \widehat{F}_{32}(\mathscr{D}^2\mathbf{Q})_{33}^{-1},\ \widehat{F}_{33}(\mathscr{D}^2\mathbf{Q})_{33}^{-1},\ 0)^{\mathrm{T}},\\
\mathbf{r}_4 = {} & (0,\ 0,\ 0,\ \widehat{F}_{31}\Omega_{1i}^{-1}A_{i1}^{31} - 1,\ \widehat{F}_{32}\Omega_{1i}^{-1}A_{i1}^{31},\ \widehat{F}_{33}\Omega_{1i}^{-1}A_{i1}^{31},\ \widehat{F}_{31}\Omega_{2i}^{-1}A_{i1}^{31}\\
& \widehat{F}_{32}\Omega_{2i}^{-1}A_{i1}^{31},\ \widehat{F}_{33}\Omega_{2i}^{-1}A_{i1}^{31},\ \widehat{F}_{31}\Omega_{3i}^{-1}A_{i1}^{31},\ \widehat{F}_{32}\Omega_{3i}^{-1}A_{i1}^{31},\ \widehat{F}_{33}\Omega_{3i}^{-1}A_{i1}^{31},\ 0)^{\mathrm{T}},\\
\mathbf{r}_5 = {} & (0,\ 0,\ 0,\ \widehat{F}_{31}\Omega_{1i}^{-1}A_{i2}^{31},\ \widehat{F}_{32}\Omega_{1i}^{-1}A_{i2}^{31} - 1,\ \widehat{F}_{33}\Omega_{1i}^{-1}A_{i2}^{31},\ \widehat{F}_{31}\Omega_{2i}^{-1}A_{i2}^{31}\\
& \widehat{F}_{32}\Omega_{2i}^{-1}A_{i2}^{31},\ \widehat{F}_{33}\Omega_{2i}^{-1}A_{i2}^{31},\ \widehat{F}_{31}\Omega_{3i}^{-1}A_{i2}^{31},\ \widehat{F}_{32}\Omega_{3i}^{-1}A_{i2}^{31},\ \widehat{F}_{33}\Omega_{3i}^{-1}A_{i2}^{31},\ 0)^{\mathrm{T}},\\
\mathbf{r}_6 = {} & (0,\ 0,\ 0,\ \widehat{F}_{31}\Omega_{1i}^{-1}A_{i1}^{32},\ \widehat{F}_{32}\Omega_{1i}^{-1}A_{i1}^{32},\ \widehat{F}_{33}\Omega_{1i}^{-1}A_{i1}^{32},\ \widehat{F}_{31}\Omega_{2i}^{-1}A_{i1}^{32} - 1\\
& \widehat{F}_{32}\Omega_{2i}^{-1}A_{i1}^{32},\ \widehat{F}_{33}\Omega_{2i}^{-1}A_{i1}^{32},\ \widehat{F}_{31}\Omega_{3i}^{-1}A_{i1}^{32},\ \widehat{F}_{32}\Omega_{3i}^{-1}A_{i1}^{32},\ \widehat{F}_{33}\Omega_{3i}^{-1}A_{i1}^{32},\ 0)^{\mathrm{T}},\\
\mathbf{r}_7 = {} & (0,\ 0,\ 0,\ \widehat{F}_{31}\Omega_{1i}^{-1}A_{i2}^{32},\ \widehat{F}_{32}\Omega_{1i}^{-1}A_{i2}^{32},\ \widehat{F}_{33}\Omega_{1i}^{-1}A_{i2}^{32},\ \widehat{F}_{31}\Omega_{2i}^{-1}A_{i2}^{32}\\
& \widehat{F}_{32}\Omega_{2i}^{-1}A_{i2}^{32} - 1,\ \widehat{F}_{33}\Omega_{2i}^{-1}A_{i2}^{32},\ \widehat{F}_{31}\Omega_{3i}^{-1}A_{i2}^{32},\ \widehat{F}_{32}\Omega_{3i}^{-1}A_{i2}^{32},\ \widehat{F}_{33}\Omega_{3i}^{-1}A_{i2}^{32},\ 0)^{\mathrm{T}},\\
\mathbf{r}_8 = {} & (0,\ 0,\ 0,\ \widehat{F}_{31}\Omega_{1i}^{-1}A_{i1}^{33},\ \widehat{F}_{32}\Omega_{1i}^{-1}A_{i1}^{33},\ \widehat{F}_{33}\Omega_{1i}^{-1}A_{i1}^{33},\ \widehat{F}_{31}\Omega_{2i}^{-1}A_{i1}^{33}\\
& \widehat{F}_{32}\Omega_{2i}^{-1}A_{i1}^{33},\ \widehat{F}_{33}\Omega_{2i}^{-1}A_{i1}^{33},\ \widehat{F}_{31}\Omega_{3i}^{-1}A_{i1}^{33} - 1,\ \widehat{F}_{32}\Omega_{3i}^{-1}A_{i1}^{33},\ \widehat{F}_{33}\Omega_{3i}^{-1}A_{i1}^{33},\ 0)^{\mathrm{T}},\\
\mathbf{r}_9 = {} & (0,\ 0,\ 0,\ \widehat{F}_{31}\Omega_{1i}^{-1}A_{i2}^{33},\ \widehat{F}_{32}\Omega_{1i}^{-1}A_{i2}^{33},\ \widehat{F}_{33}\Omega_{1i}^{-1}A_{i2}^{33},\ \widehat{F}_{31}\Omega_{2i}^{-1}A_{i2}^{33}\\
& \widehat{F}_{32}\Omega_{2i}^{-1}A_{i2}^{33},\ \widehat{F}_{33}\Omega_{2i}^{-1}A_{i2}^{33},\ \widehat{F}_{31}\Omega_{3i}^{-1}A_{i2}^{33},\ \widehat{F}_{32}\Omega_{3i}^{-1}A_{i2}^{33} - 1,\ \widehat{F}_{33}\Omega_{3i}^{-1}A_{i2}^{33},\ 0)^{\mathrm{T}},\\
\mathbf{r}_{10} = {} & (0,\ 0,\ 0,\ -\widehat{F}_{31}\Omega_{1i}^{-1}B_i^3,\ -\widehat{F}_{32}\Omega_{1i}^{-1}B_i^3,\ -\widehat{F}_{33}\Omega_{1i}^{-1}B_i^3,\ -\widehat{F}_{31}\Omega_{2i}^{-1}B_i^3\\
& -\widehat{F}_{32}\Omega_{2i}^{-1}B_i^3,\ -\widehat{F}_{33}\Omega_{2i}^{-1}B_i^3,\ -\widehat{F}_{31}\Omega_{3i}^{-1}B_i^3,\ -\widehat{F}_{32}\Omega_{3i}^{-1}B_i^3,\ -\widehat{F}_{33}\Omega_{3i}^{-1}B_i^3,\ 1)^{\mathrm{T}},\\
\mathbf{r}_{11} = {} & \tfrac{1}{2}((\mathscr{D}\mathbf{Q})_{13}^{-1},\ (\mathscr{D}\mathbf{Q})_{23}^{-1},\ (\mathscr{D}\mathbf{Q})_{33}^{-1},\ -\widehat{F}_{31}(\mathscr{D}^2\mathbf{Q})_{13}^{-1},\ -\widehat{F}_{32}(\mathscr{D}^2\mathbf{Q})_{13}^{-1},\\
& -\widehat{F}_{33}(\mathscr{D}^2\mathbf{Q})_{13}^{-1},\ -\widehat{F}_{31}(\mathscr{D}^2\mathbf{Q})_{23}^{-1},\ -\widehat{F}_{32}(\mathscr{D}^2\mathbf{Q})_{23}^{-1},\ -\widehat{F}_{33}(\mathscr{D}^2\mathbf{Q})_{23}^{-1},\\
& -\widehat{F}_{31}(\mathscr{D}^2\mathbf{Q})_{33}^{-1},\ -\widehat{F}_{32}(\mathscr{D}^2\mathbf{Q})_{33}^{-1},\ -\widehat{F}_{33}(\mathscr{D}^2\mathbf{Q})_{33}^{-1},\ 0)^{\mathrm{T}},\\
\mathbf{r}_{12} = {} & \tfrac{1}{2}((\mathscr{D}\mathbf{Q})_{12}^{-1},\ (\mathscr{D}\mathbf{Q})_{22}^{-1},\ (\mathscr{D}\mathbf{Q})_{32}^{-1},\ -\widehat{F}_{31}(\mathscr{D}^2\mathbf{Q})_{12}^{-1},\ -\widehat{F}_{32}(\mathscr{D}^2\mathbf{Q})_{12}^{-1},\\
& -\widehat{F}_{33}(\mathscr{D}^2\mathbf{Q})_{12}^{-1},\ -\widehat{F}_{31}(\mathscr{D}^2\mathbf{Q})_{22}^{-1},\ -\widehat{F}_{32}(\mathscr{D}^2\mathbf{Q})_{22}^{-1},\ -\widehat{F}_{33}(\mathscr{D}^2\mathbf{Q})_{22}^{-1},\\
& -\widehat{F}_{31}(\mathscr{D}^2\mathbf{Q})_{32}^{-1},\ -\widehat{F}_{32}(\mathscr{D}^2\mathbf{Q})_{32}^{-1},\ -\widehat{F}_{33}(\mathscr{D}^2\mathbf{Q})_{32}^{-1},\ 0)^{\mathrm{T}},
\end{aligned}$$

$$\begin{aligned}\mathbf{r}_{13} = \; & \tfrac{1}{2}((\mathscr{D}\mathbf{Q})_{11}^{-1},\ (\mathscr{D}\mathbf{Q})_{21}^{-1},\ (\mathscr{D}\mathbf{Q})_{31}^{-1},\ -\widehat{F}_{31}(\mathscr{D}^2\mathbf{Q})_{11}^{-1},\ -\widehat{F}_{32}(\mathscr{D}^2\mathbf{Q})_{11}^{-1},\\ & -\widehat{F}_{33}(\mathscr{D}^2\mathbf{Q})_{11}^{-1},\ -\widehat{F}_{31}(\mathscr{D}^2\mathbf{Q})_{21}^{-1},\ -\widehat{F}_{32}(\mathscr{D}^2\mathbf{Q})_{21}^{-1},\ -\widehat{F}_{33}(\mathscr{D}^2\mathbf{Q})_{21}^{-1},\\ & -\widehat{F}_{31}(\mathscr{D}^2\mathbf{Q})_{31}^{-1},\ -\widehat{F}_{32}(\mathscr{D}^2\mathbf{Q})_{31}^{-1},\ -\widehat{F}_{33}(\mathscr{D}^2\mathbf{Q})_{31}^{-1},\ 0)^{\mathrm{T}}.\end{aligned}$$

E

Characteristic based Riemann solver

The Riemann solver based upon characteristic variables involves large complex matrices, including those consisting of the eigenfunctions, and those associated with transformations between partial derivatives of conserved variables and partial derivatives of primitive variables. Whilst it is straightforward to construct each of these matrices separately and subsequently apply matrix/vector multiplication to arrive at the Riemann problem solution, it is intuitive to derive in greater detail the approximate solution and finally present explicit expressions for the solution vector of conserved variables $\widetilde{\mathbf{U}}$.

In the first instance an approximate solution to the Riemann problem can be derived in terms of primitive variables. Start by considering the characteristic variables:

$$
\begin{aligned}
\widetilde{\mathscr{Q}_1} =& Q_{11}\mathfrak{Q}_1^{(1)} + Q_{12}\mathfrak{Q}_2^{(1)} + Q_{13}\mathfrak{Q}_3^{(1)} + \sqrt{\lambda_{\mathrm{ac}_1}}\left(Q_{11}u_1^{(1)} + Q_{12}u_2^{(1)} + Q_{13}u_3^{(1)}\right),\\
\widetilde{\mathscr{Q}_2} =& Q_{21}\mathfrak{Q}_1^{(2)} + Q_{22}\mathfrak{Q}_2^{(2)} + Q_{23}\mathfrak{Q}_3^{(2)} + \sqrt{\lambda_{\mathrm{ac}_2}}\left(Q_{21}u_1^{(2)} + Q_{22}u_2^{(2)} + Q_{23}u_3^{(2)}\right),\\
\widetilde{\mathscr{Q}_3} =& Q_{31}\mathfrak{Q}_1^{(3)} + Q_{32}\mathfrak{Q}_2^{(3)} + Q_{33}\mathfrak{Q}_3^{(3)} + \sqrt{\lambda_{\mathrm{ac}_3}}\left(Q_{31}u_1^{(3)} + Q_{32}u_2^{(3)} + Q_{33}u_3^{(3)}\right),\\
\widetilde{\mathscr{Q}_4} =& -Q_{11}\mathfrak{Q}_1^{(4)} - Q_{12}\mathfrak{Q}_2^{(4)} - Q_{13}\mathfrak{Q}_3^{(4)} + \sqrt{\lambda_{\mathrm{ac}_1}}\left(Q_{11}u_1^{(4)} + Q_{12}u_2^{(4)} + Q_{13}u_3^{(4)}\right),\\
\widetilde{\mathscr{Q}_5} =& -Q_{21}\mathfrak{Q}_1^{(5)} - Q_{22}\mathfrak{Q}_2^{(5)} - Q_{23}\mathfrak{Q}_3^{(5)} + \sqrt{\lambda_{\mathrm{ac}_2}}\left(Q_{21}u_1^{(5)} + Q_{22}u_2^{(5)} + Q_{23}u_3^{(5)}\right),\\
\widetilde{\mathscr{Q}_6} =& -Q_{31}\mathfrak{Q}_1^{(6)} - Q_{32}\mathfrak{Q}_2^{(6)} - Q_{33}\mathfrak{Q}_3^{(6)} + \sqrt{\lambda_{\mathrm{ac}_3}}\left(Q_{31}u_1^{(6)} + Q_{32}u_2^{(6)} + Q_{33}u_3^{(6)}\right),\\
\widetilde{\mathscr{Q}_7} =& \frac{\mathfrak{F}_2}{\mathfrak{F}_1}F_{11}^{(7)} - F_{12}^{(7)},\\
\widetilde{\mathscr{Q}_8} =& \frac{\mathfrak{F}_3}{\mathfrak{F}_1}F_{11}^{(8)} - F_{13}^{(8)},\\
\widetilde{\mathscr{Q}_9} =& \frac{\mathfrak{F}_2}{\mathfrak{F}_1}F_{21}^{(9)} - F_{22}^{(9)},\\
\widetilde{\mathscr{Q}_{10}} =& \frac{\mathfrak{F}_3}{\mathfrak{F}_1}F_{21}^{(10)} - F_{23}^{(10)},\\
\widetilde{\mathscr{Q}_{11}} =& \frac{\mathfrak{F}_2}{\mathfrak{F}_1}F_{31}^{(11)} - F_{32}^{(11)},
\end{aligned}
$$

$$
\begin{aligned}
\widetilde{\mathscr{Q}_{12}} =& \frac{\mathfrak{F}_3}{\mathfrak{F}_1} F_{31}^{(12)} - F_{33}^{(12)}, \\
\widetilde{\mathscr{Q}_{13}} =& \mathscr{S}^{(13)},
\end{aligned} \tag{E.1}
$$

with

$$
\mathfrak{Q}_i^{(\cdot)} := \sum_{j,k=1}^{3} A_{ik}^{1j} F_{jk}^{(\cdot)} + b_i^1 \mathscr{S}^{(\cdot)}, \tag{E.2}
$$

$$
\mathfrak{F}_i := F_{ji} \widetilde{x}_j^1, \qquad \widetilde{x}_j^1 = \frac{(\partial \xi_1 / \partial x_j)}{\sqrt{(\partial \xi_1/\partial x_1)^2 + (\partial \xi_1/\partial x_2)^2 + (\partial \xi_1/\partial x_3)^2}}. \tag{E.3}
$$

In Eq. (E.1) those variables defined in the form $\phi^{(j)}$ denote state variables evaluated either on the left or right of the boundary, the choice of which being determined by the direction of the wave number j. All other variables are assumed to be evaluated from the averaged values across the cell boundary [cf. § 2.5.1].

Remark: Alternatively one might choose to reconstruct the primitive or conserved variables, in which case the variables $\phi^{(j)}$ would be computed using the left or right reconstructed data, as opposed to the left or right cell centred data of adjoining cells. If on the other hand one is reconstructing the characteristic variables, then $\widetilde{\mathscr{Q}}$ is computed for each cell in the stencil with the variables $\phi^{(j)}$ in each case taken to be the cell centred data for that cell. The Riemann problem solution is then found by taking from the left and right reconstructed characteristic variables the one corresponding to the individual wave directions.

To complete the solution it is assumed that using any of the above described methods one now has a single vector of characteristic variables. One need only then multiply through by the right eigenvectors to obtain explicit expressions for an approximate solution of the Riemann problem:

$$
\begin{aligned}
\widetilde{u_1} =& (\mathscr{D}\mathbf{Q})_{11}^{-1}(\widetilde{\mathscr{Q}_1} + \widetilde{\mathscr{Q}_4}) + (\mathscr{D}\mathbf{Q})_{12}^{-1}(\widetilde{\mathscr{Q}_2} + \widetilde{\mathscr{Q}_5}) + (\mathscr{D}\mathbf{Q})_{13}^{-1}(\widetilde{\mathscr{Q}_3} + \widetilde{\mathscr{Q}_6}), \\
\widetilde{u_2} =& (\mathscr{D}\mathbf{Q})_{21}^{-1}(\widetilde{\mathscr{Q}_1} + \widetilde{\mathscr{Q}_4}) + (\mathscr{D}\mathbf{Q})_{22}^{-1}(\widetilde{\mathscr{Q}_2} + \widetilde{\mathscr{Q}_5}) + (\mathscr{D}\mathbf{Q})_{23}^{-1}(\widetilde{\mathscr{Q}_3} + \widetilde{\mathscr{Q}_6}), \\
\widetilde{u_3} =& (\mathscr{D}\mathbf{Q})_{31}^{-1}(\widetilde{\mathscr{Q}_1} + \widetilde{\mathscr{Q}_4}) + (\mathscr{D}\mathbf{Q})_{32}^{-1}(\widetilde{\mathscr{Q}_2} + \widetilde{\mathscr{Q}_5}) + (\mathscr{D}\mathbf{Q})_{33}^{-1}(\widetilde{\mathscr{Q}_3} + \widetilde{\mathscr{Q}_6}), \\
\widetilde{F_{11}} =& \mathcal{F}_1 \mathcal{R}_1, \\
\widetilde{F_{12}} =& \mathcal{F}_2 \mathcal{R}_1 - \widetilde{\mathscr{Q}_7}, \\
\widetilde{F_{13}} =& \mathcal{F}_3 \mathcal{R}_1 - \widetilde{\mathscr{Q}_8}, \\
\widetilde{F_{21}} =& \mathcal{F}_1 \mathcal{R}_2, \\
\widetilde{F_{22}} =& \mathcal{F}_2 \mathcal{R}_2 - \widetilde{\mathscr{Q}_9}, \\
\widetilde{F_{23}} =& \mathcal{F}_3 \mathcal{R}_2 - \widetilde{\mathscr{Q}_{10}},
\end{aligned}
$$

$$
\begin{aligned}
\widetilde{F_{31}} =& \mathcal{F}_1\mathcal{R}_3, \\
\widetilde{F_{32}} =& \mathcal{F}_2\mathcal{R}_3 - \widetilde{\mathscr{Q}_{11}}, \\
\widetilde{F_{33}} =& \mathcal{F}_3\mathcal{R}_3 - \widetilde{\mathscr{Q}_{12}}, \\
\widetilde{\mathscr{S}} =& \widetilde{\mathscr{Q}_{13}},
\end{aligned} \tag{E.4}
$$

where

$$
\begin{aligned}
\mathcal{R}_1 :=& \frac{1}{2}\left[(\mathscr{D}^2\mathbf{Q})^{-1}_{11}(\widetilde{\mathscr{Q}_1} - \widetilde{\mathscr{Q}_4}) + (\mathscr{D}^2\mathbf{Q})^{-1}_{12}(\widetilde{\mathscr{Q}_2} - \widetilde{\mathscr{Q}_5}) + (\mathscr{D}^2\mathbf{Q})^{-1}_{13}(\widetilde{\mathscr{Q}_3} - \widetilde{\mathscr{Q}_6})\right] + \\
& \mathfrak{R}^1_{11}\widetilde{\mathscr{Q}_7} + \mathfrak{R}^2_{11}\widetilde{\mathscr{Q}_8} + \mathfrak{R}^1_{12}\widetilde{\mathscr{Q}_9} + \mathfrak{R}^2_{12}\widetilde{\mathscr{Q}_{10}} + \mathfrak{R}^1_{13}\widetilde{\mathscr{Q}_{11}} + \mathfrak{R}^2_{13}\widetilde{\mathscr{Q}_{12}} - \mathfrak{R}^3_1\widetilde{\mathscr{Q}_{13}}, \\
\mathcal{R}_2 :=& \frac{1}{2}\left[(\mathscr{D}^2\mathbf{Q})^{-1}_{21}(\widetilde{\mathscr{Q}_1} - \widetilde{\mathscr{Q}_4}) + (\mathscr{D}^2\mathbf{Q})^{-1}_{22}(\widetilde{\mathscr{Q}_2} - \widetilde{\mathscr{Q}_5}) + (\mathscr{D}^2\mathbf{Q})^{-1}_{23}(\widetilde{\mathscr{Q}_3} - \widetilde{\mathscr{Q}_6})\right] + \\
& \mathfrak{R}^1_{21}\widetilde{\mathscr{Q}_7} + \mathfrak{R}^2_{21}\widetilde{\mathscr{Q}_8} + \mathfrak{R}^1_{22}\widetilde{\mathscr{Q}_9} + \mathfrak{R}^2_{22}\widetilde{\mathscr{Q}_{10}} + \mathfrak{R}^1_{23}\widetilde{\mathscr{Q}_{11}} + \mathfrak{R}^2_{23}\widetilde{\mathscr{Q}_{12}} - \mathfrak{R}^3_2\widetilde{\mathscr{Q}_{13}}, \\
\mathcal{R}_3 :=& \frac{1}{2}\left[(\mathscr{D}^2\mathbf{Q})^{-1}_{31}(\widetilde{\mathscr{Q}_1} - \widetilde{\mathscr{Q}_4}) + (\mathscr{D}^2\mathbf{Q})^{-1}_{32}(\widetilde{\mathscr{Q}_2} - \widetilde{\mathscr{Q}_5}) + (\mathscr{D}^2\mathbf{Q})^{-1}_{33}(\widetilde{\mathscr{Q}_3} - \widetilde{\mathscr{Q}_6})\right] + \\
& \mathfrak{R}^1_{31}\widetilde{\mathscr{Q}_7} + \mathfrak{R}^2_{31}\widetilde{\mathscr{Q}_8} + \mathfrak{R}^1_{32}\widetilde{\mathscr{Q}_9} + \mathfrak{R}^2_{32}\widetilde{\mathscr{Q}_{10}} + \mathfrak{R}^1_{33}\widetilde{\mathscr{Q}_{11}} + \mathfrak{R}^2_{33}\widetilde{\mathscr{Q}_{12}} - \mathfrak{R}^3_3\widetilde{\mathscr{Q}_{13}},
\end{aligned} \tag{E.5}
$$

and

$$
\begin{aligned}
\mathfrak{R}^1_{ij} &:= \Omega^{-1}_{i1}A^{1j}_{12} + \Omega^{-1}_{i2}A^{1j}_{22} + \Omega^{-1}_{i3}A^{1j}_{32}, \\
\mathfrak{R}^2_{ij} &:= \Omega^{-1}_{i1}A^{1j}_{13} + \Omega^{-1}_{i2}A^{1j}_{23} + \Omega^{-1}_{i3}A^{1j}_{33}, \\
\mathfrak{R}^3_i &:= \Omega^{-1}_{i1}b^1_1 + \Omega^{-1}_{i2}b^1_2 + \Omega^{-1}_{i3}b^1_3.
\end{aligned} \tag{E.6}
$$

Using the above solution in terms of primitive variables it is relatively straightforward to adapt the solution to be expressed in terms of, and for, the vector of conserved variables. In Eq. (E.1) those variables denoted $\phi^{(j)}$ are taken to be auxiliary variables with the following definitions:

$$
u^{(\cdot)}_i = (\rho\mathbf{u})^{(\cdot)}_i - u_i\hat{\rho}, \tag{E.7}
$$

$$
F^{(\cdot)}_{ij} = (\rho\mathbf{F})^{(\cdot)}_{ij} - F_{ij}\hat{\rho}, \tag{E.8}
$$

$$
\begin{aligned}
\mathscr{S}^{(\cdot)} =& \frac{\mathrm{d}\mathscr{S}}{\mathrm{d}\mathscr{E}}\left[(\rho E)^{(\cdot)} - \left(u_1(\rho\mathbf{u})^{(\cdot)}_1 + u_2(\rho\mathbf{u})^{(\cdot)}_2 + u_3(\rho\mathbf{u})^{(\cdot)}_3\right) + |\mathbf{u}|/2 - \mathscr{E}\right] + \\
& \sum_{i,j=1}^{3}\frac{\mathrm{d}\mathscr{S}}{\mathrm{d}F_{ij}}\left((\rho\mathbf{F})^{(\cdot)}_{ij} - F_{ij}\hat{\rho}\right),
\end{aligned} \tag{E.9}
$$

where

$$
\hat{\rho} := \frac{1}{2}\sum_{i,j=1}^{3} F^{-\mathrm{T}}_{ij}(\rho\mathbf{F})^{(\cdot)}_{ij}, \tag{E.10}
$$

and for clarity the characteristic variables shall now be denoted $\overline{\mathscr{Q}} = \mathscr{Q}(\mathbf{U}^{(\cdot)})$. The solution is found by multiplying not only by the matrix of right eigenvectors for the quasi-linear system, but also by the transformation matrix $\mathbf{C}^{-1}$. Explicit expressions can thus again be found, but in this case are slightly more involved:

$$
\begin{aligned}
\widetilde{\rho u_1} =& u_1\mathcal{R}_{10} + \mathcal{R}_1,\\
\widetilde{\rho u_2} =& u_2\mathcal{R}_{10} + \mathcal{R}_2,\\
\widetilde{\rho u_3} =& u_3\mathcal{R}_{10} + \mathcal{R}_3,\\
\widetilde{\rho F_{11}} =& F_{11}\mathcal{R}_{10} + \mathcal{F}_1(\mathcal{R}_4 + \mathcal{R}_7),\\
\widetilde{\rho F_{12}} =& F_{12}\mathcal{R}_{10} + \mathcal{F}_2(\mathcal{R}_4 + \mathcal{R}_7) - \overline{\mathscr{Q}_7},\\
\widetilde{\rho F_{13}} =& F_{13}\mathcal{R}_{10} + \mathcal{F}_3(\mathcal{R}_4 + \mathcal{R}_7) - \overline{\mathscr{Q}_8},\\
\widetilde{\rho F_{21}} =& F_{21}\mathcal{R}_{10} + \mathcal{F}_1(\mathcal{R}_5 + \mathcal{R}_8),\\
\widetilde{\rho F_{22}} =& F_{22}\mathcal{R}_{10} + \mathcal{F}_2(\mathcal{R}_5 + \mathcal{R}_8) - \overline{\mathscr{Q}_9},\\
\widetilde{\rho F_{23}} =& F_{23}\mathcal{R}_{10} + \mathcal{F}_3(\mathcal{R}_5 + \mathcal{R}_8) - \overline{\mathscr{Q}_{10}},\\
\widetilde{\rho F_{31}} =& F_{31}\mathcal{R}_{10} + \mathcal{F}_1(\mathcal{R}_6 + \mathcal{R}_9),\\
\widetilde{\rho F_{32}} =& F_{32}\mathcal{R}_{10} + \mathcal{F}_2(\mathcal{R}_6 + \mathcal{R}_9) - \overline{\mathscr{Q}_{11}},\\
\widetilde{\rho F_{33}} =& F_{33}\mathcal{R}_{10} + \mathcal{F}_3(\mathcal{R}_6 + \mathcal{R}_9) - \overline{\mathscr{Q}_{12}},\\
\widetilde{\rho E} =& E\mathcal{R}_{10} + u_1\mathcal{R}_1 + u_2\mathcal{R}_2 + u_3\mathcal{R}_3 - T[\\
&\left(\frac{\mathrm{d}\mathscr{S}}{\mathrm{d}F_{11}}\mathcal{F}_1 + \frac{\mathrm{d}\mathscr{S}}{\mathrm{d}F_{12}}\mathcal{F}_2 + \frac{\mathrm{d}\mathscr{S}}{\mathrm{d}F_{13}}\mathcal{F}_3\right)(\mathcal{R}_5 + \mathcal{R}_8) +\\
&\left(\frac{\mathrm{d}\mathscr{S}}{\mathrm{d}F_{21}}\mathcal{F}_1 + \frac{\mathrm{d}\mathscr{S}}{\mathrm{d}F_{22}}\mathcal{F}_2 + \frac{\mathrm{d}\mathscr{S}}{\mathrm{d}F_{23}}\mathcal{F}_3\right)(\mathcal{R}_6 + \mathcal{R}_9) +\\
&\left(\frac{\mathrm{d}\mathscr{S}}{\mathrm{d}F_{31}}\mathcal{F}_1 + \frac{\mathrm{d}\mathscr{S}}{\mathrm{d}F_{32}}\mathcal{F}_2 + \frac{\mathrm{d}\mathscr{S}}{\mathrm{d}F_{33}}\mathcal{F}_3\right)(\mathcal{R}_7 + \mathcal{R}_{10}) -\\
&\frac{\mathrm{d}\mathscr{S}}{\mathrm{d}F_{12}}\overline{\mathscr{Q}_7} - \frac{\mathrm{d}\mathscr{S}}{\mathrm{d}F_{13}}\overline{\mathscr{Q}_8} - \frac{\mathrm{d}\mathscr{S}}{\mathrm{d}F_{22}}\overline{\mathscr{Q}_9} -\\
&\frac{\mathrm{d}\mathscr{S}}{\mathrm{d}F_{23}}\overline{\mathscr{Q}_{10}} - \frac{\mathrm{d}\mathscr{S}}{\mathrm{d}F_{32}}\overline{\mathscr{Q}_{11}} - \frac{\mathrm{d}\mathscr{S}}{\mathrm{d}F_{33}}\overline{\mathscr{Q}_{12}} - \overline{\mathscr{Q}_{13}}],
\end{aligned}
\tag{E.11}
$$

with

$$
\begin{aligned}
\mathcal{R}_1 :=& \frac{1}{2}\left[(\mathscr{D}\mathbf{Q})^{-1}_{11}(\overline{\mathscr{Q}_1} + \overline{\mathscr{Q}_4}) + (\mathscr{D}\mathbf{Q})^{-1}_{12}(\overline{\mathscr{Q}_2} + \overline{\mathscr{Q}_5})(\mathscr{D}\mathbf{Q})^{-1}_{13}(\overline{\mathscr{Q}_3} + \overline{\mathscr{Q}_6})\right],\\
\mathcal{R}_2 :=& \frac{1}{2}\left[(\mathscr{D}\mathbf{Q})^{-1}_{21}(\overline{\mathscr{Q}_1} + \overline{\mathscr{Q}_4}) + (\mathscr{D}\mathbf{Q})^{-1}_{22}(\overline{\mathscr{Q}_2} + \overline{\mathscr{Q}_5})(\mathscr{D}\mathbf{Q})^{-1}_{23}(\overline{\mathscr{Q}_3} + \overline{\mathscr{Q}_6})\right],\\
\mathcal{R}_3 :=& \frac{1}{2}\left[(\mathscr{D}\mathbf{Q})^{-1}_{31}(\overline{\mathscr{Q}_1} + \overline{\mathscr{Q}_4}) + (\mathscr{D}\mathbf{Q})^{-1}_{32}(\overline{\mathscr{Q}_2} + \overline{\mathscr{Q}_5})(\mathscr{D}\mathbf{Q})^{-1}_{33}(\overline{\mathscr{Q}_3} + \overline{\mathscr{Q}_6})\right],
\end{aligned}
$$

$$
\begin{aligned}
\mathcal{R}_4 :=& \frac{1}{2}\left[(\mathscr{D}^2\mathbf{Q})^{-1}_{11}(\overline{\mathscr{Q}_1}-\overline{\mathscr{Q}_4})+(\mathscr{D}^2\mathbf{Q})^{-1}_{12}(\overline{\mathscr{Q}_2}-\overline{\mathscr{Q}_5})(\mathscr{D}^2\mathbf{Q})^{-1}_{13}(\overline{\mathscr{Q}_3}-\overline{\mathscr{Q}_6})\right],\\
\mathcal{R}_5 :=& \frac{1}{2}\left[(\mathscr{D}^2\mathbf{Q})^{-1}_{21}(\overline{\mathscr{Q}_1}-\overline{\mathscr{Q}_4})+(\mathscr{D}^2\mathbf{Q})^{-1}_{22}(\overline{\mathscr{Q}_2}-\overline{\mathscr{Q}_5})(\mathscr{D}^2\mathbf{Q})^{-1}_{23}(\overline{\mathscr{Q}_3}-\overline{\mathscr{Q}_6})\right],\\
\mathcal{R}_6 :=& \frac{1}{2}\left[(\mathscr{D}^2\mathbf{Q})^{-1}_{31}(\overline{\mathscr{Q}_1}-\overline{\mathscr{Q}_4})+(\mathscr{D}^2\mathbf{Q})^{-1}_{32}(\overline{\mathscr{Q}_2}-\overline{\mathscr{Q}_5})(\mathscr{D}^2\mathbf{Q})^{-1}_{33}(\overline{\mathscr{Q}_3}-\overline{\mathscr{Q}_6})\right],\\
\mathcal{R}_7 :=& \mathfrak{R}^1_{11}\overline{\mathscr{Q}_7}+\mathfrak{R}^2_{11}\overline{\mathscr{Q}_8}+\mathfrak{R}^1_{12}\overline{\mathscr{Q}_9}+\mathfrak{R}^2_{12}\overline{\mathscr{Q}_{10}}+\mathfrak{R}^1_{13}\overline{\mathscr{Q}_{11}}+\mathfrak{R}^2_{13}\overline{\mathscr{Q}_{12}}-\mathfrak{R}^3_1\overline{\mathscr{Q}_{13}},\\
\mathcal{R}_8 :=& \mathfrak{R}^1_{21}\overline{\mathscr{Q}_7}+\mathfrak{R}^2_{21}\overline{\mathscr{Q}_8}+\mathfrak{R}^1_{22}\overline{\mathscr{Q}_9}+\mathfrak{R}^2_{22}\overline{\mathscr{Q}_{10}}+\mathfrak{R}^1_{23}\overline{\mathscr{Q}_{11}}+\mathfrak{R}^2_{23}\overline{\mathscr{Q}_{12}}-\mathfrak{R}^3_2\overline{\mathscr{Q}_{13}},\\
\mathcal{R}_9 :=& \mathfrak{R}^1_{31}\overline{\mathscr{Q}_7}+\mathfrak{R}^2_{31}\overline{\mathscr{Q}_8}+\mathfrak{R}^1_{32}\overline{\mathscr{Q}_9}+\mathfrak{R}^2_{32}\overline{\mathscr{Q}_{10}}+\mathfrak{R}^1_{33}\overline{\mathscr{Q}_{11}}+\mathfrak{R}^2_{33}\overline{\mathscr{Q}_{12}}-\mathfrak{R}^3_3\overline{\mathscr{Q}_{13}},\\
\mathcal{R}_{10} :=& F^{-\mathrm{T}}_{12}\overline{\mathscr{Q}_7}+F^{-\mathrm{T}}_{13}\overline{\mathscr{Q}_8}+F^{-\mathrm{T}}_{22}\overline{\mathscr{Q}_9}+F^{-\mathrm{T}}_{23}\overline{\mathscr{Q}_{10}}+F^{-\mathrm{T}}_{32}\overline{\mathscr{Q}_{11}}+F^{-\mathrm{T}}_{33}\overline{\mathscr{Q}_{12}}-\\
& \widetilde{x_1}(\mathcal{R}_4+\mathcal{R}_7)-\widetilde{x_2}(\mathcal{R}_5+\mathcal{R}_8)-\widetilde{x_3}(\mathcal{R}_6+\mathcal{R}_9),
\end{aligned}
\tag{E.12}
$$

where $\mathfrak{R}^1_{ij}$, $\mathfrak{R}^2_{ij}$, and $\mathfrak{R}^3_i$ are the same as in the primitive variable Riemann solver and given in Eq. (E.6).

F

Computation of the stress and acoustic tensors

The acoustic tensor is a fundamental parameter in many aspects of both the exact and numerical methods detailed in the previous chapters, and therefore warrants a detailed breakdown of the method used in computing it.

In the x_η-direction the acoustic tensor can be written

$$\mathbf{\Omega} = \begin{pmatrix} A^{\eta 1}_{11}\widehat{F}_{\eta 1} + A^{\eta 1}_{12}\widehat{F}_{\eta 2} + A^{\eta 1}_{13}\widehat{F}_{\eta 3} & A^{\eta 2}_{11}\widehat{F}_{\eta 1} + A^{\eta 2}_{12}\widehat{F}_{\eta 2} + A^{\eta 2}_{13}\widehat{F}_{\eta 3} & A^{\eta 3}_{11}\widehat{F}_{\eta 1} + A^{\eta 3}_{12}\widehat{F}_{\eta 2} + A^{\eta 3}_{13}\widehat{F}_{\eta 3} \\ A^{\eta 1}_{21}\widehat{F}_{\eta 1} + A^{\eta 1}_{22}\widehat{F}_{\eta 2} + A^{\eta 1}_{23}\widehat{F}_{\eta 3} & A^{\eta 2}_{21}\widehat{F}_{\eta 1} + A^{\eta 2}_{22}\widehat{F}_{\eta 2} + A^{\eta 2}_{23}\widehat{F}_{\eta 3} & A^{\eta 3}_{21}\widehat{F}_{\eta 1} + A^{\eta 3}_{22}\widehat{F}_{\eta 2} + A^{\eta 3}_{23}\widehat{F}_{\eta 3} \\ A^{\eta 1}_{31}\widehat{F}_{\eta 1} + A^{\eta 1}_{32}\widehat{F}_{\eta 2} + A^{\eta 1}_{33}\widehat{F}_{\eta 3} & A^{\eta 2}_{31}\widehat{F}_{\eta 1} + A^{\eta 2}_{32}\widehat{F}_{\eta 2} + A^{\eta 2}_{33}\widehat{F}_{\eta 3} & A^{\eta 3}_{31}\widehat{F}_{\eta 1} + A^{\eta 3}_{32}\widehat{F}_{\eta 2} + A^{\eta 3}_{33}\widehat{F}_{\eta 3} \end{pmatrix}. \tag{F.1}$$

Note that contrary to many other sections the repeated indices η in Eq. (F.1) refers only to the coordinate direction and does not indicate summation. The acoustic tensor, its eigensystem and the coefficients $A^{ij}_{km} = (\partial\sigma_{ik}/\partial F_{jm})/\rho$ appear in the eigenvalues and both the left- and right-eigenvectors. It is desirable therefore to evaluate the coefficients A^{ij}_{km} analytically. Computing the required derivatives of stress with respect to deformation for the coefficients is lengthy, but when decomposed become more approachable.

To begin with it is intuitive to elaborate on the definition of the stress tensor. For an isotropic hyperelastic material the internal energy density can be formulated in terms of the invariants of any chosen strain tensor, $\mathcal{I}_p$, with $p = 1, 2, 3$: $\mathscr{E} = \mathscr{E}(\mathcal{I}_1, \mathcal{I}_2, \mathcal{I}_3, \mathscr{S})$. Thus it is more convenient to formulate stress in terms of the strain tensor, instead of the deformation gradient tensor. Taking as an example the Elastic Finger tensor, $\mathbf{G} = \mathbf{F}^{-\mathrm{T}}\mathbf{F}^{-1}$, then stress is given by Eq. (2.9). Formulations of stress in terms of alternative strain tensors commonly employed in solid mechanics can be found in [28]. Using this definition of the equation of state the components of stress can be formulated in terms of density, the derivatives of internal energy density with respect to the invariants of strain, and the components of the strain tensor G,

$$\sigma_{ij} = -2\rho G_{ik}\left(\mathscr{E}_{\mathcal{I}_1}\frac{\partial\mathcal{I}_1}{\partial G_{jk}} + \mathscr{E}_{\mathcal{I}_2}\frac{\partial\mathcal{I}_2}{\partial G_{jk}} + \mathscr{E}_{\mathcal{I}_3}\frac{\partial\mathcal{I}_3}{\partial G_{jk}}\right), \tag{F.2}$$

where $\mathscr{E}_{\mathcal{I}_p} = \partial\mathscr{E}/\partial\mathcal{I}_p$ denotes derivatives of internal energy density with respect to the invariants $\mathcal{I}_p$, which will of course depend on the specific formulation of the equation of state. The derivatives of the invariants with respect to the components of the strain tensor can be found as [28]

$$\frac{\mathrm{d}\mathcal{I}_1}{\mathrm{d}G_{jk}} = \delta_{jk}, \qquad \frac{\mathrm{d}\mathcal{I}_2}{\mathrm{d}G_{jk}} = \mathcal{I}_1\delta_{jk} - G_{jk}, \qquad \frac{\mathrm{d}\mathcal{I}_3}{\mathrm{d}G_{jk}} = \mathcal{I}_3 G^{-1}_{jk},$$

where δ_{jk} is the Kronecker delta. Using these results, the stress tensor can be expressed as:

$$\sigma_{ij} = -2\rho G_{ik}\left[\mathscr{E}_{\mathcal{I}_1}\delta_{jk} + \mathscr{E}_{\mathcal{I}_2}(\mathcal{I}_1\delta_{jk} - G_{jk}) + \mathscr{E}_{\mathcal{I}_3}\mathcal{I}_3 G^{-1}_{jk}\right], \tag{F.3}$$

Thus, the stress tensor is easily computable if one knows values of $\mathbf{G}$, ρ, and the derivatives of the chosen function for internal energy density with respect to the invariants of $\mathbf{G}$.

In a similar fashion to the stress tensor, components of the tensors $\mathbf{A}^{ij}$ can be decomposed as follows:

$$A^{ij}_{km} = \frac{\mathrm{d}\sigma_{ik}}{\mathrm{d}\rho}\frac{\partial\rho}{\partial F_{jm}} + \left(\sum_{q,r=1}^{3}\frac{\mathrm{d}\sigma_{ik}}{\mathrm{d}G_{qr}}\frac{\partial G_{qr}}{\partial F_{jm}}\right) + \frac{\mathrm{d}\sigma_{ik}}{\mathrm{d}\mathscr{E}_{\mathcal{I}_1}}\frac{\partial\mathscr{E}_{\mathcal{I}_1}}{\partial F_{jm}} + \frac{\mathrm{d}\sigma_{ik}}{\mathrm{d}\mathscr{E}_{\mathcal{I}_2}}\frac{\partial\mathscr{E}_{\mathcal{I}_2}}{\partial F_{jm}} + \frac{\mathrm{d}\sigma_{ik}}{\mathrm{d}\mathscr{E}_{\mathcal{I}_3}}\frac{\partial\mathscr{E}_{\mathcal{I}_3}}{\partial F_{jm}}. \tag{F.4}$$

The derivatives in the first term in Eq. (F.4) are $\mathrm{d}\sigma_{ik}/\mathrm{d}\rho = \sigma_{ik}/\rho$ and

$$\frac{\partial\rho}{\partial F} = \frac{\rho_0}{\det|F|^2}\begin{pmatrix} F_{23}F_{32} - F_{22}F_{33} & F_{21}F_{33} - F_{23}F_{31} & F_{22}F_{31} - F_{21}F_{32} \\ F_{12}F_{33} - F_{13}F_{32} & F_{13}F_{31} - F_{11}F_{33} & F_{11}F_{32} - F_{12}F_{31} \\ F_{13}F_{22} - F_{12}F_{23} & F_{11}F_{23} - F_{13}F_{21} & F_{12}F_{21} - F_{11}F_{22} \end{pmatrix}.$$

The large number of derivatives of strain with respect to deformation in the second term in Eq. (F.4) can be found using any symbolic mathematics package. Since the stress tensor is symmetric it is necessary only to define the derivatives of six components of stress with respect to strain. Derivatives of σ_{11} with respect to $\mathbf{G}$:

$$\begin{aligned}
\frac{\partial\sigma_{11}}{\partial G_{11}} &= -2\rho\left(\frac{\partial\mathscr{E}}{\partial\mathcal{I}_1} + (G_{22}+G_{33})\frac{\partial\mathscr{E}}{\partial\mathcal{I}_2} + (-G_{23}G_{32} + G_{22}G_{33})\frac{\partial\mathscr{E}}{\partial\mathcal{I}_3}\right), \\
\frac{\partial\sigma_{11}}{\partial G_{12}} &= \frac{\partial\sigma_{11}}{\partial G_{21}} = 2\rho\left(G_{21}\frac{\partial\mathscr{E}}{\partial\mathcal{I}_2} - (G_{23}G_{31} - G_{21}G_{33})\frac{\partial\mathscr{E}}{\partial\mathcal{I}_3}\right), \\
\frac{\partial\sigma_{11}}{\partial G_{13}} &= \frac{\partial\sigma_{11}}{\partial G_{31}} = 2\rho\left(G_{31}\frac{\partial\mathscr{E}}{\partial\mathcal{I}_2} - (-G_{22}G_{31} + G_{21}G_{32})\frac{\partial\mathscr{E}}{\partial\mathcal{I}_3}\right), \\
\frac{\partial\sigma_{11}}{\partial G_{22}} &= -2\rho\left(G_{11}\frac{\partial\mathscr{E}}{\partial\mathcal{I}_2} + (-G_{13}G_{31} + G_{11}G_{33})\frac{\partial\mathscr{E}}{\partial\mathcal{I}_3}\right), \\
\frac{\partial\sigma_{11}}{\partial G_{23}} &= \frac{\partial\sigma_{11}}{\partial G_{32}} = -2\rho(G_{12}G_{31} - G_{11}G_{32})\frac{\partial\mathscr{E}}{\partial\mathcal{I}_3}, \\
\frac{\partial\sigma_{11}}{\partial G_{33}} &= -2\rho\left(G_{11}\frac{\partial\mathscr{E}}{\partial\mathcal{I}_2} + (-G_{12}G_{21} + G_{11}G_{22})\frac{\partial\mathscr{E}}{\partial\mathcal{I}_3}\right).
\end{aligned}$$

Derivatives of σ_{12} with respect to $\mathbf{G}$:

$$\begin{aligned}
\frac{\partial \sigma_{12}}{\partial G_{11}} &= 0, \\
\frac{\partial \sigma_{12}}{\partial G_{12}} &= -2\rho(\frac{\partial \mathscr{E}}{\partial \mathcal{I}_1} + G_{33}\frac{\partial \mathscr{E}}{\partial \mathcal{I}_2}), \\
\frac{\partial \sigma_{12}}{\partial G_{13}} &= 2\rho G_{32}\frac{\partial \mathscr{E}}{\partial \mathcal{I}_2}, \\
\frac{\partial \sigma_{12}}{\partial G_{21}} &= 0, \\
\frac{\partial \sigma_{12}}{\partial G_{22}} &= 0, \\
\frac{\partial \sigma_{12}}{\partial G_{23}} &= 0, \\
\frac{\partial \sigma_{12}}{\partial G_{31}} &= 0, \\
\frac{\partial \sigma_{12}}{\partial G_{32}} &= 2\rho G_{13}\frac{\partial \mathscr{E}}{\partial \mathcal{I}_2}, \\
\frac{\partial \sigma_{12}}{\partial G_{33}} &= -2\rho G_{12}\frac{\partial \mathscr{E}}{\partial \mathcal{I}_2}.
\end{aligned}$$

Derivatives of σ_{13} with respect to $\mathbf{G}$:

$$\begin{aligned}
\frac{\partial \sigma_{13}}{\partial G_{11}} &= 0, \\
\frac{\partial \sigma_{13}}{\partial G_{12}} &= 2\rho G_{23}\frac{\partial \mathscr{E}}{\partial \mathcal{I}_2}, \\
\frac{\partial \sigma_{13}}{\partial G_{13}} &= -2\rho(\frac{\partial \mathscr{E}}{\partial \mathcal{I}_1} + G_{22}\frac{\partial \mathscr{E}}{\partial \mathcal{I}_2}), \\
\frac{\partial \sigma_{13}}{\partial G_{21}} &= 0, \\
\frac{\partial \sigma_{13}}{\partial G_{22}} &= -2\rho G_{13}\frac{\partial \mathscr{E}}{\partial \mathcal{I}_2}, \\
\frac{\partial \sigma_{13}}{\partial G_{23}} &= 2\rho G_{12}\frac{\partial \mathscr{E}}{\partial \mathcal{I}_2}, \\
\frac{\partial \sigma_{13}}{\partial G_{31}} &= 0, \\
\frac{\partial \sigma_{13}}{\partial G_{32}} &= 0, \\
\frac{\partial \sigma_{13}}{\partial G_{33}} &= 0.
\end{aligned}$$

Derivatives of σ_{22} with respect to $\mathbf{G}$:

$$
\begin{aligned}
\frac{\partial \sigma_{22}}{\partial G_{11}} &= -2\rho(G_{22}\frac{\partial \mathscr{E}}{\partial \mathcal{I}_2} + (-G_{23}G_{32} + G_{22}G_{33})\frac{\partial \mathscr{E}}{\partial \mathcal{I}_3}),\\
\frac{\partial \sigma_{22}}{\partial G_{12}} &= \frac{\partial \sigma_{22}}{\partial G_{21}} = 2\rho(G_{21}\frac{\partial \mathscr{E}}{\partial \mathcal{I}_2} - (G_{23}G_{31} - G_{21}G_{33})\frac{\partial \mathscr{E}}{\partial \mathcal{I}_3}),\\
\frac{\partial \sigma_{22}}{\partial G_{13}} &= \frac{\partial \sigma_{22}}{\partial G_{31}} = -2\rho(-G_{22}G_{31} + G_{21}G_{32})\frac{\partial \mathscr{E}}{\partial \mathcal{I}_3},\\
\frac{\partial \sigma_{22}}{\partial G_{22}} &= -2\rho(\frac{\partial \mathscr{E}}{\partial \mathcal{I}_1} + (G_{11} + G_{33})\frac{\partial \mathscr{E}}{\partial \mathcal{I}_2} + (-G_{13}G_{31} + G_{11}G_{33})\frac{\partial \mathscr{E}}{\partial \mathcal{I}_3}),\\
\frac{\partial \sigma_{22}}{\partial G_{23}} &= \frac{\partial \sigma_{22}}{\partial G_{32}} = 2\rho(G_{32}\frac{\partial \mathscr{E}}{\partial \mathcal{I}_2} - dI3dG23\frac{\partial \mathscr{E}}{\partial \mathcal{I}_3}),\\
\frac{\partial \sigma_{22}}{\partial G_{33}} &= -2\rho(G_{22}\frac{\partial \mathscr{E}}{\partial \mathcal{I}_2} + (-G_{12}G_{21} + G_{11}G_{22})\frac{\partial \mathscr{E}}{\partial \mathcal{I}_3}).
\end{aligned}
$$

Derivatives of σ_{23} with respect to $\mathbf{G}$:

$$
\begin{aligned}
\frac{\partial \sigma_{23}}{\partial G_{11}} &= -2\rho G_{23}\frac{\partial \mathscr{E}}{\partial \mathcal{I}_2},\\
\frac{\partial \sigma_{23}}{\partial G_{12}} &= 0,\\
\frac{\partial \sigma_{23}}{\partial G_{13}} &= 2\rho G_{21}\frac{\partial \mathscr{E}}{\partial \mathcal{I}_2},\\
\frac{\partial \sigma_{23}}{\partial G_{21}} &= 2\rho G_{13}\frac{\partial \mathscr{E}}{\partial \mathcal{I}_2},\\
\frac{\partial \sigma_{23}}{\partial G_{22}} &= 0,\\
\frac{\partial \sigma_{23}}{\partial G_{23}} &= -2\rho(\frac{\partial \mathscr{E}}{\partial \mathcal{I}_1} + G_{11}\frac{\partial \mathscr{E}}{\partial \mathcal{I}_2}),\\
\frac{\partial \sigma_{23}}{\partial G_{31}} &= 0,\\
\frac{\partial \sigma_{23}}{\partial G_{32}} &= 0,\\
\frac{\partial \sigma_{23}}{\partial G_{33}} &= 0.
\end{aligned}
$$

Derivatives of σ_{33} with respect to $\mathbf{G}$:

$$\begin{aligned}
\frac{\partial \sigma_{33}}{\partial G_{11}} &= -2\rho(G_{33}\frac{\partial \mathscr{E}}{\partial \mathcal{I}_2} + (-G_{23}G_{32} + G_{22}G_{33})\frac{\partial \mathscr{E}}{\partial \mathcal{I}_3}),\\
\frac{\partial \sigma_{33}}{\partial G_{12}} &= \frac{\partial \sigma_{33}}{\partial G_{21}} = -2\rho(G_{23}G_{31} - G_{21}G_{33})\frac{\partial \mathscr{E}}{\partial \mathcal{I}_3},\\
\frac{\partial \sigma_{33}}{\partial G_{13}} &= \frac{\partial \sigma_{33}}{\partial G_{31}} = 2\rho(G_{31}\frac{\partial \mathscr{E}}{\partial \mathcal{I}_2} - (-G_{22}G_{31} + G_{21}G_{32})\frac{\partial \mathscr{E}}{\partial \mathcal{I}_3}),\\
\frac{\partial \sigma_{33}}{\partial G_{22}} &= -2\rho(G_{33}\frac{\partial \mathscr{E}}{\partial \mathcal{I}_2} + (-G_{13}G_{31} + G_{11}G_{33})\frac{\partial \mathscr{E}}{\partial \mathcal{I}_3}),\\
\frac{\partial \sigma_{33}}{\partial G_{23}} &= \frac{\partial \sigma_{33}}{\partial G_{32}} = 2\rho(G_{32}\frac{\partial \mathscr{E}}{\partial \mathcal{I}_2} - dI3dG23\frac{\partial \mathscr{E}}{\partial \mathcal{I}_3}),\\
\frac{\partial \sigma_{33}}{\partial G_{33}} &= -2\rho(\frac{\partial \mathscr{E}}{\partial \mathcal{I}_1} + (G_{11} + G_{22})\frac{\partial \mathscr{E}}{\partial \mathcal{I}_2} + (-G_{12}G_{21} + G_{11}G_{22})\frac{\partial \mathscr{E}}{\partial \mathcal{I}_3}).
\end{aligned}$$

Derivatives of stress in last terms on the right-hand-side of Eq. (F.4) can be found similarly. Derivatives of stress with respect to the first invariant:

$$\frac{\partial \sigma}{\partial \mathcal{I}_1} = -2\rho\mathbf{G}.$$

Derivatives of stress with respect to the second invariant:

$$\begin{aligned}
\frac{\partial \sigma_{11}}{\partial \mathcal{I}_2} &= -2\rho(G_{11}G_{22} + G_{11}G_{33} - G_{12}G_{21} - G_{13}G_{31}),\\
\frac{\partial \sigma_{12}}{\partial \mathcal{I}_2} &= \frac{\partial \sigma_{21}}{\partial \mathcal{I}_2} = -2\rho(G_{12}G_{33} - G_{13}G_{32}),\\
\frac{\partial \sigma_{13}}{\partial \mathcal{I}_2} &= \frac{\partial \sigma_{31}}{\partial \mathcal{I}_2} = -2\rho(G_{13}G_{22} - G_{12}G_{23}),\\
\frac{\partial \sigma_{22}}{\partial \mathcal{I}_2} &= -2\rho(G_{11}G_{22} + G_{22}G_{33} - G_{12}G_{21} - G_{23}G_{32}),\\
\frac{\partial \sigma_{23}}{\partial \mathcal{I}_2} &= \frac{\partial \sigma_{32}}{\partial \mathcal{I}_2} = -2\rho(G_{11}G_{23} - G_{13}G_{21}),\\
\frac{\partial \sigma_{33}}{\partial \mathcal{I}_2} &= -2\rho(G_{11}G_{33} + G_{22}G_{33} - G_{13}G_{31} - G_{23}G_{32}).
\end{aligned}$$

Derivatives of stress with respect to the third invariant:

$$\begin{aligned}
\frac{\partial \sigma_{11}}{\partial \mathcal{I}_3} &= \frac{\partial \sigma_{22}}{\partial \mathcal{I}_3} = \frac{\partial \sigma_{33}}{\partial \mathcal{I}_3} = -2\rho\mathcal{I}_3,\\
\frac{\partial \sigma_{12}}{\partial \mathcal{I}_3} &= \frac{\partial \sigma_{13}}{\partial \mathcal{I}_3} = \frac{\partial \sigma_{21}}{\partial \mathcal{I}_3} = \frac{\partial \sigma_{23}}{\partial \mathcal{I}_3} = \frac{\partial \sigma_{31}}{\partial \mathcal{I}_3} = \frac{\partial \sigma_{32}}{\partial \mathcal{I}_3} = 0.
\end{aligned}$$

The additional derivatives in the last term of Eq. (F.4) can be decomposed further using

$$\frac{\partial \mathscr{E}_{\mathcal{I}_p}}{\partial F_{jm}} = \frac{\mathrm{d}\mathscr{E}_{\mathcal{I}_p}}{\mathrm{d}\mathcal{I}_1}\frac{\partial \mathcal{I}_1}{\partial F_{jm}} + \frac{\mathrm{d}\mathscr{E}_{\mathcal{I}_p}}{\mathrm{d}\mathcal{I}_2}\frac{\partial \mathcal{I}_2}{\partial F_{jm}} + \frac{\mathrm{d}\mathscr{E}_{\mathcal{I}_p}}{\mathrm{d}\mathcal{I}_3}\frac{\partial \mathcal{I}_3}{\partial F_{jm}}. \tag{F.5}$$

Derivatives of the invariants of the elastic Finger tensor with respect to deformation can be found as

$$\frac{\mathrm{d}\mathcal{I}_1}{\mathrm{d}F_{jm}} = -2G_{jk}F^{-T}_{km}, \qquad \frac{\mathrm{d}\mathcal{I}_2}{\mathrm{d}F_{jm}} = -2(\mathbf{G} - \mathrm{Tr}(\mathbf{G})\mathbf{I})_{jk}F^{-T}_{km}, \qquad \frac{\mathrm{d}\mathcal{I}_3}{\mathrm{d}F_{jm}} = -2\mathcal{I}_3F^{-T}_{jm}.$$

giving

$$\frac{\partial \mathscr{E}_{\mathcal{I}_p}}{\partial F_{jm}} = -\frac{\mathrm{d}\mathscr{E}_{\mathcal{I}_p}}{\mathrm{d}\mathcal{I}_1}\left(2G_{jk}F^{-T}_{km}\right) - \frac{\mathrm{d}\mathscr{E}_{\mathcal{I}_p}}{\mathrm{d}\mathcal{I}_2}\left(2(\mathbf{G} - \mathrm{Tr}(\mathbf{G})\mathbf{I})_{jk}F^{-T}_{km}\right) - \frac{\mathrm{d}\mathscr{E}_{\mathcal{I}_p}}{\mathrm{d}\mathcal{I}_3}\left(2\mathcal{I}_3F^{-T}_{jm}\right). \tag{F.6}$$

Depending on the chosen form of the equation of state some of the second derivatives of internal energy density with respect to invariants may be zero.

G

Evaluation of the derivatives of wavespeeds

When evaluating the solution across rarefaction waves one requires the evaluation of the derivatives of acoustic wave speeds with respect to the deformation tensor. The problem is made determinable analytically through the following relationship:

$$\frac{\partial}{\partial F_{pq}}\left(\mathscr{D}_{kk}^2\right) = Q_{km}\frac{\partial}{\partial F_{pq}}\left(\Omega_{mj}\right)Q_{jk}^{-1}. \tag{G.1}$$

In what follows it is assumed that the solution is sought for an initial value problem orientated along the x_1-direction. Derivatives of the acoustic tensor with respect to $\mathbf{F}$ can be expressed in the following form:

$$\begin{aligned}\frac{\partial \Omega_{mj}}{\partial F_{pq}} \;=\; \frac{1}{\rho}\Bigg[& F_{11}\left(\frac{\partial \sigma_{1m}}{\partial F_{j1}\partial F_{pq}} - \frac{1}{\rho}\frac{\partial \rho}{\partial F_{pq}}\frac{\partial \sigma_{1m}}{\partial F_{j1}}\right) + \\ & F_{12}\left(\frac{\partial \sigma_{1m}}{\partial F_{j2}\partial F_{pq}} - \frac{1}{\rho}\frac{\partial \rho}{\partial F_{pq}}\frac{\partial \sigma_{1m}}{\partial F_{j2}}\right) + \\ & F_{13}\left(\frac{\partial \sigma_{1m}}{\partial F_{j3}\partial F_{pq}} - \frac{1}{\rho}\frac{\partial \rho}{\partial F_{pq}}\frac{\partial \sigma_{1m}}{\partial F_{j3}}\right)\Bigg].\end{aligned} \tag{G.2}$$

Expressions for the derivatives of density and stress with respect $\mathbf{F}$ to in Eq. (G.2) are given in Appendix F and shall thus not be repeated. It remains then to determine the second derivatives of stress.

Consider the following decomposition of the first derivatives of stress with respect to $\mathbf{F}$:

$$\frac{\partial \sigma_{ik}}{\partial F_{jm}} = \underbrace{\frac{\partial \sigma_{ik}}{\partial \rho}\frac{\partial \rho}{\partial F_{jm}}}_{(a)} + \underbrace{\frac{\partial \sigma_{ik}}{\partial G_{qr}}\frac{\partial G_{qr}}{\partial F_{jm}}}_{(b)} + \underbrace{\frac{\partial \sigma_{ik}}{\partial \mathscr{E}_{\mathcal{I}_p}}\frac{\partial \mathscr{E}_{\mathcal{I}_p}}{\partial F_{jm}}}_{(c)}, \tag{G.3}$$

for which all terms are assumed to be determinable using the method described in Appendix F. The second derivatives of stress can therefore be considered as the sum of the derivatives of terms denoted (a), (b), and (c) on the right hand side of Eq. (G.3). It is intuitive to consider each of the terms individually:

- Term (a): Derivatives of Term (a) can be expressed as

$$\frac{\partial}{\partial F_{st}}\left(\frac{\partial \sigma_{ik}}{\partial \rho}\frac{\partial \rho}{\partial F_{jm}}\right) = \frac{\partial \rho}{\partial F_{jm}}\frac{\partial}{\partial F_{st}}\left(\frac{\partial \sigma_{ik}}{\partial \rho}\right) + \frac{\partial \sigma_{ik}}{\partial \rho}\frac{\partial}{\partial F_{st}}\left(\frac{\partial \rho}{\partial F_{jm}}\right). \tag{G.4}$$

Second derivatives of density with respect to deformation gradients are easily determined using a symbolic mathematics software but are somewhat lengthy and are thus are omitted for clarity. For derivatives of $\partial\sigma_{ik}/\partial\rho$ it is recalled that these terms are functions of $\mathbf{G}$ and $\mathscr{E}_{\mathcal{I}_p}$, therefore

$$\frac{\partial}{\partial F_{st}}\left(\frac{\partial\sigma_{ik}}{\partial\rho}\right)=\frac{\partial G_{uv}}{\partial F_{st}}\frac{\partial}{\partial G_{uv}}\left(\frac{\partial\sigma_{ik}}{\partial\rho}\right)+\frac{\partial\mathscr{E}_{\mathcal{I}_p}}{\partial F_{st}}\frac{\partial}{\partial\mathscr{E}_{\mathcal{I}_p}}\left(\frac{\partial\sigma_{ik}}{\partial\rho}\right). \tag{G.5}$$

- Term (b): Derivatives of Term (b) can be expressed as

$$\frac{\partial}{\partial F_{st}}\left(\frac{\partial\sigma_{ik}}{\partial G_{qr}}\frac{\partial G_{qr}}{\partial F_{jm}}\right)=\frac{\partial\sigma_{ik}}{\partial G_{qr}}\frac{\partial}{\partial F_{st}}\left(\frac{\partial G_{qr}}{\partial F_{jm}}\right)+\frac{\partial G_{qr}}{\partial F_{jm}}\frac{\partial}{\partial F_{st}}\left(\frac{\partial\sigma_{ik}}{\partial G_{qr}}\right). \tag{G.6}$$

  Second derivatives of the strain tensor $\mathbf{G}$ with respect to $\mathbf{F}$ can again be found using a symbolic mathematics software, and are found from lengthy functions of the deformation gradients and are omitted for clarity. The term $\partial\sigma_{ik}/\partial G_{qr}$ is a function of ρ, $\mathscr{E}_{\mathcal{I}_p}$, and G, and can be found from the following decomposition:

$$\frac{\partial}{\partial F_{st}}\left(\frac{\partial\sigma_{ik}}{\partial G_{qr}}\right)=\frac{\partial\rho}{\partial F_{st}}\frac{\partial}{\partial\rho}\left(\frac{\partial\sigma_{ik}}{\partial G_{qr}}\right)+\frac{\partial G_{uv}}{\partial F_{st}}\frac{\partial}{\partial G_{uv}}\left(\frac{\partial\sigma_{ik}}{\partial G_{qr}}\right)+\frac{\partial\mathscr{E}_{\mathcal{I}_p}}{\partial F_{st}}\frac{\partial}{\partial\mathscr{E}_{\mathcal{I}_p}}\left(\frac{\partial\sigma_{ik}}{\partial G_{qr}}\right). \tag{G.7}$$

- Term (c): Derivatives of Term (b) can be expressed in the following form:

$$\frac{\partial}{\partial F_{st}}\left(\frac{\partial\sigma_{ik}}{\partial\mathscr{E}_{\mathcal{I}_p}}\frac{\partial\mathscr{E}_{\mathcal{I}_p}}{\partial F_{jm}}\right)=\underbrace{\frac{\partial\mathscr{E}_{\mathcal{I}_p}}{\partial F_{jm}}\frac{\partial}{\partial F_{st}}\left(\frac{\partial\sigma_{ik}}{\partial\mathscr{E}_{\mathcal{I}_p}}\right)}_{[1]}+\underbrace{\frac{\partial\sigma_{ik}}{\partial\mathscr{E}_{\mathcal{I}_p}}\frac{\partial}{\partial F_{st}}\left(\frac{\partial\mathscr{E}_{\mathcal{I}_p}}{\partial F_{jm}}\right)}_{[2]}. \tag{G.8}$$

  Evaluation of some of the terms on the right hand side of Eq. (G.8) can be somewhat cumbersome, hence each is considered independently in greater detail:

  - Term [1]: $\partial\sigma_{ik}/\partial\mathscr{E}_{\mathcal{I}_p}$ is a function of ρ and G, so

$$\frac{\partial}{\partial F_{st}}\left(\frac{\partial\sigma_{ik}}{\partial\mathscr{E}_{\mathcal{I}_p}}\right)=\frac{\partial\rho}{\partial F_{st}}\frac{\partial}{\partial\rho}\left(\frac{\partial\sigma_{ik}}{\partial\mathscr{E}_{\mathcal{I}_p}}\right)+\frac{\partial G_{uv}}{\partial F_{st}}\frac{\partial}{\partial G_{uv}}\left(\frac{\partial\sigma_{ik}}{\partial\mathscr{E}_{\mathcal{I}_p}}\right). \tag{G.9}$$

  - Term [2]:

$$\frac{\partial}{\partial F_{st}}\left(\frac{\partial\mathscr{E}_{\mathcal{I}_p}}{\partial F_{jm}}\right)=\frac{\partial}{\partial F_{st}}\left(\frac{\partial\mathcal{I}_1}{\partial F_{jm}}\frac{\partial\mathscr{E}_{\mathcal{I}_p}}{\partial\mathcal{I}_1}+\frac{\partial\mathcal{I}_2}{\partial F_{jm}}\frac{\partial\mathscr{E}_{\mathcal{I}_p}}{\partial\mathcal{I}_2}+\frac{\partial\mathcal{I}_3}{\partial F_{jm}}\frac{\partial\mathscr{E}_{\mathcal{I}_p}}{\partial\mathcal{I}_3}\right), \tag{G.10}$$

where

$$\frac{\partial}{\partial F_{st}}\left(\frac{\partial \mathcal{I}_q}{\partial F_{jm}}\frac{\partial \mathscr{E}_{\mathcal{I}_p}}{\partial \mathcal{I}_q}\right)=\frac{\partial \mathcal{I}_q}{\partial F_{jm}}\frac{\partial}{\partial F_{st}}\left(\frac{\partial \mathscr{E}_{\mathcal{I}_p}}{\partial \mathcal{I}_q}\right)+\frac{\partial \mathscr{E}_{\mathcal{I}_p}}{\partial \mathcal{I}_q}\frac{\partial}{\partial F_{st}}\left(\frac{\partial \mathcal{I}_q}{\partial F_{jm}}\right). \quad \text{(G.11)}$$

Outstanding terms on the right-hand-side of Eq. (G.11) can be computed according to

$$\frac{\partial}{\partial F_{st}}\left(\frac{\partial \mathscr{E}_{\mathcal{I}_p}}{\partial \mathcal{I}_q}\right)=\frac{\partial \mathcal{I}_m}{\partial F_{st}}\frac{\partial}{\partial \mathcal{I}_m}\left(\frac{\partial \mathscr{E}_{\mathcal{I}_p}}{\partial \mathcal{I}_q}\right), \quad \text{(G.12)}$$

and

$$\frac{\partial}{\partial F_{st}}\left(\frac{\partial \mathcal{I}_q}{\partial F_{jm}}\right)=\frac{\partial G_{ik}}{\partial F_{jm}}\frac{\partial}{\partial F_{st}}\left(\frac{\partial \mathcal{I}_q}{\partial G_{ik}}\right)+\frac{\partial \mathcal{I}_q}{\partial G_{ik}}\frac{\partial}{\partial F_{st}}\left(\frac{\partial G_{ik}}{\partial F_{jm}}\right), \quad \text{(G.13)}$$

where

$$\frac{\partial}{\partial F_{st}}\left(\frac{\partial \mathcal{I}_q}{\partial G_{ik}}\right)=\frac{\partial G_{jm}}{\partial F_{st}}\frac{\partial}{\partial G_{jm}}\left(\frac{\partial \mathcal{I}_q}{\partial G_{ik}}\right). \quad \text{(G.14)}$$

H

Exact solutions to selected initial value problems in non-linear elasticity

In this chapter exact solutions are given for initial value problems for hyperelastic materials in each case governed by the equation of state for internal energy density Eq. (2.82)-(2.83). The following results are presented:

- Tables H.1 and H.5 detail exact solutions for the initial conditions Eq. (2.84) assuming both left and right materials are copper, with constants given in Table 2.1.
- Tables H.2 and H.6 detail exact solutions for the initial conditions Eq. (2.85) assuming both left and right materials are copper, with constants given in Table 2.1.
- Tables H.3 and H.7 detail exact solutions for the initial conditions Eq. (2.84) assuming the left material is aluminium and the right material is copper, with constants given in Table 4.1.
- Tables H.4 and H.8 detail exact solutions for the initial conditions Eq. (2.84) assuming the left material is aluminium and right is a vacuum, with constants given in Table 4.1.

In each table wavespeeds and velocities are given in km s^{-1} and entropies in kJ g^{-1} K^{-1}.

Table H.1: Wave speeds for IVP 1 (Cu/Cu)

$\mathfrak{S}_1$	$\mathfrak{S}_2$	$\mathfrak{S}_3$	$\mathfrak{S}_4$	$\mathfrak{S}_5$	$\mathfrak{S}_6$
-5.7675	-3.1914	-2.7563	4.7731	5.1742	7.7679

Table H.2: Wave speeds for IVP 2 (Cu/Cu)

$\mathfrak{S}_1$	$\mathfrak{S}_2$	$\mathfrak{S}_3$	$\mathfrak{S}_4$	$\mathfrak{S}_5$	$\mathfrak{S}_6$
-4.8743	-1.9317	$-8.8082 \cdot 10^{-1}$	2.2419	3.0204	5.4990

Table H.3: Wave speeds for IVP 3 (Al/Cu)

$\mathfrak{S}_1$	$\mathfrak{S}_2$	$\mathfrak{S}_3$	$\mathfrak{S}_4$	$\mathfrak{S}_5$	$\mathfrak{S}_6$
-9.1130	-6.3790	-5.6614	3.8927	4.2720	6.6765

Table H.4: Wave speeds for IVP 4 (Al/Void)

$\mathfrak{S}_1$	$\mathfrak{S}_2$	$\mathfrak{S}_3$
-2.0335	-1.1796	-7.0949

Table H.5: Solution states for IVP 1

	Region					
Parameter	1	2	3	4	5	6
u_1	1.0006	1.0011	1.0003	1.0003	$9.9909 \cdot 10^{-1}$	1.0004
u_2	$-1.8458 \cdot 10^{-2}$	$-1.5632 \cdot 10^{-2}$	$2.6241 \cdot 10^{-2}$	$2.6241 \cdot 10^{-2}$	$-6.0181 \cdot 10^{-2}$	$-6.0882 \cdot 10^{-2}$
u_3	$5.9531 \cdot 10^{-2}$	$4.5669 \cdot 10^{-2}$	$5.3993 \cdot 10^{-2}$	$5.3993 \cdot 10^{-2}$	$5.4892 \cdot 10^{-2}$	$1.7898 \cdot 10^{-2}$
F_{11}	$8.7133 \cdot 10^{-1}$	$8.7144 \cdot 10^{-1}$	$8.7127 \cdot 10^{-1}$	$8.7119 \cdot 10^{-1}$	$8.7149 \cdot 10^{-1}$	$8.7122 \cdot 10^{-1}$
F_{12}	0.0000	0.0000	0.0000	0.0000	0.0000	0.0000
F_{13}	0.0000	0.0000	0.0000	0.0000	0.0000	0.0000
F_{21}	$-1.2376 \cdot 10^{-2}$	$-1.1789 \cdot 10^{-2}$	$-2.0781 \cdot 10^{-3}$	$-1.1263 \cdot 10^{-3}$	$1.8829 \cdot 10^{-2}$	$1.8976 \cdot 10^{-2}$
F_{22}	$9.5000 \cdot 10^{-1}$	$9.5000 \cdot 10^{-1}$	$9.5000 \cdot 10^{-1}$	$9.5000 \cdot 10^{-1}$	$9.5000 \cdot 10^{-1}$	$9.5000 \cdot 10^{-1}$
F_{23}	$2.0000 \cdot 10^{-2}$	$2.0000 \cdot 10^{-2}$	$2.0000 \cdot 10^{-2}$	0.0000	0.0000	0.0000
F_{31}	$-2.0210 \cdot 10^{-2}$	$-2.3090 \cdot 10^{-2}$	$-2.1159 \cdot 10^{-2}$	$-2.1095 \cdot 10^{-2}$	$-2.1302 \cdot 10^{-2}$	$-1.3591 \cdot 10^{-2}$
F_{32}	0.0000	0.0000	0.0000	0.0000	0.0000	0.0000
F_{33}	$9.0000 \cdot 10^{-1}$	$9.0000 \cdot 10^{-1}$	$9.0000 \cdot 10^{-1}$	$9.0000 \cdot 10^{-1}$	$9.0000 \cdot 10^{-1}$	$9.0000 \cdot 10^{-1}$
$\mathscr{S}$	$1.7289 \cdot 10^{-4}$	$1.7289 \cdot 10^{-4}$	$1.7290 \cdot 10^{-4}$	$1.7326 \cdot 10^{-4}$	$1.7325 \cdot 10^{-4}$	$1.7325 \cdot 10^{-4}$

Table H.6: Solution states for IVP 2

	Region					
Parameter	1	2	3	4	5	6
u_1	$2.2464 \cdot 10^{-1}$	$2.3210 \cdot 10^{-1}$	$3.2691 \cdot 10^{-1}$	$3.2691 \cdot 10^{-1}$	$3.6878 \cdot 10^{-1}$	$3.7420 \cdot 10^{-1}$
u_2	$4.9503 \cdot 10^{-1}$	$5.8153 \cdot 10^{-1}$	$1.8347 \cdot 10^{-1}$	$1.8347 \cdot 10^{-1}$	$-9.3161 \cdot 10^{-2}$	0.0000
u_3	1.0010	$9.0848 \cdot 10^{-1}$	$4.0684 \cdot 10^{-1}$	$4.0684 \cdot 10^{-1}$	$9.7935 \cdot 10^{-2}$	0.0000
F_{11}	1.0215	1.0250	1.0926	$9.5300 \cdot 10^{-1}$	$9.3384 \cdot 10^{-1}$	$9.3195 \cdot 10^{-1}$
F_{12}	0.0000	0.0000	0.0000	0.0000	0.0000	0.0000
F_{13}	0.0000	0.0000	0.0000	0.0000	0.0000	0.0000
F_{21}	$1.9082 \cdot 10^{-2}$	$5.9387 \cdot 10^{-2}$	$-2.0263 \cdot 10^{-1}$	$-9.0558 \cdot 10^{-2}$	$3.2445 \cdot 10^{-2}$	0.0000
F_{22}	1.0000	1.0000	1.0000	1.0000	1.0000	1.0000
F_{23}	$1.0000 \cdot 10^{-1}$	$1.0000 \cdot 10^{-1}$	$1.0000 \cdot 10^{-1}$	$1.0000 \cdot 10^{-1}$	$1.0000 \cdot 10^{-1}$	$1.0000 \cdot 10^{-1}$
F_{31}	$1.9161 \cdot 10^{-4}$	$-4.2937 \cdot 10^{-2}$	$-3.7940 \cdot 10^{-1}$	$-1.7201 \cdot 10^{-1}$	$-3.4107 \cdot 10^{-2}$	0.0000
F_{32}	0.0000	0.0000	0.0000	0.0000	0.0000	0.0000
F_{33}	1.0000	1.0000	1.0000	1.0000	1.0000	1.0000
$\mathscr{S}$	$1.0000 \cdot 10^{-3}$	$1.0000 \cdot 10^{-3}$	$1.0000 \cdot 10^{-3}$	$2.2945 \cdot 10^{-5}$	$2.2945 \cdot 10^{-5}$	$2.2945 \cdot 10^{-5}$

Table H.7: Solution states for IVP 3

Parameter	Region					
	1	2	3	4	5	6
u_1	$5.4828{\cdot}10^{-1}$	$5.4327{\cdot}10^{-1}$	$5.4065{\cdot}10^{-1}$	$5.4065{\cdot}10^{-1}$	$5.3958{\cdot}10^{-1}$	$5.3885{\cdot}10^{-1}$
u_2	$-4.2721{\cdot}10^{-2}$	$-7.6645{\cdot}10^{-2}$	$5.2640{\cdot}10^{-2}$	$1.6669{\cdot}10^{-2}$	$-4.8020{\cdot}10^{-2}$	$-4.7680{\cdot}10^{-2}$
u_3	$-3.0414{\cdot}10^{-3}$	$1.6339{\cdot}10^{-1}$	$1.8757{\cdot}10^{-1}$	$-4.4342{\cdot}10^{-2}$	$-4.4342{\cdot}10^{-2}$	$5.9985{\cdot}10^{-3}$
F_{11}	$8.6937{\cdot}10^{-1}$	$8.6874{\cdot}10^{-1}$	$8.6837{\cdot}10^{-1}$	$9.1882{\cdot}10^{-1}$	$9.1911{\cdot}10^{-1}$	$9.1929{\cdot}10^{-1}$
F_{12}	0.0000	0.0000	0.0000	0.0000	0.0000	0.0000
F_{13}	0.0000	0.0000	0.0000	0.0000	0.0000	0.0000
F_{21}	$-1.3844{\cdot}10^{-2}$	$-1.8102{\cdot}10^{-2}$	0.0000	0.0000	$1.7732{\cdot}10^{-2}$	$1.7648{\cdot}10^{-2}$
F_{22}	$9.5000{\cdot}10^{-1}$	$9.5000{\cdot}10^{-1}$	$9.5000{\cdot}10^{-1}$	$9.5000{\cdot}10^{-1}$	$9.5000{\cdot}10^{-1}$	$9.5000{\cdot}10^{-1}$
F_{23}	$2.0000{\cdot}10^{-2}$	$2.0000{\cdot}10^{-2}$	$2.0000{\cdot}10^{-2}$	0.0000	0.0000	0.0000
F_{31}	$-2.4272{\cdot}10^{-2}$	$-3.3847{\cdot}10^{-3}$	0.0000	0.0000	0.0000	$-1.2396{\cdot}10^{-2}$
F_{32}	0.0000	0.0000	0.0000	0.0000	0.0000	0.0000
F_{33}	$9.0000{\cdot}10^{-1}$	$9.0000{\cdot}10^{-1}$	$9.0000{\cdot}10^{-1}$	$9.0000{\cdot}10^{-1}$	$9.0000{\cdot}10^{-1}$	$9.0000{\cdot}10^{-1}$
$\mathscr{S}$	$4.2612{\cdot}10^{-4}$	$4.2615{\cdot}10^{-4}$	$4.2617{\cdot}10^{-4}$	$3.8543{\cdot}10^{-5}$	$3.8540{\cdot}10^{-5}$	$3.8538{\cdot}10^{-5}$

Table H.8: Solution states for IVP 4

	Region		
Parameter	1	2	3
u_1	2.6322	2.6317	2.6313
u_2	$2.3047 \cdot 10^{-2}$	$2.0172 \cdot 10^{-2}$	$3.9993 \cdot 10^{-2}$
u_3	$1.5159 \cdot 10^{-1}$	$1.6666 \cdot 10^{-1}$	$1.7037 \cdot 10^{-1}$
F_{11}	1.1164	1.1163	1.1161
F_{12}	0.0000	0.0000	0.0000
F_{13}	0.0000	0.0000	0.0000
F_{21}	$-5.7800 \cdot 10^{-3}$	$-6.6220 \cdot 10^{-3}$	0.0000
F_{22}	$9.5000 \cdot 10^{-1}$	$9.5000 \cdot 10^{-1}$	$9.5000 \cdot 10^{-1}$
F_{23}	$2.0000 \cdot 10^{-2}$	$2.0000 \cdot 10^{-2}$	$2.0000 \cdot 10^{-2}$
F_{31}	$-5.6540 \cdot 10^{-3}$	$-1.2382 \cdot 10^{-3}$	0.0000
F_{32}	0.0000	0.0000	0.0000
F_{33}	$9.0000 \cdot 10^{-1}$	$9.0000 \cdot 10^{-1}$	$9.0000 \cdot 10^{-1}$
$\mathscr{S}$	0.0000	0.0000	0.0000

I

Implicit evaluation of the inelastic source terms

Consider the following ordinary differential equation:

$$\frac{\mathrm{d}\mathbf{U}}{\mathrm{d}t} = \mathbf{S}^{\mathrm{P}}, \tag{I.1}$$

where

$$\mathbf{U} := (\rho\mathbf{u}, \rho, \rho F_{12}, \ldots, \rho F_{33}, \rho E), \tag{I.2}$$
$$\mathbf{S}^{\mathrm{P}} := (\mathbf{0}, 0, \varphi_{12}, \ldots, \varphi_{33}, 0), \tag{I.3}$$

with

$$\varphi_{ij} := \chi\sigma'_{ik}(\rho\mathbf{F})_{kj}, \qquad \chi := \frac{1}{2G\tau}. \tag{I.4}$$

If it is assumed that the term $\mathbf{S}^{\mathrm{P}}$ is, or could be, stiff then the simplest stable method of discretising Eq. (I.1) is the forward Euler method:

$$\mathbf{U}^{n+1} = \mathbf{U}^{*} + \mathbf{S}^{\mathrm{P}}\left(\mathbf{U}^{n+1}\right), \tag{I.5}$$

where $\mathbf{U}^{*}$ is the last known solution vector. In χ it is assumed that the shear modulus G is a constant, and that the relaxation time of tangential stress τ is a function of the shear stress intensity σ_{EQ} and temperature: $\tau = \tau(\sigma_{\mathrm{EQ}}, T)$.

To evaluate the implicit function Eq. (I.5) the following vector is defined:

$$\mathscr{R} := \frac{1}{\Delta t}\left(\mathbf{U}^{n+1} - \mathbf{U}^{*}\right) + \mathbf{S}^{\mathrm{P}}. \tag{I.6}$$

In order to satisfy Eq. (I.5) the following equality is required:

$$\mathscr{R} = 0, \tag{I.7}$$

which can be viewed as a non-linear set of equations in terms of $\mathbf{U}^{n+1}$, and can be solved using Newton's method:

$$\left(\mathbf{U}^{n+1}\right)^{m} = \left(\mathbf{U}^{n+1}\right)^{m-1} - \left(\frac{\partial\mathscr{R}}{\partial\mathbf{U}^{n+1}}\right)^{-1}\left(\left(\mathbf{U}^{n+1}\right)^{m-1}\right)\mathscr{R}\left(\left(\mathbf{U}^{n+1}\right)^{m-1}\right). \tag{I.8}$$

It is easy to see that the Jacobian in Eq. (I.8) can be written

$$\frac{\partial \mathscr{R}}{\partial \mathbf{U}^{n+1}} = \frac{1}{\Delta t}\mathbf{I} + \frac{\partial \mathbf{S}^{\mathrm{P}}\left(\mathbf{U}^{n+1}\right)}{\partial \mathbf{U}^{n+1}}. \tag{I.9}$$

The difficulty therefore lies in computing the Jacobian matrix $\partial \mathbf{S}^{\mathrm{P}}/\partial \mathbf{U}$ which can be written

$$\frac{\partial \mathbf{S}^{\mathrm{P}}}{\partial \mathbf{U}} = \begin{pmatrix} 0 & 0 & 0 & 0 & 0 \\ 0 & \mathbf{A}^{11} & \mathbf{A}^{12} & \mathbf{A}^{13} & \mathbf{b}^1 \\ 0 & \mathbf{A}^{21} & \mathbf{A}^{22} & \mathbf{A}^{23} & \mathbf{b}^2 \\ 0 & \mathbf{A}^{31} & \mathbf{A}^{32} & \mathbf{A}^{33} & \mathbf{b}^3 \\ 0 & 0 & 0 & 0 & 0 \end{pmatrix}. \tag{I.10}$$

Recall the definition of the vector of conserved variables in Eq. (I.2), then the coefficients $\mathbf{A}^{ij} = [A^{ij}_{kl}]$, $\mathbf{b}^i = [b^i_j]$ in Eq. (I.10) can be defined as follows:

$$\begin{aligned} A^{ij}_{kl} &= \frac{\partial}{\partial(\rho\mathbf{F})_{kl}}\left(\chi\sigma'_{im}(\rho\mathbf{F})_{mj}\right), \\ &= \chi\sigma'_{ij}\delta_{kl} + \chi(\rho\mathbf{F})_{mk}\underbrace{\frac{\partial\sigma'_{im}}{\partial(\rho\mathbf{F})_{jl}}}_{(a)} + \sigma'_{im}(\rho\mathbf{F})_{mk}\underbrace{\frac{\partial\chi}{\partial(\rho\mathbf{F})_{jl}}}_{(b)} + \sigma'_{ij}\underbrace{\frac{\partial(\rho\mathbf{F})_{11}}{\partial(\rho\mathbf{F})_{jl}}}_{(c)}\delta_{1k}, \end{aligned} \tag{I.11}$$

for $j = l \neq 1$;

$$\begin{aligned} A^{ij}_{kl} &= \frac{\partial}{\partial\rho}\left(\chi\sigma'_{im}(\rho\mathbf{F})_{mj}\right), \\ &= \chi(\rho\mathbf{F})_{mk}\underbrace{\frac{\partial\sigma'_{im}}{\partial\rho}}_{(d)} + \sigma'_{im}(\rho\mathbf{F})_{mk}\underbrace{\frac{\partial\chi}{\partial\rho}}_{(e)} + \sigma'_{ij}\underbrace{\frac{\partial(\rho\mathbf{F})_{11}}{\partial(\rho)}}_{(f)}\delta_{1k}, \end{aligned} \tag{I.12}$$

for $j = l = 1$; and

$$\begin{aligned} b^i_j &= \sigma'_{im}(\rho\mathbf{F})_{mj}\frac{\partial\chi}{\partial(\rho E)}, \\ &= \sigma'_{im}(\rho\mathbf{F})_{mj}\underbrace{\frac{\partial T}{\partial(\rho E)}}_{(g)}\frac{\partial\chi}{\partial T}. \end{aligned} \tag{I.13}$$

Note that the above definitions are all invalid when $i = k = 1$ since $S^{\mathrm{P}}_4 = 0$, and hence:

$$A^{1j}_{1l} = 0, \qquad b^1_1 = 0. \tag{I.14}$$

In Eq. (I.11)-(I.13) certain terms have been singled out as requiring further expansion to enable a straightforward analytic evaluation and shall be considered separately as follows (note that in each case the above respective definitions of the valid range for each of the indices i, j, k, l strictly applies):

- Term (a): Derivatives of the stress deviator with respect to $(\rho\mathbf{F})$, with ρ and (ρE) held constant, can be decomposed as follows:

$$\frac{\partial \sigma'_{im}}{\partial(\rho\mathbf{F})_{jl}} = \frac{\partial \sigma_{im}}{\partial(\rho\mathbf{F})_{jl}} - \frac{1}{3}\left(\frac{\partial \sigma_{11}}{\partial(\rho\mathbf{F})_{jl}} + \frac{\partial \sigma_{22}}{\partial(\rho\mathbf{F})_{jl}} + \frac{\partial \sigma_{33}}{\partial(\rho\mathbf{F})_{jl}}\right)\delta_{im}, \tag{I.15}$$

  where in terms of derivatives with respect to primitive variables the following relationships can be substituted:

$$\frac{\partial \sigma_{im}}{\partial(\rho\mathbf{F})_{jl}} = \frac{\partial F_{11}}{\partial(\rho\mathbf{F})_{jl}}\frac{\partial \sigma_{im}}{\partial F_{11}} + \frac{1}{\rho}\frac{\partial \sigma_{im}}{\partial F_{jl}}. \tag{I.16}$$

  To evaluate the first term, F_{11} can be considered a function of the conserved variables:

$$F_{11} = F_{11}\left(\rho, (\rho\mathbf{F})_{12}, \ldots, (\rho\mathbf{F})_{33}\right), \tag{I.17}$$

  and it can be subsequently shown that

$$\frac{\partial F_{11}}{\partial(\rho\mathbf{F})} = \frac{1}{\rho}\frac{\partial(\rho F)_{11}}{\partial(\rho\mathbf{F})}, \tag{I.18}$$

  where the last term on the right hand side is evaluated in Term (c).

- Term (b): Based upon the definition of the relaxation time as a function of the equivalent stress and temperature, the following can be derived:

$$\frac{\partial \chi}{\partial(\rho\mathbf{F})_{ij}} = \frac{\partial \chi}{\partial \sigma_{\text{EQ}}}\frac{\partial \sigma_{\text{EQ}}}{\partial J_2}\frac{\partial J_2}{\partial(\rho\mathbf{F})_{ij}} + \frac{\partial \chi}{\partial T}\frac{\partial T}{\partial(\rho\mathbf{F})_{ij}}. \tag{I.19}$$

  Here the fact that the tangential stress intensity is a function of the second invariant of the deviatoric stress tensor has been used: $\sigma_{\text{EQ}} = \sqrt{3J_2/4}$ where $J_2 = \sigma'^2_{11} + \sigma'^2_{22} + \sigma'^2_{33} + 2(\sigma'^2_{12} + \sigma'^2_{23} + \sigma'^2_{31})$. Derivatives appearing in the first term of Eq. (I.19) are found easily:

$$\frac{\partial \sigma_{\text{EQ}}}{\partial J_2} = \frac{3}{4}\frac{1}{\sigma_{\text{EQ}}}, \tag{I.20}$$

  and

$$\begin{aligned}\frac{\partial J_2}{\partial(\rho\mathbf{F})_{ij}} \;=\; & 2\left[\sigma'_{11}\frac{\partial \sigma'_{11}}{\partial(\rho\mathbf{F})_{ij}} + \sigma'_{22}\frac{\partial \sigma'_{22}}{\partial(\rho\mathbf{F})_{ij}} + \sigma'_{33}\frac{\partial \sigma'_{33}}{\partial(\rho\mathbf{F})_{ij}} + \right. \\ & \left. 2\left(\sigma'_{12}\frac{\partial \sigma'_{12}}{\partial(\rho\mathbf{F})_{ij}} + \sigma'_{13}\frac{\partial \sigma'_{13}}{\partial(\rho\mathbf{F})_{ij}} + \sigma'_{23}\frac{\partial \sigma'_{23}}{\partial(\rho\mathbf{F})_{ij}}\right)\right]\end{aligned} \tag{I.21}$$

where one can refer back to Term (a) for the outstanding derivatives.

The last term in Eq. (I.19) can be expanded as follows:

$$\frac{\partial T}{\partial(\rho\mathbf{F})_{ij}} = \frac{\partial T}{\partial \mathscr{S}}\frac{\partial \mathscr{S}}{\partial(\rho\mathbf{F})_{ij}}, \tag{I.22}$$

$$= \frac{\partial T}{\partial \mathscr{S}}\left(\frac{\partial \mathscr{S}}{\partial \mathcal{I}_1}\frac{\partial \mathcal{I}_1}{\partial(\rho\mathbf{F})_{ij}} + \frac{\partial \mathscr{S}}{\partial \mathcal{I}_2}\frac{\partial \mathcal{I}_2}{\partial(\rho\mathbf{F})_{ij}}\right), \tag{I.23}$$

where

$$\frac{\partial \mathcal{I}_p}{\partial(\rho\mathbf{F})_{ij}} = \sum_{k,m=1}^{3}\frac{\partial \mathcal{I}_p}{\partial G_{km}}\frac{\partial G_{km}}{\partial(\rho\mathbf{F})_{ij}}, \tag{I.24}$$

$$= \sum_{k,m=1}^{3}\frac{\partial \mathcal{I}_p}{\partial G_{km}}\left(\frac{\partial F_{11}}{\partial(\rho\mathbf{F})_{ij}}\frac{\partial G_{km}}{\partial F_{11}} + \frac{1}{\rho}\frac{\partial G_{km}}{\partial F_{ij}}\right). \tag{I.25}$$

Thus the result is determined either in terms of derivatives with respect to primitive variables or derivatives that have already been detailed.

- Term (c): To determine the required derivatives it is necessary to recall that $(\rho\mathbf{F})_{11}$ can be expressed as a function of the conserved variables:

$$(\rho\mathbf{F})_{11} = (\rho\mathbf{F})_{11}\left(\rho, (\rho\mathbf{F})_{12}, \ldots, (\rho\mathbf{F})_{33}\right). \tag{I.26}$$

Hence the following explicit expressions can be obtained:

$$\frac{\partial(\rho\mathbf{F})_{11}}{\partial(\rho\mathbf{F})_{12}} = \frac{F_{23}F_{31} - F_{21}F_{33}}{F_{23}F_{32} - F_{22}F_{33}}, \tag{I.27}$$

$$\frac{\partial(\rho\mathbf{F})_{11}}{\partial(\rho\mathbf{F})_{13}} = -\frac{F_{22}F_{31} - F_{21}F_{32}}{F_{23}F_{32} - F_{22}F_{33}}, \tag{I.28}$$

$$\frac{\partial(\rho\mathbf{F})_{11}}{\partial(\rho\mathbf{F})_{21}} = \frac{F_{13}F_{32} - F_{12}F_{33}}{F_{23}F_{32} - F_{22}F_{33}}, \tag{I.29}$$

$$\frac{\partial(\rho\mathbf{F})_{11}}{\partial(\rho\mathbf{F})_{22}} = -\frac{F_{13}F_{31} - F_{11}F_{33}}{F_{23}F_{32} - F_{22}F_{33}}, \tag{I.30}$$

$$\frac{\partial(\rho\mathbf{F})_{11}}{\partial(\rho\mathbf{F})_{23}} = \frac{F_{12}F_{31} - F_{11}F_{32}}{F_{23}F_{32} - F_{22}F_{33}}, \tag{I.31}$$

$$\frac{\partial(\rho\mathbf{F})_{11}}{\partial(\rho\mathbf{F})_{31}} = -\frac{F_{13}F_{22} - F_{12}F_{23}}{F_{23}F_{32} - F_{22}F_{33}}, \tag{I.32}$$

$$\frac{\partial(\rho\mathbf{F})_{11}}{\partial(\rho\mathbf{F})_{32}} = \frac{F_{13}F_{21} - F_{11}F_{23}}{F_{23}F_{32} - F_{22}F_{33}}, \tag{I.33}$$

$$\frac{\partial(\rho\mathbf{F})_{11}}{\partial(\rho\mathbf{F})_{33}} = -\frac{F_{12}F_{21} - F_{11}F_{22}}{F_{23}F_{32} - F_{22}F_{33}}. \tag{I.34}$$

- Term (d): Similarly to Term (a) derivatives of the stress deviator with respect to density can be decomposed as follows:

$$\frac{\partial \sigma'_{ij}}{\partial \rho} = \frac{\partial \sigma_{ij}}{\partial \rho} - \frac{1}{3}\left(\frac{\partial \sigma_{11}}{\partial \rho} + \frac{\partial \sigma_{22}}{\partial \rho} + \frac{\partial \sigma_{33}}{\partial \rho}\right)\delta_{ij}. \tag{I.35}$$

Furthermore:

$$\begin{aligned}\frac{\partial \sigma_{ij}}{\partial \rho} \;=\; & \frac{\partial F_{11}}{\partial \rho}\frac{\partial \sigma_{ij}}{\partial F_{11}} - \frac{1}{\rho}\left(F_{12}\frac{\partial \sigma_{ij}}{\partial F_{12}} + F_{13}\frac{\partial \sigma_{ij}}{\partial F_{13}} + F_{21}\frac{\partial \sigma_{ij}}{\partial F_{21}} + F_{22}\frac{\partial \sigma_{ij}}{\partial F_{22}}\right. \\ & \left. + F_{23}\frac{\partial \sigma_{ij}}{\partial F_{23}} + F_{31}\frac{\partial \sigma_{ij}}{\partial F_{31}} + F_{32}\frac{\partial \sigma_{ij}}{\partial F_{32}} + F_{33}\frac{\partial \sigma_{ij}}{\partial F_{33}}\right).\end{aligned} \tag{I.36}$$

As a result of Eq. (I.18) the following expression can be substituted:

$$\begin{aligned}\frac{\partial F_{11}}{\partial \rho} \;=\; & -\frac{1}{\rho^3(F_{23}F_{32} - F_{22}F_{33})}\left(\rho^2\rho_0 - (\rho\mathbf{F})_{13}(\rho\mathbf{F})_{22}(\rho\mathbf{F})_{31} + \right. \\ & \left. (\rho\mathbf{F})_{12}(\rho\mathbf{F})_{23}(\rho\mathbf{F})_{31} + (\rho\mathbf{F})_{13}(\rho\mathbf{F})_{21}(\rho\mathbf{F})_{32} - (\rho\mathbf{F})_{12}(\rho\mathbf{F})_{21}(\rho\mathbf{F})_{33}\right).\end{aligned} \tag{I.37}$$

- Term (e): In the same way as in Term (b) the required derivatives can be computed according to the following:

$$\frac{\partial \chi}{\partial \rho} = \frac{\partial \chi}{\partial \sigma_{\mathrm{EQ}}}\frac{\partial \sigma_{\mathrm{EQ}}}{\partial J_2}\frac{\partial J_2}{\partial \rho} + \frac{\partial \chi}{\partial T}\frac{\partial T}{\partial \rho}, \tag{I.38}$$

where Eq. (I.20) is required and

$$\begin{aligned}\frac{\partial J_2}{\partial \rho} \;=\; & 2\left[\sigma'_{11}\frac{\partial \sigma'_{11}}{\partial \rho} + \sigma'_{22}\frac{\partial \sigma'_{22}}{\partial \rho} + \sigma'_{33}\frac{\partial \sigma'_{33}}{\partial \rho} + \right. \\ & \left. 2\left(\sigma'_{12}\frac{\partial \sigma'_{12}}{\partial \rho} + \sigma'_{13}\frac{\partial \sigma'_{13}}{\partial \rho} + \sigma'_{23}\frac{\partial \sigma'_{23}}{\partial \rho}\right)\right]\end{aligned} \tag{I.39}$$

The last term in Eq. (I.38) can be found as

$$\frac{\partial T}{\partial \rho} = \left.\frac{\partial T}{\partial \rho}\right|_{\mathscr{S}} + \left.\frac{\partial T}{\partial \mathscr{S}}\right|_{\rho}\frac{\partial \mathscr{S}}{\partial \rho}, \tag{I.40}$$

where

$$\frac{\partial \mathscr{S}}{\partial \rho} = \left.\frac{\partial \mathscr{S}}{\partial \mathscr{E}}\right|_{(\rho\mathbf{F})}\left.\frac{\partial \mathscr{E}}{\partial \rho}\right|_{(\rho\mathbf{u}),(\rho E)} + \left.\frac{\partial \mathscr{S}}{\partial \rho}\right|_{\mathscr{E},(\rho\mathbf{F})}, \tag{I.41}$$

with

$$\left.\frac{\partial \mathscr{S}}{\partial \rho}\right|_{\mathscr{E},(\rho\mathbf{F})} = \frac{\partial \mathscr{S}}{\partial \mathcal{I}_1}\frac{\partial \mathcal{I}_1}{\partial F_{11}} + \frac{\partial \mathscr{S}}{\partial \mathcal{I}_2}\frac{\partial \mathcal{I}_2}{\partial F_{11}} + \frac{2\rho}{\rho_0^2}\frac{\partial \mathscr{S}}{\partial \mathcal{I}_3}. \tag{I.42}$$

Finally it is easy to show that

$$\left.\frac{\partial \mathscr{E}}{\partial \rho}\right|_{(\rho \mathbf{u}),(\rho E)} = \frac{1}{\rho}\left(|\mathbf{u}|^2 - E\right). \tag{I.43}$$

- Term (f): From Eq. (I.26) the following result can be derived

$$\frac{\partial(\rho \mathbf{F})_{11}}{\partial \rho} = -\frac{2\rho_0}{F_{23}F_{32} - F_{22}F_{33}}. \tag{I.44}$$

- Term (g): Derivatives of the constitutive equation for temperature can expanded as follows:

$$\frac{\partial T}{\partial(\rho E)} = \frac{\partial \mathscr{E}}{\partial(\rho E)}\frac{\partial \mathscr{S}}{\partial \mathscr{E}}\frac{\partial T}{\partial \mathscr{S}}, \tag{I.45}$$

where

$$\frac{\partial \mathscr{E}}{\partial(\rho E)} = \frac{1}{\rho}, \qquad \frac{\partial \mathscr{S}}{\partial \mathscr{E}} = \frac{1}{T}. \tag{I.46}$$

J

Symmetry boundary conditions

Within the computational mesh, it is assumed that the first 'real' computational cell is denoted $\alpha = N_{\mathrm{f}}$ where α is used to denote either i, j, k depending on whether the boundary conditions are being applied to the left x_1- , x_2-, or x_3-boundary; and N_{f} is the number of fictitious cells. Where symmetry boundary conditions apply the following provides the proper reflection of vector and tensor variables:

$$\mathbf{u}_\alpha = \mathbf{R}^{\mathrm{SBC}}\mathbf{u}_{2N_{\mathrm{f}}-\alpha-1}, \tag{J.1}$$
$$\mathbf{F}_\alpha = \mathbf{R}^{\mathrm{SBC}}\mathbf{F}_{2N_{\mathrm{f}}-\alpha-1}\mathbf{R}^{\mathrm{SBC}}, \tag{J.2}$$
$$\mathscr{S}_\alpha = \mathscr{S}_{2N_{\mathrm{f}}-\alpha-1}, \tag{J.3}$$

for the range $0 \leq \alpha \leq N_{\mathrm{f}} - 1$. For the boundaries in each coordinate direction the required rotation matricies are as follows:

- x_1-direction:
$$\mathbf{R}^{\mathrm{SBC}} = \begin{pmatrix} -1 & 0 & 0 \\ 0 & 1 & 0 \\ 0 & 0 & 1 \end{pmatrix} \tag{J.4}$$
- x_2-direction:
$$\mathbf{R}^{\mathrm{SBC}} = \begin{pmatrix} 1 & 0 & 0 \\ 0 & -1 & 0 \\ 0 & 0 & 1 \end{pmatrix} \tag{J.5}$$
- x_3-direction:
$$\mathbf{R}^{\mathrm{SBC}} = \begin{pmatrix} 1 & 0 & 0 \\ 0 & 1 & 0 \\ 0 & 0 & -1 \end{pmatrix} \tag{J.6}$$